Stony Brook University

Resurgence and the Large N Expansion

A Dissertation Presented

by

Ricardo Nuno Melo de Carmo Vaz

to

The Graduate School

in Partial Fulfillment of the Requirements

for the Degree of

Doctor of Philosophy

in

Physics

Stony Brook University

August 2015

Stony Brook University

The Graduate School

Ricardo Nuno Melo de Carmo Vaz

We, the dissertation committee for the above candidate for the
Doctor of Philosophy degree, hereby recommend
acceptance of this dissertation.

Christopher Herzog – Dissertation Advisor
Associate Professor, Department of Physics and Astronomy

George Sterman – Chairperson of Defense
Distinguished Professor, Department of Physics and Astronomy

Abhay Deshpande
Professor, Department of Physics and Astronomy

Martin Roček
Professor, Department of Physics and Astronomy

Michael Anderson
Professor, Department of Mathematics

This dissertation is accepted by the Graduate School.

Charles Taber
Dean of the Graduate School

Abstract of the Dissertation

Resurgence and the Large N Expansion

by

Ricardo Nuno Melo de Carmo Vaz

Doctor of Philosophy

in

Physics

Stony Brook University

2015

In this dissertation we focus on recent developments in the study of resurgence and the large N expansion. It is a well known fact that perturbative expansions, such as the large N expansion, are divergent asymptotic series. This is a signal that there are non-perturbative effects of the form e^{-N} that also need to be considered, and our original perturbative series should be upgraded to one including powers of both $1/N$ and e^{-N}, which is called a *transseries*. The machinery needed to tackle transseries was developed in the 1980s under the formalism of so-called *resurgence*. Using its tools we can derive a web of large-order relations showing how coefficients of the transseries, perturbative and non-perturbative, are connected to each other, and this is the origin of the term *resurgence*. This tells us that the perturbative part already "knows" all about the non-perturbative effects.

Matrix models appear in multiple contexts in theoretical physics, and this was the arena chosen to test and understand the ideas of resurgence, particularly the matrix model with a quartic potential. We consider different phases of the quartic matrix model, with special focus on the two-cut phase, in order to test the predictions of resurgence and study their implications.

In the second part of the dissertation we used our knowledge of resurgent transseries and the quartic matrix model to address a different type of question. Namely, can we make use of an expansion at large N to generate results at finite N? We did this by comparing an analytical solution of the quartic matrix model at finite N to a resummation of the transseries. Moving around in parameter space we saw how the non-perturbative sectors could go from irrelevant to absolutely crucial in order to generate the correct answer at finite N.

This work was supported by Fundação para a Ciência e Tecnologia,
within the POPH/FSE programme, under the grant SFRH/BD/70613/2010

Contents

List of Figures

List of Tables

Acknowledgments

First of all, I would like to thank my advisor Chris Herzog. His approach to Physics strikes the right balance between a formal component and physical intuition, and this is what every (young) physicist should aim for. While some of our projects did not reach positive conclusions I still learned a lot, and I enjoyed the freedom to work in other research avenues.

I am very grateful to Ricardo Schiappa for giving me the chance to take part in very interesting projects where I felt more at home, especially during times where my availability was not ideal. The results of these projects are presented in this thesis and I look forward to the research problems that will follow.

I am also thankful to Ricardo Couso-Santamaría and Kuo-Wei Huang for fruitful and enjoyable collaborations in the recent past. I have also benefited a lot from discussions with Inês Aniceto and Marcel Vonk.

Much credit is also due to the YITP for providing a very active research environment. In particular, I am indebted to Michael Anderson, Barry McCoy, Leonardo Rastelli, Martin Roček, Peter van Nieuwenhuizen and Warren Siegel for their advanced courses and/or seminars. Finally, I want to thank Adrián, Andrea, Arthur, Chia-Yi, Gustavo, Jean-Paul, Jun, Oumarou, Sujan and others for great experiences related to Physics, football [1], food, latin-american music, etc. And of course, I thank Madalena for everything.

Last, but not least, I am grateful to my family for their support.

[1] For some reason this is called "soccer" in the US.

Publication List

Publications related to this dissertation

[1] **"The Resurgence of Instantons: Multi-Cut Stokes Phases and the Painlevé II Equation"**
R. Schiappa and R. Vaz.
arXiv:1302.5138 [hep-th]
10.1007/s00220-014-2028-7
Commun. Math. Phys. **330**, 655 (2014)

[2] **"Finite N from Resurgent Large N"**
R. Couso-Santamaría, R. Schiappa and R. Vaz.
arXiv:1501.01007 [hep-th]
10.1016/j.aop.2015.02.019
Annals Phys. **356**, 1 (2015)

Other publications

[3] **"Linear Resistivity from Non-Abelian Black Holes"**
C. P. Herzog, K. W. Huang and R. Vaz.
arXiv:1405.3714 [hep-th]
10.1007/JHEP11(2014)066
JHEP **1411**, 066 (2014)

Chapter 1

Introduction

In modern physics, when tasked with the computation of a given physical quantity, *e.g.* partition functions, ground-state energies, cross-sections, transport coefficients, it is increasingly likely that we are not able to find an exact solution to the problem. The standard way forward is through perturbation theory. This involves identifying a parameter g, for example a coupling constant, which can be tuned to be small, and then expand whatever observable we want to compute, call it F, in powers of g

$$F(g) = F_0 + F_1\, g + F_2\, g^2 + \dots \tag{1.1}$$

A familiar example is the computation of energy levels of the harmonic oscillator with a quartic perturbation (also known as the anharmonic oscillator). Another one is the $g-2$ anomalous magnetic moment of the electron, which has been tested to remarkably high precision. And the first impression is that, should we have infinite computational ability, we can compute higher and higher orders in perturbation theory and add them up towards a more accurate result. But this is not true. If we keep on adding the contributions will start growing and the result will diverge. These are typically asymptotic series, with the coefficients F_g growing factorially $F_g \sim g!$, and they have zero radius of convergence. In quantum field theories, there is a general argument by Dyson [4] on why this happens, and the familiar lore is that this factorial growth is connected to the rapid growth in the number of Feynman diagrams at each order [5]. While there may be subtleties with this argument [6, 7], the factorial divergence of perturbative series has been observed many a time, for instance in quantum mechanics [8, 9], in matrix models [10, 11], and even generally in string theories [12].

So these asymptotic series with zero radius of convergence clearly cannot amount to the whole story. Actually, the divergence of perturbation theory conceals a window into the world of nonperturbative physics. The divergence of the perturbative series is connected to the existence of nonperturbative [1] effects of the form $\mathrm{e}^{-1/g}$ [12, 13]. We are interested in

[1] We will also refer to these effects, interchangeably, as *instantons*.

understanding these effects for multiple reasons [14] . We may have a maximalist perspective of wanting to completely understand the observable in question. These exponentially small effects may be physically significant by themselves, like they are in the case of radioactive decay. But there is also the Stokes phenomenon [15] to take into account, and as parameters in the setup change, the asymptotic behavior of the observable may change as well, even getting to a scenario where what once was exponentially small becomes the leading order effect. Having said all this, it should be clear that we need something more general than our starting perturbative expansion. In fact, it is eloquently put in [14], that these "[non-perturbative] features are like mathematical stealth aircraft, flying unseen by the radar of conventional asymptotics". Therefore, we will instead be working with a formal object that includes both perturbative and nonperturbative components, which is called a transseries [16]

$$F(g) = \sum_n F_n^{(0)} g^n + \sum_i \mathrm{e}^{-A_i/g} \sum_m F_m^{(i)} g^m \,. \tag{1.2}$$

The A_i factors control the strength of the nonperturbative effects and we will always refer to them as instanton actions. In the expression above we see that we have our old perturbative expansion, and then a collection of nonperturbative sectors (about which we are not being too specific), each of them with an exponential weight and its own asymptotic expansion. From a path integral perspective, the first term corresponds to an expansion around the $g = 0$ vacuum, and it is then followed by the contributions from different non-trivial saddles, each of them having a *perturbative* expansion around a *nonperturbative* saddle.

Naïvely it might seem like we have just increased the complexity of our approach for no strong reason, but we shall see that this is not the case. The appropriate mathematical formalism for dealing with transseries was developed in the remarkable work of Jean Écalle in the 1980s [17–19], and it is now generally known as "resurgence". When dealing with divergent sums, a natural object to consider is the Borel transform and then perform its inverse in order to associate a value to the original sum. The obstacle in doing this lies in the singularities of the Borel transform, and these are also deeply connected to the non-perturbative component of the transseries. The resurgence toolbox allows us to precisely study the behavior of transseries around singularities. This is very important because we may have different transseries solutions with different asymptotic profiles in different regions of the complex plane, which are separated by these directions with singularities, and the computation of so-called *alien derivatives* is the gateway towards gluing transseries across singular directions, or from a different perspective, understanding how a transseries "jumps" across a singular directions. Finally, in what is perhaps the most significant consequence of resurgence, we derive a web of (large-order) relations which connect all the sectors of the transseries, perturbative and nonperturbative, amongst each other. This implies that the coefficients $F_m^{(i)}$ above are not random, rather they are related to coefficients in different sectors; they *resurge* in different sectors. It also means, we should stress, that our plain

and honest perturbative expansion already knows all about nonperturbative physics, and vice-versa. While the ideas of resurgence were relatively unknown to the Physics community, they were applied successfully to certain problems in quantum mechanics [20–22]. They were certainly more familiar in certain areas of Mathematics, especially the study of ODEs [23, 24]. But it was the landmark work of Aniceto, Schiappa and Vonk [25] that brought these ideas into the language of string and gauge theories through the type of perturbative series that will be the main focus of this dissertation: the large N expansion.

The large N expansion, also known as the $1/N$ expansion, dates back to the seminal paper by 't Hooft [26] in which he proposed "$1/N$" as a suitable expansion parameter for SU(N) gauge theories as a way around the fact that the coupling constant of QCD could not be used as such. Since then, the large N expansion has been the source of many fascinating results and ideas, perhaps none more so than large N duality [27, 28]. In this setup the partition function of a given gauge theory defines, nonperturbatively, a dual large N closed string background, described by geometry related to this large N limit. A more complete picture is perhaps the one of [29]. Here the gauge theory side is a matrix model with a given potential V, and its large N limit yields a closed string background described by the B-model topological string on a particular non-compact Calabi-Yau background. Additionally, the nonperturbative e^{-N} effects on the closed string side are understood physically as being associated to D-branes [30, 31]. At this stage we segue into the class of large N gauge theories that we wish to address: matrix models, or random matrix integrals. These are the simplest gauge theories, since they are theories in zero dimension (they have no propagating degrees of freedom). Despite this apparent simplicity, random matrices manage to spring up in the most disparate of scenarios, from real life problems of a chaotic transportation system [32] or airplane boarding [33], to problems in pure mathematics involving knot invariants [34] or zeros of the Riemann zeta function [35], and even applications to biology [36] (the full spectrum can be seen here [37]). One could possibly argue that they play the role of "special functions", through which the solutions to various problems can be expressed, in modern mathematical physics [38]. In more familiar grounds, it was found within the context of the AGT correspondence [39, 40] that certain quantities could be realized by Penner-type matrix models [41, 42]. More recently it was found that the partition functions of certain supersymmetric theories could be reduced, via the method of localization, to (multi-)matrix models [43, 44]. Among the theories with matrix model descriptions, ABJM is the one where the most knowledge of nonperturbative effects has been extracted [45–47].

The choice of matrix models as the arena to test nonperturbative phenomena has other advantages beyond their (relative) simplicity and versatility. For concreteness, let us write

down the partition function of the Hermitian one-matrix model,

$$Z(N,g_s)=\frac{1}{\mathrm{vol}(\mathrm{U}(N))}\int \mathrm{d}M\,\mathrm{e}^{-\frac{1}{g_s}V(M)}=\frac{1}{N!}\int\prod_{i=1}^{N}\frac{\mathrm{d}\lambda_i}{2\pi}\,\Delta^2(\lambda_i)\mathrm{e}^{-\frac{1}{g_s}\sum_{i=1}^{N}V(\lambda_i)}\,, \tag{1.3}$$

where the diagonal representation on the right-hand side is derived through a standard gauge-fixing procedure. For now the details are not important, so we will just say that V is the potential, which from this point forward can be taken to be a polynomial, $\Delta^2(\lambda_i)$ is the Vandermonde determinant

$$\Delta^2(\lambda_i)=\prod_{i<j}(\lambda_i-\lambda_j)^2\,, \tag{1.4}$$

and g_s is the coupling constant, called *string* coupling for historical reasons. This can be thought of as a gas of particles in a one-dimensional potential V and with a logarithmic repulsion (after moving the $\Delta(\lambda_i)$ to the exponent). Typically we work in what is known as the 't Hooft large N limit, which corresponds to having large N and small g_s with the 't Hooft coupling $t=g_sN$ fixed, and t becomes a modulus of the problem. It is known that in the large N limit the matrix eigenvalues condense in segments centered on the critical points of the potential, forming cuts. The simplest case is a one-cut configuration, with eigenvalues along a single interval, but in general we get a multi-cut eigenvalue configuration. Then we can define an eigenvalue density along these cuts, or more generally a spectral curve on the whole complex plane. This is a Riemann surface with s cuts, with its discontinuities across the cuts determining the eigenvalue density. From these objects we can compute the perturbative coefficients F_g of the free energy $F=\log Z$. These very elegant methods were introduced in the early 80s [48, 49] (see [50] for an excellent review), later given a more geometrical identity in [51], and then finally solved purely in terms of the spectral curve [52, 53]. Moreover, the instanton effects in matrix models have long been understood as eigenvalue tunneling [12, 54–56]. In other words, suppose we have an $s-$cut configuration and we choose a given distribution $\{N_i\}$, meaning we put N_i eigenvalues in the $i-$th cut. This is also referred to as a choice of background. Then we can use the spectral curve that describes this background to compute perturbative contributions to the free energy, but different backgrounds $\{N_i'\}$ are never seen because they are instantons. They are nonperturbative effects [2]. The research program of studying nonperturbative effects in matrix models, with special focus on polynomial (particularly quartic) potentials started with [10] and carried on in [11, 16, 57–60] before culminating in the general exposition of [25], which tackled the one-cut quartic matrix model and its double-scaling limit, described by the Painlevé I equation. In the end the nonperturbative effects are derived and interpreted through different methods (spectral curve methods or orthogonal polynomials), and finally the transseries structure and the predictions from resurgence, such as the tight web of connections between different

[2] We will discuss this in greater detail. The basic idea is that a background independent partition function is obtained by a sum over all instanton sectors, and this is precisely a transseries.

instanton sectors we alluded to above, were tested to great precision. These methods and results were then extended to the two-cut quartic matrix model and its double-scaling limit (described by the Painlevé II equation) in [1]. The study of multi-cut solutions is in general very difficult, and as shown in [1] (and reproduced below), the generalization of the one-cut techniques is non-trivial. But there are still several open questions, both from physical or more formal perspectives, that we will return to in the main text.

In a recent paper [2] we took the large N expansion and resurgence transseries a step further in order to address an important question, namely how we can make use of them in order to make meaningful predictions at *finite* N, *e.g.* for $N = 3$. The best model in which this question can be answered is the one-cut quartic matrix model [10, 16, 25, 49]. Not only are we able to extract a very large amount of transseries coefficients, but for (small) finite N the partition function can be computed analytically. This way we can make a comparison between the exact result and the resummation of the transseries for finite N. Naturally, it is very interesting to understand the role played by the nonperturbative sectors. What was found in [2], which will be discussed below, is that moving the 't Hooft parameter t around the complex plane we encounter several different possibilities. We can have a great match between both results including just the perturbative part, meaning $\sigma = 0$. Or we can find, after crossing a Stokes line, that the instanton sectors are turned on and provide a match with higher and higher accuracy. Or we can even find, after crossing anti-Stokes lines, that the perturbative contribution totally misses the analytical result, but then the nonperturbative ones come in to save the day and match the right result. Additionally, we are also interested in knowing the properties of the partition function as a function of *complex* N. It was discovered [61] that in certain ABJ(M) theories the nonperturbative contributions truncate at a low order, and the authors were able to show that the partition function $Z(N)$ is in fact an entire function of N (*i.e.* it is holomorphic for any complex value of N). This is a remarkable feature given that the starting point is an object defined for positive, integer, N. For the one-cut quartic matrix model there is no equivalent truncation, and we have the entire tower of nonperturbative sectors to handle. So while we are not able to completely prove that the partition function is an entire function, we were able to interpolate continuously to negative and complex values of N, and our evidence suggests that it should indeed be an entire function of complex N.

Before wrapping up this section we should mention other areas where the ideas of resurgence have been applied and explored. One of them, which is connected to matrix models [10, 29, 62] is topological string theory (see [50, 63] for reviews). In [64–66] the focus was the holomorphic anomaly equation which governs the B-model topological string (perturbative) free energy [67]. In the aforementioned works the authors managed to generalize the holomorphic anomaly equations to a nonperturbative framework and test the resulting transseries in specific examples. There are several interesting features, including different

instanton actions with alternating dominance of the large-order behavior in different regions of moduli space and a multi-sheeted Borel plane that sometimes sees the singularities jump from one sheet to another. Applications to more "realistic" theories, particularly ones mimicking certain properties of QCD, such as confinement or asymptotic freedom, have been undertaken with great success by Dunne, Ünsal, and collaborators [68–79]. One of the main accomplishments has been the understanding of infra-red renormalons, which also manifest themselves as Borel singularities, in the transseries and resurgence framework. Another interesting application was the cusp anomalous dimension, a well-known observable in $\mathcal{N} = 4$ Yang-Mills theory, satisfying the so-called Beisert-Eden-Staudacher equation [80] which is valid at any coupling. The recent works [81, 82] built upon previous results and built full transseries solutions. These were used to check large-order relations as well as, in the same spirit of [2], generate solutions at finite coupling and interpolate between weak and strong coupling. Finally, some features of resurgence were observed in the gradient expansion of hydrodynamics [83]. This is very interesting because the model in question is used to describe a longitudinally-expanding quark gluon plasma, and the nonperturbative effects are interpreted as quasinormal modes.

The remainder of this dissertation is organized as follows:

- In chapter 2 we present a short introduction into transseries and resurgence. We try to go over the main ideas but without an excessive amount of technical detail. We begin by looking at the Borel transform and the ambiguities that arise in Borel resummation due to singularities. We then define transseries as the formal solutions we should be considering. The tools of resurgence, namely alien calculus, allow us to compute the discontinuity of transseries across the singular directions as well as derive relations between different sectors of the transseries. In the end we use the example of Painlevé I to illustrate some of the ideas, as well as introduce some features of the "real" transseries we encounter in later examples.

- Chapter 3 is dedicated to introducing large N matrix models and the techniques used to solve them. We start by studying spectral curve methods in multi-cut setups. We then consider the orthogonal polynomial approach which in turn allows for a straightforward transseries generalization, and we also present some predictions from resurgence, already written in the appropriate notation, to be tested in chapter 4. We also perform a derivation in $\mathbb{Z}_2$ configurations that provides another check on the transseries solution as well as a physical interpretation of the instanton sectors. This is followed by a short discussion on background independence.

- Chapter 4 studies the resurgent structure of the quartic matrix model. We briefly review some results from the one-cut solution, which are later needed in 6, and then focus our attention in the two-cut solution and its double-scaling limit, described by

Painlevé II. We analyze some novel features, test large-order resurgence relations to high precision and also extract several (previously unknown) Stokes constants.

- Besides the one- and two-cut phases, there are different types of eigenvalue configurations in the quartic matrix model. In chapter 5 we report on some ongoing work concerning trivalent-tree distributions. We present some numerical evidence of this phase, its large t limit and some of the open questions that need to be addressed.

- In chapter 6 we show how large N resurgent transseries can be used in order to make finite N predictions. We work in the one-cut phase of the quartic matrix model, and compare a Borel-Padé-Écalle resummation to an analytical calculation of the matrix model partition function at small N. Moving the 't Hooft coupling around the complex plane we run into Stokes and anti-Stokes lines, and this in turn changes the role that the instanton sectors play at finite N. Finally, we explore the partition function for complex values of N and present some evidence that it is an entire function on complex-N plane.

- We summarize our results and discuss open problems and future research directions in chapter 7.

- In the appendices we present some of the transseries data that was computed. Appendix A concerns the one-cut solution, used in chapter 6. Appendices B and C contain data from the two-cut solution, and D has data from Painlevé II, and they are all connected to chapter 4.

Chapter 2

Resurgent Transseries

2.1 Introduction

We have outlined in the introduction that typically perturbative expansions are asymptotic, and if we just keep adding more and more terms they will eventually diverge. As such, a natural question to pose is: how do we associate a number to a divergent sum? In this chapter we try to address this question rigorously and introduce some of the main ideas of transseries and resurgence [17–19]. The material described below is covered in many references with different degrees of depth, technical detail and mathematical flavor [20, 23–25, 58, 66, 84–90]. Out of these we should point out that [84] is the most recent one and already takes some of the recent applications into account. We will follow the approach of [25] more closely because it is formulated in the same language of our examples in chapters 4 and 6.

Throughout this introduction we will be talking about a general quantity $F(z)$ without specifying anything about its origin. Should this be too abstract, the reader could think of it as a solution to a given ODE. Our example at the end focuses precisely on an ODE, the Painlevé I equation. The results extend naturally to the finite difference equations we study later [91, 92], but we will not delve into this in detail. Some of the most technically heavy large-order resurgence relations will be postponed until section 3.2.3. Even there we will not provide the full derivations, some of which can be found in [25].

2.2 Asymptotic Series and Borel Resummation

As we announced before, our starting point is a perturbative expansion for an abstract quantity $F(z)$ around $z \sim \infty$

$$F(z) \simeq \sum_{g=0}^{\infty} \frac{F_g}{z^g} \,. \tag{2.1}$$

We say that a function $\Phi(z)$ is asymptotic to it in the sense of Poincaré if

$$\lim_{z\to\infty}\left(\Phi(z)-\sum_{g=0}^{N}\frac{F_g}{z^g}\right)z^N=0 \tag{2.2}$$

for all N. Asymptotic series are not necessarily divergent, but we will work under that assumption from this point forward. In particular, we will be interested in a special type of divergent series which are of Gevrey-1 type. A power series such as (2.1) is of Gevrey-1 type if we can find two positive numbers, c and A, such that

$$|F_g|\leq c\,g!\,A^{-g} \tag{2.3}$$

for all g. In words, the coefficients F_g grow factorially fast. This type of series is asymptotic and is commonly found in perturbative solutions to problems across many different fields. In practice, divergent asymptotic series are characterized by the fact that the partial sums will approach the true value $\Phi(z)$ and then, as N grows, they will diverge. So a natural first question to ask is how to associate a value to a divergent series. The most straightforward answer is to do *optimal truncation*, which is to say we look for the value of N that minimizes $|F_g/z^g|$ and truncate the sum at this point. If z is large enough, so that $1/z$ is a good choice for an expansion parameter, then we can approximate

$$\left|F_N z^{-N}\right|\simeq c\,N!\,A^{-N}|z|^{-N}\,, \tag{2.4}$$

and using Stirling's approximation of the factorial this can be rewritten as

$$c\,\exp\left\{N\left(\log N-1-\log|A\,z|\right)\right\}\,. \tag{2.5}$$

At large N the exponent will be minimal at

$$N_\star=|A\,z|\,. \tag{2.6}$$

The error in the optimal truncation can then be estimated from the next term in the series

$$\varepsilon(z)\simeq|F_{N_\star+1}z^{-(N_\star+1)}|\simeq\widehat{c}\,\mathrm{e}^{-A|z|}\,, \tag{2.7}$$

making use of Stirling's approximation once more. This error is exponentially small and nonperturbative in nature. This is an indication the perturbative expansion is not enough to fully determine $\Phi(z)$ as we are missing nonperturbative information. To completely understand the picture nonperturbatively, and there are plenty of reasons to do so [14], we need to go beyond optimal truncation and into the realm of Borel resummation.

The Borel transform of a Gevrey-1 asymptotic series such as (2.1) is a linear operator $\mathcal{B}$

defined as [1]

$$\mathcal{B}\left[F\right](\xi) = \sum_{g=1}^{+\infty} \frac{F_g}{(g-1)!}\xi^{g-1} \tag{2.8}$$

We note that the constant term is not included above, and we will return to this shortly. The Borel transform takes us from our original series to a new series in the variable ξ, which lives in the (complex) Borel-plane. Moreover, there is a very interesting map from the standard operations (*e.g.* multiplication, taking derivatives, etc) we could perform on our original series to different operations on the side of the Borel transform. This is laid out in detail in [84], where the original and the Borel sides are respectively labeled as "multiplicative" and "convolutive". For example, a derivative $\partial_z F(z)$ on the multiplicative side becomes a multiplication $-\xi\,\mathcal{B}[F](\xi)$, it follows straight from the definition (2.8). We could also use this property recursively to show that $F(z+w)$ becomes $\mathrm{e}^{-\xi w}\mathcal{B}[F](\xi)$. But the most important feature is that the Borel transform now has a finite radius of convergence [85] and it is an analytic function in a disk around $\xi = 0$ [2]. The radius of convergence corresponds to the distance from the origin to the closest singularity, and as we shall see, the singularities of the Borel transform play a crucial role within the framework of resurgence. The second step in Borel resummation is the inversion of the Borel transform through a directional Laplace transform, which is formally written as

$$\mathcal{S}_\theta F(z) = F_0 + \int_0^{\mathrm{e}^{\mathrm{i}\theta}\infty} \mathrm{d}\xi\, \mathcal{B}\left[F\right](\xi)\, \mathrm{e}^{-\xi z}\,, \tag{2.9}$$

where we have brought back the constant term. This is called the *Borel resummation along* θ and it has, by construction, the same asymptotic expansion as $F(z)$. It also may provide an answer to our original question, namely how to associate a value to a divergent series. However, we cannot carry out the integration if there are singularities in the Borel plane along the θ ray. We can avoid the singularities by defining *lateral* Borel resummations $\mathcal{S}_{\theta^\pm}$ going slightly above or below θ. These two lateral resummations define different functions and introduce an ambiguity in the reconstruction of the original funcion, rendering $F(z)$ non-Borel summable. More specifically, these different integration contours generate functions that have the same asymptotic behaviour but differ by exponentially small terms [20]. Let us assume that the Borel transform has only one singularity along θ, a simple pole at a distance A from the origin. Then the difference of the two contours becomes a contour integral around A

$$\mathcal{S}_{\theta^+} F(z) - \mathcal{S}_{\theta^-} F(z) \propto \oint_{(A)} \mathrm{d}\xi\, \frac{\mathrm{e}^{-\xi z}}{\xi - A} \propto \mathrm{e}^{-Az}\,. \tag{2.10}$$

[1] A more general factorial growth of the form $(ag! + b)$ would just require some straightforward modifications, and we will focus on this simplest possibility.

[2] If our starting series had a finite radius of convergence its Borel transform would be an entire function on the complex plane.

As we reconstruct the original function along different (singular) directions we pick up further nonperturbative ambiguities. To understand these we need to go to the toolbox of resurgence and use *alien calculus*. The reason why we placed our singularity at a distance A is no accident. With the help of alien calculus we shall see how the singularities in the Borel plane are precisely what controls the large-order growth of the perturbative expansion (2.3). At this point we may also wonder how the Borel transforms can, in practice, help us with our original issue of associating a number to a divergent sum. The way forward is through using *Borel-Padé* approximants, which consist in computing a Padé approximant of the Borel transform. This transforms a polynomial (in practice we can only compute a finite amount of terms) into a rational function which mimicks the singularity structure of the Borel transform. This object can then be inverted using Laplace transforms. We will not say more about Borel-Padé in this introduction, but we will return to it and make use of it in 6.

2.3 Transseries

We have tried to argue up to now that the divergence of perturbation theory and the singularity structure of the Borel plane conceal important information about nonperturbative physics, meaning we have to go beyond the perturbative expansion (2.1) if we wish to find a complete, nonperturbative, answer to our problem. We do this by introducing a so-called *transseries* [16]. This is a double expansion, in powers of both $1/z$ and e^{-Az}, for some constant $A \in \mathbb{C}$.

$$F(z,\sigma) = \sum_{n=0}^{+\infty} \sigma^n \mathrm{e}^{-nAz} \sum_{g=0}^{+\infty} \frac{F_g^{(n)}}{z^{g+\beta_n}} \,. \tag{2.11}$$

This is a formal object that contains in it a perturbative sector ($n = 0$) and a tower of nonperturbative ones ($n \geq 1$) which have themselves a perturbative expansion at each level. It should, after an appropriate resummation, generate the full nonperturbative answer for the problem we are interested in. For historical reasons we will also refer to the nonperturbative sectors as "instanton sectors", even when there is no such physical interpretation. The ingredients in (2.11) are the following:

- σ is called a transseries parameter and it serves as a counting parameter to keep track of the instanton sector. This is a parameter that is fixed by some physical condition, or by a boundary condition in an ordinary differential equation.

- A will be referred to as the instanton action regardless of its physical interpretation. Once again, the choice of notation has everything to do with what we saw in the previous sections, namely the closest singularity in the Borel plane and the large-order growth of perturbation theory. This is in fact the first sign of resurgence, a connection between perturbative and nonperturbative objects. The instanton action is not an

arbitrary quantity, and it can be explicitly computed by plugging the transseries ansatz (2.11) into whatever differential/difference equation we are interested in solving. We will see this in several examples.

- β_n is just a characteristic exponent to allow for the sums to start at some non-zero power of $1/z$.

- We will define

$$F(z,\sigma) = \sum_{n=0}^{+\infty} \sigma^n \, \mathrm{e}^{-nAz} F^{(n)}(z); \quad F^{(n)}(z) \equiv \sum_{g=0}^{+\infty} \frac{F_g^{(n)}}{z^{g+\beta_n}} \, . \tag{2.12}$$

  $F^{(n)}$ is the n-instanton contribution, and the sum is also asymptotic. The coefficient $F_g^{(n)}$ is the g-loop contribution around the n-instanton configuration.

Up to now we have been talking about one-parameter transseries. There are many natural generalizations we can think of. For instance, we can imagine having multiple instanton actions which lead to a multi-parameter transseries of the form

$$F(z,\sigma) = \sum_{\boldsymbol{n}\in\mathbb{N}^p} \boldsymbol{\sigma}^{\boldsymbol{n}} \mathrm{e}^{-\boldsymbol{n}\cdot\boldsymbol{A}z} \sum_{g=0}^{+\infty} \frac{F_g^{(\boldsymbol{n})}}{z^{g+\beta_{\boldsymbol{n}}}} \, , \tag{2.13}$$

where all the quantities were promoted to p-vectors, $\boldsymbol{\sigma}^{\boldsymbol{n}} = \prod_{j=1}^p \sigma_j^{n_j}$, $\boldsymbol{n}\cdot\boldsymbol{A} = \sum_{j=1}^p n_j A_j$. In the specific cases addressed below we will encounter two-parameter transseries, with instanton actions $\pm A$. We will discuss this in more detail when we study the example of Painlevé I in section 2.6. Another generalization we will encounter is the appearance of another monomial, $\log z$, making the transseries a triple expansion, with powers of $1/z$, e^{-Az} and $\log z$. We will save further details on the appearance of logarithmic sectors for specific examples. It is also possible for the transseries to contain other nonanalytic functions of z at $z=\infty$ [93], but we will not entertain these possibilities.

At this stage transseries are just formal objects, and there are several aspects to take into account if we are using them to describe physical quantities. First of all, an expression such as (2.11) only makes sense if $\mathbb{R}\mathrm{e}(A\,z) > 0$, so that the instanton sectors are suppressed with respect to the perturbative one. We will discuss this in detail in the context of matrix models in section 3.3.2. Nonperturbative sectors which are exponentially large with respect to the perturbative part naturally need to be turned off (*i.e.* their transseries parameter σ_j is set to 0) before any meaningful resummation is performed, but they still need to be taken into account. For one, they are still involved in large-order relations that connect them to other sectors. Not only that, it may be that as we move the coupling around the complex plane we cross a Stokes line which will turn on these sectors, and they may end up being physically

relevant. This is what is known as Stokes phenomenon, and one of the simplest examples where this is realized is the Airy equation [87, 94]. Another practical question to pose is on the reality of the transseries. It is often the case that we are interested in computing an observable for some positive real value of the coupling. But equally often the positive real axis will be a singular direction. The Borel resummation of a full transseries, which is called Borel-Écalle resummation, has the remarkable property of resolving any and all nonperturbative ambiguities. We saw above how the resummation of the perturbative series generated an ambiguity (2.10). But remarkably the resummation of higher instanton sectors generates similar ambiguities that end up all canceling out, leaving behind an unambiguous result. In the case of positive real coupling, this means a real result. This cancellation mechanism was observed in a constructive way in quantum mechanics [95, 96], and then recently in certain quantum field theories in two and four dimensions [76, 79]. This procedure, also called *median* resummation, was then laid out systematically in [97], where the reality properties were translated into conditions fixing the imaginary part of the transseries parameter.

Example Before moving on it may be beneficial to look at a simple example to illustrate some of the features of the past two sections. For this we look at the Euler equation [85, 87]

$$\varphi'(z) + A\,\varphi(z) = \frac{A}{z}\,, \tag{2.14}$$

which has an irregular singularity at $z = \infty$. We can construct a power series solution which looks like

$$\varphi^{(0)}(z) = \sum_{n=0}^{+\infty} \frac{c_n}{z^{n+1}}\ , \quad c_n = A^{-n} n!\ , \tag{2.15}$$

so our choice of notation is not innocent. This solution ticks all the boxes above, it is asymptotic and Gevrey-1, with coefficients growing factorially. And it is easy to see that (2.14) actually admits a one-parameter family of solutions of the form

$$\varphi(z) = \varphi^{(0)}(z) + C\,\mathrm{e}^{-Az}\,, \tag{2.16}$$

for some constant C. This is just the familiar method of finding a solution to a differential equation as a solution to the homogeneous equation added to a particular solution. But (2.16) is also an example of a *transseries*, and possibly the simplest transseries we can think of. It has only one nonperturbative sector with only one term in it. The constant C plays the role of the transseries parameter, and as we have mentioned before, it needs a boundary condition to be fixed. Let us now set $A = -1$ and look at Borel resummation. The asymptotic series is now

$$\varphi^{(0)}(z) = \sum_{n=0}^{+\infty} \frac{(-1)^n\, n!}{z^{n+1}}\ , \tag{2.17}$$

and its Borel transform is easily found to be

$$\mathcal{B}\left[\varphi^{(0)}\right](\xi) = \sum_{n=1}^{+\infty} (-1)^{n-1}\,\xi^{n-1} = \frac{1}{1+\xi}\,. \tag{2.18}$$

We see that it only has a singularity at $\xi = -1$. As a consequence of that, we are allowed to perform Borel resummation along the positive real axis

$$\mathcal{S}_0\varphi^{(0)}(z) = \int_0^{+\infty} \mathrm{d}\xi\, \frac{\mathrm{e}^{-\xi z}}{1+\xi} = \mathrm{e}^{z}\,\Gamma(0,z)\,, \tag{2.19}$$

where the last equality is nothing more than the definition of the incomplete gamma function $\Gamma(0,z)$. This solution can be analytically extended to the entire half-plane $\mathbb{R}\mathrm{e}\, z > 0$. Things are a bit more interesting if we try to invert the Borel transform along the negative real axis. Because of the singularity at $\xi = -1$, we have to take lateral resummations going either above or below the singularity

$$\mathcal{S}_{\pi^\pm}\varphi^{(0)}(z) = \int_0^{\mathrm{e}^{\mathrm{i}\pi^\pm}\infty} \mathrm{d}\xi\, \frac{\mathrm{e}^{-\xi z}}{1+\xi}\,. \tag{2.20}$$

In line with what we described before, we can compute the difference between the two lateral resummations, which amount to picking up the residue at $\xi = -1$,

$$\mathcal{S}_{\pi^+}\varphi^{(0)}(z) - \mathcal{S}_{\pi^-}\varphi^{(0)}(z) = 2\pi\mathrm{i}\,\mathrm{Res}_{\xi=-1}\left(\frac{\mathrm{e}^{-\xi z}}{1+\xi}\right) = 2\pi\mathrm{i}\,\mathrm{e}^{z}\,. \tag{2.21}$$

This term is exponentially small along the negative real axis, and it is precisely the kind of non-analytic term we added in (2.16). To recap, we have seen how the factorial growth of the asymptotic (perturbative) series is associated to a singularity in the Borel plane, and the ambiguity in resumming along singular directions is what compels us to include the non-analytic terms that make up the transseries.

2.4 Alien Calculus and Stokes Automorphism

When we introduced Borel resummation in section 2.2 we saw how the singularities of the Borel transform produce nonperturbative ambiguities, depending on the choice of lateral resummation. The work of Écalle included the development of the so-called *alien calculus* ("calcul étranger") [17–19] in order to systematically study the transseries singularities in the Borel plane. The central objects, to be defined shortly, are the alien derivatives Δ_ω, where ω labels the singularities of the Borel transform. A given Gevrey-1 series such as (2.1) is said to be a simple resurgent function if its Borel transform $\mathcal{B}[F](\xi)$ has only simple

poles or logarithmic branch cuts as singularities. That is, if ω is a singular point, then in its vicinity

$$\mathcal{B}[F](\xi) = \frac{\alpha_\omega}{2\pi\mathrm{i}(\xi-\omega)} + \Psi_\omega(\xi-\omega)\frac{\log(\xi-\omega)}{2\pi\mathrm{i}} + \tilde{\Psi}_\omega(\xi-\omega)\,, \tag{2.22}$$

with $\alpha_\omega \in \mathbb{C}$ and $\Psi_\omega, \tilde{\Psi}_\omega$ are holomorphic near the origin. We should mention that, under some reasonable extra conditions, simple resurgent functions allow for the resummation of power series along any direction of the ξ-plane, giving rise to a family of functions $\{\mathcal{S}_\theta F(z)\}$ which are holomorphic in given wedges of the complex plane [85, 88, 98]. Going back to (2.22), we can rewrite it in a slightly different fashion

$$\mathcal{B}[F](\xi) = \frac{\alpha_\omega}{2\pi\mathrm{i}(\xi-\omega)} + \mathcal{B}[\psi_\omega](\xi-\omega)\frac{\log(\xi-\omega)}{2\pi\mathrm{i}} + \text{holomorphic}\,. \tag{2.23}$$

We can now define the alien derivative Δ_ω. If we denote by U the set of singularities of $\mathcal{B}[F](\xi)$, then

$$\left(\Delta_\omega F\right)(z) = \alpha_\omega + \psi_\omega(z)\,, \tag{2.24}$$

if $\omega \in U$ and $(\Delta_\omega F) = 0$ otherwise. It should be noted that the alien derivative acts on an asymptotic series and returns another asymptotic series [3]. It can be shown that it has the right properties a derivative should have, namely being linear and obeying the Leibniz role. More importantly, it has the following property

$$[\partial_z, \Delta_\omega] = \omega\,\Delta_\omega \tag{2.25}$$

which will turn out to be very useful. So we see in (2.24) that the alien derivative encodes the singular behaviour of the Borel transform, and this will be the key to connecting different sectorial solutions – understanding the "jumps" across singular directions. With this in mind, we can see how the alien derivative provides a way to calculate the difference between lateral Borel resummations

$$\mathcal{S}_{\theta^+}F(z) - \mathcal{S}_{\theta^-}F(z) \tag{2.26}$$

We now define the Stokes automorphism $\underline{\mathfrak{S}}_\theta$ along direction θ

$$\mathcal{S}_{\theta^+} \equiv \mathcal{S}_{\theta^-} \circ \underline{\mathfrak{S}}_\theta\,, \tag{2.27}$$

which maps a simple resurgent function onto another. This can also be written as

$$\mathcal{S}_{\theta^+} - \mathcal{S}_{\theta^-} = -\mathcal{S}_{\theta^-} \circ \mathrm{Disc}_\theta\,, \tag{2.28}$$

[3] Typically $\psi_\omega(z)$ will be another sector in the transseries, or a combination of those. This will become more evident later on.

where $\text{Disc}_\theta = 1 - \underline{\mathfrak{S}}_\theta$ encodes the discontinuity across this direction. These objects are written in terms of alien derivatives through an exponentiation

$$\underline{\mathfrak{S}}_\theta = \exp\left(\sum_{\{\omega_\theta\}} \mathrm{e}^{-\omega_\theta z}\, \Delta_{\omega_\theta}\right) . \tag{2.29}$$

In this expression ω_θ is the set of Borel singularities along the θ-direction. We refer to [99] for a detailed derivation of this result. It involves a rigorous analysis of the integration contours involved. In particular the discontinuity Disc_θ can be seen as a sum over all Hankel contours which encircle each singularity from above the singular line before running off to infinity below it. This is shown in Fig. 2.1. In this context it is more useful to write out the

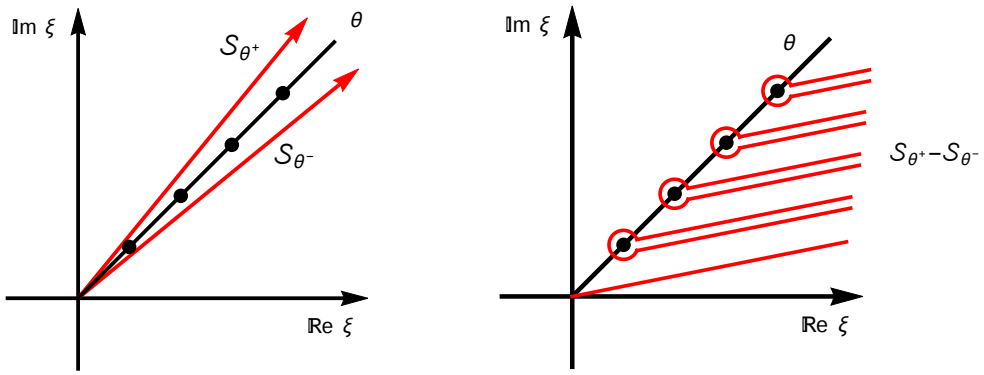

Figure 2.1: Lateral Borel resummations (left) and the difference between them (right). The discontinuity across θ can be seen as a sum over Hankel contours which encircle the singularities and then go off to infinity.

Stokes automorphism more explicitly [25], and for that we will consider the direction $\theta = 0$, the positive real axis, with Borel singularities located at points nA, with $n \in \mathbb{N}^\star$. This is generally what happens when we have a multi-instanton expansion such as (2.11). In this case we have

$$\underline{\mathfrak{S}}_0 = \exp\left(\sum_{\ell=1}^{+\infty} \Delta_{\ell A}\right) = 1 + \mathrm{e}^{-Az}\Delta_A + \mathrm{e}^{-2Az}\left(\Delta_{2A} + \frac{1}{2}\Delta_A^2\right) + \cdots \tag{2.30}$$

This formula shows how the understanding of the discontinuity across a singular direction is reliant upon the knowledge of the alien derivatives at the singularities. But, as it turns out, the alien derivatives are not the most straightforward objects to compute. Instead, we

introduce the *pointed* alien derivative [4]

$$\dot{\Delta}_\omega \equiv \mathrm{e}^{-\omega z}\Delta_\omega \,, \tag{2.31}$$

turning (2.29) into a sum of pointed alien derivatives. It is also easy to check, using (2.25), that this object commutes with the standard derivative

$$\left[\partial_z, \dot{\Delta}_\omega\right] = 0 \,. \tag{2.32}$$

This is a significant fact. We also point out that a derivative with respect to the transseries parameter, ∂_σ, also commutes with $\dot{\Delta}_\omega$. So now, for concreteness, let us suppose that the transseries $F(z,\sigma)$ (2.11) is an ansatz for a solution of some differential equation in the variable z, and for simplicity take it to be a first order equation. If we apply $\dot{\Delta}_\omega$ to this equation, the commutativity with the z-derivative means we find a linear differential equation for $\dot{\Delta}_\omega F(z,\sigma)$. But we can also apply ∂_σ to the equation and use the same reasoning. The conclusion is that $\dot{\Delta}_\omega F(z,\sigma)$ and $\partial_\sigma F(z,\sigma)$ satisfy the same first order differential equation (in the variable z), which means they must be proportional to each other

$$\dot{\Delta}_\omega F(z,\sigma) = S_\omega(\sigma)\, \partial_\sigma F(z,\sigma) \,. \tag{2.33}$$

The proportionality factor $S_\omega(\sigma)$ can only depend on σ and should be regular at $\sigma = 0$. Equation (2.33) is known as a *bridge* equation, providing a bridge between alien calculus and regular calculus. On the left hand side we have the (pointed) alien derivatives, capturing the behaviour around the Borel singularities, and on the right hand side we have our original asymptotic series, multiplied by an object we will discuss in detail below. The argument we have presented can be generalized to higher-order differential equations [5], and in the case of a multi-parameter transseries the right hand side becomes a linear combination of derivatives with respect to the different σ_j, multiplied by different factors $S_\omega^{(j)}$.

We will now look at the multiplier $S_\omega(\sigma)$ in more detail. Reverting to our specific case of singularities $\omega = \ell A \,, \ell = 1, 2, \ldots$, along the positive real axis, plugging our formal transseries expansions in (2.33) lead us to derive the following condition [6]

$$S_\ell = 0 \,, \;\; \text{if} \;\; \ell > 1 \quad \Leftrightarrow \quad \Delta_{\ell A} F(z,\sigma) = 0 \,, \;\; \text{if} \;\; \ell > 1 \tag{2.34}$$

[4] A more appropriate translation would be "dotted" alien derivative!

[5] It also applies to finite difference equations which will be studied later on [91, 92].

[6] We will abbreviate $S_{\ell A}(\sigma)$ by $S_\ell(\sigma)$.

In general we could think of $S_\ell(\sigma)$ as being a generic series in powers of σ, but matching the appropriate powers in (2.33) implies [7]

$$S_\ell(\sigma) = S_\ell\, \sigma^{1-\ell}\,, \quad \ell \leq 1\,, \tag{2.35}$$

and S_ℓ is called a Stokes constant. So the alien derivatives we may have are

$$\Delta_{\ell A} F^{(n)} = 0\,, \;\; \ell > 1\,; \;\; \Delta_{\ell A} F^{(n)} = S_\ell (n+\ell) F^{(n+\ell)}\,, \;\; \ell \leq 1\,. \tag{2.36}$$

We see that the knowledge of all alien derivatives hinges on these unknown Stokes constants $S_\ell \in \mathbb{C}$, $\ell = 1, -1, -2, \ldots$. These are analytic invariants of the differential equation in question and key to the nonperturbative construction of the solution. In our concrete examples we shall extract some of these constants numerically, but a general analytical procedure to do so is not known. If we go back to our Stokes automorphism (2.30), there is a significant simplification since all alien derivatives with $\ell > 1$ vanish, leaving us with

$$\underline{\mathfrak{S}}_0 = 1 + \mathrm{e}^{-Az}\Delta_A + \frac{1}{2}\mathrm{e}^{-2Az}\Delta_A^2 + \frac{1}{3!}\mathrm{e}^{-3Az}\Delta_A^2 + \cdots \tag{2.37}$$

Combining this with an iterative use of (2.36), we are left with only one Stokes constant and find the action of the Stokes automorphism on a given transseries sector

$$\underline{\mathfrak{S}}_0 F^{(n)} = \sum_{\ell=0}^{+\infty} \binom{n+\ell}{n} S_1^\ell\, \mathrm{e}^{-\ell A z} F^{(n+\ell)}\,. \tag{2.38}$$

The bridge equations (2.33) actually provide much more information besides the discontinuity across the positive real axis. Indeed, if we now consider the negative real axis, the Stokes automorphism has the form

$$\underline{\mathfrak{S}}_\pi = \exp\left(\sum_{\ell=1}^{+\infty} \Delta_{-\ell A}\right) = 1 + \mathrm{e}^{Az}\Delta_{-A} + \mathrm{e}^{2Az}\left(\Delta_{-2A} + \frac{1}{2}\Delta_{-A}^2\right) + \cdots \tag{2.39}$$

It is clear from (2.36) that there are now many more non-vanishing alien derivatives and many more Stokes constants. The task of computing the Stokes automorphism along $\theta = \pi$ is conceptually clear but technically involved since there is now the need to compute multiple alien derivatives which do not commute. We will not go through the details and refer to the derivation in [25]. Instead we will just present the final result which we will make use of in

[7] This is no longer as simple when dealing with multi-parameter transseries. In that case $S_\ell(\sigma_j)$ is a series in powers of all the σ_j [25].

concrete examples,

$$\underline{\mathfrak{S}}_{\pi} F^{(n)} = F^{(n)} + \sum_{\ell=1}^{n-1} \mathrm{e}^{\ell A z} \sum_{k=1}^{\ell} \frac{1}{k!} \sum_{0<\gamma_0<\gamma_1<\cdots<\gamma_k=\ell} \left(\prod_{j=1}^{k} (n-\gamma_j) S_{-\mathbf{d}\gamma_j} \right) F^{(n-\ell)} \,. \tag{2.40}$$

Here we have defined the partitions $\mathbf{d}\gamma_j \equiv \gamma_j - \gamma_{j-1}$. Some examples for the formula above are

$$\underline{\mathfrak{S}}_{\pi} F^{(0)} = F^{(0)} \,, \tag{2.41}$$

$$\underline{\mathfrak{S}}_{\pi} F^{(1)} = F^{(1)} \,, \tag{2.42}$$

$$\underline{\mathfrak{S}}_{\pi} F^{(2)} = F^{(2)} + S_{-1} \, \mathrm{e}^{Az} \, F^{(1)} \,, \tag{2.43}$$

$$\underline{\mathfrak{S}}_{\pi} F^{(3)} = F^{(3)} + 2 S_{-1} \, \mathrm{e}^{Az} \, F^{(2)} + \left(S_{-2} + S_{-1}^2 \right) \mathrm{e}^{2Az} \, F^{(1)} \,. \tag{2.44}$$

Before ending this section we should say a few words about Stokes constants. If we go back to the Stokes automorphism along $\theta = 0$ (2.38), and we insert it in the whole transseries, we find

$$\underline{\mathfrak{S}}_{0} F(z,\sigma) = \sum_{n=0}^{+\infty} \sigma^n \, \mathrm{e}^{-nAz} \left(\sum_{\ell=0}^{+\infty} \binom{n+\ell}{n} S_1^{\ell} \, \mathrm{e}^{-\ell A z} F^{(n+\ell)} \right) = F(z, \sigma + S_1) \,. \tag{2.45}$$

Going back to the definition of $\underline{\mathfrak{S}}_{\theta}$ in terms of the lateral resummations, this means

$$\mathcal{S}_{0^+} F(z,\sigma) = \mathcal{S}_{0^-} F(z, \sigma + S_1) \tag{2.46}$$

The reason why these numbers were labelled "Stokes constants" should now be apparent, because the result above is nothing more than the Stokes phenomenon of classical asymptotics. This singular direction is a Stokes line in the original z variable, and if we move across it there is a "jump" in the transseries parameter σ. We can imagine a case where $\sigma = 0$ before we cross the Stokes line, meaning all the nonperturbative sectors are turned off, and then after we cross σ jumps to a nonzero value and they spring to life [8]. We see how Stokes phenomenon naturally shows up in the resurgence framework, and how the Stokes constants hold the key to connecting solutions in different sectors of the complex plain. It is important to point out that performing the same exercise across $\theta = \pi$ is much more challenging and involves many more Stokes constants (see [97] for details).

[8] We will see this in detail in chapter 6.

2.5 Large-order Relations

At this stage it is worth summarizing our long and technical journey through resurgence and alien calculus. We started off with a general asymptotic series, and we saw how Borel resummation gave rise to nonperturbative ambiguities across singular directions in the Borel plane. The framework of alien calculus allows us to treat these singularities in a systematic fashion, and then the bridge equation(s) allow for the computation of alien derivatives. In the end we were able to write down the Stokes automorphisms along singular directions $\theta = 0$ (2.38) and $\theta = \pi$ (2.40), which is the relevant setup going forward, and these objects tell us how to "jump" across singular directions. In other words, they connect solutions on different sectors/wedges of the complex plane, and depend on the Stokes constants which are invariants of the problem in question. In the simplest case (2.46) all we are dealing with is the Stokes phenomenon of classical asymptotics. But we have announced several times that all the coefficients in the transseries are not random, but they are connected via relations that we will derive shortly. And this is why we talk about "resurgent" transseries. Perturbative and nonperturbative (multi-instanton) sectors are related to other sectors, *i.e.* they *resurge* in other sectors.

The final ingredient we require is Cauchy's theorem [20]. If a given function $F(z)$ has a branch-cut along a direction θ and is analytic everywhere else, then it can be written as

$$F(z) = \int_0^{\mathrm{e}^{\mathrm{i}\theta}\infty} \frac{\mathrm{d}w}{2\pi\mathrm{i}} \frac{\mathrm{Disc}_\theta F(w)}{w - z} - \oint_{(\infty)} \frac{\mathrm{d}w}{2\pi\mathrm{i}} \frac{F(w)}{w - z} \tag{2.47}$$

In the cases we are interested in we never encounter a pole at infinity, so we will drop the last term [9]. Focusing on the perturbative sector, we already computed its discontinuities. From (2.38) and (2.41) we have

$$\mathrm{Disc}_0\, F^{(0)} = -\sum_{\ell=1}^{+\infty} S_1^\ell\, \mathrm{e}^{-\ell A z} F^{(\ell)}\,, \tag{2.48}$$

$$\mathrm{Disc}_\pi\, F^{(0)} = 0\,. \tag{2.49}$$

These discontinuities mean $F^{(0)}$ has a branch cut in the positive real axis in the Borel plane. If we now insert (2.48) into (2.47), and expand all sectors into their formal power series

[9] In [9, 100] it is shown via scaling arguments that there is no contribution from $z = \infty$.

(2.12), we arrive at [10]

$$F_g^{(0)} \simeq \sum_{k=1}^{+\infty} \frac{S_1^k}{2\pi \mathrm{i}} \frac{\Gamma(g-k\beta)}{(kA)^{g-k\beta}} \sum_{h=1}^{+\infty} \frac{\Gamma(g-k\beta-h+1)}{\Gamma(g-k\beta)} F_h^{(k)} (kA)^{h-1} . \tag{2.50}$$

This expression becomes more insightful if we spell out some terms

$$\begin{aligned} F_g^{(0)} \simeq & \frac{S_1}{2\pi \mathrm{i}} \frac{\Gamma(g-\beta)}{A^{g-\beta}} \left(F_1^{(1)} + \frac{A}{g-\beta-1} F_2^{(1)} + \cdots \right) + \\ & + \frac{S_1^2}{2\pi \mathrm{i}} \frac{\Gamma(g-2\beta)}{(2A)^{g-2\beta}} \left(F_1^{(2)} + \frac{2A}{g-2\beta-1} F_2^{(2)} + \cdots \right) + \\ & + \frac{S_1^3}{2\pi \mathrm{i}} \frac{\Gamma(g-3\beta)}{(3A)^{g-3\beta}} \left(F_1^{(3)} + \frac{3A}{g-3\beta-1} F_2^{(3)} + \cdots \right) + \cdots \end{aligned} \tag{2.51}$$

This is a well-known result, or a generalization of it. We see on the first line the features that we have mentioned from the start, a large-order factorial growth "controlled" by the instanton action A [11]. The leading term is the one-instanton, one-loop coefficient $F_1^{(1)}$ which is then followed by $1/g$ corrections with contributions from higher loops. We then have a tower of contributions from the instanton sectors with the same structure, suppressed by a factor n^{-g}. This result was already seen in matrix model or topological string contexts in [10, 16], but it is worth taking a moment to underline its implications. What (2.51) tells us is that the perturbative component of the transseries contains all the information about the nonperturbative contributions, even if it is buried in the large-order asymptotics, and depending only on a single Stokes constant.

The same procedure can be applied to any multi-instanton sector to generate other large-order relations. The main difference is that now the discontinuities both at $\theta = 0$ and $\theta = \pi$ contribute, which is equivalent to saying that the Borel transforms of these sectors have branch cuts along both positive and negative real axes. These expressions tend to get long and cumbersome very quickly, so we will introduce the necessary ones later on, already in the language of the examples we are interested in. But an interesting feature that we can see from (2.38) and (2.40) is that there is now both *forwards* and *backwards* resurgence. The coefficients of the perturbative expansion around the n-instanton sector are related to the coefficients in higher sectors via the discontinuity across 0 and to the coefficients from lower sectors through the discontinuity at π, but now with more Stokes constants involved. We will return these relations in the following chapters.

[10] For shortness of notation we are already jumping to the case in our examples where $\beta_n = n\,\beta$ for some value of β. In the general case we need only replace $k\beta \to \beta_k - \beta_0$.

[11] Notice that $\frac{F_{g+1}^{(0)}}{F_g^{(0)}} \sim 1/A$.

2.6 Example: Painlevé I

Before ending this chapter it will be useful to present an example to illustrate some of the ideas we have presented up to now more concretely. We will consider the Painlevé I equation

$$u^2(z) - \frac{1}{6}u''(z) = z \tag{2.52}$$

This equation has made various appearances in the literature in different contexts [12]. It can be realized from a double-scaling limit of the quartic matrix model, for example. But, more importantly, the (2,3) minimal string theory, which describes pure gravity in two dimensions [101], has its free energy F related to a solution of Painlevé I. In detail

$$u(z) = -F''(z)\,, \tag{2.53}$$

and the variable z is essentially the string coupling constant. Some references that study Painlevé I include [10, 16, 25, 102, 103]. Some of the properties of the (two-parameter) transseries solution of Painlevé I were first understood in [103]. What we will present in this section is just a very small sample of the deep analysis carried out in [25].

We begin by looking at a perturbative solution to (2.52). For large z it scales as $u(z) \sim \sqrt{z}$, and beyond that the perturbative solution is a power series in powers of $z^{-5/2}$

$$u_{\text{pert}}(z) = \sqrt{z}\left(1 - \frac{1}{48}z^{-5/2} - \frac{49}{4608}z^{-5} - \frac{1225}{55296}z^{-15/2} - \cdots\right). \tag{2.54}$$

While this is an expansion in powers of $z^{-5/2}$, we know that the perturbative free energy will be an expansion in powers of the closed string coupling constant. On the other hand, nonperturbative effects are associated to D-branes, and consequently to open strings, so they will be series expansions in powers of the open string coupling constant

$$x \equiv z^{-5/4}\,. \tag{2.55}$$

We also want to absorb the leading $\sqrt{z}$ factor by redefining

$$u(x) \equiv \left.\frac{u(z)}{\sqrt{z}}\right|_{z=x^{-4/5}}. \tag{2.56}$$

This turns our original equation (2.52) into the following equation for $u(x)$

$$u^2(x) + \frac{1}{24}x^2\,u(x) - \frac{25}{96}x^3\,u'(x) - \frac{25}{96}x^4\,u''(x) = 1\,. \tag{2.57}$$

[12] It can also be written with different normalizations.

We are finally ready to introduce a transseries ansatz for $u(x)$, and it takes the following form

$$u(x,\sigma) = \sum_{n=0}^{+\infty} \sigma^n \, \mathrm{e}^{-nA/x} \, u^{(n)}(x) \, ; \tag{2.58}$$

$$u^{(0)}(x) = \sum_{g=0}^{+\infty} u_{2g}^{(0)} x^{2g+\beta_0} \, ; \quad u^{(n)}(x) = \sum_{g=0}^{+\infty} u_g^{(n)} x^{g+\beta_n} \, , n \geq 1 \, . \tag{2.59}$$

The instanton action is $A = \frac{8\sqrt{3}}{5}$. By plugging (2.58) into (2.57) we get a recursive equation allowing us to find the coefficients $u_g^{(n)}$ order by order. The technical details are not very important at this stage, we will do this with all the steps when we study Painlevé II in section 4.4. The first few sectors of the solution are

$$u^{(0)} = 1 - \frac{1}{48}x^2 - \frac{49}{4608}x^4 - \frac{1225}{55296}x^6 - \cdots \, , \tag{2.60}$$

$$u^{(1)} = x^{1/2} - \frac{5}{64\sqrt{3}}x^{3/2} + \frac{75}{8192}x^{5/2} - \frac{341239}{23592960}x^{7/2} + \cdots \, , \tag{2.61}$$

$$u^{(2)} = \frac{1}{6}x - \frac{55}{576\sqrt{3}}x^2 + \frac{1325}{36864}x^3 - \frac{3363653}{53084160\sqrt{3}}x^4 + \cdots \, . \tag{2.62}$$

From these results we can see that $\beta_0 = 0$, $\beta_1 = 1/2$ and $\beta_2 = 1$. There are some subtleties that we are going to skip over now, related to certain parameters in the transseries that need to be fixed and the β_n factors. We refer to [25] or to section 3.2.3 for more on this. We could go on and compute more sectors to very high orders [13], but for now our goal is different. We are going to see in detail how a large-order relation such as (2.51) can be studied and tested to high precision.

2.6.1 Testing Large-Order Relations

The main technique used to test large-order relations is Richardson extrapolation [104]. Suppose we have a sequence of quantities Q_g, which could, for instance, be the quantities on the left-hand side of (2.51). We are interested in the limit $\lim_{g\to+\infty} Q_g$, but in practice we can only compute the Q_g up to a certain $g_{\max}$. Then $Q_{g_{\max}}$ is an approximation to the limit but it is not good enough. This is where Richardson extrapolation comes in to *accelerate* the convergence. If we have a sequence

$$Q_g = q_0 + \frac{q_1}{g} + \frac{q_2}{g^2} + \dots \, , \tag{2.63}$$

[13] See Appendix A in [25].

and q_0 is the number we want to extract, then we define the N-th Richardson transform as a modified sequence

$$Q_g^{[N]} \equiv \sum_{k=0}^{N} (-1)^{N-k} \frac{(g+k)^N}{k!(N-k)!} Q_{g+k} \,. \tag{2.64}$$

The Richardson transform essentially works by removing the sub-leading tail in (2.63) and taking us closer to the limit. For instance, the N-th Richardson transform will look like

$$Q_g^{[N]} = q_0 + \frac{q_{N+1}}{g^{N+1}} + \mathcal{O}\left(g^{-N-2}\right) \,. \tag{2.65}$$

We should point out that if our original list $\{Q_g\}$ has K elements, its N-th Richardson transform will have $K-N$ elements, so there is naturally a limit to how many Richardson transforms one can take. Let us now see how this works in practice by returning to our Painlevé I example. First we should write (2.51) adapted to the Painlevé I expansions we wrote above. The relation we want to test is then

$$\begin{aligned} u_{2g}^{(0)} \;\simeq\; & \frac{S_1}{2\pi \mathrm{i}} \frac{\Gamma(2g-1/2)}{A^{2g-1/2}} \left(u_0^{(1)} + \frac{A}{2g-3/2} u_1^{(1)} + \cdots \right) + \\ & + \frac{S_1^2}{2\pi \mathrm{i}} \frac{\Gamma(2g-1)}{(2A)^{2g-1}} \left(u_0^{(2)} + \frac{2A}{2g-2} u_1^{(2)} + \cdots \right) + \mathcal{O}(3^{-g}) \end{aligned} \tag{2.66}$$

The first quantity to test is the instanton action. To do that we consider the sequence $Q_g = \frac{u_{2(g+1)}}{4g^2 u_{2g}}$ which allows for the extraction of A

$$Q_g = \frac{1}{A^2} \left(1 + \frac{1+2\beta}{2g} + \mathcal{O}\left(\frac{1}{g^2}\right) \right) \tag{2.67}$$

In Fig. 2.2 (left) we see the original sequence (blue) and then its fourth (green) and eight (red) Richardson transforms. Our original sequence goes up to $g_{\max} = 200$ but in the plot we show up to $g = 20$ because the convergence is very fast. In table 2.1 we show the final term in each Richardson transform $Q^{[N]}_{g_{\max}-N}$ (raised to the power $-1/2$) is getting closer to the exact result $A = \frac{8\sqrt{3}}{5}$. We have said before that $\beta = 1/2$, but we can also check this by looking at the sequence

$$\frac{1}{2} \left\{ 1 - 2g \left(A^2 Q_g - 1 \right) \right\} \sim \beta = 1/2 \,. \tag{2.68}$$

In Fig. 2.2 (right) this convergence is clearly seen. Then we can move on to the one-loop coefficient, which needs to be tested together with the Stokes factor S_1, but as we shall see we are free to set $u_0^{(1)} = 1$. The sequence now is

$$\frac{2\pi \mathrm{i}\, A^{2g-1/2}}{\Gamma(2g-1/2)} u_{2g}^{(0)} \sim S_1 \, u_0^{(1)} \,. \tag{2.69}$$

# of R.T.	$A - \left(Q^{[N]}_{g_{\max}-N}\right)^{-1/2}$
0	3.5×10^{-11}
4	4.0×10^{-13}
8	1.3×10^{-19}
12	3.9×10^{-25}
16	5.8×10^{-30}

Table 2.1: Difference between the instanton action A and the last term in the N-th Richardson transform, raised to the power $-1/2$, for various values of N. The convergence is very quick and at $N = 16$ there are 30 matching decimal places.

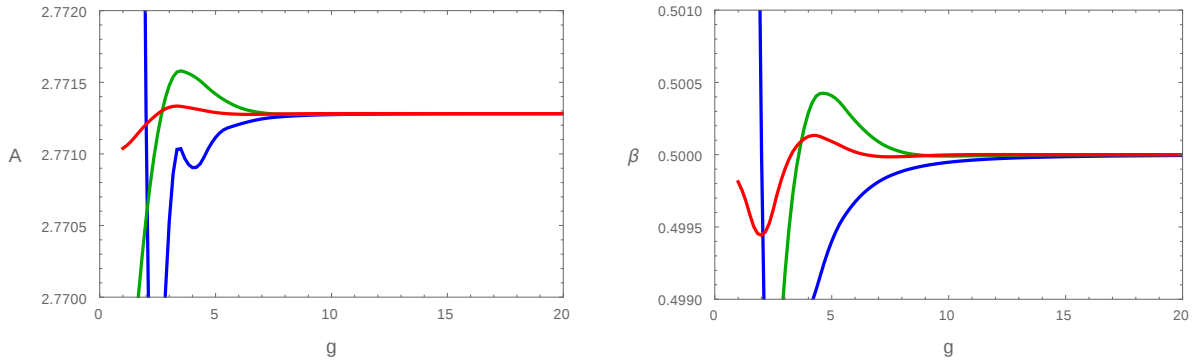

Figure 2.2: Left: Sequence $Q_g^{-1/2}$ (blue) along with its fourth (green) and eighth (red) Richardson transforms. After eight Richardson transforms the error is of the order $10^{-17}\%$; Right: Similar but now for the sequence $\frac{1}{2}\{1 - 2g\,(A^2 Q_g - 1)\}$, which asymptotes to $\beta = 1/2$. After eight Richardson transforms the error also $\sim 10^{-17}\%$

In Fig. 2.3 (left) we confirm the well known result $S_1 = -\mathrm{i}\,\frac{3^{1/4}}{2\sqrt{\pi}}$ [10, 102, 105]. Finally we can look at

$$\frac{2g}{A}\left(\frac{2\pi \mathrm{i} A^{2g-1/2}}{\Gamma(2g-1/2)} u_{2g}^{(0)} - u_0^{(1)}\right) \sim u_1^{(1)}\,, \tag{2.70}$$

and see in Fig. 2.3 (right) how it converges towards $u_1^{(1)} = \frac{5}{64\sqrt{3}} = 0.0451055\ldots$. We could now proceed order by order, subtracting coefficients from the left-hand side and testing higher-loop terms in the one-instanton sector. But the more challenging task is finding a way to test the two-instanton terms, which are suppressed by a factor of 2^{-2g}. In (2.66) we would want to remove the first line from the left-hand side in order to examine the second line. But the first line is an asymptotic series, so we cannot just keep adding terms. Optimal truncation is also not useful because it has an exponentially small error, and the terms we want to see are also exponentially suppressed, so they will not be visible. The

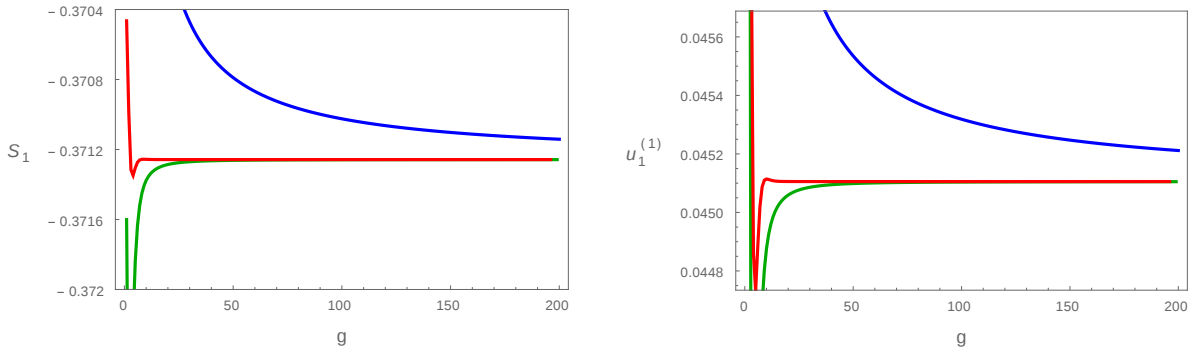

Figure 2.3: Left: Sequence $\frac{2\pi \mathrm{i}\, A^{2g-1/2}}{\Gamma(2g-1/2)} u_{2g}^{(0)}$ (blue) which should asymptote to S_1 ($u_0^{(1)}$ is set to 1), alongside its first (green) and fourth (red) Richardson transforms. The error after four Richardson transforms is of the order $10^{-11}\%$; Right: Similar for sequence $\frac{2g}{A}\left(\frac{2\pi \mathrm{i} A^{2g-1/2}}{\Gamma(2g-1/2)} u_{2g}^{(0)} - u_0^{(1)}\right) \sim u_1^{(1)}$. The error after four Richardson transforms is also $\sim 10^{-11}\%$.

way forward is through Borel-Padé approximations [16, 106]. These are approximants to the Borel transform (2.8) which can then be inverted in order to associate a number to these asymptotic series. By using Borel-Padé approximants, the authors of [25] were able to test asymptotic relations up to 7 (!) instantons. We will not discuss this method further because we will not make use of it. The resurgent relations that we will consider later will only be tested at the level of the leading sums on the right-hand side. We will consider relations involving higher instanton sectors (on the left-hand side), but not look into exponentially suppressed effects on the right-hand side. We will, nevertheless, make use of Borel-Padé approximants in chapter 6. But we will not be looking to approximate asymptotic sums in large-order relations, we will approximate the asymptotic sums in the transseries itself (*i.e.* the expansions at each instanton level).

2.6.2 Two-parameter Transseries: Overview

As we prepare to move on to our target, the $1/N$ expansion, we shall briefly overview some results that we have already announced. Namely, we need to deal with *two*-parameter transseries. We will introduce the notation and briefly discuss some of the new features.

It was first noticed in [103], and then fully explored in [25], that one should actually consider a two-parameter transseries, with exponentials of both $+A$ and $-A$. They are of the form

$$u(x,\sigma_1,\sigma_2) = \sum_{n=0}^{+\infty}\sum_{m=0}^{+\infty} \sigma_1^n \sigma_2^m \, \mathrm{e}^{-(n-m)A/x} \Phi_{(n|m)}(x)\,. \tag{2.71}$$

The one-parameter transseries we presented above corresponds to the $(n|0)$ slice of (2.71). This immediately introduces a few interesting features. First of all, there are now sectors which are exponentially *large* when compared to the perturbative $(0|0)$ sector. The obvious question to ask is: what is the physical interpretation of these effects? We will refer to these sectors as "generalized instantons". At the moment there still is no clear understanding of these contributions, but resurgence certainly forces them to be there. In [25] there is some discussion on possible interpretations of the generalized instantons, and we will also delve into them later on. It could very well be that the question can be avoided and there are never exponentially large effects to be interpreted. When resumming a transseries to generate a number, as we will do in chapter 6, contributions of the form $\exp(S)$ with $\mathbb{R}\mathrm{e}\, S > 0$ need to have their transseries parameter turned off, even though their coefficients are non-vanishing. So these sectors, while being connected to all others via resurgence, do not contribute to the final result. A different scenario we can envision is having $\mathbb{R}\mathrm{e}\left(\frac{A}{x}\right) = 0$ and then all sectors can contribute equally to give rise to an oscillatory result. [14]

Also noteworthy is the appearance of sectors with $n = m$ which carry no exponential weight. The two-parameter transseries has several features which are explained in detail in [25] and which we will also talk about. For example, it has the feature of being *resonant*, which means there are some coefficients which are not fixed by the equation. This is related to a reparametrization invariance we have, that is, we are free to make a change of variables (under certain conditions) to our transseries parameters. But most striking property, to which we alluded before, is the fact that $\Phi_{(n|m)}$ are no longer just power series in x. Instead, powers of $\log(x)$ also appear [15]. Specifically, they are

$$\Phi_{(n|m)}(x) = \sum_{k=0}^{\min(n,m)} \log^k x \sum_{g=0}^{+\infty} u_g^{(n|m)[k]}\, x^{g+\beta_{nm}^{[k]}}\,, \tag{2.72}$$

so that in the end each term in the transseries carries a four labels (n, m, k, g). There are more interesting properties, but we refer to [25] or to our examples below for specifics. Additionally, our derivations in sections 2.4 and 2.5 also need to be generalized. Most of the steps are straightforward but the formulae become very cumbersome. For starters, the bridge equations (2.33) now read

$$\dot{\Delta}_{\ell A} F(z, \sigma_1, \sigma_2) = S_\ell(\sigma_1, \sigma_2)\, \partial_{\sigma_1} F(z, \sigma_1, \sigma_2) + \widetilde{S}_\ell(\sigma_1, \sigma_2)\, \partial_{\sigma_2} F(z, \sigma_1, \sigma_2)\,, \tag{2.73}$$

and many more Stokes constants now enter the game. The derivations of asymptotic relations connecting different (generalized) instanton sectors are carefully derived in [25]. We will simply present in section 3.2.3 the ones we are interested in using and testing.

[14] We will say more about this in the context of the large N expansion.

[15] This was first realized in [103].

Chapter 3

Large N Matrix Models

The contents of this chapter appear in [1]:
"The Resurgence of Instantons: Multi-Cut Stokes Phases and the Painleve II Equation",
R. Schiappa, and R. Vaz,
arXiv:1302.5138 [hep-th], Commun. Math. Phys. **330**, 655-721 (2014)
DOI: 10.1007/s00220-014-2028-7

3.1 Introduction

Following what we introduced in chapters 1 and 2, in order to understand nonperturbative effects and the consequences of resurgence we now turn our attention to a special setup: the large N expansion of matrix models. We outlined several reasons, of both physical and practical nature, that justify this choice. This is a subject with a long history, and our work builds upon the recent developments [10, 11, 16, 57, 59, 60, 103, 107, 108] and specially [25]. We can start from the matrix model free energy, $F = \log Z$, where the partition function was written in (1.3), which has an expansion

$$F = \sum_{g=0}^{+\infty} g_s^{2g-2} F_g(t) \, . \tag{3.1}$$

As we discussed, we work in the 't Hooft large N limit, which amounts to having large N, small g_s and the 't Hooft coupling $t = g_s N$ fixed. This is a topological expansion with coefficients F_g growing as $(2g)!$, which are linked to $\exp(-N)$ effects, and this was the beginning of our journey in chapter 2. So everything we developed, such as the transseries expansions and the large-order relations connecting different multi-instanton sectors, will manifest itself in this problem. In particular, we will encounter two-parameter transseries like the ones we introduced in the Painlevé I example, and these contain "generalized" multi-instantons with instanton actions of opposite sign compared to the "physical" multi-instantons. We did not

say much about this feature before because the subject is very technical, but we will discuss this more closely in this chapter.

It is very well known that, at large N, matrix eigenvalues cluster into the cuts of a corresponding spectral geometry [48]. Within the context of large N duality, this was later understood as relating matrix models to B-model topological string theory in local Calabi-Yau geometries [29, 62, 109] (see [50] for an excellent review). Depending on the potential appearing in the matrix partition function, and the phase in which the model is to be found, generically the spectral geometry will correspond to a multi-cut configuration. This is an important point, specially in light of the question: is it always the case that, as one considers the large N limit of some given gauge theory, one will find an expansion of 't Hooft type with a closed string dual? Within the matrix model context, this question was first raised in [110] and answered negatively.

Let us dwell on this point for a moment as it is also at the basis of the class of examples we choose to address in this work. The nature of the large N asymptotic limit depends very much on which gauge theoretic phase one considers [108, 110] and is analogous to the study of Stokes phenomena in classical analysis. When considering single-cut models, one finds the familiar $1/N^2$ expansion [51–53], *i.e.*, one finds a topological genus expansion with a closed string dual. However, this is not usually the case when considering multi-cut models, where one finds large N theta-function asymptotics instead [58, 59, 110], *i.e.*, there is no genus expansion and possibly no closed string dual. These two distinct large N asymptotics are associated to what we call Stokes and anti-Stokes phases, respectively, generalizing the usual Stokes and anti-Stokes lines in classical analysis [87]. In fact, in the Stokes phase the single cut would correspond to the leading saddle, with pinched cuts corresponding to exponentially suppressed saddles [10]. On the other hand, in the anti-Stokes phase the many cuts correspond to many different saddles of similar order, where their joint contribution translates into an oscillatory large N behavior [110]. Of course one should start the analysis in the opposite direction: having identified Stokes and anti-Stokes phases with particular large N asymptotics, one may then ask what spectral geometry configurations appear in each distinct phase. The point of interest to us in here is that there are regions of moduli space where the Stokes phase is actually realized by a *multi*-cut configuration (essentially, by configurations where all cuts are equal, *i.e.*, they have the precise same eigenvalue filling). It is this type of multi-cut configurations which we investigate and explore in this work, within the framework of resurgent transseries.

This chapter is organized as follows. We begin in section 3.2 by reviewing background material concerning both matrix models and resurgent transseries. We briefly review the saddle-point approach to solving multi-cut matrix models. We do not take the usual step of starting with the one-cut solution, but all results can be trivially reduced to the one-cut case by taking $s = 1$, where s is the number of cuts [1]. The next step is introducing the

[1]The generalization in the other direction is anything but trivial, and in practice multi-cut models are

orthogonal polynomial method, which is the best way to generate large-order data that can be tested. We do this in a one-cut scenario because the generalization of this method to a multi-cut setup is not at all clear. There is a way of doing it in a $\mathbb{Z}_2$ configuration, but we will introduce it later. The orthogonal polynomial approach is also naturally extended when we turn to transseries solutions for the different quantities we are interested in computing. We will review the two-parameter transseries we briefly introduced in section 2.6 but now within the context of large N matrix models. More importantly, the large-order relations for various multi-instanton sectors, which we will be interested in testing in concrete examples, will be presented. We will only sketch the derivation of the various formulae. In section 3.3 we address the multi-instanton analysis when we have two cuts with $\mathbb{Z}_2$ symmetry (ensuring we are in a multi-cut Stokes phase). This is done using methods of spectral geometry which essentially generalize previous work in [10, 57]. Elliptic functions and theta functions which, due to the elliptic nature of the spectral curve, appear during the calculation, end up canceling in the final result thus providing further evidence on the nature of the Stokes phase. This is actually an interesting point of the calculation, as, on what concerns the perturbative sector, it was source to some confusion in early studies of $\mathbb{Z}_2$ symmetric spectral configurations. In fact, the original saddle-point calculation of the two-point resolvent in a $\mathbb{Z}_2$ symmetric distribution of eigenvalues [111, 112], with an explicit elliptic function dependence, did not match the corresponding orthogonal polynomial calculation [113–115], which saw no trace of these elliptic functions. The reason for this was that [111, 112] worked in a fixed canonical ensemble, while in the spectral curve approach to solving some given multi-cut scenario one needs to address the full grand-canonical ensemble as later explained in [110]. We shall explicitly see in section 3.3 what is the counterpart of those ideas within the multi-instanton context.

3.2 Revisiting Multi-Cut Matrix Models

Let us begin by setting our notation concerning both saddle-point and orthogonal polynomial approaches to solving matrix models, with emphasis on multi-cut configurations. We shall also review the required background in order to address the construction of (large N) resurgent transseries solutions for these multi-cut configurations, when in their Stokes phases.

3.2.1 The Saddle-Point Analysis

Let us first address the saddle-point approximation to computing the one-matrix model partition function (within the hermitian ensemble, $\beta = 1$) in a general multi-cut set-up; see, *e.g.*, [48, 50, 57, 101, 111]. In such configurations the N eigenvalues condense into s different

very hard to solve.

cuts $\mathcal{C}_1 \cup \cdots \cup \mathcal{C}_s = [x_1, x_2] \cup \cdots \cup [x_{2s-1}, x_{2s}]$, and, in diagonal gauge, the partition function is written as

$$Z(N_1, \ldots, N_s) = \frac{1}{N_1! \cdots N_s!} \int_{\lambda_{k_1}^{(1)} \in C_1} \cdots \int_{\lambda_{k_s}^{(s)} \in C_s} \prod_{i=1}^{N} \left(\frac{\mathrm{d}\lambda_i}{2\pi} \right) \Delta^2(\lambda_i)\, \mathrm{e}^{-\frac{1}{g_s} \sum_{i=1}^{N} V(\lambda_i)}, \tag{3.2}$$

with 't Hooft coupling $t = N g_s$ (fixed in the 't Hooft limit). In the above expression the $\{\lambda_{k_I}^{(I)}\}$ are the eigenvalues sitting on the I-th cut, with $k_I = 1, \ldots, N_I$ and $\sum_{I=1}^{s} N_I = N$, and $\Delta(\lambda_i)$ is the Vandermonde determinant. In this picture it is natural to consider the hyperelliptic Riemann surface which corresponds to a double-sheet covering of the complex plane, $\mathbb{C}$, with precisely the above cuts. One can then define A-cycles as the cycles around each cut, whereas B-cycles go from the endpoint of each cut to infinity on one of the two sheets and back again on the other. For shortness, we shall refer to $\mathcal{C}$ as the contour encircling all the cuts, *i.e.*, $\mathcal{C} = \bigcup_{I=1}^{s} A^I$.

The large N saddle-point solution is usefully encoded in the planar resolvent, defined in closed form as

$$\omega_0(z) = \frac{1}{2t} \oint_{\mathcal{C}} \frac{\mathrm{d}w}{2\pi \mathrm{i}} \frac{V'(w)}{z - w} \sqrt{\frac{\sigma_s(z)}{\sigma_s(w)}}, \tag{3.3}$$

where we have defined

$$\sigma_s(z) \equiv \prod_{k=1}^{2s} (z - x_k) \tag{3.4}$$

and where one still needs to specify the endpoints of the s cuts, $\{x_k\}$. One may now describe the large N matrix model geometry via the corresponding spectral curve, $y(z)$, which is given in terms of the resolvent by

$$y(z) = V'(z) - 2t\, \omega_0(z) \equiv M(z) \sqrt{\sigma_s(z)}. \tag{3.5}$$

If the potential $V(z)$ in the matrix model partition function (3.2) is such that $V'(z)$ is a rational function with simple poles at $z = \beta_i$, $i = 1, 2, ..., k$ and with residues α_i at each pole, the expression for $M(z)$ in the expression above is simply

$$M(z) = \oint_{(\infty)} \frac{\mathrm{d}w}{2\pi \mathrm{i}} \frac{V'(w)}{w - z} \frac{1}{\sqrt{\sigma_s(w)}} + \sum_{i=1}^{k} \frac{\alpha_i}{(\beta_i - z) \sqrt{\sigma_s(\beta_i)}}. \tag{3.6}$$

At this stage one still needs to specify the endpoints of the cuts. If the eigenvalue distribution across all cuts is properly normalized, the planar resolvent will have the asymptotic behavior $\omega_0(z) \sim \frac{1}{z}$ as $z \to +\infty$. In turn, this asymptotic condition implies the following set of

constraints

$$\oint_{\mathcal{C}} \frac{\mathrm{d}w}{2\pi \mathrm{i}} \frac{w^n\, V'(w)}{\sqrt{\sigma_s(w)}} = 2t\, \delta_{ns}, \tag{3.7}$$

with $n = 0, 1, \ldots, s$. These are $s+1$ conditions for $2s$ unknowns, where the remaining $s-1$ conditions still need to be specified and they come from the number of eigenvalues N_I one chooses to place at each cut. This distribution of eigenvalues may be equivalently described by the partial 't Hooft moduli $t_I = g_s N_I$, which may be written directly in terms of the spectral curve:

$$t_I = \frac{1}{4\pi \mathrm{i}} \oint_{A^I} \mathrm{d}z\, y(z), \qquad I = 1, 2, \ldots, s. \tag{3.8}$$

Notice that, as expected, these are only $s-1$ conditions as they are not all independent, *i.e.*, $\sum_{I=1}^{s} t_I = t$. Both constraints (3.7) and moduli (3.8) now determine the full spectral geometry.

It is also useful to define the holomorphic effective potential

$$V'_{\mathrm{h;eff}}(z) = y(z). \tag{3.9}$$

In this case, the effective potential is given by the real part of the holomorphic effective potential, in such a way that

$$V_{\mathrm{eff}}(\lambda) = \mathbb{R}\mathrm{e} \int^{\lambda} \mathrm{d}z\, y(z). \tag{3.10}$$

3.2.2 The Approach via Orthogonal Polynomials

While saddle-point analysis is the appropriate framework to describe the spectral geometry of multi-cut configurations, it gets a bit more cumbersome when one wishes to address the computation of the full free energy. In the 't Hooft limit, where $N \to +\infty$ with $t = g_s N$ held fixed, the perturbative, large N, topological expansion of the free energy is given by[2]

$$F(g_s, \{t_I\}) = \log Z \simeq \sum_{g=0}^{+\infty} g_s^{2g-2} F_g(t_I). \tag{3.11}$$

Computing this genus expansion out of a hyperelliptic spectral curve has a long history – starting in [51, 111], passing through [110], and recently culminating in the recursive procedure of [52, 53] – and it is in fact an intricate problem in algebraic geometry [53].

An easier approach to computing the free energy of a matrix model is to use the method of orthogonal polynomials; see, *e.g.*, [25, 49, 50, 101]. On the other hand, this method is less general as it is not applicable to arbitrary multi-cut configurations. However, as we shall

[2] Throughout this work we shall use the symbol $\simeq$ to signal when in the presence of an asymptotic series [25].

also see in the course of this dissertation, orthogonal polynomials do work when addressing multi-cut Stokes phases. As such, let us swiftly review this method in the context of the one-cut solution (the multi-cut extension will be addressed later). Considering the partition function (3.2) with a single cut, one may consider the positive-definite measure on $\mathbb{R}$ given by

$$\mathrm{d}\mu(z) = \mathrm{e}^{-\frac{1}{g_s}V(z)}\,\frac{\mathrm{d}z}{2\pi}. \tag{3.12}$$

Normalized orthogonal polynomials with respect to this measure are introduced as $p_n(z) = z^n + \cdots$, with inner product

$$\int_{\mathbb{R}} \mathrm{d}\mu(z)\, p_n(z) p_m(z) = h_n \delta_{nm}, \qquad n \geq 0. \tag{3.13}$$

As the Vandermonde determinant may be written $\Delta(\lambda_i) = \det p_{j-1}(\lambda_i)$, the partition function of our matrix model may be computed as

$$Z = \prod_{n=0}^{N-1} h_n = h_0^N \prod_{n=1}^{N} r_n^{N-n}, \tag{3.14}$$

where we have defined $r_n = \frac{h_n}{h_{n-1}}$ for $n \geq 1$. These r_n coefficients further appear in the recursion relations

$$p_{n+1}(z) = (z + s_n)\, p_n(z) - r_n\, p_{n-1}(z), \tag{3.15}$$

together with coefficients $\{s_n\}$ which will vanish for an even potential. Plugging the above (3.15) in the inner product (3.13) one obtains a recursion relation directly for the r_n coefficients [49].

One example of great interest to us in the present work is that of the quartic potential $V(z) = \frac{\mu}{2}z^2 + \frac{\lambda}{4!}z^4$. In this case it follows that $s_n = 0$ and [49]

$$r_n \left(\mu + \frac{\lambda}{6}\left(r_{n-1} + r_n + r_{n+1}\right)\right) = n g_s. \tag{3.16}$$

The free energy of the quartic matrix model (normalized against the Gaussian weight $V_{\mathrm{G}}(z) = \frac{1}{2}z^2$, as usual) then follows straight from the definition of the partition function (3.14)

$$\mathcal{F} \equiv F - F_{\mathrm{G}} = \log\frac{Z}{Z_{\mathrm{G}}} \simeq \sum_{g=0}^{+\infty} g_s^{2g-2}\mathcal{F}_g(t) = \frac{t}{g_s}\log\frac{h_0}{h_0^{\mathrm{G}}} + \frac{t^2}{g_s^2}\frac{1}{N}\sum_{n=1}^{N}\left(1 - \frac{n}{N}\right)\log\frac{r_n}{r_n^{\mathrm{G}}}. \tag{3.17}$$

This genus expansion is made explicit by first understanding the large N expansion of the r_n recursion coefficients. Changing to continuum variables as $x \equiv n g_s$, with $x \in [0, t]$ in the 't Hooft limit, and defining $\mathcal{R}(x) = r_n$ with $\mathcal{R}^{\mathrm{G}}(x) = x$, the above example of the quartic

potential (3.16) becomes [25, 49]

$$\mathcal{R}(x)\left\{\mu+\frac{\lambda}{6}\left(\mathcal{R}(x-g_s)+\mathcal{R}(x)+\mathcal{R}(x+g_s)\right)\right\}=x. \tag{3.18}$$

As $\mathcal{R}(x)$ is even in the string coupling, it admits the usual asymptotic large N expansion

$$\mathcal{R}(x)\simeq\sum_{g=0}^{+\infty}g_s^{2g}R_{2g}(x), \tag{3.19}$$

allowing for a recursive solution for the $R_{2g}(x)$. In particular, in the continuum limit the sum in (3.17) may be computed via the Euler-Maclaurin formula (with B_{2k} the Bernoulli numbers and $x=t\,\xi$)

$$\lim_{N\to+\infty}\frac{1}{N}\sum_{n=1}^{N}\Psi\left(\frac{n}{N}\right)\simeq\int_0^1\mathrm{d}\xi\,\Psi(\xi)+\frac{1}{2N}\Psi(\xi)\Big|_{\xi=0}^{\xi=1}+\sum_{k=1}^{+\infty}\frac{1}{N^{2k}}\frac{B_{2k}}{(2k)!}\Psi^{(2k-1)}(\xi)\Big|_{\xi=0}^{\xi=1}, \tag{3.20}$$

yielding

$$\begin{aligned}\mathcal{F}(t,g_s)\;\simeq\;&\frac{t}{2g_s}\left(2\log\frac{h_0}{h_0^{\mathrm{G}}}-\log\frac{\mathcal{R}(x)}{x}\Big|_{x=0}\right)+\frac{1}{g_s^2}\int_0^t\mathrm{d}x\,(t-x)\log\frac{\mathcal{R}(x)}{x}+\\&+\sum_{g=1}^{+\infty}g_s^{2g-2}\frac{B_{2g}}{(2g)!}\frac{\mathrm{d}^{2g-1}}{\mathrm{d}x^{2g-1}}\left[(t-x)\log\frac{\mathcal{R}(x)}{x}\right]\Big|_{x=0}^{x=t}.\end{aligned} \tag{3.21}$$

Then it is just a matter of plugging (3.19) into the right-hand side and extract the $\mathcal{F}_{2g}$ order by order. This analysis was first presented in [49] and was recently extended to a full resurgent transseries analysis in [25], and we refer the reader to these references for further details. We shall later see how it generalizes to accommodate the two-cut Stokes phase of the quartic matrix model. We also note that, while (3.21) has been used several times [1, 10, 25, 49, 50], we have found that some times it is more useful to compute the free energy slightly differently. Instead of using Euler-Maclaurin, we start from the Toda-like relation [3]

$$\frac{Z_{N+1}\,Z_{N-1}}{Z_N^2}=r_N\,, \tag{3.22}$$

which is trivially proven using (3.14). Then we just have to apply the same continuum limit to find

$$\mathcal{F}(t-g_s)+\mathcal{F}(t+g_s)-2\mathcal{F}(t)=\log\left(\frac{\mathcal{R}(t)}{t}\right). \tag{3.23}$$

[3] This derivation is presented in [16].

This is actually the equation used to extract multi-instanton coefficients for the free energy. If we introduce a transseries ansatz like (2.12) into (3.23) we get algebraic equations for the $\mathcal{F}_g^{(n)}$ coefficients. [4] But we can also use it for the perturbative coefficients. Expanding both sides with expansions like (3.19), we get second order differential equations for the perturbative coefficients $\mathcal{F}_{2g}$. These are easily integrated, and the condition $\mathcal{F}_{2g}\Big|_{\lambda=0} = 0$, which is a consequence of the Gaussian normalization, is enough to fix the integration constants. See appendix A for details on this procedure for the one-cut quartic matrix model.

3.2.3 Transseries and Resurgence: Basic Formulae

The discussion so far has focused upon the large N, perturbative construction of the matrix model free energy (3.11). If, on the other hand, one wishes to go beyond the perturbative analysis in order to build a fully nonperturbative solution to a given matrix model, one needs to make use of resurgent transseries. This subject was discussed in the introduction. In this section, we shall review some of these aspects now in the appropriate notation and setup, and present the formulae that will be tested later. We refer the reader to [25] for more details.

Resurgent transseries essentially encode the full (generalized) multi-instanton content of a given non-linear system and, as such, yield nonperturbative solutions to these problems as expansions in both powers of the coupling constant and the (generalized) multi-instanton number(s). In general, many distinct instanton actions may appear and, as such, transseries will depend upon as many free parameters[5] as there are distinct instanton actions. For most of this dissertation, and similarly to what was found in [25] for the one-cut quartic matrix model and the Painlevé I equation [103], a two-parameter transseries will be sufficient to describe the two-cut quartic matrix model and the Painlevé II equation. These two-parameter transseries, as we showed in the example of Painlevé I in section 2.6.2, generalize the one-parameter cases which were first introduced in the matrix model context in [16].

Similarly to what was discussed above and in [25], we only need to consider the special case of a two-parameter transseries *ansatz* with instanton action A and "generalized instanton" action $-A$. This may be written as

$$F(z,\sigma_1,\sigma_2) = \sum_{n=0}^{+\infty}\sum_{m=0}^{+\infty} \sigma_1^n \sigma_2^m F^{(n|m)}(z), \tag{3.24}$$

where z is the coupling parameter (here chosen $\sim 1/g_s$) and σ_1, σ_2 are the transseries parameters. Further, the above $(n|m)$ sectors label generalized multi-instanton contributions

[4] With a two-parameter transseries this is not always the case. The $(n|n)$ sectors, the perturbative being one of them, we get differential equations.

[5] Free parameters which are essentially parameterizing the corresponding nonperturbative ambiguities.

of the form

$$F^{(n|m)}(z) \equiv \mathrm{e}^{-(n-m)Az}\,\Phi_{(n|m)}(z) \simeq \mathrm{e}^{-(n-m)Az}\sum_{g=1}^{+\infty}\frac{F_g^{(n|m)}}{z^{g+\beta_{nm}}}. \tag{3.25}$$

In this expression β_{nm} is a characteristic exponent, to which we shall later return when needed. We explained in the introduction how resurgent transseries are defined along wedges in the complex z-plane and they are "glued" along Stokes lines (directions where the Borel transform has singularities) in order to construct the full analytic solution. This "gluing" is achieved via the Stokes automorphism $\underline{\mathfrak{S}}_\theta$ which essentially acts upon the transseries (3.24) by shifting its parameters. For example, we saw how given a one-parameter transseries with a Stokes line on the positive real axis, the gluing is achieved by shifting $\sigma \to \sigma + S_1$ as one crosses from the upper to the lower positive-half-plane, where S_1 is the Stokes constant associated to that particular Stokes line – although, generically, there may be an infinite number of distinct Stokes constants. In our two-parameter case, there are two sets of Stokes coefficients, $S_\ell^{(k)}$ and $\widetilde{S}_\ell^{(k)}$, labeled by integers k and ℓ with $k \geq 0$. Do notice that not all of these coefficients are independent and in [25] some empirical relations between them have been found, in the Painlevé I context. We refer the reader to that reference for further details.

The main point of interest to us in this subsection concerns large-order analysis [20], and how resurgent analysis improves it [25, 103]. We are going to re-derive some of the formulae from chapter 2 in the two-parameter context and similar formulae for higher instanton sectors a well. Recall that if a given function $F(z)$ has a branch-cut in the complex plane along some direction θ, being analytic elsewhere, then

$$F(z) = \frac{1}{2\pi\mathrm{i}}\int_0^{\mathrm{e}^{\mathrm{i}\theta}\cdot\infty} \mathrm{d}w\,\frac{\mathrm{Disc}_\theta\, F(w)}{w-z}, \tag{3.26}$$

where we have assumed that there is no contribution arising from infinity [9, 20]. The key point now is that the aforementioned Stokes automorphism $\underline{\mathfrak{S}}_\theta$, which may be expressed as a multi-instanton expansion, relates to this branch-cut discontinuity as

$$\underline{\mathfrak{S}}_\theta = \mathbf{1} - \mathrm{Disc}_\theta, \tag{3.27}$$

in such a way that the discontinuity itself may be written in terms of multi-instanton data. For instance, starting with the perturbative sector, it was shown in [25] that in the two-parameter transseries set-up (3.24) there will be two branch-cuts, along $\theta = 0$ and $\theta = \pi$,

such that with $\beta_{00} = 0$ one finds

$$\begin{aligned} \text{Disc}_{\,0}\,\Phi_{(0|0)} &= -\sum_{k=1}^{+\infty}\left(S_1^{(0)}\right)^k \mathrm{e}^{-kAz}\,\Phi_{(k|0)}, \qquad (3.28)\\ \text{Disc}_{\,\pi}\,\Phi_{(0|0)} &= -\sum_{k=1}^{+\infty}\left(\widetilde{S}_{-1}^{(0)}\right)^k \mathrm{e}^{kAz}\,\Phi_{(0|k)}. \qquad (3.29)\end{aligned}$$

Using (3.25) and (3.26), we then find the perturbative asymptotic coefficients to obey the following relation

$$\begin{aligned} F_g^{(0|0)} \simeq & \sum_{k=1}^{+\infty}\frac{\left(S_1^{(0)}\right)^k}{2\pi\mathrm{i}}\frac{\Gamma\left(g-\beta_{k,0}\right)}{(kA)^{g-\beta_{k,0}}}\sum_{h=1}^{+\infty}\frac{\Gamma\left(g-\beta_{k,0}-h+1\right)}{\Gamma\left(g-\beta_{k,0}\right)}F_h^{(k|0)}\,(kA)^{h-1}+\\ &+\sum_{k=1}^{+\infty}\frac{\left(\widetilde{S}_{-1}^{(0)}\right)^k}{2\pi\mathrm{i}}\frac{\Gamma\left(g-\beta_{0,k}\right)}{(-kA)^{g-\beta_{0,k}}}\sum_{h=1}^{+\infty}\frac{\Gamma\left(g-\beta_{0,k}-h+1\right)}{\Gamma\left(g-\beta_{0,k}\right)}F_h^{(0|k)}\,(-kA)^{h-1}\,. \qquad (3.30)\end{aligned}$$

What this expression shows is that the asymptotic coefficients of the perturbative sector, for large g, are precisely controlled by the coefficients of the (generalized) multi-instanton sectors, $(n|0)$ and $(0|n)$. Of course that besides the coefficients $F_g^{(n|0)}$ and $F_g^{(0|n)}$, the perturbative coefficients also depend on the two Stokes constants, $S_1^{(0)}$ and $\widetilde{S}_{-1}^{(0)}$, and these still need to be determined. For the moment, let us just note that the leading large-order growth is dictated by the Stokes constants and the one-loop (generalized) one-instanton coefficients $F_1^{(1|0)}$ and $F_1^{(0|1)}$. Higher loop coefficients in the $(1|0)$ and $(0|1)$ sectors yield corrections in $1/g$, whereas the higher $(n|0)$ and $(0|n)$ sectors yield corrections which are suppressed as $1/n^g$.

As we turn to the models of interest to us in the present work – such as matrix models or topological strings – there are a few extra points to consider. First, the perturbative sector (3.11) is given by a topological genus expansion, in powers of $2g-2$, where the string coupling is $z = 1/g_s$. Secondly, as we address matrix models or topological strings, one needs to consider a version of the multi-instanton sectors (3.25) where both the action A and the perturbative coefficients $F_g^{(n|m)}$ become functions of the partial 't Hooft moduli (or geometric moduli) t_I. But, more importantly, due to resonance effects which will later appear in either the quartic matrix model or the Painlevé II equation, one also needs to consider the inclusion of logarithmic sectors as [25, 103]:

$$\begin{aligned} F^{(n|m)}(g_s,\{t_I\}) &\simeq \mathrm{e}^{-(n-m)\frac{A(t_I)}{g_s}}\sum_{k=0}^{k_{nm}}\log^k g_s\sum_{g=0}^{+\infty}g_s^{g+\beta_{nm}^{[k]}}F_g^{(n|m)[k]}(t_I)\\ &\equiv \mathrm{e}^{-(n-m)\frac{A(t_I)}{g_s}}\,\Phi_{(n|m)}(g_s,\{t_I\}). \qquad (3.31)\end{aligned}$$

We shall later uncover that the maximum logarithmic power is $k_{nm} = k_{mn} = \min(n,m) - m\,\delta_{nm}$ and that $\beta^{[k]}_{nm} = \beta^{[k]}_{mn} = \beta(m+n) - [(k_{nm}+k)/2]_I$, where $[\bullet]_I$ is the integer part of the argument and where $\beta = 1/2$. In practice, this essentially means that all we have done up to now was for the $k = 0$ "sector", and that the $\beta^{[k]}_{nm}$ coefficients take into account the fact that the perturbative expansions may in fact begin at some negative integer. Going back to the perturbative $(0|0)$ sector in (3.11), we know that $F^{(0|0)}$ is given by a genus expansion containing only powers of the closed[6] string coupling g_s^2. Thus, one needs to impose $F^{(0|0)}_{2n+1} = 0$ in (3.30), which will produce a series of relations between the $(0|k)$ and $(k|0)$ contributions since its right-hand-side must vanish order by order in both $\frac{1}{g}$ and k^{-g}. As further explained in [25], in the end we find that for all k and g,

$$\left(S_1^{(0)}\right)^k F_g^{(k|0)[0]} = (-1)^{g+\beta^{[0]}_{0,k}} \left(\widetilde{S}_{-1}^{(0)}\right)^k F_g^{(0|k)[0]}. \tag{3.32}$$

When working out the full details of either the two-cut quartic matrix model or the Painlevé II equation, we shall find further relations between different coefficients $F_g^{(n|m)[k]}$, either when m and n are exchanged, or relating the $k \neq 0$ coefficients to the $k = 0$ coefficients. In some cases, these will imply further relations between different Stokes constants.

Finally, using the above relations (3.32) back in the large-order formula for the perturbative sector (3.30), we obtain the asymptotic large-order behavior of the perturbative coefficients in the string genus expansion (3.11) as

$$F^{(0|0)}_{2g} \simeq \sum_{k=1}^{+\infty} \frac{\left(S_1^{(0)}\right)^k}{\mathrm{i}\pi} \frac{\Gamma\left(2g-\beta^{[0]}_{k,0}\right)}{(kA)^{2g-\beta^{[0]}_{k,0}}} \sum_{h=0}^{+\infty} \frac{\Gamma\left(2g-h-\beta^{[0]}_{k,0}\right)}{\Gamma\left(2g-\beta^{[0]}_{k,0}\right)} F_h^{(k|0)[0]} (kA)^h . \tag{3.33}$$

This procedure may be extended in order to find the large-order behavior of all (generalized) multi-instanton sectors. In particular, we are here interested in the large-order behavior of the physical multi-instanton series $F^{(n|0)}$. The precise calculation is a bit more cumbersome due to the logarithmic sectors appearing in (3.31), and we refer the reader to

[6] One has to be a bit careful with the precise meaning of the labels: in full rigor, the coefficients F_g in (3.11) precisely stand for $F^{(0|0)}_{2g}$ in the present transseries language, as can be seen by comparing against (3.25).

[25] for full details. The final result is

$$
\begin{aligned}
F_g^{(n|0)[0]} \simeq & \sum_{k=1}^{+\infty} \binom{n+k}{n} \frac{(S_1^{(0)})^k}{2\pi \mathrm{i}} \frac{\Gamma(g+\beta_{n,0}^{[0]}-\beta_{n+k,0}^{[0]})}{(kA)^{g+\beta_{n,0}^{[0]}-\beta_{n+k,0}^{[0]}}} \sum_{h=1}^{+\infty} \frac{\Gamma(g+\beta_{n,0}^{[0]}-\beta_{n+k,0}^{[0]}-h)}{\Gamma(g+\beta_{n,0}^{[0]}-\beta_{n+k,0}^{[0]})} F_h^{(n+k|0)[0]} (kA)^h \\
& + \sum_{k=1}^{+\infty} \left\{ \frac{1}{2\pi \mathrm{i}} \sum_{m=1}^{k} \frac{1}{m!} \sum_{\ell=0}^{m} \sum_{\gamma_i \in \Gamma(m,k)} \sum_{\delta_j \in \Gamma(m,m-\ell+1)} \left(\prod_{j=1}^{m} \Sigma(n,j) \right) \right\} \times \\
& \times \sum_{r=0}^{k_{n+\ell-k,\ell}} \frac{\Gamma(g+\beta_{n,0}^{[0]}-\beta_{n+\ell-k,\ell}^{[r]})}{(-kA)^{g+\beta_{n,0}^{[0]}-\beta_{n+\ell-k,\ell}^{[r]}}} \sum_{h=0}^{+\infty} \frac{\Gamma(g+\beta_{n,0}^{[0]}-\beta_{n+\ell-k,\ell}^{[r]}-h)}{\Gamma(g+\beta_{n,0}^{[0]}-\beta_{n+\ell-k,\ell}^{[r]})} F_h^{(n+\ell-k|\ell)[r]} (-kA)^h \times \\
& \times \left\{ \delta_{r0} + \Theta(r-1) \left(B_{kA}(a) + \partial_a \right)^{r-1} B_{kA}(a) \right\} \Big|_{a=g+\beta_{n,0}^{[0]}-\beta_{n+\ell-k,\ell}^{[r]}-h-1} .
\end{aligned}
\tag{3.34}
$$

Let us define the many ingredients in this expression (but, again, we refer the reader to [25] for the full details). The sums over γ_i and δ_j are sums over Young diagrams, where a diagram $\gamma_i \in \Gamma(k,\ell) : 0 < \gamma_1 \leq \cdots \leq \gamma_k = \ell$ has length $\ell(\Gamma) = k$, and where the maximum number of boxes for each γ_i is $\ell(\Gamma^T) = \ell$. The sum over δ_s is similar, now with $0 < \delta_1 \leq \delta_2 \leq \cdots \leq \delta_k = k-m+1$ and $0 < \delta_s \leq s+1$. These δ_s form a diagram $\Gamma(k, k-m+1)$ that has length $\ell(\Gamma) = k$ and $\ell(\Gamma^T) = k-m+1$, with an extra condition that each component $\delta_s \in \Gamma(k, k-m+1)$ has at most $s+1$ boxes. For these definitions to be consistent we still have to set $\gamma_0 \equiv 0$, $\delta_0 \equiv 1$, as well as the Stokes constants $S_0^{(k)} = \widetilde{S}_0^{(k)} = S_{-k}^{(k)} \equiv 0$. Next, defining $\mathbf{d}\gamma_j \equiv \gamma_j - \gamma_{j-1}$, and similarly for $\mathbf{d}\delta_s$, one has

$$
\Sigma(n,j) \equiv \left((j+1-\delta_j)\, \widetilde{S}_{-\mathbf{d}\gamma_j}^{(\mathbf{d}\delta_j)} + (n-\gamma_j+j+1-\delta_j)\, S_{-\mathbf{d}\gamma_j}^{(\mathbf{d}\gamma_j+\mathbf{d}\delta_j)} \right) \Theta\left(j+1-\delta_j\right), \tag{3.35}
$$

where $\Theta(x)$ is the Heaviside step-function. Finally, we have introduced the function

$$
B_s(a) \equiv \psi(a+1) - \log(-s) \equiv \widetilde{B}_s(a) - \mathrm{i}\pi, \tag{3.36}
$$

with $\psi(z) = \frac{\Gamma'(z)}{\Gamma(z)}$ the digamma function.

There are a few relevant features to be found in (3.34). Besides the multitude of (generalized) multi-instanton sectors and Stokes constants that now play a role, there is also a new type of large-order effect. In fact, and unlike the usual perturbative case which had a leading large-order growth of $g!$, essentially arising from the gamma function dependence, we now find a large-order growth of the type $g! \log g$, arising from the digamma function, and this is actually a *leading* effect as compared to the $g!$ growth. The first signs of this effect were found in [103], in the context of the Painlevé I equation, and further studied in [25].

3.3 Multi-Instanton Analysis for $\mathbb{Z}_2$-Symmetric Systems

Having reviewed the main background ingredients required for our analysis, we may now proceed with our main goal and address the nonperturbative study of Stokes phases associated to multi-cut configurations. These phases arise when all cuts are equally filled and, to be very concrete and present fully explicit formulae, we shall next focus on two-cut set-ups (see [57] as well). In this case, equal filling also implies that the configuration is $\mathbb{Z}_2$-symmetric. As we shall see in detail throughout this section, this symmetry implies that hyperelliptic integrals which appear in the calculation will reduce to elliptic integrals, and that, physically, the system will be found in a Stokes phase. Notice that, strictly within the orthogonal polynomial framework, it was already noticed in [54] that equal filling of the cuts would lead to a Stokes phase.

3.3.1 Computing the Multi-Instanton Sectors

Let us begin by considering the multi-instanton sectors of a two-cut matrix model. We shall do this by following the strategy in [57], *i.e.*, we shall consider the two-cut spectral geometry as a degeneration from a three-cut configuration. In principle one could also consider degenerations from more complicated configurations if one were to introduce several distinct instanton actions, but for our purposes degenerations from three cuts will suffice. In this case, a reference filling of eigenvalues across the cuts is of the form (N_1, N_2, N_3), with $N_1 + N_2 + N_3 = N$, the degeneration will simply be $N_2 \to 0$, and the $\mathbb{Z}_2$ symmetry will eventually demand $N_1 = N_3$.

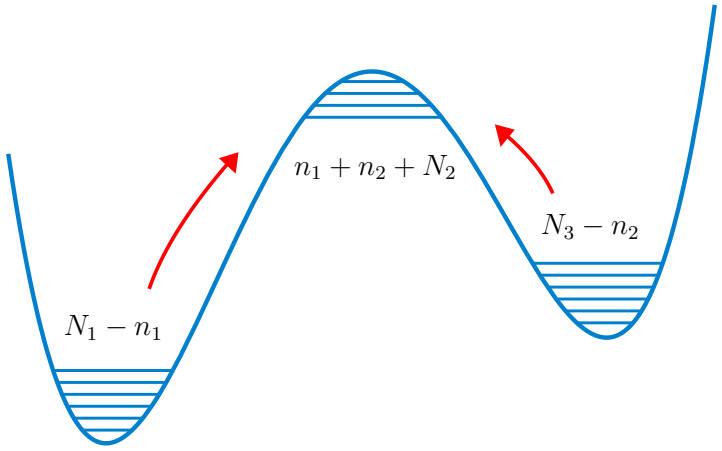

Figure 3.1: Eigenvalue tunneling as the multi-instanton sectors of a three-cut matrix model.

In matrix models, (multi) instantons are associated to (multiple) eigenvalue tunneling [10, 55, 57, 105] and, as such, the multi-instanton sectors are described by tunneling eigenvalues in-between the three cuts, as shown in figure 3.1 (it is simple to see that two integers, n_1

and n_2, are enough to parameterize all possible exchanges of eigenvalues between three cuts, *i.e.*, all possible background choices). In the particular case of the $\mathbb{Z}_2$-symmetric two-cut configuration, the reference background is of the form

$$\left(\frac{N}{2}, 0, \frac{N}{2}\right). \tag{3.37}$$

As we shall see later on, the one-instanton sector will correspond to summing over all configurations which leave a single eigenvalue on the middle-cut. From the spectral geometry viewpoint, the $\mathbb{Z}_2$ symmetry essentially places the cuts at $[-b,-a]\cup[a,b]$ and the spectral curve (3.5) becomes

$$y(z) = M(z)\sqrt{(z^2-a^2)\,(z^2-b^2)}, \tag{3.38}$$

where $M(z)$ is given by (3.6). In this configuration, the pinching cycle will be found at $z=0$. The action associated to eigenvalue tunneling essentially measures their energy difference in-between cuts [10, 55, 57, 105], as given by the holomorphic effective potential (3.9), and in the particular case of this $\mathbb{Z}_2$-symmetric configuration with equal filling it is simple to check that the equal filling essentially translates to

$$\int_{-a}^{a} \mathrm{d}z\, y(z) = 0. \tag{3.39}$$

This condition will further imply that one may completely evaluate all data in the spectral geometry just by using the asymptotics of the resolvent (3.7). One is left with one instanton action to evaluate, describing tunneling from each of the (equal) cuts up to the pinched cycle[7] located at x_0 such that $M(x_0)=0$ [10]. In here $x_0=0$ and

$$A = \int_{a}^{0} \mathrm{d}z\, y(z). \tag{3.40}$$

Having briefly explained the set-up, one may proceed and compute the partition functions associated to the relevant configurations along the lines in [57]. Let now $y(z)$ be the spectral curve (3.5) of the *three*-cut configuration, with cuts $[x_1,x_2]\cup[x_3,x_4]\cup[x_5,x_6]$. Let us consider the aforementioned set-up with N_1-n_1, $N_2+(n_1+n_2)$ and N_3-n_2 eigenvalues in the first, second and third cuts, respectively, and let us consider the associated multi-instanton amplitude written in terms of the 't Hooft moduli (3.8)

$$Z^{(n_1,n_2)} \equiv \frac{Z\left(t_1-n_1 g_s, t_2+n_1 g_s+n_2 g_s, t_3-n_2 g_s\right)}{Z\left(t_1,t_2,t_3\right)}, \tag{3.41}$$

[7] This is the non-trivial saddle located outside the cut, where eigenvalues may tunnel to [10].

with $t_1 + t_2 + t_3 = t$. For convenience we introduce the variables

$$s_1 = \frac{1}{2}(t_1 - t_2 - t_3), \tag{3.42}$$

$$s_2 = \frac{1}{2}(t_3 - t_2 - t_1), \tag{3.43}$$

and use them to expand the exponent of (3.41) above (*i.e.*, the difference of free energies between the "eigenvalue-shifted" configuration and the reference background), around $g_s = 0$ and for $n_1, n_2 \ll N$. One simply finds[8]

$$Z^{(n_1,n_2)} = \exp\left(-\frac{1}{g_s}\sum_{i=1}^{2} n_i\,\partial_{s_i}F_0\right)\exp\left(\frac{1}{2}\sum_{i,j=1}^{2} n_i n_j\,\partial_{s_i}\partial_{s_j}F_0\right)\Big\{1 + \mathcal{O}(g_s)\Big\}. \tag{3.44}$$

In this expression we find two, in general different, actions

$$A_i = \partial_{s_i}F_0, \qquad i = 1, 2, \tag{3.45}$$

which may be computed in terms of geometric data if we use the special geometry relations

$$\frac{\partial F_0}{\partial t_I} = \oint_{B^I} \mathrm{d}z\, y(z). \tag{3.46}$$

In the present three-cut configuration, the two actions are then given by

$$A_1 = \frac{\partial F_0}{\partial s_1} = \int_{x_2}^{x_3} \mathrm{d}z\, y(z), \tag{3.47}$$

$$A_2 = \frac{\partial F_0}{\partial s_2} = \int_{x_5}^{x_4} \mathrm{d}z\, y(z), \tag{3.48}$$

and they have the usual geometric interpretation appearing in figure 3.2, generalizing the one-cut case appearing in [10, 57]. The extension to an arbitrary number of cuts is straightforward. The other feature we find in (3.44) are the second derivatives of F_0, and for those it is convenient to introduce the (symmetric) period matrix

$$\tau_{ij} \equiv \frac{1}{2\pi\mathrm{i}}\frac{\partial^2 F_0}{\partial s_i \partial s_j}. \tag{3.49}$$

Having understood the general form of the multi-instanton amplitudes, we still need to understand the precise nature of the multi-instanton expansion. The grand-canonical parti-

[8] For shortness we shall many times omit the arguments; it should be clear that whenever we write F_0 we always mean the reference configuration $F_0(t_1, t_2, t_3)$, and similarly in other cases.

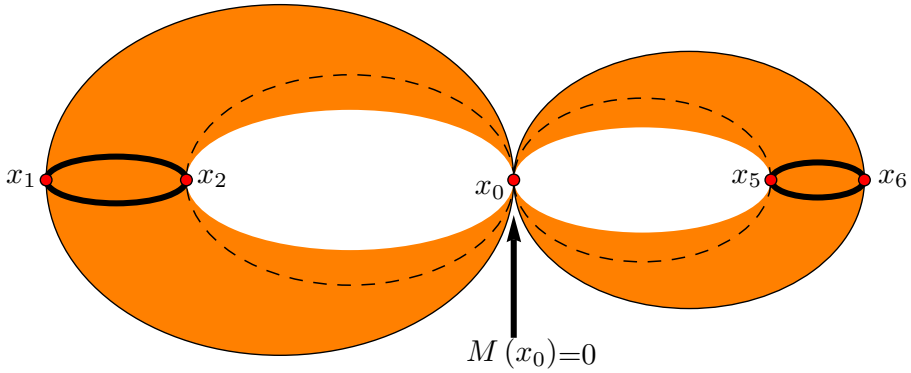

Figure 3.2: The two-cut spectral curve $y(z)$ is a genus one curve, with a pinched cycle at the non-trivial saddle x_0 which is obtained by taking $x_3 \to x_4$ in the three-cut geometry (in the $\mathbb{Z}_2$ symmetric scenario $x_0 = 0$). The instanton actions A_1 and A_2 naturally appear as B-cycles in this spectral geometry.

tion function is obtained as a sum over all possible eigenvalue distributions into the multiple cuts, with their total number fixed. In our case, and making use of the multi-instanton amplitudes (3.41), this translates to

$$Z(N) = \sum_{n_1=-N_2+N_3}^{N_1} \sum_{n_2=-n_1-N_2}^{N_3} Z^{(n_1,n_2)}. \tag{3.50}$$

Let us now consider the reference background of interest to us, *i.e.*, the $\mathbb{Z}_2$-symmetric two-cut configuration describing a multi-cut Stokes phase. This background has moduli $t_1 = t_3 = \frac{t}{2}$ and $t_2 = 0$, in which case both instanton actions will be equal $A_1 = A_2 \equiv A$, as well as $\tau_{11} = \tau_{22}$. Changing variables from n_1 and n_2 to $\ell = n_1 + n_2$ and $m = n_1 - n_2$, we may write the multi-instanton amplitudes (3.44) as

$$Z^{(\ell,m)} = \exp\left(-\frac{\ell A}{g_s}\right) \exp\left(\frac{\mathrm{i}\pi}{2}\left(\tau_{11}+\tau_{12}\right)\ell^2\right) \exp\left(\frac{\mathrm{i}\pi}{2}\left(\tau_{11}-\tau_{12}\right)m^2\right) \Big\{1+\mathcal{O}(g_s)\Big\}, \tag{3.51}$$

where it now becomes clear that it is $\ell = n_1 + n_2 \geq 0$ which will label the multi-instanton sectors. Of course this further implies that we still need to sum over the "relative" index m in order to obtain the "purely" ℓ-instanton amplitude: it is this sum over m which essentially moves our calculation to the grand-canonical ensemble. In other words, the grand-canonical partition function (3.50) is of the schematic form

$$Z(N) = \mathcal{Z}^{(\ell=0)} + \mathcal{Z}^{(\ell=1)} + \mathcal{Z}^{(\ell=2)} + \cdots = \mathcal{Z}^{(\ell=0)} \left(1 + \frac{\mathcal{Z}^{(\ell=1)}}{\mathcal{Z}^{(\ell=0)}} + \frac{\mathcal{Z}^{(\ell=2)}}{\mathcal{Z}^{(\ell=0)}} + \ldots\right), \tag{3.52}$$

where now each term $\mathcal{Z}^{(\ell)}$ contains a sum over all possible values of $m = n_1 - n_2$ that satisfy $n_1 + n_2 = \ell$. Fixing ℓ eigenvalues on the middle-cut implies that we only have $N - \ell$ available eigenvalues to place in each of the two side-cuts, which yields the limits on the m-sum. But because m jumps by values of two, it turns out that it is actually more convenient to change variables and use as the "relative" index $m = 2r - \ell$. Overall, we find

$$\begin{aligned}\mathcal{Z}^{(\ell)} = \quad & \exp\left(-\frac{\ell A}{g_s}\right)\exp\left(\frac{\mathrm{i}\pi}{2}\left(\tau_{11}+\tau_{12}\right)\ell^2\right)\times \\ & \times\sum_{r=-N/2+\ell}^{N/2}\exp\left(\frac{\mathrm{i}\pi}{2}\left(\tau_{11}-\tau_{12}\right)\left(2r-\ell\right)^2\right)\Big\{1+\mathcal{O}(g_s)\Big\}. \end{aligned} \tag{3.53}$$

With a certain abuse of notation, we shall immediately identify the ℓ-th instanton amplitude as

$$Z^{(\ell)} = \frac{\mathcal{Z}^{(\ell)}}{\mathcal{Z}^{(0)}}, \tag{3.54}$$

where all that is now missing is the explicit evaluation of the many different ingredients which appear above, in particular explicitly evaluating the sum.

Let us begin by addressing the period matrix (3.49), *i.e.*, the second derivatives of the planar free energy. Using the special geometry relation (3.46) and the explicit form of the spectral curve (3.5), it follows that

$$\frac{\partial^2 F_0}{\partial s_i \partial s_j} = (-1)^{j+1}\int_{x_{2j}}^{x_{2j+1}} \mathrm{d}z\,(-2)\frac{\partial(t\omega_0(z))}{\partial s_i}, \tag{3.55}$$

where the derivative of the resolvent has the form[9]

$$\frac{\partial(t\omega_0(z))}{\partial s_i} = \frac{C_0^{(i)}(t,s_k) + C_1^{(i)}(t,s_k)\,z}{\sqrt{\sigma_3(z)}}. \tag{3.56}$$

The coefficients which appear in this expression, $C_0^{(i)}(t,s_k)$ and $C_1^{(i)}(t,s_k)$, may be fixed by taking derivatives of the partial 't Hooft moduli (3.8), and by using the definition of the variables $\{s_i\}$, (3.42) and (3.43), as

$$\frac{\partial t_I}{\partial s_i} = \begin{pmatrix}+1\\0\\-1\end{pmatrix} = -\frac{1}{2\pi\mathrm{i}}\oint_{A^I}\mathrm{d}z\,\frac{C_0^{(i)}(t,s_k) + C_1^{(i)}(t,s_k)\,z}{\sqrt{\sigma_3(z)}}, \qquad i=1,2, \quad I=1,2,3. \tag{3.57}$$

[9]In order to check this relation one explicitly uses (3.5) and (3.6) when taking derivatives, and this will yield the polynomial structure in z. In order to fix the degree of this polynomial, one compares the asymptotics as $z \to +\infty$ on both sides of the equation. Generically, the degree will depend on the number of cuts as $s-2$.

Note that although this relation corresponds to a system of 6 equations for 4 unknowns, two of the equations are redundant as we can deform contours in order to find $\sum_I \oint_{A^I} = 0$ (there is no residue at infinity). If we now define the integrals

$$\mathcal{K}_I = \oint_{A^I} \frac{\mathrm{d}z}{2\pi\mathrm{i}} \frac{1}{\sqrt{\sigma_3(z)}} \quad \text{and} \quad \mathcal{L}_I = \oint_{A^I} \frac{\mathrm{d}z}{2\pi\mathrm{i}} \frac{z}{\sqrt{\sigma_3(z)}}, \tag{3.58}$$

then we can express all the coefficients $C_j^{(i)}$ in terms of these integrals as

$$C_0^{(1)} = \frac{\mathcal{L}_1 + \mathcal{L}_2}{\mathcal{L}_1\mathcal{K}_2 - \mathcal{L}_2\mathcal{K}_1}, \qquad C_0^{(2)} = \frac{\mathcal{L}_2 + \mathcal{L}_3}{\mathcal{L}_3\mathcal{K}_2 - \mathcal{L}_2\mathcal{K}_3}, \tag{3.59}$$

$$C_1^{(1)} = \frac{\mathcal{K}_1 + \mathcal{K}_2}{\mathcal{L}_2\mathcal{K}_1 - \mathcal{L}_1\mathcal{K}_2}, \qquad C_1^{(2)} = \frac{\mathcal{K}_2 + \mathcal{K}_3}{\mathcal{L}_2\mathcal{K}_3 - \mathcal{L}_3\mathcal{K}_2}. \tag{3.60}$$

So far these results are only formal: hyperelliptic integrals are hard to evaluate. However, they may in fact be explicitly evaluated when one imposes $\mathbb{Z}_2$ symmetry into the problem. In this case, one places the cuts as $[-b,-a]\cup[-c,c]\cup[a,b]$ (where we shall later be interested in the $c \to 0$ degeneration) and it immediately follows that

$$\mathcal{K}_1 = \mathcal{K}_3 = -\frac{1}{2}\mathcal{K}_2 \equiv -\mathcal{K}, \tag{3.61}$$

$$\mathcal{L}_1 = -\mathcal{L}_3 \equiv -\mathcal{L}, \quad \mathcal{L}_2 = 0, \tag{3.62}$$

leading to the (simplified) coefficients

$$C_0^{(1)} = C_0^{(2)} = \frac{1}{2\mathcal{K}}, \tag{3.63}$$

$$-C_1^{(1)} = C_1^{(2)} = \frac{1}{2\mathcal{L}}. \tag{3.64}$$

As they will be needed in the following, let us also introduce the B-cycle integrals:

$$\widetilde{\mathcal{K}} \equiv \int_{-a}^{-c} \frac{\mathrm{d}z}{\sqrt{\sigma_3(z)}} = \int_{c}^{a} \frac{\mathrm{d}z}{\sqrt{\sigma_3(z)}}, \tag{3.65}$$

$$\widetilde{\mathcal{L}} \equiv -\int_{-a}^{-c} \mathrm{d}z \frac{z}{\sqrt{\sigma_3(z)}} = \int_{c}^{a} \mathrm{d}z \frac{z}{\sqrt{\sigma_3(z)}}. \tag{3.66}$$

All these A and B-cycle integrals may be explicitly evaluated, and expressed in terms of complete *elliptic* integrals of the first kind, $K(k^2)$, with k being the elliptic modulus. This is also the technical reason why one may find Stokes phases within multi-cut configurations: symmetries (in this case a $\mathbb{Z}_2$ symmetry) may effectively reduce hyperelliptic geometries to

elliptic ones! The results are

$$\mathcal{K} = -\int_a^b \frac{\mathrm{d}x}{\pi} \frac{1}{\sqrt{|\sigma_3(x)|}} = -\frac{1}{\pi b\sqrt{a^2-c^2}} K\left(\frac{c^2\left(b^2-a^2\right)}{b^2\left(c^2-a^2\right)}\right), \tag{3.67}$$

$$\mathcal{L} = \int_{-b}^{-a} \frac{\mathrm{d}x}{\pi} \frac{x}{\sqrt{|\sigma_3(x)|}} = -\frac{1}{\pi\sqrt{a^2-c^2}} K\left(\frac{b^2-a^2}{c^2-a^2}\right), \tag{3.68}$$

and, for (3.65) and (3.66),

$$\widetilde{\mathcal{K}} = \frac{1}{a\sqrt{b^2-c^2}} K\left(\frac{b^2\left(c^2-a^2\right)}{a^2\left(c^2-b^2\right)}\right), \tag{3.69}$$

$$\widetilde{\mathcal{L}} = \frac{1}{\sqrt{b^2-a^2}} K\left(\frac{a^2-c^2}{a^2-b^2}\right). \tag{3.70}$$

Having explicitly evaluated all integrals, we may now start assembling these results back into our original formulae and address the degeneration limit $c \to 0$. In order to do that, it is first important to notice that this limit must be taken carefully as the free energy is not analytic in the 't Hooft modulus associated to the shrinking cycle [57]. This may be explicitly seen by splitting the free energies as

$$F_g(t_1,t_2,t_3) = F_g^{\mathrm{G}}(t_2) + \widehat{F}_g(t_1,t_2,t_3), \tag{3.71}$$

where $F_g^{\mathrm{G}}(t_2)$ are the genus g free energies of the Gaussian model depending on the vanishing 't Hooft modulus, which, at genus $g=0$ and $g=1$, have a dependence as $\log t_2$. As explained in [57], for the ℓ-instanton sector it is not appropriate to look at the integration over the ℓ eigenvalues in the collapsing cycle as a large N approximation; rather one should *exactly* evaluate the Gaussian partition function associated to this cycle, which is

$$Z_\ell^{\mathrm{G}} = \frac{g_s^{\ell^2/2}}{(2\pi)^{\ell/2}} G_2\left(\ell+1\right) \tag{3.72}$$

with $G_2\left(\ell+1\right)$ the Barnes function. Then, the partition function around the ℓ-instanton configuration should be properly written as

$$Z^{(\ell)} = Z_\ell^{\mathrm{G}}\, \widehat{Z}^{(\ell)}, \tag{3.73}$$

where all "hatted" quantities in $\widehat{Z}^{(\ell)}$ are now regularized and analytic in the $t_2 \to 0$ limit.

The instanton action is the simplest quantity to evaluate as it is in fact regular in the

$t_2 \to 0$ limit. One simply finds

$$\widehat{A} = \int_a^c \mathrm{d}z\, \widetilde{M}(z)\sqrt{(z^2-a^2)(z^2-b^2)(z^2-c^2)} \xrightarrow[c\to 0]{} \int_a^0 \mathrm{d}z\, M(z)\sqrt{(z^2-a^2)(z^2-b^2)}, \tag{3.74}$$

where $M(z) = z\widetilde{M}(z)$. To compute the period matrix we must first address the second derivatives of the planar free energy, (3.55), which are given by

$$\partial_{s_1}^2 F_0 \equiv \partial_{s_2}^2 F_0 = \frac{1}{\mathcal{K}}\int_c^a \frac{\mathrm{d}z}{\sqrt{\sigma_3(z)}} + \frac{1}{\mathcal{L}}\int_c^a \mathrm{d}z\, \frac{z}{\sqrt{\sigma_3(z)}} = \frac{\widetilde{\mathcal{K}}}{\mathcal{K}} + \frac{\widetilde{\mathcal{L}}}{\mathcal{L}}, \tag{3.75}$$

and by

$$\partial_{s_1}\partial_{s_2} F_0 = \frac{\widetilde{\mathcal{K}}}{\mathcal{K}} - \frac{\widetilde{\mathcal{L}}}{\mathcal{L}}. \tag{3.76}$$

With these results, the period matrix follows immediately. In particular we obtain

$$\tau_{11} + \tau_{12} = -\frac{\mathrm{i}}{\pi}\frac{\widetilde{\mathcal{K}}}{\mathcal{K}}, \tag{3.77}$$

$$\tau_{11} - \tau_{12} = -\frac{\mathrm{i}}{\pi}\frac{\widetilde{\mathcal{L}}}{\mathcal{L}}. \tag{3.78}$$

The need for regulation of the shrinking cycle is now very clean. In fact, if one takes the $c \to 0$ limit in (3.77) above one obtains

$$\lim_{c\to 0} \mathrm{i}\pi\,(\tau_{11}+\tau_{12}) \sim 2\lim_{c\to 0}\log c + \log\left(\frac{b^2-a^2}{16a^2b^2}\right) + \cdots. \tag{3.79}$$

However, as explained, this logarithmic divergence – which emerges in one of the elliptic integrals – will be precisely canceled by the "Gaussian divergence" arising from the shrinking cycle. The regulation is simply [57]

$$\partial_s^2 \widehat{F}_0 = \lim_{c\to 0}\left(\partial_s^2 F_0 - \log t_2\right), \tag{3.80}$$

where the vanishing 't Hooft modulus is, via (3.8),

$$t_2 = \frac{1}{2\pi}\int_{-c}^{c} \mathrm{d}z\, \widetilde{M}(z)\sqrt{(z^2-a^2)(z^2-b^2)(z^2-c^2)}. \tag{3.81}$$

Changing variables $z \to z/c$, expanding the result in powers of c and performing the inte-

gration, it follows[10]

$$t_2 = \frac{1}{4}\widetilde{M}\, ab\, c^2 \left(1 + \mathcal{O}(c^2)\right), \tag{3.82}$$

which will indeed cancel the divergence above. As for the combination (3.78), it has a regular $c \to 0$ limit. Using known properties of elliptic integrals [116] one may compute

$$\tau_{11} - \tau_{12} = \frac{\mathrm{i}}{2}\frac{K(1-k^2)}{K(k^2)} \equiv \frac{\mathrm{i}}{2}\frac{K'}{K}, \tag{3.83}$$

where the elliptic modulus in this $\mathbb{Z}_2$-symmetric limit is simply given by $k = \frac{b-a}{b+a}$.

Finally, in order to obtain the multi-instanton amplitudes (3.54), all one has to do is evaluate the sums in (3.53). When $\ell = 0$, the sum in (3.53) yields the Jacobi (elliptic) theta-function given by

$$\vartheta_3\left(z \,|\, q\right) = 1 + 2\sum_{r=1}^{+\infty} q^{r^2}\cos\left(2rz\right). \tag{3.84}$$

In fact, using this definition it is straightforward to evaluate

$$\lim_{N\to+\infty}\sum_{r=-N/2}^{N/2}\exp\left(\frac{\mathrm{i}\pi}{2}\left(\tau_{11}-\tau_{12}\right)(2r)^2\right) = \vartheta_3\left(0\,\middle|\,\mathrm{e}^{-\pi\frac{K'}{K}}\right). \tag{3.85}$$

When $\ell \neq 0$, and using simple properties of theta-functions [117], one may obtain instead[11]

$$\lim_{N\to+\infty}\sum_{r=-N/2+\ell}^{N/2}\exp\left(\frac{\mathrm{i}\pi}{2}\left(\tau_{11}-\tau_{12}\right)(2r-\ell)^2\right) = k^{\frac{1-(-1)^\ell}{4}}\,\vartheta_3\left(0,\mathrm{e}^{-\pi\frac{K'}{K}}\right). \tag{3.86}$$

As we use both results above in the ratio (3.54) for the ℓ-instanton partition function, we observe the remarkable cancelation of the elliptic/theta function contribution: the only trace of their existence which remains is that the result will have a different k-dependence, depending on whether the instanton number is even or odd. That neither elliptic nor theta functions should be present in the final result is of course what one would have expected, when addressing a Stokes phase of a given matrix model. As such, our final result is

$$Z^{(\ell)} = \frac{g_s^{\ell^2/2}}{(2\pi)^{\ell/2}}\, G_2\left(\ell+1\right) k^{\frac{1-(-1)^\ell}{4}}\,\hat{q}^{\frac{\ell^2}{2}}\,\exp\left(-\frac{\ell\widehat{A}}{g_s}\right)\Big\{1+\mathcal{O}(g_s)\Big\}, \tag{3.87}$$

[10] In the purely three-cut scenario it is simple to check that $\widetilde{M}$ is just a constant; more on this in the following.

[11] The periodicity of the theta-function $\vartheta_3\left(z + n\,\pi \,|\, q\right) = \vartheta_3\left(z \,|\, q\right)$ implies that only the parity of ℓ is relevant.

where

$$\hat{q}^{\frac{1}{2}} \equiv \frac{\sqrt{b^2-a^2}}{2\sqrt{\widetilde{M}}\,(ab)^{3/2}}. \tag{3.88}$$

In the following sections we shall test this result with great accuracy, by matching against large-order data. Besides the instanton action we shall give particular attention to testing the one-loop coefficient in the one-instanton sector (which also relates to one of the Stokes constants [10, 25]) which, written in terms of spectral geometry data, is very simply given by

$$S_1^{(0)} F_0^{(1|0)} = \frac{1}{2\sqrt{2\pi\widetilde{M}}}\,\frac{b-a}{(ab)^{3/2}}. \tag{3.89}$$

3.3.2 Stokes Phases and Background Independence

In the previous subsection we used saddle-point analysis in order to explicitly find all multi-instanton amplitudes in a two-cut matrix model (at least to leading order in the string coupling). As we have seen, the situation with a multiple number of cuts is – as long as one can evaluate all hyperelliptic integrals – a straightforward extension from the single-cut case [10, 57, 110]. Another interesting aspect of our line of work is that all these analytical results may be numerically tested to very high precision by making the match against large-order analysis; see, *e.g.*, [9–11, 16, 20, 25, 57, 60, 103, 107, 108]. As such, the obvious question to address now is whether obtaining large-order data for all the (generalized) multi-instanton coefficients $F_g^{(n|m)}$ is feasible, and perhaps also a simple extension from the one-cut case. In general, this is *not* the case and producing large-order data in multi-cut situations is a much harder problem; see, *e.g.*, [57, 60].

While there are several approaches to constructing large-order data, in this work we shall focus solely in the orthogonal polynomial method [49] (more generally, the transseries approach as developed in [16, 25]). As mentioned, in general this method is in fact *not* applicable to multi-cut configurations and what we shall discuss now is how this situation changes if we focus on a given Stokes phase of our system. As we also discussed in the introduction, some of the earlier work done in the exploration of the phase spaces of matrix models with multi-welled potentials was carried out in the orthogonal polynomial framework; see, *e.g.*, [54, 118–122]. Such works were mainly based on numerical computations of the recursion coefficients, r_n, appearing in the string equation (equation (3.16) in the case of the quartic model) and the main discovery concerned the appearance of multi-branch solutions at large N, as we illustrate in figure 3.3.

Let us consider the case of the quartic potential $V(z) = \frac{\mu}{2}z^2 + \frac{\lambda}{4!}z^4$ which, when $\mu = -1$ and $\lambda = 6$, is depicted in the first image of figure 3.3. With a large N choice of $N = 1000$ eigenvalues, and given the string equation for this model presented in (3.16), one may numerically iterate the recursion in order to compute the coefficients r_n and the result is shown in the second image of figure 3.3 (in here we have used the same numerical method

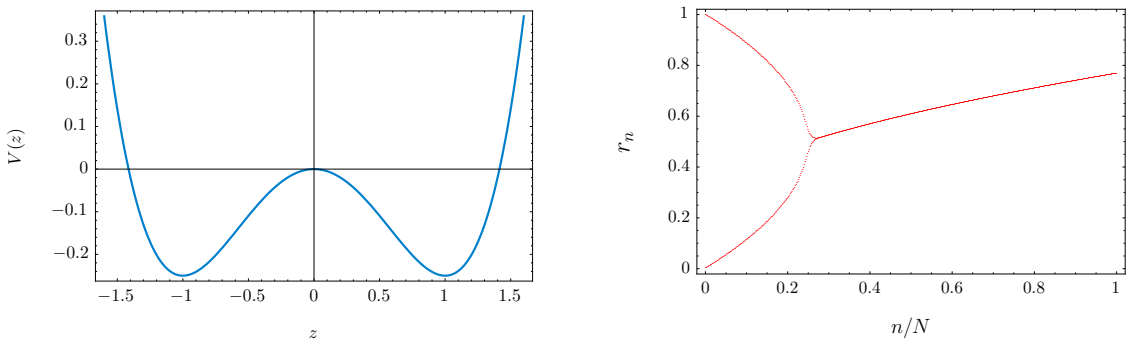

Figure 3.3: Numerical data for the quartic potential. The first image shows the quartic potential $V(z) = \frac{\mu}{2}z^2 + \frac{\lambda}{4!}z^4$ with $\mu = -1$ and $\lambda = 6$, while the second image displays the corresponding recursion coefficients r_n recursively obtained from the string equation (3.16) (in the plots with choosing $N = 1000$ and after 4000 iterations in the numerical method described in [120, 121]).

as in [120, 121]). What this plot tells us is that, in some region of parameter space, the large N behavior of the r_n coefficients falls into a single branch, whereas in another region the even and odd coefficients actually split into alternating branches, with period two. As we shall show in the next section, this splitting of branches is telling us how the continuum limit should be taken in a multi-cut Stokes phase and, as such, how orthogonal polynomials may be used to generate large-order results. In other words, if the recursion coefficients have a periodic large N behavior, the free energy will have a well-defined topological expansion with exponentially suppressed instanton corrections – characteristic of a Stokes phase – and orthogonal polynomials may be simply used. Furthermore, notice that the variable n/N in the horizontal axis becomes the 't Hooft parameter in the continuum limit. In this case, note that the two branches merge near $n/N = 1/4$ which in the continuum language corresponds to $\lambda t = 3/2$. This critical point actually occurs when the two cuts of the quartic matrix model collide, and at this point the system is described in the double-scaling limit by the Painlevé II equation. We shall have more to say about this in a later section.

It is important to distinguish the Stokes phase, where the free energy has a "good" large N 't Hooft expansion, from more complicated cases which may also appear as transitions occur to other phases. For instance, a different behavior is shown in figure 3.4, obtained from the string equation of a sixth-order potential. We no longer find just periodic behavior, but also regions of *quasi-periodic* behavior (as shown in [110]): this quasi-periodicity is a sign of the theta-functions which control the recursion coefficients in this phase and which appear as one constructs the grand-canonical partition function of the matrix model as a sum over all choices of filling fractions [110]. This was recently made explicit in [58, 59], with the construction of general, nonperturbative, background independent partition functions for matrix models and topological strings in terms of theta functions. In this case, the free energy has an asymptotic large N behavior which is also controled by theta functions and

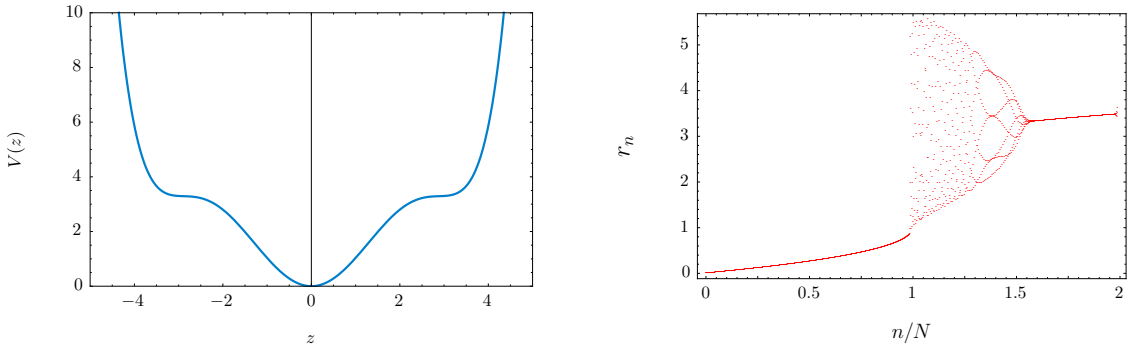

Figure 3.4: Numerical data for a sixth-order potential. The first image shows a sixth-order potential, while the second image displays the corresponding recursion coefficients r_n recursively obtained from its string equation (with $N = 1000$ and after 4000 iterations in the numerical method described in [120, 121]).

a *naïve* use of orthogonal polynomials will not work; rather one has to use the full power of resurgent transseries.

In summary, one may be faced with at least two different phases or backgrounds when addressing multi-cut configurations: either periodic or quasi-periodic behavior of the recursion coefficients, corresponding to either Stokes or anti-Stokes phases. In the Stokes phase the large N asymptotics is essentially given by an 't Hooft topological genus expansion, while in the anti-Stokes phase the asymptotics is of theta-function type. These issues were addressed in [108] and we refer the reader to their excellent discussion (where the authors of [108] used the terminology of "boundary" and "interior" points to denote what we here call Stokes and anti-Stokes regions). In particular, an expansion around a given background is well-defined when either [108]:

1. In a Stokes region, one will find an admissible large N 't Hooft genus expansion in powers of $1/N^2$, with exponentially suppressed multi-instanton corrections, if

$$\mathbb{R}\mathrm{e}\left(\frac{A(t)}{g_s}\right) > 0. \tag{3.90}$$

2. In an anti-Stokes region, the free energy will display theta-function asymptotics [58, 59]. This expansion will be admissible if the filling fractions are real, $\frac{N_i}{N} \in \mathbb{R}$, and if

$$\mathbb{R}\mathrm{e}\left(\frac{\partial_{s_i} F_0}{g_s}\right) = 0. \tag{3.91}$$

The conditions of admissibility were first discussed in [55, 105], and later further addressed in [123–125] where they were shown to be equivalent to having the spectral curve as a Boutroux

curve. Let us now stress that our construction in the previous subsection precisely fulfills the first condition above. In fact we were able to find a well-defined (exponentially suppressed) multi-instanton expansion, which is clear both from the general structure of (3.52) as well as from our final result (3.87). In this process, the $\mathbb{Z}_2$ symmetry plays an important role since it is the equality of the two instanton actions what allows us to write down a multi-instanton expansion for the (grand-canonical) partition function. Of course we still must make sure that the examples we shall address next also satisfy this condition.

Chapter 4

Quartic Matrix Model I: Stokes Phases

Most of the contents of this chapter appear in [1]:
"The Resurgence of Instantons: Multi-Cut Stokes Phases and the Painleve II Equation",
R. Schiappa, and R. Vaz,
arXiv:1302.5138 [hep-th], Commun. Math. Phys. **330**, 655-721 (2014)
DOI: 10.1007/s00220-014-2028-7

4.1 Introduction

After our journey through nonperturbative effects in matrix models, our next goal is to illustrate how the multi-instanton effects we have uncovered in the previous section make their appearance in different examples, and how we may test them by comparing against large-order analysis. We will begin by presenting an overview of the one-cut quartic matrix model, as it is the simplest Stokes phase of the quartic matrix model. This solution was studied recently in [10, 25, 57]. We will present some results, and some of them will be needed later in chapter 6. We then focus our attention on the quartic matrix model in its two-cut Stokes phase, as this is a particularly clean application of all our nonperturbative machinery. Our analysis follows in a somewhat parallel spirit to [25], in particular as we construct a two-parameter transseries solution in this phase. Instantons in this example are associated to B-cycle eigenvalue tunneling [10], which we discussed in detail in the previous section, and we provide tests of our analytical results by comparing against the large-order behavior of perturbation theory. Earlier results addressing the asymptotics of this model were presented in [126] and we extend them in here within the context of transseries and resurgent analysis. We notice that one of the key points that allowed us to solve for the nonperturbative structure of a multi-cut configuration in the previous section was its $\mathbb{Z}_2$ symmetry and, as such, this will be a required ingredient also for our following examples. In section 4.4 we turn

to the asymptotics of multi-instanton sectors, and we do this in the natural double-scaling limit of the two-cut quartic matrix model, which is the Painlevé II equation. This equation describes 2d supergravity, or type 0B string theory [127–130], and we fully construct its two-parameter transseries solution, checking the existence of generalized multi-instanton sectors via resurgent analysis. Earlier results addressing the asymptotics of this model were presented in [131] and we extend them in here within the context of transseries and resurgent analysis. In particular, we compute many new Stokes constants for this system (in this way verifying and generalizing the one known Stokes constant [132]), and present the complete nonperturbative free energy of type 0B string theory. Let us also stress that, due to the nature of the large-order analysis, we have generated a large amount of data concerning both the two-cut quartic matrix model and the Painlevé II equation. Due to space constraints it is impossible to list all such results in the main text, but we do present some of this data in a few appendices.

As an aside, we should point out that not all nonperturbative effects arise from what we may call B-cycle instantons [10], *i.e.*, instantons whose action is given by a B-cycle integration of the spectral curve one-form as in figure 3.2. In fact, in some cases one needs to consider A-cycle instantons instead [11], *i.e.*, instantons whose action arises from integrating the spectral curve one-form along an A-cycle and thus, because of (3.8), instantons which have an almost "universal" structure. We will not consider A-cycle instantons in this discussion, but in [1] the "triple" Penner matrix model, which could be considered in the context of studying four-point correlation functions in the AGT set-up [39], is discussed. This is an interesting example because it is actually exactly solvable via so-called generalized Gegenbauer polynomials, and the instantons can be read off from a multi-sheeted holomorphic effective potential and multiple actions corresponding to "jumps" between sheets.

4.2 The One-Cut Phase

The one-cut solution to the quartic matrix model is very natural to consider. Some references where it has been studied in detail include [10, 16, 25, 49, 50, 57]. It is a Stokes phase that verifies the Boutroux conditions we laid out in section 3.3.2. Defining the potential

$$V(z) = \frac{1}{2}z^2 - \frac{\lambda}{4!}z^4\,, \tag{4.1}$$

we can derive the spectral curve using conditions (3.6) and (3.7) specified to a one-cut setup. It bears mentioning that this is the only situation where the asymptotic condition on the resolvent (3.7) is sufficient to fully determine the endpoints of the cuts. In multi-cut configurations the filling fractions need to be specified, which is why it is very rare to find an explicit solution to a multi-cut matrix model. Some cases, such as the $\mathbb{Z}_2$-symmetric two-cut quartic we will study below, are aided by symmetry, which automatically enforces

equal filling of the cuts. Going back to the one-cut phase, the spectral curve is found to be

$$y(z) = \left(1 - \frac{\lambda}{6}(z^2 + 2\alpha^2)\right)\sqrt{z^2 - 4\alpha^2}\,, \tag{4.2}$$

with a cut $\mathcal{C} = [-2\alpha, +2\alpha]$, and

$$\alpha^2(t) = \frac{1}{\lambda}\left(1 - \sqrt{1 - 2\lambda t}\right) \tag{4.3}$$

encoding all the dependence on the 't Hooft parameter t. The construction of the instanton sectors from a spectral geometry perspective, correctly portraying them as eigenvalue tunneling (or B-cycle instantons), was developed in [10] and [57] using different methods. The "differential" methods of [57] were generalized before in section 3.3. Physically we have a cut centered around the origin, and then two non-trivial saddles [1], one on either side of the cut. From the picture of the quartic model as, in general, a three-cut problem, this amounts to filling out the middle-cut and closing the other two. Instanton effects then naturally correspond to the opening of the other cuts, or in other words, to dragging eigenvalues from the cut to the top of the "hills". The instanton action is then cast as a cycle integral of the spectral curve, which can also be seen as measuring the difference in heights of the holomorphic effective potential. We refer the reader to [10, 57] for details. The instanton action is given by

$$A(t) = \frac{1}{2\lambda}\sqrt{3 - 3\lambda\alpha^2}\sqrt{3 - \lambda\alpha^2} - \frac{\alpha^2}{2}(2 - \lambda\alpha^2)\log\left[\frac{3 - 2\lambda\alpha^2 + \sqrt{3 - 3\lambda\alpha^2}\sqrt{3 - \lambda\alpha^2}}{\lambda^2\alpha^2}\right]. \tag{4.4}$$

The spectral curve methods are very useful to understand the origin of the nonperturbative effects, but not the most efficient in terms of computational power. Especially if we have in mind that we are looking to test large-order relations that require lots of data. But nevertheless, the computation of the instanton action, and of the one-instanton one-loop coefficient, as we showed for the $\mathbb{Z}_2$-symmetric setups above, are very important in the end. These are quantities that are also computed via orthogonal polynomials / transseries, so by checking that both calculations lead to the same result we have a guarantee that we are working with the right transseries expansion.

The calculation of large-order perturbative and nonperturbative data relies on the orthogonal polynomial method, and the central object is the string equation, which for the quartic potential takes the form

$$r_n\left(1 - \frac{\lambda}{6}\left(r_{n-1} + r_n + r_{n+1}\right)\right) = n\, g_s\,. \tag{4.5}$$

[1] These saddles satisfy the condition $M(z) = 1 - \frac{\lambda}{6}(z^2 + 2\alpha^2) = 0$.

We have already explained the procedure that follows in section 3.2.2, so we can jump straight to the main point. We work with a two-parameter transseries for the continuous version of r_n, $\mathcal{R}(x)$ [2],

$$\mathcal{R}(x) = \sum_{n=0}^{+\infty}\sum_{m=0}^{+\infty} \sigma_1^n \sigma_2^m \, \mathcal{R}^{(n|m)}(x)\,; \quad \mathcal{R}^{(n|m)}(x) \simeq \mathrm{e}^{-(n-m)A(x)/g_s} \sum_{g=\beta_{nm}}^{+\infty} g_s^g \, R_g^{(n|m)}(x)\,. \tag{4.6}$$

This ansatz is inserted into the string equation and solved iteratively for the coefficients $R_g^{(n|m)}$. Some equations are algebraic, others are differential, and there are also some nice features such as resonance which we will discuss below. For the purposes of chapter 6 we have solved the one-cut quartic matrix model with a one-parameter transseries [3], and results and further details are shown in Appendix A. We refer the reader to [25] for a more in-depth analysis of all these topics. Before moving on, we just recall that the one-cut quartic matrix model has a very interesting double-scaling limit when $t \to 1/2$. This corresponds to the endpoints of the cut colliding with the non-trivial saddles, and the critical model is described by the Painlevé I equation which we briefly discussed in the introduction. As we will see when we look at Painlevé II, obtained as a double-scaling limit of the two-cut quartic solution, these special points increase our computational ability dramatically. This is because the coefficients $R_g^{(n|m)}(x)$ become numbers, instead of functions. As a consequence, much more data can be extracted and higher instanton large-order relations can be tested (see [25] for very high instanton tests done for Painlevé I).

4.3 The Two-Cut Phase

Let us now address the quartic matrix model in its two-cut Stokes phase, starting with the matrix model partition function (3.2) with a quartic potential. We should begin by making a comment on the conventions. For practical reasons, this section will have different conventions for the quartic potential compared to the previous one. We are going to stick to the conventions of [1], which is to take

$$V(z) = -\frac{1}{2}z^2 + \frac{\lambda}{4!}z^4, \qquad \lambda > 0, \tag{4.7}$$

This way we avoid the risk of generating wrong or inconsistent results, and any transposition to different conventions will always be an obvious task [4]. We shall first fully work out its two-cut spectral geometry and use this data to obtain explicit formulae for all the nonper-

[2] We are leaving the logarithmic terms aside for now.

[3] In the two-parameter language this amounts to looking only at the $(n|0)$ slice.

[4] In practice, we need to take λ to $-\lambda$ and $z \to \mathrm{i}z$, so this moves the cuts to the imaginary axis. When dealing with orthogonal polynomials, or transseries, there is also a simple change in the string equations which would just imply a flipped sign $x \to -x$ in all results.

turbative quantities we addressed earlier in subsection 3.3.1. Then, we will use orthogonal polynomials and resurgent transseries in order to, on one hand, readdress the results of subsection 3.3.1, and, on the other hand, produce large-order data that will be used to test and confirm our overall nonperturbative picture.

Beginning with the spectral curve (3.5), it is simple to compute

$$M(z) = \frac{\lambda}{6} z \tag{4.8}$$

from (3.6), and the endpoints of the cuts follow from the asymptotic constraints (3.7) as

$$a^2 = \frac{6}{\lambda}\left(1 - \sqrt{\frac{2\lambda t}{3}}\right) \quad \text{and} \quad b^2 = \frac{6}{\lambda}\left(1 + \sqrt{\frac{2\lambda t}{3}}\right). \tag{4.9}$$

Integrating the spectral curve, the holomorphic effective potential (3.9) follows:

$$\begin{aligned} V_{\text{h;eff}}(z) = \frac{\lambda}{48}\Bigg\{ & \left(2z^2 - a^2 - b^2\right)\sqrt{\left(z^2 - a^2\right)\left(z^2 - b^2\right)} - \\ & - \left(b^2 - a^2\right)^2 \log\left(\frac{\sqrt{z^2 - a^2} + \sqrt{z^2 - b^2}}{\sqrt{b^2 - a^2}}\right)\Bigg\}. \end{aligned} \tag{4.10}$$

The real part of this potential is shown in figure 4.1 where the symmetric cuts and the pinched cycle are very clearly identifiable. Given this result, one may immediately compute the instanton action, with either (3.40) or (3.74), as

$$A(\lambda, t) = V_{\text{h;eff}}(0) - V_{\text{h;eff}}(a) = \frac{3}{2\lambda}\sqrt{1 - \frac{2\lambda t}{3}} - t \log\left(\frac{\sqrt{3} + \sqrt{3 - 2\lambda t}}{\sqrt{2\lambda t}}\right). \tag{4.11}$$

In its domain of validity, $0 < \lambda t < \frac{3}{2}$, this action is indeed real positive as expected.

Similarly to what was done in the one-cut case with the quartic matrix model [10, 25], one may now test all our nonperturbative formulae against large-order data in a simple and explicit example. Of course one first needs to generate the large-order data itself and, for the present two-cut scenario, the procedure will be slightly more involved than the one in [10, 25] (which, on what concerned the perturbative sector, was a simple extension of the pioneering work in [49]). Let us also stress that because this data precisely constructs the large N expansion in this phase, it will further confirm that it is in fact of 't Hooft type, *i.e.*, a Stokes phase. The analysis starts by addressing orthogonal polynomials in this model,

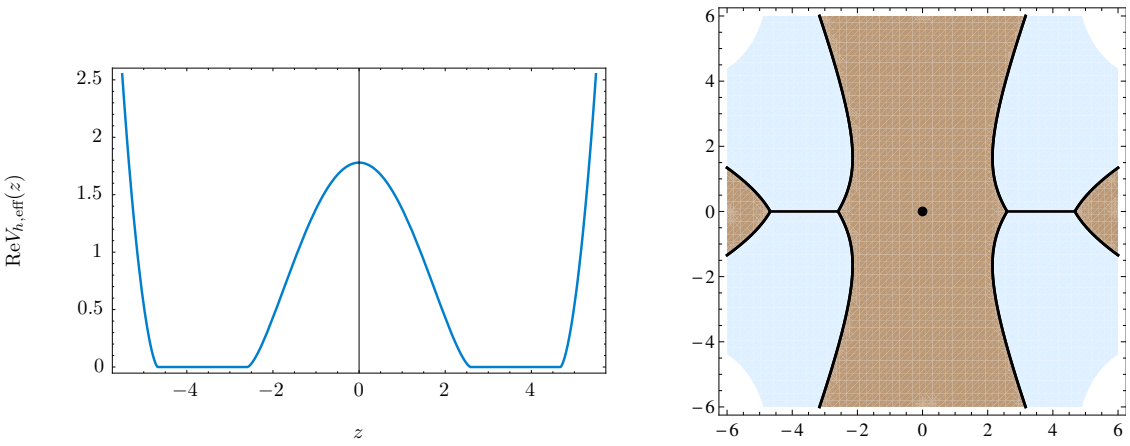

Figure 4.1: The real part of the holomorphic effective potential for the two-cut quartic matrix model, (4.10), both on the real axis (left) and on the complex plane (right), when $t = 1$ and $\lambda = 0.42$. The brown areas indicate when $\mathbb{R}\mathrm{e}\, V_{\mathrm{h;eff}}(z) > 0$ and the blue ones when $\mathbb{R}\mathrm{e}\, V_{\mathrm{h;eff}}(z) < 0$. The horizontal black lines are precisely the cuts of the spectral curve and the black dot the pinched cycle.

whose string equation (3.16) is currently written as

$$r_n \left\{ -1 + \frac{\lambda}{6} \left(r_{n-1} + r_n + r_{n+1} \right) \right\} = n g_s. \tag{4.12}$$

Recall from our review in subsection 3.2.2 that, in the one-cut case, the recursion coefficients r_n approach a single function $\mathcal{R}(x)$ with genus expansion (3.19) in its perturbative sector. This function satisfies a finite difference equation, (3.18), which was solved using resurgent transseries in [16, 25]. The key point here is that transseries solutions allow for an inclusion of *all* multi-instanton sectors, as we briefly mentioned in (3.24), going beyond the usual large N expansion. Furthermore, the free energy follows as (3.21). This time around, with two cuts, as we discussed previously and plotted in figure 3.3, a numerical solution of the above recursive equation (4.12), approaches, in the large N limit, *two* distinct functions. Thus, what one now has to do is to generalize the aforementioned framework into a period two *ansatz*, as first suggested in [118, 119, 122, 133]. As such, we shall consider

$$r_n \;\to\; \mathcal{P}(x), \qquad n \text{ even}, \tag{4.13}$$

$$r_n \;\to\; \mathcal{Q}(x), \qquad n \text{ odd}. \tag{4.14}$$

In this case, the large N limit of our recursion (4.12) will split into two coupled equations

$$\mathcal{P}(x)\left\{-1+\frac{\lambda}{6}\left(\mathcal{Q}(x-g_s)+\mathcal{P}(x)+\mathcal{Q}(x+g_s)\right)\right\} = x, \tag{4.15}$$

$$\mathcal{Q}(x)\left\{-1+\frac{\lambda}{6}\left(\mathcal{P}(x-g_s)+\mathcal{Q}(x)+\mathcal{P}(x+g_s)\right)\right\} = x, \tag{4.16}$$

and these are the equations we wish to solve via transseries methods, following the work in [25].

Two-Parameter Transseries Solution to the String Equations

In [1] we solve the string equations, (4.15) and (4.16), in small steps, starting with a perturbative expansion, then looking at a one-parameter transseries, and finally looking at a two-parameter transseries. But given everything we have discussed up to now, we can start immediately with the two-parameter transseries similar to (4.6)

$$\mathcal{P}(x)=\sum_{n=0}^{+\infty}\sum_{m=0}^{+\infty}\sigma_1^n\sigma_2^m\,\mathcal{P}^{(n|m)}(x), \qquad \mathcal{Q}(x)=\sum_{n=0}^{+\infty}\sum_{m=0}^{+\infty}\sigma_1^n\sigma_2^m\,\mathcal{Q}^{(n|m)}(x), \tag{4.17}$$

where each $P^{(n|m)}(x)$ sector (and similarly for $Q^{(n|m)}(x)$) has an expansion of the form [5]

$$\mathcal{P}^{(n|m)}(x)\simeq \mathrm{e}^{-(n-m)A(x)/g_s}\sum_{g=\beta_{nm}}^{+\infty} g_s^g\,P_g^{(n|m)}(x). \tag{4.18}$$

We are of course assuming that $\mathcal{P}(x)$ and $\mathcal{Q}(x)$ have the same type of expansion, particularly that they have the same instanton action, but this is essentially forced by the equations. If they had different transseries structures the equations would decouple and become trivial. At the same time, we will compute the perturbative sectors of both $\mathcal{P}(x)$ and $\mathcal{Q}(x)$ and later check that they are governed by the same instanton action, thus justifying our assumption *a posteriori*. Looking at the perturbative sector, recall that we have expansions in g_s^2,

$$\mathcal{P}^{(0|0)}(x)\simeq\sum_{g=0}^{+\infty} g_s^{2g}P_{2g}^{(0|0)}(x), \qquad \mathcal{Q}^{(0|0)}(x)\simeq\sum_{g=0}^{+\infty} g_s^{2g}Q_{2g}^{(0|0)}(x). \tag{4.19}$$

[5] It will not be relevant for the examples shown here, but in general $\beta_{nm}=-\min(m,n)$.

At genus zero, for instance, it is then simple to obtain

$$P_0^{(0|0)}(x) = \frac{3}{\lambda}\left(1-\sqrt{1-\frac{2\lambda x}{3}}\right), \tag{4.20}$$

$$Q_0^{(0|0)}(x) = \frac{3}{\lambda}\left(1+\sqrt{1-\frac{2\lambda x}{3}}\right), \tag{4.21}$$

where we have assumed that $\mathcal{P} \neq \mathcal{Q}$, *i.e.*, explicitly imposed the period-two *ansatz* [119, 122, 133]. In the domain of validity of the two-cut phase, $0 < \lambda x < \frac{3}{2}$, this in fact corresponds to two distinct (real) functions which meet at the (critical) point $\lambda x = \frac{3}{2}$, where $P_0^{(0|0)} = \frac{3}{\lambda} = Q_0^{(0|0)}$. Beyond the perturbative level, we can look at (4.15) and (4.16) at order $\sigma_1^1\,\sigma_2^0\,g_s^0$ to find an equation for the instanton action,

$$\cosh^2\left(A'(x)\right) = \frac{3}{2\lambda x}. \tag{4.22}$$

Notice that there are four sign ambiguities in this equation: two from the quadratic power and two from the (even) hyperbolic cosine function. For the moment we shall assume the quadratic sign ambiguity arises as an artifact of the period-two *ansatz*, and thus only address the $\cosh z$ sign ambiguity (which is now equivalent to the one in the one-cut case [16, 25]), leaving the complete exploration of the four sign ambiguities for future work. In this case one obtains for the instanton action:

$$A(x) = \pm\frac{\sqrt{9-6\lambda x}}{2\lambda} \mp x\,\operatorname{arccosh}\left(\sqrt{\frac{3}{2\lambda x}}\right) + 2\pi\mathrm{i}\,x\,p + c_{\text{int}}, \tag{4.23}$$

where $p \in \mathbb{Z}$. We shall set both the integer ambiguity p and the integration constant c_{int} to zero so that later this result will yield the Painlevé II instanton action, in the corresponding double-scaling limit. As for the sign ambiguity, notice that choosing the upper sign makes this expression precisely match the instanton action as computed via spectral geometry methods, (4.11).

In general, as one plugs the expansions (4.17) back into the string equations, (4.15) and (4.16), one can equate the terms with given powers σ_1^n and σ_2^m and find the following two

coupled equations

$$x\,\delta_{n0}\,\delta_{m0} \;=\; -\mathcal{P}^{(n|m)}(x) + \tag{4.24}$$
$$+\frac{\lambda}{6}\sum_{n_1=0}^{n}\sum_{m_1=0}^{m}\mathcal{P}^{(n_1|m_1)}(x)\left\{\mathcal{Q}^{(n-n_1|m-m_1)}(x-g_s)+\mathcal{P}^{(n-n_1|m-m_1)}(x)+\mathcal{Q}^{(n-n_1|m-m_1)}(x+g_s)\right\},$$
$$x\,\delta_{n0}\,\delta_{m0} \;=\; -\mathcal{Q}^{(n|m)}(x) + \tag{4.25}$$
$$+\frac{\lambda}{6}\sum_{n_1=0}^{n}\sum_{m_1=0}^{m}\mathcal{Q}^{(n_1|m_1)}(x)\left\{\mathcal{P}^{(n-n_1|m-m_1)}(x-g_s)+\mathcal{Q}^{(n-n_1|m-m_1)}(x)+\mathcal{P}^{(n-n_1|m-m_1)}(x+g_s)\right\}.$$

If one next expands these equations in powers of the string coupling, g_s, this will produce – at each order – systems of either algebraic or (linear) differential equations which allow us to find the coefficients $P_g^{(n|m)}(x)$ and $Q_g^{(n|m)}(x)$ in terms of the "earlier" ones $P_{g'}^{(n'|m')}(x)$ and $Q_{g'}^{(n'|m')}(z)$ with $n'\leq n$, $m'\leq m$ and $g'\leq g$ (and their derivatives). As a technical aside, let us also note that the many exponentials appearing in (4.24) and (4.25) via (4.18) will bring down extra powers of the string coupling. In fact, we shall always have in mind the following expansions:

$$\exp\left(-n\,\frac{A(x\pm g_s)}{g_s}\right)=\exp\left(-n\,\frac{A(x)}{g_s}\right)\times \mathrm{e}^{\mp nA'(x)}\sum_{\ell'=0}^{+\infty}\frac{1}{\ell'!}\left(-n\sum_{\ell=2}^{+\infty}(\pm 1)^{\ell}\,g_s^{\ell-1}\,\frac{A^{(\ell)}(x)}{\ell!}\right)^{\ell'}. \tag{4.26}$$

From here on, the extraction of the $P_g^{(n|m)}$ and $Q_g^{(n|m)}$ coefficients is absolutely straightforward with the help of a computer, very much in line with the strategy used in [25]. Most of our explicit results are collected in appendix B, but for completeness we next discuss a couple of examples. First of all, we are going to make a smart choice of variables and re-define the leading perturbative coefficients as

$$P_0^{(0|0)}(x) \;=\; \frac{3-\sqrt{9-6\lambda x}}{\lambda}\equiv\frac{3-p}{\lambda}, \tag{4.27}$$
$$Q_0^{(0|0)}(x) \;=\; \frac{3+\sqrt{9-6\lambda x}}{\lambda}\equiv\frac{3+p}{\lambda}. \tag{4.28}$$

Here we have defined $p\equiv\sqrt{9-6\lambda x}$, as rewriting and solving most equations in terms of this variable will make life much easier. The remaining perturbative coefficients are recursively obtained from algebraic equations and this is generically the case for most of the $(n|m)$ sectors (see the appendix B for further details and explicit expressions).

One exception to the aforementioned straightforward algebraic procedure is when $n=m\pm 1$. In this case one finds the phenomenon of resonance, also discussed in the present context in [25, 103], and one needs to solve a (linear) differential equation instead. Let us

illustrate this situation in the one-instanton sector $(1|0)$. One finds, at order g_s^0,

$$P_0^{(1|0)} + \frac{3-p}{3}\cosh\left(A'(x)\right) Q_0^{(1|0)} = 0, \tag{4.29}$$

$$Q_0^{(1|0)} + \frac{3+p}{3}\cosh\left(A'(x)\right) P_0^{(1|0)} = 0. \tag{4.30}$$

These two equations do not allow us to solve for both $P_0^{(1|0)}$ and $Q_0^{(1|0)}$, but only for their ratio $P_0^{(1|0)}/Q_0^{(1|0)}$. On the other hand, eliminating $P_0^{(1|0)}$ and $Q_0^{(1|0)}$, one may instead find a differential equation for the instanton action – which we have solved earlier in (4.23). Proceeding to next order, g_s^1, the equations read[6]

$$P_1^{(1|0)} + \frac{(3-p)\,p}{9\lambda}\sinh\left(A'\right) Q_0^{(1|0)\prime} + \frac{3-p}{6}\cosh\left(A'\right)\left(2Q_1^{(1|0)} - Q_0^{(1|0)} A''\right) = 0, \tag{4.31}$$

$$Q_1^{(1|0)} + \frac{(3+p)\,p}{9\lambda}\sinh\left(A'\right) P_0^{(1|0)\prime} + \frac{3+p}{6}\cosh\left(A'\right)\left(2P_1^{(1|0)} - P_0^{(1|0)} A''\right) = 0. \tag{4.32}$$

The situation is the same as in the $(1|0)$ sector at order g_s^0. All we can now do is to eliminate the ratio $P_1^{(1|0)}/Q_1^{(1|0)}$ and use our knowledge of the lower sectors – namely the relation between $P_0^{(1|0)}$ and $Q_0^{(1|0)}$, and the result for the instanton action – in order to obtain a linear differential equation yielding

$$Q_0^{(1|0)} = \sqrt{\frac{3+p}{p}} \qquad \text{and} \qquad P_0^{(1|0)} = -\sqrt{\frac{3-p}{p}}. \tag{4.33}$$

These examples show a feature which is characteristic of resonance and of the $n = m \pm 1$ sectors, namely, that the equations we obtain at order g_s^k produce differential equations whose solutions yield the instanton coefficients at order $k-1$. At this stage the reader may object that the differential equations alone are not enough if one does not specify boundary conditions. In fact, all integration constants involved in this procedure must be fixed by using data available in the double-scaling limit and we shall postpone that discussion for the next section (although we have already used this fact in fixing the integration constants in (4.33) above).

Other interesting features appear in the higher multi-instanton sectors, and many of these were first uncovered in the one-cut example studied in [25]. For example starting in the $(2|1)$ sector, logarithms make their appearance into the game and they recursively propagate to the ensuing higher sectors. Akin to what happened in [25], these logarithms are indeed expected in the construction of the transseries solution and, again, we shall further discuss

[6] Notice that these equations involve derivatives of $P_0^{(1|0)}(x)$ and $Q_0^{(1|0)}(x)$. All derivatives are with respect to x, so Jacobians need to be included when switching to the new variable p.

this issue in the next section, within the analysis of the Painlevé II equation. Another interesting feature happens when $n = m$ (and the exponential term cancels). In this case, we find that all the coefficients $P_g^{(n|n)}$ (respectively Q) with *odd* g vanish, and the perturbative expansion in (4.18) contains only powers of g_s^2, *i.e.*, it is an expansion in the *closed* string coupling. As aforementioned, further data is presented in appendix B, where we also find general patterns for the multi-instanton coefficients and relate the logarithmic sectors with the non-logarithmic ones.

The Nonperturbative Free Energy and Large-order Analysis

In order to test the multi-instanton results obtained in section 3.3, one needs to match them against the large-order behavior of the free energy, and this is what we shall now address. As such, we will derive the nonperturbative free energy of the two-cut quartic matrix model out of the transseries solution to the string equations (4.15) and (4.16) we have just obtained, even though we will not be interested in extracting as much data. For this we assume that the free energy has a similar two-parameter transseries

$$\mathcal{F}(t) = \sum_{n=0}^{+\infty} \sum_{m=0}^{+\infty} \sigma_1^n \sigma_2^m \, \mathcal{F}^{(n|m)}(t) \, ; \quad \mathcal{F}^{(n|m)}(x) \simeq \mathrm{e}^{-(n-m)A(t)/g_s} \sum_{g=\beta^{\mathcal{F}}_{nm}}^{+\infty} g_s^g \, \mathcal{F}_g^{(n|m)}(t) \, . \tag{4.34}$$

The starting point in this construction is expression (3.14), which yields the partition function in terms of the orthogonal-polynomial recursion coefficients r_n. Since in the present configuration these recursion coefficients split into two different branches at large N, it is useful to first rewrite (3.14) for $2N$ eigenvalues (and thus with 't Hooft coupling $t = 2Ng_s$) as

$$Z = h_0^{2N} \prod_{i=1}^{2N} r_i^{2N-i} = h_0^{2N} \prod_{i=1}^{N} r_{2i}^{2N-2i} \prod_{j=1}^{N} r_{2j-1}^{2N-(2j-1)} . \tag{4.35}$$

Similarly to what was done in (3.17), the free energy follows by taking the logarithm of the above expression (and normalizing against the Gaussian weight, as usual). One finds:

$$\mathcal{F} = \frac{t}{g_s} \log \frac{h_0}{h_0^{\mathrm{G}}} + \frac{t^2}{g_s^2} \frac{1}{2N} \sum_{n=1}^{N} \left(1 - \frac{n}{N}\right) \log \frac{r_{2n}}{r_{2n}^{\mathrm{G}}} + \frac{t^2}{g_s^2} \frac{1}{2N} \sum_{n=1}^{N} \left(1 - \frac{n-\frac{1}{2}}{N}\right) \log \frac{r_{2n-1}}{r_{2n-1}^{\mathrm{G}}} . \tag{4.36}$$

It is now clear the reason why we rewrote the partition function (3.14) as (4.35) above: because of the even/odd split in (4.13) and (4.14), the large N limit of (4.36) will precisely construct the free energy out of $\mathcal{P}(x)$ and $\mathcal{Q}(x)$. In the continuum limit the first sum in (4.36), which we will denote by the "even" sum, is essentially the same as the sum in (3.17) and thus may be computed via the Euler-Maclaurin formula (3.20). The second sum in (4.36), the "odd" sum, is a bit more subtle and requires slight modifications. In fact, from (4.28),

recall that $\lim_{x\to 0} Q_0^{(0|0)}(x) \neq 0$ making $Q_0^{(0|0)}(x)/x$ ill-defined at the origin (alongside with its derivatives), but this problem is solved by simply considering the Gaussian contribution separately in the "odd" sector. Furthermore, the "odd" Euler-Maclaurin formula is now written as (following a similar analysis in [134])

$$\lim_{N\to+\infty} \frac{1}{N}\sum_{n=1}^{N} \Phi\left(\frac{n-\frac{1}{2}}{N}\right) \simeq \int_0^1 \mathrm{d}\xi\, \Phi(\xi) - \sum_{k=1}^{+\infty} \frac{1}{N^{2k}} \frac{\left(1-2^{1-2k}\right) B_{2k}}{(2k)!} \Phi^{(2k-1)}(\xi)\Big|_{\xi=0}^{\xi=1}. \quad (4.37)$$

Assembling all contributions together, our formula for the free energy finally takes a familiar form [16, 49, 50]

$$\begin{aligned}\mathcal{F}(t) \;\simeq\; & \frac{t}{2g_s}\left(2\log\frac{h_0}{h_0^{\mathrm{G}}} - \log\frac{\mathcal{P}(x)}{x}\Big|_{x=0}\right) + \frac{1}{g_s^2}\,\mathfrak{G}(t,g_s) + \frac{1}{2g_s^2}\int_0^t \mathrm{d}x\,(t-x)\log\frac{\mathcal{P}(x)}{x} + \\ & + \frac{1}{2g_s^2}\int_0^t \mathrm{d}x\,(t-x)\log\mathcal{Q}(x) + \frac{1}{2}\sum_{g=1}^{+\infty} g_s^{2g-2}\,\frac{2^{2g}\,B_{2g}}{(2g)!}\,\frac{\mathrm{d}^{2g-1}}{\mathrm{d}x^{2g-1}}\left[(t-x)\log\frac{\mathcal{P}(x)}{x}\right]\Big|_{x=0}^{x=t} - \\ & - \frac{1}{2}\sum_{g=1}^{+\infty} g_s^{2g-2}\,\frac{(2^{2g}-2)\,B_{2g}}{(2g)!}\,\frac{\mathrm{d}^{2g-1}}{\mathrm{d}x^{2g-1}}\left[(t-x)\log\mathcal{Q}(x)\right]\Big|_{x=0}^{x=t}. \end{aligned} \quad (4.38)$$

The function $\mathfrak{G}(t,g_s)$ comes from the Gaussian normalization in the "odd" part and is given by

$$\mathfrak{G}(t,g_s) \equiv -\sum_{k=1}^{N} (2N-2i+1)\log\left((2i-1)\,g_s\right). \quad (4.39)$$

When computing the free energy, this expression may be first evaluated exactly and then expanded in powers of the string coupling.

Let us note that while at the perturbative level, *i.e.*, when $n = 0 = m$, the Euler-Maclaurin recipe (4.38) is an efficient way to produce large-order data, the same is not valid when addressing the (generalized) multi-instanton sectors (more on this next). In any case, using the expansions (4.18) when $n = 0 = m$ (which we have described how to compute in the paragraphs above, and whose data we have presented in appendix B) and inserting them into a *Mathematica* script encoding the Euler-Maclaurin expansion, we have computed the coefficients $\mathcal{F}_g^{(0|0)}$ in the perturbative free energy of the $\mathbb{Z}_2$-symmetric two-cut quartic matrix model up to genus $g = 20$ and some partial results are presented in greater detail in appendix C.

In order to obtain data concerning the higher instanton sectors in an effective way, and while remaining within the orthogonal polynomial framework, one uses a small trick due to [16]. Starting off with the partition function, written as either (3.14) or (4.35), it is simple to show that (subscripts in the partition function indicate the total number of eigenvalues

considered)

$$\frac{Z_{2(N+1)}\,Z_{2(N-1)}}{Z_{2N}^2} = r_{2N+1}\,r_{2N}^2\,r_{2N-1}, \tag{4.40}$$

which, at the free energy level, may be written as

$$\mathcal{F}(t+2g_s) - 2\mathcal{F}(t) + \mathcal{F}(t-2g_s) = \log\left(\mathcal{Q}\left(t+g_s\right)\mathcal{P}^2\left(t\right)\mathcal{Q}\left(t-g_s\right)\right). \tag{4.41}$$

This expression is, in fact, a rewriting of the Euler-Maclaurin formula (4.38), but from a computational point-of-view it also makes it much easier to extract large-order data.

We may now finally address tests of our multi-instanton formulae using large-order analysis, and further compute Stokes coefficients for the problem at hand. The main quantity we wish to focus upon is the one-instanton, one-loop coefficient $\mathcal{F}_0^{(1|0)}$. At this stage, its calculation is simple if we are to use (4.41) above: all one has to do is to plug in two-parameter transseries *ansätze* for all quantities and it quickly follows that, for $n=1$, $m=0$ and at order g_s^0, one has

$$4\sinh^2\left(A'(x)\right)\mathcal{F}_0^{(1|0)} = 2\left(\frac{P_0^{(1|0)}(x)}{P_0^{(0|0)}(x)} + \cosh\left(A'(x)\right)\frac{Q_0^{(1|0)}(x)}{Q_0^{(0|0)}(x)}\right). \tag{4.42}$$

If we plug in our results for the perturbative contributions, (4.27) and (4.28), for the one-instanton contributions, (4.33), and for the instanton action, (4.23), we finally obtain

$$\mathcal{F}_0^{(1|0)} = -\frac{\lambda}{2}\sqrt{\frac{3-p}{p^3}}. \tag{4.43}$$

As we have discussed in detail in 3.2.3, a key point about this quantity is that it controls the leading large-order growth of the asymptotic perturbative expansion, as explicitly shown in (3.33). For completeness, let us just recall that expression in here:

$$\mathcal{F}_g^{(0|0)} \sim \frac{S_1^{(0)}}{\mathrm{i}\pi}\frac{\Gamma\left(2g+b\right)}{A^{2g+b}}\left\{\mathcal{F}_0^{(1|0)} + \frac{A}{2g+b-1}\,\mathcal{F}_1^{(1|0)} + \cdots\right\}. \tag{4.44}$$

Many large-order tests may now be carried out; let us here mention a few of those following [10] (but, let us note, many more higher-precision tests may be carried through, as in [25], and these we leave for future work). One obvious test concerns the instanton action, which may be numerically extracted from the sequence:

$$\alpha_g^{(\mathcal{F})} = \frac{\mathcal{F}_{g+1}^{(0|0)}}{4g^2\mathcal{F}_g^{(0|0)}} \sim \frac{1}{A^2}\left(1 + \frac{2b+1}{2g} + \cdots\right). \tag{4.45}$$

The parameter b will be equal to $-5/2$, but that can be tested as well, *e.g.*, using the

sequence:

$$b \sim \frac{1}{2}\left(2g\left(A^2\alpha_g^{(\mathcal{F})}-1\right)-1\right)+\cdots . \tag{4.46}$$

Finally, one approach to testing the one-loop coefficient is to use the sequence:

$$\beta_g^{(\mathcal{F})} = \frac{\mathrm{i}\pi}{S_1^{(0)}}\frac{A^{2g+b}\,\mathcal{F}_g^{(0|0)}}{\Gamma\left(2g+b\right)} \sim \mathcal{F}_0^{(1|0)}+\cdots . \tag{4.47}$$

We should note that all sequences above have been built with free energy quantities but, of course, one may also perform the exact analogue large-order tests directly using the solutions to the string equations, $\mathcal{P}(x)$ and $\mathcal{Q}(x)$. In fact, all these quantities have their large-order behavior dictated by the very same instanton action[7] and, as such, we shall use either $\mathcal{P}(x)$ or $\mathcal{Q}(x)$ whenever possible as we have obtained far more large-order data for these quantities than for the free energy. We shall denote those corresponding sequences with the respective superscript. We also note that all these quantities have "closed string" expansions (*i.e.*, in powers of g_s^2) in their $(0|0)$ sectors, so the sequences above are tested for *even* g.

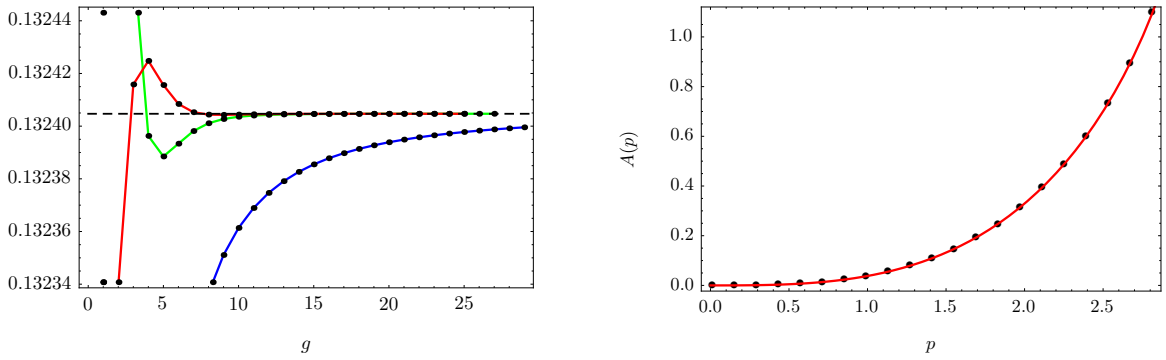

Figure 4.2: The first image depicts a test of the instanton action using the sequence $\alpha_g^{(\mathcal{P})}$ and its first Richardson transforms, when $\lambda = 0.5$ and $p = 1.2$. The large-order convergence towards the correct result is clear (the dashed horizontal line is the analytical prediction), with an error of $10^{-6}\%$ after just four Richardson transforms. The second image shows a test of the instanton action at fixed $\lambda = 1$ but with varying p, after implementing four Richardson transforms. Large-order data makes up the dots, while the analytical prediction is given as the solid red line. Again, the match is extremely clear.

The first natural test to do concerns the instanton action, which is shown in figure 4.2. Clearly, there is a very strong agreement between the "theoretical" prediction (be it from either saddle-point (4.11) or transseries (4.23) approaches) and the "numerical" data. On the

[7] This was previously shown via the string equations, but we also checked it numerically to very high precision.

left of figure 4.2 we have plotted data at a particular point in moduli space[8], namely, $\lambda = 0.5$ and $p = 1.2$, concerning the sequence $\alpha_g^{(\mathcal{P})}$ and its first sequential Richardson extrapolations (see, *e.g.*, [10] for a short discussion of Richardson transforms and their role in accelerating the convergence of a given sequence, within the present matrix model context). That the large-order data approaches the analytic prediction is very clear: after just four Richardson transforms the error is already of the order $10^{-6}\%$ at genus $g = 60$. On the right of figure 4.2 we have fixed $\lambda = 1$ but vary p over its full range. Once again we check that the numerical data (the black dots in the figure), after just four Richardson transforms, is never further than $10^{-6}\%$ away from the analytical prediction (the solid red line), thus fully validating our results.

As we move on to testing the one-instanton, one-loop coefficient, it is important to first recall that the transseries framework only predicts large-order behavior up to the Stokes factors – in this case up to the Stokes factor $S_1^{(0)}$, see (4.44). However, we also have computed the same quantity via spectral curve analysis (3.89) (this was one of the main results in section 3.3.1) and, following [10, 16, 25], the spectral curve result should provide for the full answer, Stokes factor included. Consequently, the calculation of $S_1^{(0)}\, F_0^{(1|0)}$ in (3.89) and the calculation of $F_0^{(1|0)}$ in (4.43) combine to predict the Stokes parameter as

$$S_1^{(0)} = -\mathrm{i}\sqrt{\frac{6}{\pi\lambda}}. \tag{4.48}$$

It is quite interesting to compare the result for this "simplest" Stokes constant (at least that one constant which may be analytically computed from saddle-point analysis), in the present two-cut configuration, with the analogue Stokes constant for the one-cut configuration in [16, 25]. For the quartic matrix model one thus finds:

$$S_1^{(0)}\Big|_{\text{two-cut}} = -\sqrt{2}\, S_1^{(0)}\Big|_{\text{one-cut}}. \tag{4.49}$$

With the knowledge of this Stokes constant (which we should more properly denote by $S_1^{(0)\mathcal{F}}$ since it refers to the free energy), we can proceed to test the relation (4.47) for the sequence β_g. Since besides the free energy the quantities $\mathcal{P}(x)$ and $\mathcal{Q}(x)$ also obey a relation similar to (4.47), a natural question to ask is whether the Stokes constant for these different quantities is the same. Indeed we find that it is the case, namely that

$$S_1^{(0)\mathcal{F}} = S_1^{(0)\mathcal{P}} = S_1^{(0)\mathcal{Q}} \equiv S_1^{(0)}. \tag{4.50}$$

This is to say that, when testing the asymptotic relation (4.47) for either $\beta_g^{(\mathcal{P})}$, $\beta_g^{(\mathcal{Q})}$ or $\beta_g^{(\mathcal{F})}$, we find that the relation holds to very high accuracy with the Stokes constants being the same in all three cases. On the other hand, the value of b is different, with $b = -1/2$ for

[8] Recall the domain of validity of the two-cut Stokes phase, $0 < \lambda x < \frac{3}{2}$, or, equivalently, $0 < p < 3$.

$\beta_g^{(\mathcal{P})}$ and $\beta_g^{(\mathcal{Q})}$ and $b = -5/2$ for $\beta_g^{(\mathcal{F})}$ (see [25] for a discussion of this point). With this knowledge, we have tested our instanton predictions with the sequences $\beta_g^{(\mathcal{P},\mathcal{Q})}$, finding that the numerical data has an error smaller than $10^{-5}\%$ at genus $g = 60$ as compared to the analytical prediction for $S_1^{(0)} P_0^{(1|0)}$ (or Q), within most of the allowed range for λ and the variable p. Note, however, that $P_0^{(1|0)}$ (and also Q) diverges as one approaches $p \to 0$, making the convergence of numerical data to analytical prediction naturally a bit worse once we get too close to $p = 0$. These results are illustrated in figure 4.3. On the left of this figure we have fixed $\lambda = 0.5$ and $p = 1.5$, and plotted the sequence $\beta_g^{(\mathcal{P})}$ alongside with its Richardson transforms. It is again very clear how the data approaches the analytical prediction (the horizontal dashed line). On the right of figure 4.3 we have fixed $\lambda = 1$ and changed p over its full range, plotting the fourth Richardson transform of the sequence $\beta_g^{(\mathcal{P})}$ (black dots) and the analytical prediction (solid red line). The agreement is, once again, evident. Let us mention that the very same tests may also be carried out for the free energy. In this case, we find an equally conclusive agreement, albeit with a smaller accuracy ($10^{-3}\%$) as we have less large-order data available.

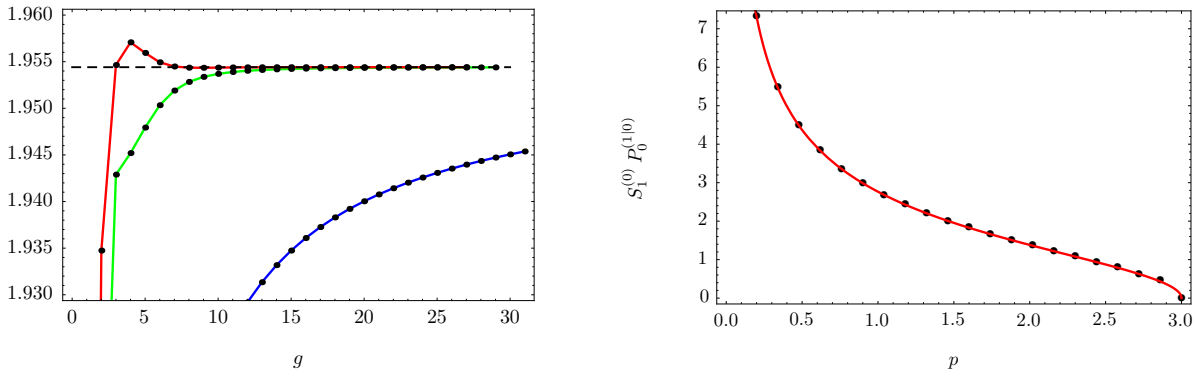

Figure 4.3: The first image depicts a test of the one-instanton, one-loop coefficient using the sequence $\beta_g^{(\mathcal{P})}$ and its first Richardson transforms, when $\lambda = 0.5$ and $p = 1.5$. The large-order convergence towards the correct result is clear (the dashed horizontal line is the analytical prediction), with an error of the order of $10^{-6}\%$. The second image shows a test of the one-instanton, one-loop coefficient at fixed $\lambda = 1$ but with varying p over its full range, after implementing just four Richardson transforms on the sequence $\beta_g^{(\mathcal{P})}$. Large-order data makes up the dots, while the analytical prediction is given as the solid red line. As in previous cases, the agreement is extremely clear.

At this stage one could proceed along the lines in [25] and test both multi-instanton formulae as well as the validity of generalized multi-instanton sectors appearing via our resurgence formulae. This would involve techniques of Borel-Padé resummation and, as such, within the context of the two-cut Stokes phase of the quartic matrix model, we shall leave these precision tests for future work. Do notice that we shall, nonetheless, test the

validity of our multi-instanton formulae in the double-scaling limit towards the Painlevé II equation in a following section.

4.4 Asymptotics of Instantons in the Painlevé II Equation

The analysis in the previous section allowed us to check the validity of our one-instanton results, for the Stokes phase of two distinct multi-cut models. In particular, we have checked both the instanton action (3.74) and the one-loop one-instanton coefficient (3.89), predicted in section 3.3, to very high precision. But our saddle-point analysis also yields multi-instanton results, as for instance in (3.87), and the general structure of resurgent transseries solutions further predicts many, new, generalized multi-instanton sectors, as discussed in subsection 3.2.3. As such, we would now like to check all this multi-instantonic structure, and we shall do so within the context of 2d supergravity, or type 0B string theory, by analyzing the Painlevé II equation. This equation arises as a double-scaling limit from the two-cut quartic matrix model we have previously analyzed, but is simpler to analyze from a numerical point-of-view than the full off-critical matrix model.

4.4.1 Painlevé II and Resurgent Transseries

Recalling the discussions in subsections 3.3.2 and 4.3, it should be obvious that the two-cut quartic matrix model has a natural critical point. This is cleary depicted in figure 3.3, which shows a critical point for the recursion coefficients at $\lambda t = 3/2$. At this point a phase transition takes place, from the two-cut phase to an unstable one-cut phase. In the double-scaling limit, this critical point is precisely described by the Painlevé II equation. At the critical point, and referring to figure 4.1, the two cuts collide with each other, having the non-trivial saddle for the eigenvalue instantons at this collision point. In practice what this means is that the smaller endpoints of the cuts will vanish, with $a \to 0$ (and with the non-trivial saddle kept fixed at the origin, $x_0 = 0$). In terms of λ, t and g_s, the double-scaling limit is defined as

$$g_s \to 0, \qquad \lambda \to \lambda_{\rm c} = \frac{3}{2}, \qquad t \to 1, \tag{4.51}$$

with the variable

$$z = (1-t)\, g_s^{-\frac{2}{3}} \tag{4.52}$$

kept fixed in this limit. As mentioned, it is known that in this limit the matrix model describes 2d supergravity or type 0B minimal superstrings, see, *e.g.*, [127, 129, 130, 132, 135], and that the physics is encoded in the Painlevé II equation. This differential equation precisely appears as we take the double-scaling limit in the string equations (4.15) and (4.16), as discussed in, *e.g.*, [127, 133]. Let us quickly review this point, following [101], as

this will also be important as we connect transseries solutions off and at criticality: start with the string equations (4.15) and (4.16), and introduce scaling *ansätze* for both $P(x)$ and $Q(x)$ [127]

$$P(x) \rightarrow 2\left(1 - g_s^{1/3}\, u(z) + g_s^{2/3}\, v(z)\right), \tag{4.53}$$
$$Q(x) \rightarrow 2\left(1 + g_s^{1/3}\, u(z) + g_s^{2/3}\, v(z)\right). \tag{4.54}$$

Plugging these expressions into (an appropriate rewriting of) the string equations, it is simple to obtain in the double-scaling limit

$$4u(z)v(z) - 2u''(z) = 0, \tag{4.55}$$
$$2u^2(z) - 8v(z) - 2z = 0. \tag{4.56}$$

The first equation is readily solved for $v(z)$ which may then be replaced in the second one. As such, one finally obtains a second-order differential equation for $u(z)$,

$$2u''(z) - u^3(z) + z\, u(z) = 0. \tag{4.57}$$

The equation above is the Painlevé II equation in the normalization used in, *e.g.*, [132, 135]. We are using a slightly different normalization, which follows with a simple rescaling of u and z as $u \to 2^{1/3}\, u$ and $z \to 2^{2/3}\, z$. Then the Painlevé II equation becomes

$$u''(z) - 2u^3(z) + 2z\, u(z) = 0\,, \tag{4.58}$$

which, in particular, also matches the normalization used in [16]. The perturbative solution corresponds to an expansion around $z \sim +\infty$ where one has $u_{\text{pert}}(z) \sim \sqrt{z}$.

From here on, the procedure to compute the resurgent transseries solution to the Painlevé II equation (4.58) follows in parallel, step by step, with what was done in [25]. The one-parameter transseries solution to (4.58) was addressed in [16], from where we recall the following points. First, the perturbative solution to (4.58) yields

$$x = z^{-3/2} \tag{4.59}$$

as the *open* string coupling. In this case, one may immediately write down an one-parameter transseries solution to the Painlevé II equation of the form [16, 25]

$$u(x) \simeq x^{-1/3} \sum_{n=0}^{+\infty} \sigma^n\, \mathrm{e}^{-nA/x}\, x^{n\beta} \sum_{g=0}^{+\infty} u_g^{(n)}\, x^g, \tag{4.60}$$

where A is the instanton action and β a characteristic exponent. Then, plugging this ex-

pression back into the Painlevé II equation, a solution of this form exists if

$$A = \pm\frac{4}{3}, \qquad \beta = \frac{1}{2}. \tag{4.61}$$

As discussed in [25, 103] and earlier in this dissertation, when building nonperturbative solutions with transseries it is important to take into consideration all possible values of the instanton action – in fact, via resurgence, deep in the asymptotics of the solution one will find the need for *both* signs, and thus the need for the two-parameter transseries *ansatz*. As such, we shall now focus on the two-parameter case (but we will also recover some of the results in [16] along the way).

Let us begin by writing the Painlevé II equation in terms of a different variable

$$w = x^{1/2} = z^{-3/4}. \tag{4.62}$$

This is motivated by having found $\beta = \frac{1}{2}$ above: in the two-parameter case the prefactors will not be of the simple form $x^{n\beta}$ but will depend on two integers, say n and m. As we shall see, it will be more convenient to include these contributions inside the perturbative expansions and, as such, to work directly with the variable x^{β}. For simplicity of the calculation, it is also convenient to remove the overall factor of $z^{1/2}$ in front of the solution. This motivates us to introduce the new variables (with a slight, but obvious, abuse of notation)

$$u(w) \equiv \left.\frac{u(z)}{\sqrt{z}}\right|_{z=w^{-4/3}}. \tag{4.63}$$

It is then a straightforward exercise to rewrite the original equation in terms of this new function

$$\frac{9}{16}w^6\,u''(w) + \frac{9}{16}w^5\,u'(w) - 2u^3(w) - \left(\frac{w^4}{4} - 2\right)u(w) = 0. \tag{4.64}$$

Our goal is to solve this equation with a two-parameter transseries *ansatz*, along the lines in [25], as (we remind the reader that $w^2 = x$ is the open string coupling)

$$u\left(w, \sigma_1, \sigma_2\right) = \sum_{n=0}^{+\infty}\sum_{m=0}^{+\infty} \sigma_1^n \sigma_2^m\, \mathrm{e}^{-(n-m)A/w^2}\, \Phi_{(n|m)}(w). \tag{4.65}$$

At this stage one might be tempted to assume $\Phi_{(n|m)}(w)$ as a power series in w but, due to resonance effects, this will not work (see [25, 103]): in order to obtain a solution one further needs to add terms multiplying powers of $\log w$. As such we shall use the following *ansatz*

for the asymptotic expansions around generalized multi-instanton sectors

$$\Phi_{(n|m)}(w) = \sum_{k=0}^{\min(n,m)} \log^k(w) \cdot \Phi^{[k]}_{(n|m)}(w) \simeq \sum_{k=0}^{\min(n,m)} \log^k w \cdot \sum_{g=0}^{+\infty} u_g^{(n|m)[k]}\, w^g. \tag{4.66}$$

In this case, finding a two-parameter transseries solution to the Painlevé II equation now translates to determining the full list of coefficients $u_g^{(n|m)[k]}$. Inserting our *ansätze* (4.66) and (4.65) back into Painlevé II (4.64), yields the recursion relation which constructs this transseries:

$$\begin{aligned}
&2 \sum_{n_1=0}^{n} \sum_{n_2=0}^{n-n_1} \sum_{m_1=0}^{m} \sum_{m_2=0}^{m-m_1} \sum_{k_1=0}^{k} \sum_{k_2=0}^{k-k_1} \sum_{g_1=0}^{g} \sum_{g_2=0}^{g-g_1} u_{g_1}^{(n_1|m_1)[k_1]}\, u_{g_2}^{(n_2|m_2)[k_2]}\, u_{g-g_1-g_2}^{(n-n_1-n_2|m-m_1-m_2)[k-k_1-k_2]} \\
&= \left(\frac{9}{4}A^2(n-m)^2+2\right) u_g^{(n|m)[k]} + \frac{9}{4}A(n-m)(k+1)\, u_{g-2}^{(n|m)[k+1]} + \\
&+ \frac{9}{4}A(n-m)(g-3)\, u_{g-2}^{(n|m)[k]} + \frac{9}{16}(k+2)(k+1)\, u_{g-4}^{(n|m)[k+2]} \\
&+ \frac{9}{8}(k+1)(g-4)\, u_{g-4}^{(n|m)[k+1]} + \frac{140+9g(g-8)}{16}\, u_{g-4}^{(n|m)[k]}.
\end{aligned} \tag{4.67}$$

The above recursion now allows us to see resonance explicitly. Let us consider the case where $|n-m|=1$ and look for the leading terms in the recursion, the $u_g^{(n|m)[k]}$ coefficients. The first term on the second line above is $6u_g^{(n|m)[k]}$, but the sum in the first line also contains terms with this factor; they are:

$$2u_g^{(n|m)[k]}\, u_0^{(0|0)[0]}\, u_0^{(0|0)[0]} + 2u_0^{(0|0)[0]}\, u_g^{(n|m)[k]}\, u_0^{(0|0)[0]} + 2u_0^{(0|0)[0]}\, u_0^{(0|0)[0]}\, u_g^{(n|m)[k]} \tag{4.68}$$

such that the leading terms in the recursion will cancel[9]. As explained in greater detail in [25] this cancelation describes resonance in the Painlevé II equation and thus the need to introduce the "$[k]$-sectors", which will still allow us to find a solution for the recursion in spite of the aforementioned cancelation. We refer the reader to [25] for further details on this phenomenon.

Another issue which arises when solving the above recursion deals with reparameterization invariance of the transseries: there is an obvious freedom to choose the parameterization of the transseries coefficients σ_1 and σ_2 which translates to a long list of free coefficients, *i.e.*, coefficients in the transseries which are *not* fixed by the recursion. Do notice that this is not a problem, but rather a requirement from the transseries structure, but we refer the reader to [25] for further details on this phenomenon. The punch line is that one needs to choose a prescription to fix these free coefficients. As it turns out, the most natural choice is to set as many free coefficients to zero as possible, as this will also yield the simplest final results.

[9] Recall that $\lim_{z\to+\infty} u_{\text{pert}}(z) \sim \sqrt{z}$, so that one has $u_0^{(0|0)[0]} = 1$.

We shall fix the reparameterization invariance by setting

$$u_1^{(m+1|m)[0]} = 0, \qquad \forall m \geq 1, \qquad \text{and} \qquad u_1^{(n|n+1)[0]} = 0, \qquad \forall n \geq 1. \tag{4.69}$$

Having addressed the aforementioned subtleties, all that is left to do is to iterate the recursion in a computer. Results for the lowest sectors follow as

$$\Phi^{[0]}_{(0|0)}(w) = 1 - \frac{1}{16}w^4 - \frac{73}{512}w^8 - \frac{10657}{8192}w^{12} - \frac{13912277}{524288}w^{16} - \cdots, \tag{4.70}$$

$$\Phi^{[0]}_{(1|0)}(w) = w - \frac{17}{96}w^3 + \frac{1513}{18432}w^5 - \frac{850193}{5308416}w^7 + \frac{407117521}{2038431744}w^9 - \cdots, \tag{4.71}$$

$$\Phi^{[0]}_{(2|0)}(w) = \frac{1}{2}w^2 - \frac{41}{96}w^4 + \frac{5461}{9216}w^6 - \frac{1734407}{1327104}w^8 + \frac{925779217}{254803968}w^{10} - \cdots, \tag{4.72}$$

$$\Phi^{[0]}_{(1|1)}(w) = -3w^2 - \frac{291}{128}w^6 - \frac{447441}{32768}w^{10} - \frac{886660431}{4194304}w^{14} - \frac{13316458344441}{2147483648}w^{18} - \cdots \tag{4.73}$$

Let us note that, as expected, the first three lines above containing physical multi-instanton sectors precisely agree with the results in [16] (once we translate from our notation to theirs). Results concerning generalized multi-instanton sectors are new, and we present more details of this explicit transseries solution to the Painlevé II equation in appendix D.

We end this subsection with a few more comments on the (logarithmic) structure of the transseries solution and how it relates – in the double-scaling limit – to the transseries solution of the two-cut quartic matrix model we have discussed in subsection 4.3 and in appendix B. The first thing to notice is that it is simple to determine the lowest order for which the coefficients $u_g^{(n|m)[k]}$ are non-vanishing; let us call this number $2\beta_{nm}^{[k]}$. The result, which can be immediately checked from the results above and in appendix D, is the following

$$2\beta_{nm}^{[k]} = n + m - 2\left[\frac{k_{nm} + k}{2}\right]_I, \tag{4.74}$$

with $[\star]_I$ denoting the integer part, and

$$k_{nm} = \min(n, m) - m\,\delta_{nm}. \tag{4.75}$$

Next, and similarly to what was found for the Painlevé I equation in [25], the logarithmic sectors turn out to be related to each other and, in particular, to the non-logarithmic sectors. In fact, we here find a formula very similar to the expression (5.40) in [25], which reads

$$u_g^{(n|m)[k]} = \frac{1}{k!}\Big(8\,(m-n)\Big)^k u_g^{(n-k|m-k)[0]}. \tag{4.76}$$

This relation will be very useful in reducing the number of independent Stokes constants which enter the game; it provides relations between many of them in the same way as the

analogue Painlevé I expression was very helpful in [25]. As a final point in discussing the structure of the Painlevé II transseries solution, let us see how to make the bridge back to the two-cut string equations (4.15) and (4.16). Its two-parameter transseries solution, *i.e.*, its coefficients $P^{(n|m)}$ and $Q^{(n|m)}$ in (4.17), must agree, in the double-scaling limit, with the coefficients of our present solution $u^{(n|m)}$. That this has to be the case is clear since the Painlevé II equation itself was derived from the aforementioned string equations via (4.53) and (4.54). But our point here is that this may be made explicit as we find:

$$-\left(C\sqrt{g_s}\right)^{n+m} g_s^{g-1/3} P_g^{(n|m)[0]} \xrightarrow[\text{DSL}]{} z^{-\frac{3(n+m)+6g-2}{4}} u_{2g+n+m}^{(n|m)[0]}. \tag{4.77}$$

In this expression, the "DSL" arrow simply means that we have applied the double-scaling limit (4.51) and (4.52) to the left-hand-side. On the right-hand-side the coefficients which appear are the ones associated to the original variables, *i.e.*, where we have inverted the redefinitions of u and z we did before. There is a similar expression involving the Q coefficients which relates to the one above by a simple change of sign, as can be seen in (4.54). Finally, the constant C is given by

$$C = \frac{2 \cdot 3^{1/2}}{\sqrt{\lambda}}. \tag{4.78}$$

4.4.2 The Resurgence of Multi-instantons and Stokes Coefficients

We shall now turn to the resurgence of the generalized multi-instanton $(n|m)[k]$ sectors. The resurgence formulae we have discussed in subsection 3.2.3 will verify the validity of these multi-instanton sectors, and they will further allow – upon consistency – to extract many unknown Stokes constants. We shall only focus on effects at exponential order 1^{-g} and our analysis will be less detailed than the one in [25] where, using more refined techniques, it was possible to "dig" deep in the asymptotics and study effects at orders 2^{-g}, 3^{-g}, *et cetera*. Nonetheless, our results will fully validate the two-parameter multi-instantonic structure of the Painlevé II solutions.

Let us begin by addressing the Stokes constant $S_1^{(0)}$. On what concerns large-order behavior, this constant appears in the perturbative $(0|0)$ sector and we may use the large-order expression (3.33) to write in the present case

$$u_{4g}^{(0|0)[0]} \simeq \frac{S_1^{(0)}}{\mathrm{i}\pi} \frac{\Gamma\left(2g-\frac{1}{2}\right)}{A^{2g-\frac{1}{2}}} \sum_{h=0}^{+\infty} u_{2h+1}^{(1|0)[0]} A^h \frac{\Gamma\left(2g-h-\frac{1}{2}\right)}{\Gamma\left(2g-\frac{1}{2}\right)} + \mathcal{O}(2^{-g}). \tag{4.79}$$

Given this expression, it is immediate to construct the sequence

$$\frac{\mathrm{i}\pi\, A^{2g-\frac{1}{2}}}{\Gamma\left(2g-\frac{1}{2}\right)} u_{4g}^{(0|0)[0]} \tag{4.80}$$

which is asymptotic to $S_1^{(0)}$. Taking its Richardson extrapolation, it follows an extremely precise check on the well-known result (see, *e.g.*, [16, 132]), where we found a match of the first 30 decimal places after $N = 20$ Richardson transforms

$$S_1^{(0)} = -\frac{\mathrm{i}}{\sqrt{2\pi}} = -0.3989422804014327...\,\mathrm{i}. \tag{4.81}$$

There is a simple relation between the above Stokes constant at criticality, and the corresponding Stokes constant off-criticality, (4.48), which is similar to the relation between the corresponding Stokes constants in [25] – *i.e.*, Stokes constant for Painlevé I and for the one-cut quartic matrix model. Namely, we find[10]

$$S_1^{(0)}\Big|_{\text{PII}} = \frac{S_1^{(0)}\Big|_{\text{QMM}}}{C}, \tag{4.82}$$

where the constant C was defined above. Naturally, this expression is simply encoding the double-scaling limit at the level of Stokes constants (see [25] for other Stokes constants).

As we move forward there is one point to have in mind: except for a limited set of empirical relations they satisfy among themselves – which we shall discuss in the following – there are no further analytical predictions for all other Stokes constants. As such, we need to compute them at the same time we test resurgence in an independent fashion. This is done in two steps [25, 103]: we choose one resurgent formula and validate it via *some* resurgent relations; then we use *different* resurgent relations in this formula to numerically compute new Stokes constants. As one iterates this procedure towards several Stokes constants and several multi-instanton sectors, consistency independently double-checks both the Stokes constants and the resurgence of instantons.

In this spirit, let us move on to the multi-instanton sectors and address the Stokes constant $S_{-1}^{(2)}$ which appears in the $(2|0)$ sector. If we apply our large-order formula for multi-instanton sectors, (3.34), with two physical instantons, $n = 2$ and $m = 0$, and focus

[10]For shortness we will avoid the labels referring to either "Painlevé II" or "Quartic Matrix Model" throughout the rest of the chapter. All constants discussed from here onwards refer to the critical (double-scaled) model.

only on the leading contributions to the asymptotics, $k=1$, we arrive at

$$
\begin{aligned}
u_{2g+2}^{(2|0)[0]} \simeq & \frac{3S_1^{(0)}}{2\pi\mathrm{i}} \frac{\Gamma\left(g-\frac{1}{2}\right)}{A^{g-\frac{1}{2}}} \sum_{h=0}^{+\infty} \frac{\Gamma\left(g-h-\frac{1}{2}\right)}{\Gamma\left(g-\frac{1}{2}\right)} u_{2h+3}^{(3|0)[0]} A^h + \\
& + \frac{S_{-1}^{(2)}}{2\pi\mathrm{i}} \frac{\Gamma\left(g+\frac{1}{2}\right)}{(-A)^{g+\frac{1}{2}}} \sum_{h=0}^{+\infty} \frac{\Gamma\left(g-h+\frac{1}{2}\right)}{\Gamma\left(g+\frac{1}{2}\right)} u_{2h+1}^{(1|0)[0]} (-A)^h + \\
& + \frac{\widetilde{S}_{-1}^{(0)}}{2\pi\mathrm{i}} \frac{\Gamma\left(g-\frac{1}{2}\right)}{(-A)^{g-\frac{1}{2}}} \sum_{h=0}^{+\infty} \frac{\Gamma\left(g-h-\frac{1}{2}\right)}{\Gamma\left(g-\frac{1}{2}\right)} u_{2h+3}^{(2|1)[0]} (-A)^h + \\
& + \frac{\widetilde{S}_{-1}^{(0)}}{4\pi\mathrm{i}} \frac{\Gamma\left(g+\frac{1}{2}\right)}{(-A)^{g+\frac{1}{2}}} \sum_{h=0}^{+\infty} \frac{\Gamma\left(g-h+\frac{1}{2}\right)}{\Gamma\left(g+\frac{1}{2}\right)} u_{2h+1}^{(2|1)[1]} (-A)^h \left\{ \psi\left(g-h+\frac{1}{2}\right) - \log(A) - \mathrm{i}\pi \right\}.
\end{aligned}
\tag{4.83}
$$

A novel feature of this case is that, adding to the familiar $g!$ large-order growth, the digamma function further produces effects which grow as $g! \log g$ and which will in fact be the *dominant* effects [11]. One procedure to extract and confirm the new Stokes coefficients associated to this expression, via Richardson transforms and when in the presence of $\log g$ factors, was introduced in [103] within the context of the Painlevé I equation and further extended in [25]. Let us see how to address this issue. We move a factor of

$$
2\pi\mathrm{i} \frac{A^{g+\frac{1}{2}}}{\Gamma\left(g+\frac{1}{2}\right)} \tag{4.84}
$$

to the left-hand-side of the above equation, and expand its right-hand-side in powers of $1/g$. In this way, one obtains a sequence with the following asymptotic behavior:

$$
A_g \sim B_g \log g + C_g, \qquad \text{where} \qquad B_g \simeq \sum_{k=0}^{+\infty} \frac{b_k}{g^k}, \quad C_g \simeq \sum_{k=0}^{+\infty} \frac{c_k}{g^k}. \tag{4.85}
$$

To extract the leading coefficient, b_0, we may construct a new sequence,

$$
\widetilde{A}_g = g\left(A_{g+1} - A_g\right), \tag{4.86}
$$

which behaves as

$$
\widetilde{A}_g \sim \widetilde{B}_g \log g + \widetilde{C}_g, \qquad \text{where} \qquad \widetilde{B}_g \simeq \sum_{k=1}^{+\infty} \frac{\widetilde{b}_k}{g^k}, \quad \widetilde{C}_g \simeq b_0 + \sum_{k=1}^{+\infty} \frac{\widetilde{c}_k}{g^k}, \tag{4.87}
$$

[11] The successful testing of this relation also provides validation on the need for a two-parameter transseries. Had we only taken a one-parameter transseries, then (4.83) would have only the first two lines on the right-hand side and we would empirically find such a relation to be false. There are contributions at leading order to the $(2|0)[0]$ asymptotics coming from generalized instanton sectors.

thus isolating the coefficient we are looking for. In fact, should we apply a couple of Richardson transform (at least two), we remove the subleading tails in $1/g^k$ and in $\log g/g^k$ and immediately obtain b_0 numerically. Similarly, if we want to find b_1, we can define

$$A_g^{(1)} = g\left(\widetilde{A}_g - b_0\right), \tag{4.88}$$

and now apply the Richardson transforms to the sequence $\widetilde{A}_g^{(1)} = g\left(A_{g+1}^{(1)} - A_g^{(1)}\right)$ in order to extract the coefficient $-b_1$. As we move on to the extraction of the c_i coefficients, the procedure is more or less straightforward. For instance, if we subtract the leading logarithm to the left-hand-side of the original sequence, the new sequence[12]

$$P_g = A_g - b_0\,\log g \tag{4.89}$$

will now yield c_0. Along the same lines, $P_g^{(1)} = A_g - (b_0 + b_1/g)\log g$ allows us to extract $-c_1$, and so on. Applying all this in our present context we now have to consider the sequence[13]

$$A_g = 2\pi\mathrm{i}\,\frac{A^{g+\frac{1}{2}}}{\Gamma\left(g+\frac{1}{2}\right)}\,u_{2g+2}^{(2|0)[0]}, \tag{4.90}$$

where we should notice that, due to the factors of $(-1)^g$ in (4.83), we need to look separately at the sequences for g odd and for g even. For simplicity, we shall only discuss the even case, but the odd one is completely analogous. If we now use the sequence (4.86) to compute $\widetilde{A}_{2g}$, we expect it to converge towards the leading coefficient multiplying $\log g$ in the resurgent relation (4.83). What is this number? Using the value of $u_1^{(2|1)[1]} = -8$ (simply obtained for instance via (4.76)) and using the fact[14] that $\widetilde{S}_{-1}^{(0)} = -\mathrm{i}\,S_1^{(0)}$, if the resurgent formulae hold in the present context then this number should be equal to the analytical value

$$-\frac{\mathrm{i}\,\widetilde{S}_{-1}^{(0)}}{2}\,u_1^{(2|1)[1]} = 1.59576\ldots\,. \tag{4.91}$$

Let us then turn to the sequence and analyze it. This is shown on the first image of figure 4.4, where we plot the original sequence and some of its Richardson transforms. After $N = 20$ Richardson transforms we find the numerical value of 1.59573... which differs from the prediction above by less than 0.01%, thus fully validating our resurgent multi-instanton structure.

Taking our analysis one step further, we may now extract a new Stokes constant by looking at the leading non-logarithmic term, which may be computed using the sequence

[12] Notice that we can subtract further logarithmic terms in order to accelerate the convergence.

[13] A trivial word on notation: A is the instanton action, A_g the sequence we are addressing.

[14] At this precise moment this only adds numerical evidence to the fact that $\widetilde{S}_{-1}^{(0)} = -\mathrm{i}\,S_1^{(0)}$. But, as we shall see in the following, we can actually show that this relation is true, so we may as well use it already.

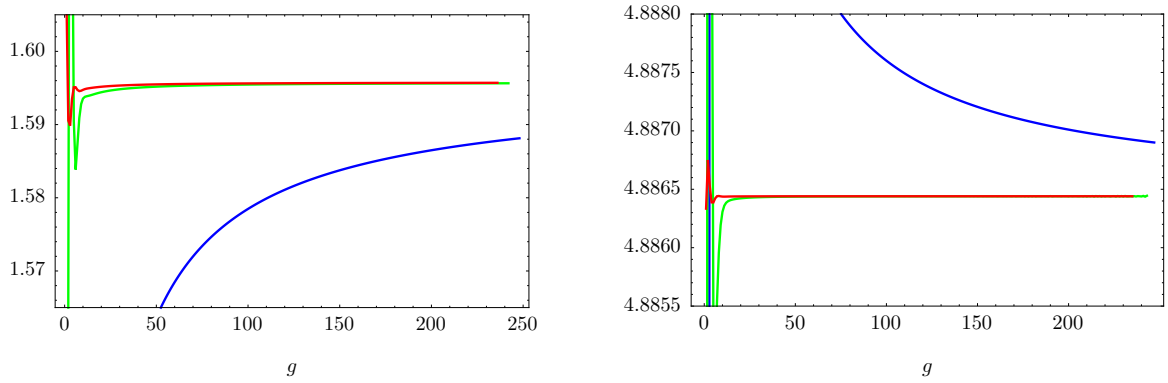

Figure 4.4: The left image shows the sequence $\widetilde{A}_{2g}$ built from (4.90) (blue) alongside with its fifth (green) and twentieth (red) Richardson transforms. This can be shown to quickly converge towards our prediction (4.91) with errors $\sim 0.01\%$. The right image shows the sequence P_g in (4.89) (blue) alongside its fifth (green) and twentieth (red) Richardson transforms. This quickly converges towards our prediction (4.93).

(4.89). According to the same large-order resurgent relation, (4.83), this term should be

$$-\frac{\mathrm{i}\,\widetilde{S}_{-1}^{(0)}}{2}\,u_1^{(2|1)[1]}\,(\log A+\mathrm{i}\pi)-\mathrm{i}\,S_{-1}^{(2)}\,u_1^{(1|0)[0]}, \tag{4.92}$$

where we do not know the value of the Stokes constant $S_{-1}^{(2)}$. However, we may find it by analyzing the sequence (4.89), as shown in the second image of figure 4.4: after $N = 20$ Richardson iterations we extract the numerical prediction

$$S_{-1}^{(2)} = -5.3455144... - 5.013256493...\,\mathrm{i}. \tag{4.93}$$

Before moving on with further Stokes constants, let us make a remark concerning the new Stokes constant we have just computed, (4.93): it is a complex number, with both real and imaginary contributions. But, as explained in detail in [25], there are many relations between the Stokes constants and a large number of these depend on each other (although it is unclear how many truly independent Stokes constants exist). Some of these relations may be derived from the general structure of the string genus expansion, and are thus model-independent; while others were found "experimentally", and will thus depend upon which equation is under analysis (but see [25] for more details on both these points). In particular, all Stokes constants of the form $S_\ell^{(n)}$ and $\widetilde{S}_\ell^{(n)}$ with $\ell > 0$ are *purely* imaginary. We will thus only list this type of Stokes constants. We shall discuss how these relations arise when we discuss the $(1|1)$ sector below; for the moment let us just mention that, for (4.93) above, the relation

which involves $\widetilde{S}_1^{(2)}$ out of $S_{-1}^{(2)}$ is

$$\widetilde{S}_1^{(2)} = -\mathrm{i}\, S_{-1}^{(2)} + 4\pi\mathrm{i}\, S_1^{(0)} = 5.3455144...\,\mathrm{i}. \tag{4.94}$$

Having successfully addressed a two-instanton sector, let us next address a sector involving generalized instantons. In this case, the simplest choice is to study a generalized "closed string" sector; the example where we have $n = 1 = m$ and $k = 0$. By "closed string" we mean that sectors of the type $(n|n)$ are expected to have an asymptotic expansion in powers of the *closed* string coupling $g_s^2 \sim w^4$ rather than in powers of the *open* string coupling $g_s \sim w^2$, as can be seen in (4.73). In this case the $(1|1)$ sector has no logarithmic contributions and the relevant large-order relation is

$$\begin{aligned}
&\frac{2\pi\mathrm{i}\, A^{g+\frac{1}{2}}}{\Gamma\left(g+\frac{1}{2}\right)}\, u_{2g+2}^{(1|1)[0]} \simeq \\
&S_1^{(1)} \sum_{h=0}^{+\infty} \frac{\Gamma\left(g-h+\frac{1}{2}\right)}{\Gamma\left(g+\frac{1}{2}\right)}\, u_{2h+1}^{(1|0)[0]}\, A^h + 2S_1^{(0)}\, A \sum_{h=0}^{+\infty} \frac{\Gamma\left(g-h-\frac{1}{2}\right)}{\Gamma\left(g+\frac{1}{2}\right)}\, u_{2h+3}^{(2|1)[0]}\, A^h - \\
&-2S_1^{(0)} \sum_{h=0}^{+\infty} \frac{\Gamma\left(g-h+\frac{1}{2}\right)}{\Gamma\left(g+\frac{1}{2}\right)}\, u_{2h+1}^{(2|1)[1]}\, A^h\, \widetilde{B}_A\left(g-h-\frac{3}{2}\right) - \\
&-\frac{\mathrm{i}\,\widetilde{S}_{-1}^{(1)}}{(-1)^g} \sum_{h=0}^{+\infty} \frac{\Gamma\left(g-h+\frac{1}{2}\right)}{\Gamma\left(g+\frac{1}{2}\right)}\, u_{2h+1}^{(0|1)[0]}\, (-A)^h + \frac{2\mathrm{i}\,\widetilde{S}_{-1}^{(0)}}{(-1)^g}\, A \sum_{h=0}^{+\infty} \frac{\Gamma\left(g-h-\frac{1}{2}\right)}{\Gamma\left(g+\frac{1}{2}\right)}\, u_{2h+3}^{(1|2)[0]}\, (-A)^h + \\
&+\frac{2\mathrm{i}\,\widetilde{S}_{-1}^{(0)}}{(-1)^g} \sum_{h=0}^{+\infty} \frac{\Gamma\left(g-h+\frac{1}{2}\right)}{\Gamma\left(g+\frac{1}{2}\right)}\, u_{2h+1}^{(1|2)[1]}\, (-A)^h\, B_A\left(g-h-\frac{3}{2}\right).
\end{aligned} \tag{4.95}$$

As we have just mentioned, the $(1|1)[0]$ sector will have a standard, topological perturbative expansion, which implies that all terms above with odd g will have to vanish. In other words, imposing $u_{2(2g+1)+2}^{(1|1)[0]} = 0$ will result in a tower of relations between the Stokes constants appearing on the right-hand-side of (4.95), as this expression needs to vanish order by order in both powers of $1/g^k$ and $\log g/g^k$. For example, expanding the digamma functions we find that imposing that the term proportional to $\log g$ vanishes will imply the condition

$$S_1^{(0)} - \mathrm{i}\,\widetilde{S}_{-1}^{(0)} = 0 \quad \Rightarrow \quad \widetilde{S}_{-1}^{(0)} = -\mathrm{i}\, S_1^{(0)}, \tag{4.96}$$

which we had already put forward and checked numerically – now being "theoretically" justified. On the other hand, the term at order $\mathcal{O}(1)$ yields a relation involving two unknown constants,

$$S_1^{(1)} + \mathrm{i}\,\widetilde{S}_{-1}^{(1)} + 8\pi\mathrm{i}\, S_1^{(0)} = 0, \tag{4.97}$$

where we have used (4.76) to relate $u_1^{(1|2)[1]} = 8u_1^{(0|1)[0]}$. Continuing along these lines and

looking at further required cancelations, one may use this procedure in order to extract similar relations between further Stokes constants, such as (4.94) which we have discussed above. Our goal now is to apply the same reasoning as used within the (2|0) sector in order to compute this new Stokes constant, $S_1^{(1)}$ (and, along the way, $\widetilde{S}_{-1}^{(1)}$ as well). This is very similar to what we have done before, with the slight difference that now only the sequences for even g are relevant. Once again the term proportional to $\log g$ offers just a consistency check on the resurgent structure of the transseries solution and on (already) known Stokes constants, and we show in figure 4.5 that this is indeed working perfectly: the relevant sequence, after Richardson extrapolation, converges towards the correct number, $-S_1^{(0)}\, u_1^{(2|1)[1]} + \mathrm{i}\, \widetilde{S}_{-1}^{(2)}\, u_1^{(1|2)[1]}$, with an error smaller than 0.001%.

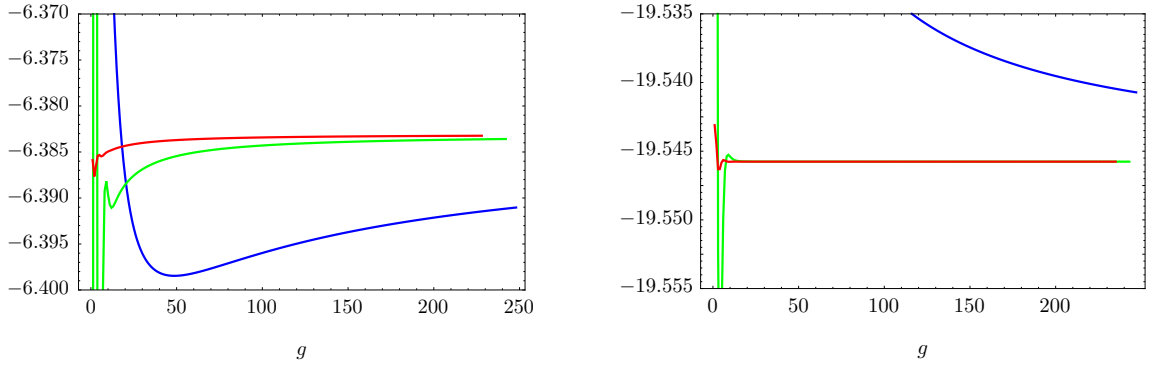

Figure 4.5: The left image shows the sequence which tests the leading, $\log g$, coefficient of the large-order relation (4.95) (blue), alongside with its fifth (green) and twentieth (red) Richardson transforms. This sequence quickly converges towards the expected limit $-S_1^{(0)}\, u_1^{(2|1)[1]} + \mathrm{i}\, \widetilde{S}_{-1}^{(2)}\, u_1^{(1|2)[1]}$ with an error smaller than 0.001%. The right image shows the sequence which tests the leading, order $\mathcal{O}(1)$, term in the large-order relation (4.95) (blue), alongside its fifth (green) and twentieth (red) Richardson transforms. Again, this quickly leads to our prediction (4.98).

The new constants we are after appear at order $\mathcal{O}(1)$, without logarithmic contributions. After using the relevant sequence, (4.89), we find, as we show in figure 4.5, a fast convergence towards the number $\xi = -19.54576...\,\mathrm{i}$ that resurgence sets to

$$\xi = S_1^{(0)}\, u_1^{(2|1)[1]}\, \log A + S_1^{(1)}\, u_1^{(1|0)[0]} - \mathrm{i}\, \widetilde{S}_{-1}^{(1)}\, u_1^{(0|1)[0]} - \mathrm{i}\, \widetilde{S}_{-1}^{(0)}\, u_1^{(1|2)[1]}\, (\log A + \mathrm{i}\pi)\,. \tag{4.98}$$

Using this result together with the previous relation, (4.97), we find $S_1^{(1)}$ (which is, as expected, a purely imaginary number)

$$S_1^{(1)} = -10.6910288...\,\mathrm{i}. \tag{4.99}$$

The (independent) Stokes constants we have computed are summarized in table 4.1. It

		Precision	From
$S_1^{(0)}$	$-0.39894228...$ i	∞	$\Phi^{[0]}_{(0\|0)}$
$S_1^{(1)}$	$-10.6910288...$ i	7	$\Phi^{[0]}_{(1\|1)}$
$\widetilde{S}_1^{(2)}$	$5.3455144...$ i	7	$\Phi^{[0]}_{(2\|0)}$

Table 4.1: The independent Stokes constants we have calculated. The third column gives the number of decimal places to which the answer is explicitly computed, while the fourth column shows the instanton sector where each constant appears for the first time. All constants we address first appear at order 1^{-g}.

is interesting to notice that a further "experimental" relation $\widetilde{S}_1^{(2)} = -\frac{1}{2}\, S_1^{(1)}$ is (apparently) true in this case. The exact same relation was also found in [25], in the context of the Painlevé I equation, alongside with some other extra relations, all of them emerging from purely numerical relations. We expect that by examining further data in the present Painlevé II context also many similar relations will be found. However, at this stage, we have no first principles explanation for these extra relations: determining the minimal set of independent Stokes constants is a very interesting open problem for future research.

4.4.3 The Nonperturbative Free Energy of Type 0B String Theory

The final point we wish to address is the construction of the nonperturbative free energy for 2d supergravity or 1d type 0B string theory. In fact, using the results of our transseries analysis of the Painlevé II equation, we may now build its associated double-scaled free energy. This free energy is obtained from the solution of the Painlevé II equation via [127, 129, 130, 135]

$$F''_{\rm ds}(z) = -\frac{1}{4}\, u(z)^2. \tag{4.100}$$

For convenience, from this point on we shall drop the double-scaled label, but we will always be talking about the free energy at the critical point. The first thing to notice is that there is now a fundamental difference with respect to the Painlevé I case, studied in [25]: the relation between the (twice derived) free energy and the solution of the differential equation is no longer linear. Nonetheless, the right-hand-side of (4.100) still has a transseries expansion

$$-\frac{1}{4}\, u(z)^2 \equiv \sum_{n=0}^{+\infty} \sum_{m=0}^{+\infty} \sigma_1^n \sigma_2^m\, \mathrm{e}^{-(n-m)\, A\, z^{3/2}}\, \varphi_{(n|m)}(z), \tag{4.101}$$

but where now one has

$$\varphi_{(n|m)}(z) = \sum_{n'=0}^{n} \sum_{m'=0}^{m} \Phi_{(n'|m')}(z)\, \Phi_{(n-n'|m-m')}(z) \simeq \sum_{g=0}^{+\infty} \frac{\widetilde{u}_g^{(n|m)}}{z^{\frac{3g}{4}}}. \tag{4.102}$$

Relating this expression to the free energy now just requires a double-integration, as follows from (4.100). Let us begin by looking at the perturbative sector, where we bring back the $\sqrt{z}$ factor we had pulled out in (4.63). In this case, the integration leads to

$$F^{(0|0)}(z) = -\frac{1}{4} \iint \mathrm{d}z\, z \left(\Phi_{(0|0)}(z)\right)^2 = -\frac{z^3}{24} - \frac{\log(z)}{32} + \frac{3}{512 z^3} + \frac{63}{4096 z^6} + \cdots . \tag{4.103}$$

As a check on this result, notice that if we apply the double-scaling limit, (4.51) and (4.52), to the quartic matrix model free energies, $F_g(t)$, which we have computed via the Euler-Maclaurin formula in (4.38) (the first few of which are presented in appendix C), and if we further implement the rescalings $u \to 2^{1/3}\, u$ and $z \to 2^{2/3}\, z$ associated to our choice of normalization, then the answer one obtains precisely matches the above result.

Having understood how to construct the free energy in the perturbative sector, one may move on towards multi-instanton sectors. Beginning with the one-instanton sector arising from the product $\Phi_{(0|0)}(z)\, \Phi_{(1|0)}(z)$, the first coefficient to compute is simply given by

$$-\frac{1}{2}\sigma_1\, u_1^{(1|0)[0]} \iint \mathrm{d}z\, z^{1/4}\, \mathrm{e}^{-Az^{3/2}} = -\frac{1}{8}\, \sigma_1\, u_1^{(1|0)[0]}\, z^{-3/4}\, \mathrm{e}^{-Az^{3/2}} + \cdots . \tag{4.104}$$

In the expression above we have kept only the leading term and we have explicitly displayed the coefficient $u_1^{(1|0)[0]}$. Recall that when solving the Painlevé II equation we chose to set $u_1^{(1|0)[0]} = 1$, and recall that this freedom in choosing the normalization was a consequence of a reparameterization invariance of the double-transseries solution [25]. One now needs to readdress this point in order to properly fix the free energy transseries. As shown in [25], rescaling the transseries parameters as $\sigma_1 = c_1\, \widehat{\sigma}_1$ and $\sigma_2 = c_2\, \widehat{\sigma}_2$ makes the following quantities scale accordingly

$$\Phi_{(n|m)} = c_1^{-n}\, c_2^{-m}\, \widehat{\Phi}_{(n|m)}, \tag{4.105}$$

$$S_\ell^{(k)} = c_1^{1-k}\, c_2^{1-k-\ell}\, \widehat{S}_\ell^{(k)}, \tag{4.106}$$

$$\widetilde{S}_\ell^{(k)} = c_1^{1+\ell-k}\, c_2^{1-k}\, \widehat{\widetilde{S}}_\ell^{(k)}. \tag{4.107}$$

The convenient scaling to do, when dealing with the free energy, is

$$\sigma_{1,2} = S_1^{(0)}\, \sigma_{1,2}^F. \tag{4.108}$$

In fact, this immediately implies that the leading coefficient of the one-instanton free energy

is

$$F_0^{(1|0)[0]} = -\frac{1}{8}\, S_1^{(0)}\, u_1^{(1|0)[0]} = \frac{\mathrm{i}}{8\sqrt{2\pi}}, \tag{4.109}$$

and thus the free energy Stokes constant is very simply

$$S_1^{(0)F} = 1. \tag{4.110}$$

This convenient normalization may further be double-checked by using the large-order connection (4.44)

$$F_g^{(0|0)[0]} \sim \frac{S_1^{(0)F}}{\mathrm{i}\pi}\, \frac{\Gamma\left(2g-\frac{5}{2}\right)}{A^{2g-\frac{5}{2}}}\, F_0^{(1|0)[0]}. \tag{4.111}$$

After just a few Richardson transforms we find that (4.110) is indeed consistent. It is important to remark that *physical* quantities should not depend on normalization choices, so that only combinations which are left invariant by the above rescalings are physical. In this particular case, the physical quantity is

$$S_1^{(0)F} \cdot F_0^{(1|0)[0]}. \tag{4.112}$$

Had we chosen to have $\sigma_1^F = \sigma_1$, then we would have found $S_1^{(0)F} = S_1^{(0)}$, but the combination above would not have changed. A longer discussion on normalizations may be found in [25].

We are now ready to proceed and explicitly compute generalized $(n|m)$ multi-instanton sectors in the free energy of 2d supergravity or 1d type 0B string theory. From the point-of-view of the double-integration, the only complicated sectors are the ones with logarithms. In fact, when $n = m$ the procedure is immediate and a straightforward generalization of what we did for the perturbative $(0|0)$ sector in (4.103). As such, and always having in mind that we are now dealing with the function $u(z)^2$, in (4.101), we have for general $n \neq m$,

$$\sigma_1^n \sigma_2^m\, \mathrm{e}^{-(n-m)A/w^2}\, \varphi_{(n|m)}^{[0]}(w) \simeq \sigma_1^n \sigma_2^m\, \mathrm{e}^{-(n-m)A/w^2} \sum_{g=0}^{+\infty} \widetilde{u}_{2g+2\beta_{nm}^{[0]}}^{(n|m)[0]}\, w^{2g+2\beta_{nm}^{[0]}}. \tag{4.113}$$

It can be shown – and easily checked – that the relation (4.76) connecting logarithmic $(n+k|m+k)[k]$ to non-logarithmic $(n|m)[0]$ sectors still holds in the precise same form for $\varphi_{(n|m)}^{[k]}$ and its components. In this case, it is convenient to assemble together all sectors which are related to the $(n|m)[0]$ sector; due to the aforementioned relation each of these is of the form (transseries parameters and logarithmic factor included)

$$\frac{1}{k!}\left(8\,(m-n)\,\sigma_1\sigma_2\,\log w\right)^k \sigma_1^n \sigma_2^m\, \mathrm{e}^{-(n-m)A/w^2}\, \varphi_{(n|m)}^{[0]}(w). \tag{4.114}$$

Finally summing over k, one finds

$$\varphi^{[\mathrm{sum}]}_{(n|m)}(w) = \mathrm{e}^{8(m-n)\sigma_1\sigma_2\ \log w}\,\varphi^{[0]}_{(n|m)}(w) = w^{8(m-n)\sigma_1\sigma_2}\,\varphi^{[0]}_{(n|m)}(w). \tag{4.115}$$

In order to do the double-integration, let us first move back to the z variable so that the $(n|m)$ contribution becomes

$$\sigma_1^n\sigma_2^m\,\mathrm{e}^{-(n-m)Az^{3/2}}\sum_{g=0}^{+\infty}\widetilde{u}^{(n|m)[0]}_{2g+2\beta^{[0]}_{nm}}\,z^{-\frac{3g+3\beta^{[0]}_{nm}-2}{2}+\frac{8(n-m)\sigma_1\sigma_2}{A}}. \tag{4.116}$$

The double-integration may now be carried through using that

$$\iint \mathrm{d}z\,z^q\,\mathrm{e}^{-\ell Az^{3/2}} = \frac{2}{3\ell A}\,z^{q+1/2}\,\mathrm{e}^{-\ell Az^{3/2}}\sum_{m=1}^{+\infty}a_m(q)\cdot\left(-\ell Az^{3/2}\right)^{-m}, \tag{4.117}$$

where the coefficients $a_m(q)$ are given by

$$a_m(q) = \frac{\Gamma\left(m-\frac{2q+1}{3}\right)}{\Gamma\left(-\frac{2q+1}{3}\right)} - \frac{\Gamma\left(m-\frac{2q-1}{3}\right)}{\Gamma\left(-\frac{2q-1}{3}\right)}. \tag{4.118}$$

Notice that the $a_m(q)$ coefficients are polynomials in q of degree $m-1$. Further, given the integrand in (4.116), the variable q is actually linear in $\sigma_1\sigma_2$ and, as such, the $a_m(q)$ coefficients will be polynomials of degree $m-1$ in $\sigma_1\sigma_2$. This effectively means that the double-integration of the $(n|m)$ sector of $u(z)^2$ contributes not only to the $(n|m)$ sector of the free energy, but to all other $(n+r|m+r)$ sectors as well (with $r>0$).

We are now essentially done. Using a computer, we can apply the integral (4.117) systematically and find that the free energy has the structure

$$F(z,\sigma_1^F,\sigma_2^F) = \sum_{n=0}^{+\infty}\sum_{m=0}^{+\infty}\left(S_1^{(0)}\right)^{n+m}\left(\sigma_1^F\right)^n\left(\sigma_2^F\right)^m\mathrm{e}^{-(n-m)Az^{3/2}}\,z^{\frac{3}{\pi}(m-n)\sigma_1^F\sigma_2^F}\,F^{(n|m)}(z), \tag{4.119}$$

where the "coefficients" $F^{(n|m)}(z)$ will be asymptotic expansions in powers of $z^{-3/2}$ (both integer and half-integer, and also containing the occasional logarithm). The first few sectors

of the critical free energy are the following

$$F^{(0|0)}(z) = -\frac{1}{24}z^3 - \frac{1}{32}\log z + \frac{3}{512}z^{-3} + \frac{63}{4096}z^{-6} + \cdots, \tag{4.120}$$

$$F^{(1|0)}(z) = -\frac{1}{8}z^{-\frac{3}{4}} + \frac{65}{768}z^{-\frac{9}{4}} - \frac{19273}{147456}z^{-\frac{15}{4}} + \frac{13647905}{42467328}z^{-\frac{21}{4}} - \cdots, \tag{4.121}$$

$$F^{(1|1)}(z) = \frac{4}{3}z^{\frac{3}{2}} + \frac{25}{96}z^{-\frac{3}{2}} + \frac{6323}{24576}z^{-\frac{9}{2}} + \frac{5015413}{3145728}z^{-\frac{15}{2}} + \cdots, \tag{4.122}$$

$$F^{(2|0)}(z) = -\frac{1}{32}z^{-\frac{3}{2}} + \frac{59}{1536}z^{-3} - \frac{9745}{147456}z^{-\frac{9}{2}} + \frac{3335669}{21233664}z^{-6} - \cdots, \tag{4.123}$$

$$F^{(2|1)}(z) = -\frac{9}{16}z^{-\frac{9}{4}} + \frac{737}{512}z^{-\frac{15}{4}} - \frac{398375}{98304}z^{-\frac{21}{4}} + \frac{142017823}{9437184}z^{-\frac{27}{4}} - \cdots, \tag{4.124}$$

$$F^{(2|2)}(z) = -3\log z + \frac{111}{64}z^{-3} + \frac{54507}{8192}z^{-6} + \frac{15245711}{196608}z^{-9} + \cdots, \tag{4.125}$$

$$F^{(3|0)}(z) = -\frac{1}{96}z^{-\frac{9}{4}} + \frac{59}{3072}z^{-\frac{15}{4}} - \frac{7645}{196608}z^{-\frac{21}{4}} + \frac{1836031}{18874368}z^{-\frac{27}{4}} - \cdots, \tag{4.126}$$

$$F^{(3|1)}(z) = -\frac{17}{64}z^{-3} + \frac{1211}{1536}z^{-\frac{9}{2}} - \frac{655883}{294912}z^{-6} + \frac{161783969}{21233664}z^{-\frac{15}{2}} - \cdots, \tag{4.127}$$

$$F^{(3|2)}(z) = \frac{17}{8}z^{-\frac{9}{4}} - \frac{2267}{384}z^{-\frac{15}{4}} + \frac{3488915}{147456}z^{-\frac{21}{4}} - \frac{251878099}{2654208}z^{-\frac{27}{4}} + \cdots, \tag{4.128}$$

$$F^{(3|3)}(z) = \frac{17}{3}z^{-\frac{3}{2}} + \frac{35675}{2304}z^{-\frac{9}{2}} + \frac{11452163}{81920}z^{-\frac{15}{2}} + \frac{157674856009}{58720256}z^{-\frac{21}{2}} + \cdots \tag{4.129}$$

In the list above we presented the sectors $(n|m)$ with $n \geq m$. The coefficients with $n < m$ differ at most by signs, obeying the rule

$$F_g^{(m|n)} = (-1)^{g+[n/2]_I} F_g^{(n|m)}, \qquad n > m. \tag{4.130}$$

The starting powers in the free energy coefficients $F^{(n|m)}$ can be easily related to the starting powers $\beta_{nm}^{[0]}$ of the Painlevé II coefficients $u^{(n|m)}$, for instance by looking at (4.117). At the end of the day we find

$$F^{(n|n)} \sim z^{-\frac{3}{2}\beta_{nn}^{[0]}+3}, \tag{4.131}$$

$$F^{(n|m)} \sim z^{-\frac{3}{2}\beta_{nm}^{[0]}}, \qquad n \neq m, \tag{4.132}$$

where $\beta_{nm}^{[0]}$ was defined above in (4.74). For completeness, we also recall that the logarithmic sectors are "hidden" inside the term

$$z^{\frac{3}{\pi}(m-n)\sigma_1^F\sigma_2^F} = \exp\left(\frac{3}{\pi}(m-n)\,\sigma_1^F\sigma_2^F\,\log z\right). \tag{4.133}$$

As a final point, we should also comment on the Stokes constants for the free energy. Since

the Stokes constants for $u(z)$ and $u(z)^2$ are the same, the Stokes constants for the free energy are related to those of Painlevé II via the rescalings described above, (4.106) and (4.107), and so

$$S_\ell^{(k)F} = \ell^2 \left(S_1^{(0)}\right)^{2k+\ell-2} S_\ell^{(k)}, \tag{4.134}$$

$$\widetilde{S}_\ell^{(k)F} = \ell^2 \left(S_1^{(0)}\right)^{2k-\ell-2} \widetilde{S}_\ell^{(k)}. \tag{4.135}$$

The extra ℓ^2 appearing above comes from taking two derivatives on the factor $\exp\left(\pm \ell A z^{3/2}\right)$. On what concerns the independent Stokes constants we computed in section 4.4.2, the respective values for the independent free energy Stokes constants are presented in table 4.2.

		Precision
$S_1^{(0)F}$	1.0000000000...	∞
$S_1^{(1)F}$	$-4.26510341...$ i	8
$\widetilde{S}_1^{(2)F}$	2.13255170... i	8

Table 4.2: The independent Stokes constants for the free energy of 2d supergravity or 1d type 0B string theory. They are related to the Stokes constants of the Painlevé II equation via (4.134) and (4.135).

Chapter 5

Quartic Matrix Model II: Phase Diagram and Trivalent Phase

The contents of this chapter will appear in [136], with R. Couso-Santamaría and R. Schiappa.

5.1 Introduction

The one- and two-cut phases of the quartic matrix model are very well understood at this stage [1, 25], as we highlighted in the previous chapter. These are Stokes phases with the standard $1/N$ expansion, which we discussed in 3.3.2. There is a perturbative series in powers of $1/N^2$ and then a non-perturbative completion into a transseries including powers of both $\exp(-A/g_s)$ and $1/N$. Furthermore, the coefficients of different instanton sectors and loop orders, $\mathcal{R}_g^{(n|m)}$ [1], are very tightly bound together by the asymptotic relations that come out of resurgence.

With this in mind, it is natural to wonder if the quartic matrix model has other kinds of phases. In particular, if it has phases with the oscillatory large N asymptotics, as we have discussed before. And the answer is positive. These *anti-Stokes* phases are now being understood [136–138] and in some sense they will close the story of the quartic matrix model. There are two types of such phases to consider. One where there are three cuts, which we will loosely refer to as "anti-Stokes" phase, and another where the eigenvalues condense along a trivalent-tree graph, which we will refer to as "trivalent phase" and devote most of our attention to. In section 5.2 we will use a numerical method to generate the eigenvalue distributions and study the phase diagram. This study was done, albeit from a slightly different perspective, by Bertola and Tovbis [125], and the existence of these trivalent-tree distributions was first discussed by David [105]. Then in section 5.3 we will discuss some

[1] Similarly for $\mathcal{P}$, $\mathcal{Q}$ or $\mathcal{F}$

aspects of the trivalent phase, mostly as a result of numerical methods.

The great interest in these phases can be divided into two camps. On one hand, we have stressed how inside Stokes phases the transseries expansion is well understood and everything falls into place. However, as we will show below, these phases are bound by anti-Stokes lines. These are lines in the complex plane where $\mathbb{R}\mathrm{e}\frac{A(t)}{g_s} = 0$, and at this point the perturbative and instanton sectors are all of the same order. So crossing these lines is akin to a phase transition. The goal is then to understand how the transseries can be reorganized into a (generalized) theta function. As always, we will want to match, for example, a result obtained directly in the trivalent phase to one "engineered" out of the one-cut solution. If these transitions can be brought totally under control, there is the hope that all the different phases can be connected and described by a single object, which would be the *full*, grand-canonical, background-independent, partition function of the quartic matrix model. The second perspective is related to the "universality" of matrix models. They tend to appear, in different shapes and sizes, in many different areas of theoretical physics, as we outlined in the introduction. And, as we shall see in the phase diagram below, the trivalent phase stretches out to infinity in the complex plane (of the 't Hooft parameter), so it is in some sense the generic phase of the quartic matrix model. It is then logical to ask if this type of trivalent (or multivalent in general) distribution also exists in more complicated matrix models. That is, to ask if there are phases of large N gauge theories, for example ABJM, which are currently not known and have oscillatory large N asymptotics. This is of course a subject for future investigation.

5.2 Phase Diagram of the Quartic Matrix Model

We will investigate the different phases of the quartic matrix model by resorting to numerical methods. But rather than using a relaxation method such as the one in section 3.3.2, we will instead solve the recursion (3.16)

$$r_n - \frac{\lambda}{6}\, r_n \left(r_{n-1} + r_n + r_{n+1}\right) = n g_s \tag{5.1}$$

directly. In other words, we need to compute r_1 and r_2 and then we can plug them into the recursion to extract the subsequent r_n. But to do this we need to address an issue that was not important up to now, namely the choice of integration contour(s). When we wrote down the matrix integral (1.3) we purposely overlooked the fact that the integration runs over an integration contour γ. The only constraint on γ is that it must reach infinity along directions through which the weight $\mathrm{e}^{-\frac{1}{g_s}V(z)}$ decays exponentially. Or more generally it can be a combination of contours falling off to infinity in the appropriate regions. These regions are angular wedges with openings of $\pi/4$ centered around the rays $\Omega_j = \left\{z : \arg z = \frac{(2j-1)\pi}{4} + \frac{\arg\,(t/\lambda)}{4}\right\}$,

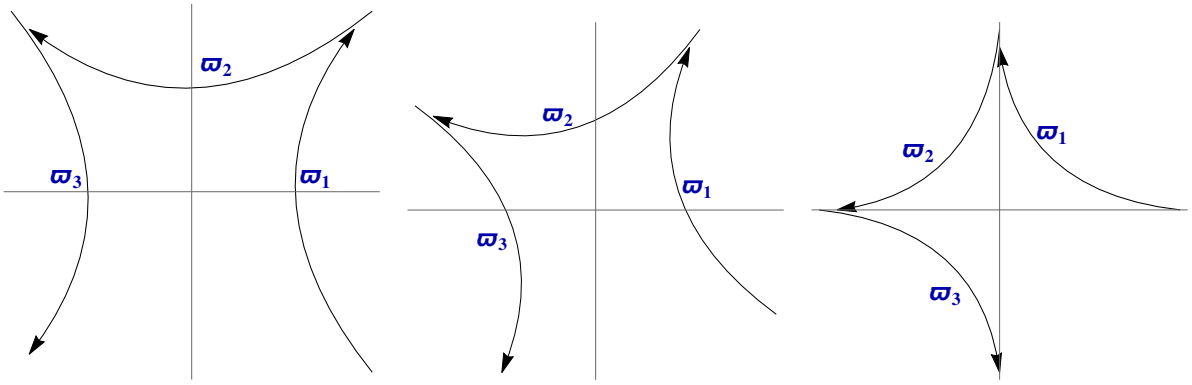

Figure 5.1: Basis of integration contours for $\arg t = 0$ (left), $\arg t = \pi/3$ (middle) and $\arg t = \pi$ (right), and real λ.

$j = 1, 2, 3, 4$ [2]. So an integration contour can be specified by two integers (j_a, j_b) indicating that the contours starts from infinity along Ω_{j_a} and goes off to infinity again along Ω_{j_b}. There are six such combinations, but we can choose a basis of three homologically independent contours. We will take as a basis the contours [3]

$$\{\varpi_1, \varpi_2, \varpi_3\} = \{(4,1),\, (1,2),\, (2,3)\}\,, \tag{5.2}$$

and for different values of $\arg t$ these can be seen in figure 5.1. After choosing a basis there is now the matter of choosing the weights ϱ_j assigned to each contour, and we are now defining orthogonal polynomials with the following procedure

$$h_n\, \delta_{n,m} = \sum_{k=1}^{3} \varrho_k \int_{\varpi_k} \mathrm{d}z\, \mathrm{e}^{-\frac{1}{g_s}V(z)} p_n(z)\, p_m(z)\,, \tag{5.3}$$

with $\varrho_1 + \varrho_2 + \varrho_3 = 1$. The multiple possibilities in terms of weight assignments are listed in detail in [125], but we shall focus solely on the "symmetric" combination

$$\varrho_1 = \varrho_3 = \frac{1}{4}\,, \varrho_2 = \frac{1}{2}\,. \tag{5.4}$$

We could also entertain the possibility of having $\varrho_1 = \varrho_3 = a$, $\varrho_2 = 1 - 2a$, but since our approach for now is mostly qualitative the choice (5.4) is enough. The dependence on the contour weights is also worthy of investigation [136], since there is a chance they may be related to transseries parameters. The main advantage of this symmetric choice is that it

[2] Given our excess of variables, the quartic coupling λ will always be fixed, either to 1 or -1 depending on what is more convenient. The 't Hooft coupling t, and consequently g_s is allowed to have complex values.

[3] The reader should notice that the different conventions used above for the one- and two-cut solutions allow us to integrate along the real axis.

fixes $s_n = 0$ in (3.15). This means an orthogonal polynomial setup with r_n coefficients alone is enough to generate anti-Stokes and trivalent distributions.

The procedure is now straightforward. We start by computing h_0, h_1 and h_2 from the definition (5.3). These can be expressed in terms of hypergeometric functions, and from them we find $r_1 = h_1/h_0$, $r_2 = h_2/h_1$. This is all the input needed for the recursion, and the r_n for $N \sim 1000$ can be found with a *Mathematica* code within a few minutes. The main difficulty is that the initial data should have enough precision to carry through to the end. The knowledge of the r_n is enough to compute the partition function (and the free energy), and these are numerical predictions to be tested later against the analytical description of the trivalent phase. But for now we are more concerned with the phase diagram, so the next step is to build the orthogonal polynomials from the recursion coefficients. This simply involves the using the definition

$$p_{n+1} = z\, p_n - r_{n-1}\, p_{n-1}\,. \tag{5.5}$$

From the highest polynomial, p_N, we get a prediction for the eigenvalue distribution by computing its zeros. For finite N it is not true that the eigenvalues, solutions of the equations of motion, coincide with the zeros of the highest polynomial. But in the large N limit the eigenvalues condense in cuts and the zeros will certainly become dense in the same cuts. So as long as our inferences are qualitative in nature and N is sufficiently large there should be no issues, and we will refer to zeros and eigenvalues interchangeably. In the Fig. 5.2 we show several distributions alongside the ray $\theta = \pi/6$. We see that we start with a one-cut solution when $|t| = 1/3$. Then as $|t|$ increases this cut will grow until a certain point, and then the two cuts, one on each side, start opening up and we have a three-cut configuration like the middle-picture. As $|t|$ increases even further the three cuts eventually collide and two extra legs grow out to generate the trivalent configuration seen on the right. In Fig. 5.3 we do the same alongside the ray $\theta = 3\pi/4$. Here we start with two cuts, then with $|t|$ getting larger a third one opens up in the middle, and then after they collide we move into the trivalent configuration. We can look at the different configurations and track where the phase transitions occur, and similarly to [125] we find the phase diagram shown in Figure 5.4. Furthermore, we know that the boundaries of the one- and two-cut phases are precisely the sets of points where $\mathbb{R}\mathrm{e}\, A_{\text{1-cut}}(t) = 0$ and $\mathbb{R}\mathrm{e}\, A_{\text{2-cut}}(t) = 0$, where $A_{\text{1-cut}}(t)$ is (4.4) and $A_{\text{2-cut}}(t)$ is (4.11). What is more surprising is the fact that the outer boundary, separating the anti-Stokes and trivalent phases, is governed by the one-cut action with the "wrong" choice of square root in (4.3). That is, instead of (4.3) we define

$$\alpha_\pm^2 = \frac{1}{\lambda}\left(1 \pm \sqrt{1 - 2\lambda t}\right)\,, \tag{5.6}$$

so that $A_{\text{1-cut}}(t) = 0$ corresponds to (4.4) with $\alpha_-(t)$. Then this outer boundary is where

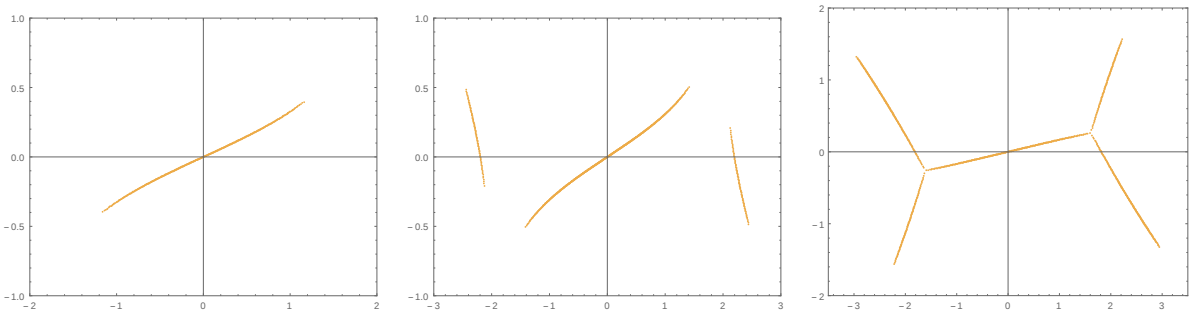

Figure 5.2: Eigenvalue distributions with $\arg t = \pi/6$ and: a) $|t| = 1/3$ (left), corresponding to a one-cut configuration; b) $|t| = 3/5$ (middle), corresponding to a three-cut (anti-Stokes) configuration; c) $|t| = 3$ (right), corresponding to a trivalent configuration.

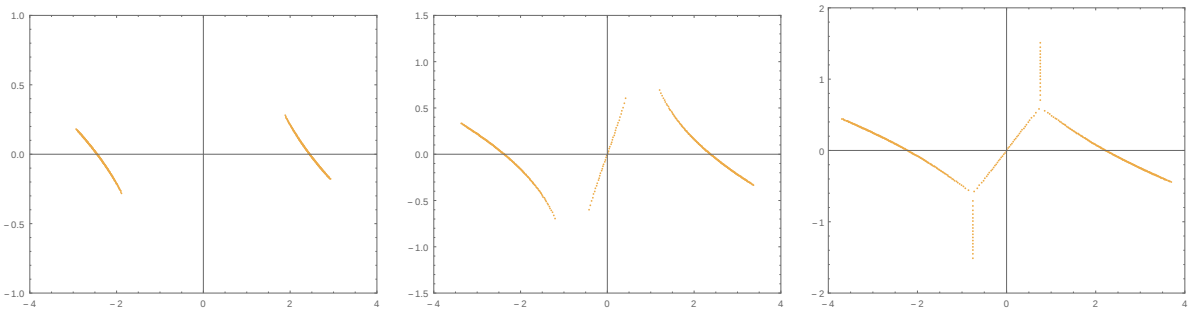

Figure 5.3: Eigenvalue distributions with $\arg t = 3\pi/4$ and: a) $|t| = 1/3$ (left), corresponding to a two-cut configuration; b) $|t| = 3/2$ (middle), corresponding to a three-cut (anti-Stokes) configuration; c) $|t| = 3$ (right), corresponding to a trivalent configuration.

$\mathbb{R}\mathrm{e}\, A_{\text{1-cut}}(t)\Big|_{\alpha(t)\to\alpha_+(t)} = 0$. While an unstable one-cut solution with this choice $\alpha_+(t)$ is expected to exist, it is an open problem to physically explain why it is the one signaling the appearance, and energetic dominance, of trivalent structures.

5.3 Trivalent-tree phase

For all the reasons discussed above, the trivalent phase is expected to provide very interesting results and perspectives. While this study is not over yet, we can discuss some preliminary results and open problems.

Having gathered significant numerical data concerning the trivalent treelike phase of the quartic matrix model, let us now address this phase from an (analytical) spectral geometry standpoint. There are several aspects one should consider. First, one needs to construct the spectral geometry configuration. At the computational level it turns out this is similar to the multi-cut case [57, 110, 111], but also including some novelties dealing with the

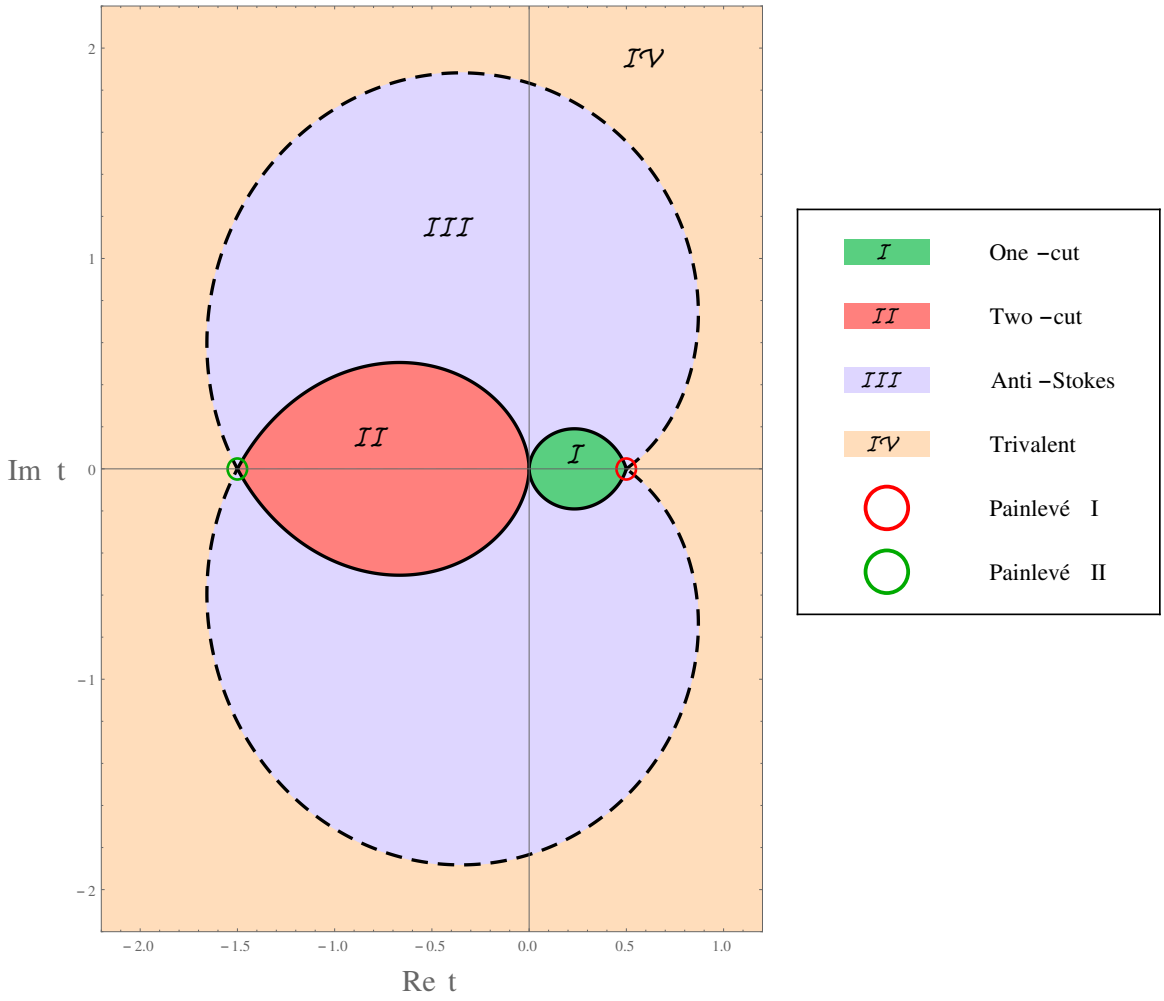

Figure 5.4: Quartic matrix model phase diagram. There are two "lobes" (green and red) where the Stokes phases, one- and two-cut, are thermodynamically favored. Then there is an anti-Stokes three-cut phase (light blue) and the general (orange) distribution outside of this is a trivalent one. The lines, dashed and solid, are anti-Stokes lines, corresponding to the condition $\mathbb{R}\mathrm{e}(A(t)/t) = 0$ for the different actions. The red and green circles are the points where the (double-scaled) system is described by Painlevé I and II equations, respectively.

definitions of A- and B- cycles, and what physical role they play. Secondly, one may ask what the nature of the nonperturbative effects is, since they are usually associated to eigenvalue tunneling (see, *e.g.*, [10, 55]). On the one hand the trivalent configuration is similar to the ones addressed in [11], in the sense that there are no non-trivial saddles outside of the (trivalent) cut configuration. One could then expect for instanton effects associated to A-cycle eigenvalue tunneling as in [11]. But, on the other hand, it turns out that due to its trivalent nature the cut configuration actually has more than two endpoints and,

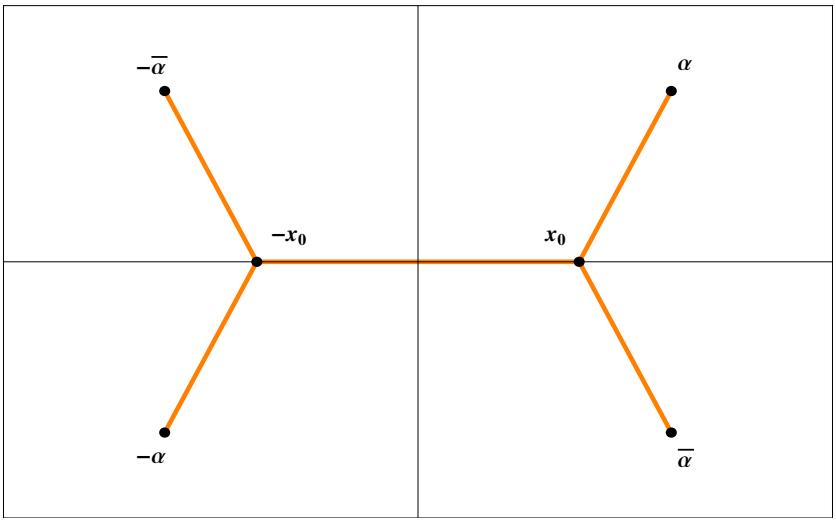

Figure 5.5: The trivalent-tree configuration for the quartic matrix model, with 't Hooft coupling positive real, larger than the Painlevé I critical point ($t = 1/2$). The branch-points of the configuration depend on $x_0 \in \mathbb{R}$ and $\alpha \in \mathbb{C}$, yielding three (real) unknowns to determine in order to completely fix the spectral geometry.

consequently, one requires equilibrium conditions[4] in between these many endpoints of the trivalent cut. In this sense, the instanton effects could actually be more reminiscent of the multi-cut B-cycle eigenvalue tunneling type [1, 10, 57]. While our expectation is that oscillatory large N asymptotics will be found, it is still an open problem at this stage. Another open problem to address concerns the (eventual) difference between the anti-Stokes and trivalent phases from the point of view of the $1/N$ expansion.

5.3.1 Constructing Trivalent Spectral Configurations

In the previous section 5.2 we have gathered a large amount of numerical evidence that, within the positive real axis and past the Painlevé I critical point, the relevant trivalent spectral configuration of the quartic matrix model is as illustrated in figure 5.5, with $x_0 \in \mathbb{R}$ and $\alpha \in \mathbb{C}$. This means we have three real unknowns to determine, in order to fully specify the geometry.

Let us briefly discuss how this calculation carries through in the present trivalent context (although we always have in mind the configuration of figure 5.5, the first couple of paragraphs that follow will be generic). In the large N continuum limit, the matrix model

[4]Do notice that one may also think of the A-cycle eigenvalue tunneling of [11] as a (trivial) equilibrium condition in-between the two extrema of the same single cut. In this sense both A- and B- cycle conditions are just conditions describing energy differences between pairs of branch-points of the spectral curve.

equations of motion become (see [50] for a review)

$$\frac{1}{t}\,V'(z) = \omega_0(z+\mathrm{i}\epsilon) + \omega_0(z-\mathrm{i}\epsilon), \tag{5.7}$$

where we have denoted by $\omega_0(z)$ the genus zero resolvent,

$$\omega(z) = \frac{1}{N}\left\langle \mathrm{Tr}\frac{1}{z-M}\right\rangle \quad \text{with} \quad \omega_0(z) = \int_{\mathcal{C}} \mathrm{d}\lambda\, \frac{\rho(\lambda)}{z-\lambda}, \tag{5.8}$$

and where $\rho(\lambda)$ is the eigenvalue density. It is now important to notice that, as written, with the $\pm\mathrm{i}\epsilon$ prescription for the jump across a cut, (5.7) is appropriate to, say, a multi-cut configuration where all cuts lay along the real axis. For a configuration such as the one in figure 5.5, with cuts along complex directions, this prescription must be (easily) replaced with left/right shifts along the normal direction to the cut, and we implicitly assume this is done as we write (5.7). Further, this equation is a local condition, essentially valid everywhere but at branch points.

Under the assumption that a phase transition into the trivalent region will not change the hyperelliptic nature of the spectral geometry [105, 124], and regarding any trivalent vertex just as any other branch point, the solution to (5.7) is the usual one,

$$\omega_0(z) = \frac{1}{2t}\oint_{\mathcal{C}} \frac{\mathrm{d}w}{2\pi\mathrm{i}}\,\frac{V'(w)}{z-w}\sqrt{\prod_{k=1}^{2s}\frac{z-x_k}{w-x_k}}, \tag{5.9}$$

with $2s$ now the number of branch points, $\{x_k\}$, including either trivalent vertices or endpoints of the cuts, and $\mathcal{C}$ a large contour encircling the trivalent configuration. In order to solve the problem one thus has to fix $2s$ (generically complex) unknowns. The usual large z asymptotics of the resolvent yield the familiar $s+1$ complex constraints (with $n=0,\ldots,s$)

$$\oint_{\mathcal{C}} \frac{\mathrm{d}w}{2\pi\mathrm{i}}\,\frac{w^n\,V'(w)}{\sqrt{\prod_{k=1}^{2s}(w-x_k)}} = 2t\,\delta_{ns}. \tag{5.10}$$

The remaining $s-1$ complex constraints arise just as in the usual multi-cut case [105, 111], considering cycles in-between all possible branch points. These constraints are know as the Boutroux conditions [105, 124]. Introducing the spectral curve via its standard definition $y(z) = V'(z) - 2t\,\omega_0(z)$, these conditions say that

$$\mathbb{R}\mathrm{e}\oint_{\gamma} \mathrm{d}z\, y(z) = 0, \tag{5.11}$$

for *any* cycle γ on the curve, *i.e.*, all cycles of the spectral curve one-form must be purely

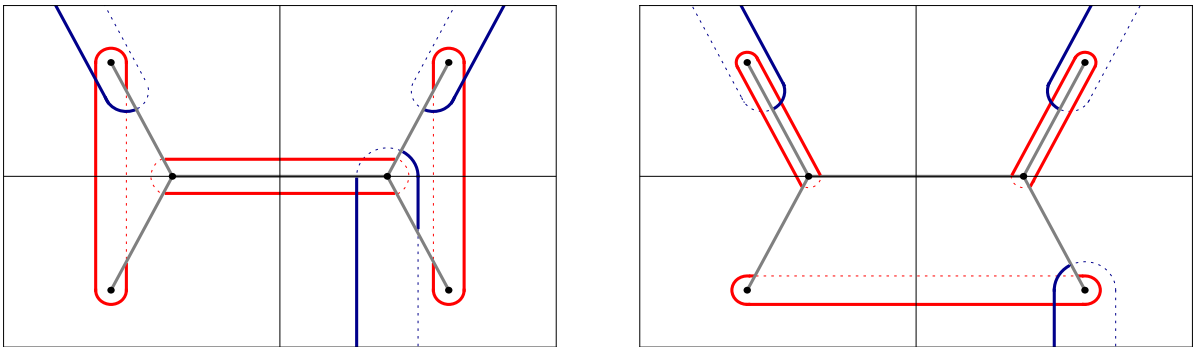

Figure 5.6: Different choices of A- and B- cycles for the trivalent-cut configuration. Notice that in both images we have included several examples, even non-homotopically-independent choices. We have plotted A-cycles in red and B-cycles in dark blue, but it is simple to see that upon compactification and homotopy, one can turn A-cycles into B-cycles and vice-versa [59]. This means their choice is not as rigid as in standard multi-cut configurations and all they have to obey is their standard definition $A_i \cap B_j = \delta_{ij}$.

imaginary. The Boutroux conditions are real constraints and, because with $2s$ branch points one finds $2s-2$ homologically independent cycles, they amount to the missing $s-1$ complex constraints that finally fully specify the spectral geometry.

The Boutroux conditions are very physical in the usual multi-cut scenario, with all cuts along the real axis (and with the canonical choice of A-cycles encircling cuts and B-cycles in-between cuts). In this case A-cycles are automatically purely imaginary and thus unconstrained (leading to the partial 't Hooft moduli familiar in topological string large N dualities [29]), while B-cycles are automatically purely real and thus forced to vanish (leading to the usual multi-cut equilibrium conditions [111]). In the trivalent case there is no canonical choice of A- and B-cycles; in fact there is now no clean topologically distinction between them as illustrated in figure 5.6. This is of course not an issue, as a Boutroux condition (5.11) is naturally assigned to every pair of branch points. We shall see this explicitly in the following.

Finally, recall that also the eigenvalue density follows from the discontinuity[5] of the planar resolvent along any corresponding cut-leg, in-between two branch points,

$$\rho(\lambda) = -\frac{1}{2\pi \mathrm{i}} \left(\omega_0(\lambda + \mathrm{i}\epsilon) - \omega_0(\lambda - \mathrm{i}\epsilon)\right). \tag{5.12}$$

In particular, due to the hyperelliptic nature of the spectral curve, there are no eigenvalues at any of the branch points, be them endpoints of the cut configuration or trivalent vertices. Further, there is no monodromy at any branch point.

All this said, let us focus on our case of interest, the quartic matrix model with potential

[5]The same remarks concerning how to properly define (5.7) along complex directions also hold in here.

$V(z) = \frac{1}{2}z^2 - \frac{\lambda}{24}z^4$, where λ is the quartic coupling constant. Using the *ansatz* (5.9) for the resolvent associated to the configuration of figure 5.5, it now follows

$$\omega_0(z) = \frac{1}{2t}\oint_{\mathcal{C}} \frac{\mathrm{d}w}{2\pi\mathrm{i}}\,\frac{V'(w)}{z-w}\sqrt{\frac{(z^2-\alpha^2)\,(z^2-\bar{\alpha}^2)\,(z^2-x_0^2)}{(w^2-\alpha^2)\,(w^2-\bar{\alpha}^2)\,(w^2-x_0^2)}}, \tag{5.13}$$

where, as mentioned earlier, there are three real unknowns to fix (while $x_0 \in \mathbb{R}$, $\alpha \in \mathbb{C}$). The conditions (5.10) yield four equations, of which only two are non-trivial,

$$x_0^2 + \alpha^2 + \bar{\alpha}^2 = \frac{12}{\lambda}, \tag{5.14}$$

$$x_0^4 + \alpha^4 + \bar{\alpha}^4 = \frac{24}{\lambda^2}\,(3 - 2\lambda t)\,. \tag{5.15}$$

To fix the last real constraint, use the spectral curve

$$y(z) = -\frac{\lambda}{6}\sqrt{(z^2-\alpha^2)\,(z^2-\bar{\alpha}^2)\,(z^2-x_0^2)} \tag{5.16}$$

and all we lack is to apply the Boutroux condition (5.11). Considering the basic cycles illustrated in figure 5.7, we need to look for a combination of cycles that can yield a physical condition. For instance, how many eigenvalues lie on the middle-cut and how many lie on the outer legs. The task is straightforward but technically involved, as the integrals will be realized as combinations of elliptic integrals, and those always require some care in dealing with the choices of branch cuts.

In the meantime we can look for further numerical information in the trivalent phase. In particular, we can use our numerical eigenvalue distributions to compute eigenvalue densities, and these will also provide a useful test for the analytical spectral curve [6]. This is shown below in Fig. 5.8 for $t = 2+\mathrm{i}$ and $t = 20$, and $N = 500$. We proceed by fitting a straight line through all the five segments in the configuration, projecting the eigenvalues onto these lines and then essentially breaking each segment into intervals and counting how many eigenvalues lie in each interval. For this reason the densities sometimes appear to be flat, but that is just a consequence of the finite number of eigenvalues. By increasing the number of eigenvalues or reducing the number of intervals the pictures look better. We notice that as $|t|$ increases we approach the pure quartic limit, and as such there are less eigenvalues of the middle cut as it shrinks. This limit is discussed below.

5.3.2 Pure Quartic Limit

The trivalent phase has an interesting limit as $|t| \to \infty$. As we increase t along any ray, the middle-cut shrinks and in the end the eigenvalue distribution is a $\mathbb{Z}_4$ symmetric cross. The

[6] Recall that the eigenvalue density is given by the discontinuity of the spectral curve across branch cuts.

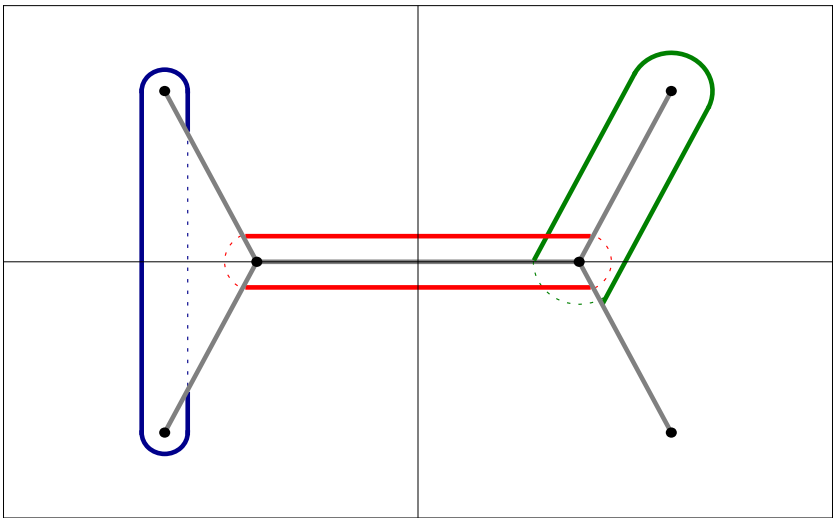

Figure 5.7: The "elementary" compact cycles in the trivalent configuration. Notice that there are four cycles of the "green" type; one around each of the outer legs . Further, there are also six cycles of the "blue" type; one joining each pair of "exterior" branch points.

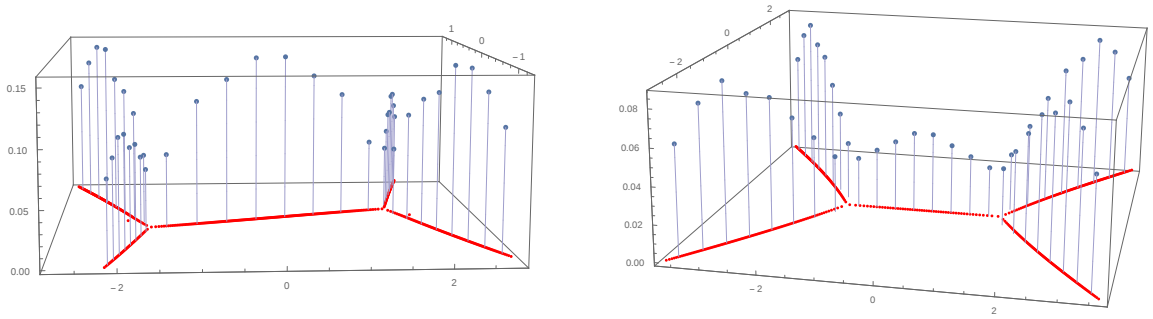

Figure 5.8: Numerical calculation of eigenvalue densities. The red dots are the eigenvalues (in rigor, they are the zeros of orthogonal polynomials), and the blue dots above are an estimate of the density of eigenvalues along each segment. Both plots have $N = 500$, the left one corresponds to $t = 2 + \mathrm{i}$ and the right one to $t = 20$.

shrinking of the middle-cut can be seen in Figure 5.9 (left). This means that for (infinitely) large t the quartic matrix model is reduced to a "pure" quartic matrix model (meaning the potential has only the z^4 term). This could be expected from the starting matrix integral.

Namely we could re-scale the variables as $z \to \sqrt{g_s}\, z$, such that the exponent becomes

$$\frac{1}{g_s} V(z) \to \frac{1}{2} z^2 + \frac{\lambda\, g_s^2}{4!} z^4 \,. \tag{5.17}$$

Since t is proportional to g_s the quartic term is clearly dominant in this limit. We can also provide numerical evidence of this aspect by comparing the eigenvalue distributions of quartic and pure quartic models, using the recursion as described in 5.2 [7]. If we label the eigenvalues as $\{\lambda\}$ and $\{\lambda^{\rm PQ}\}$, we can see from the (log)plot of the total distance between eigenvalues, $\sum_i \left|\lambda_i - \lambda_i^{\rm PQ}\right|^2$, in Fig. 5.9 (right) that these get smaller and smaller as $|t| \to \infty$, meaning the quartic distribution approaches the pure quartic one. In both figures we have

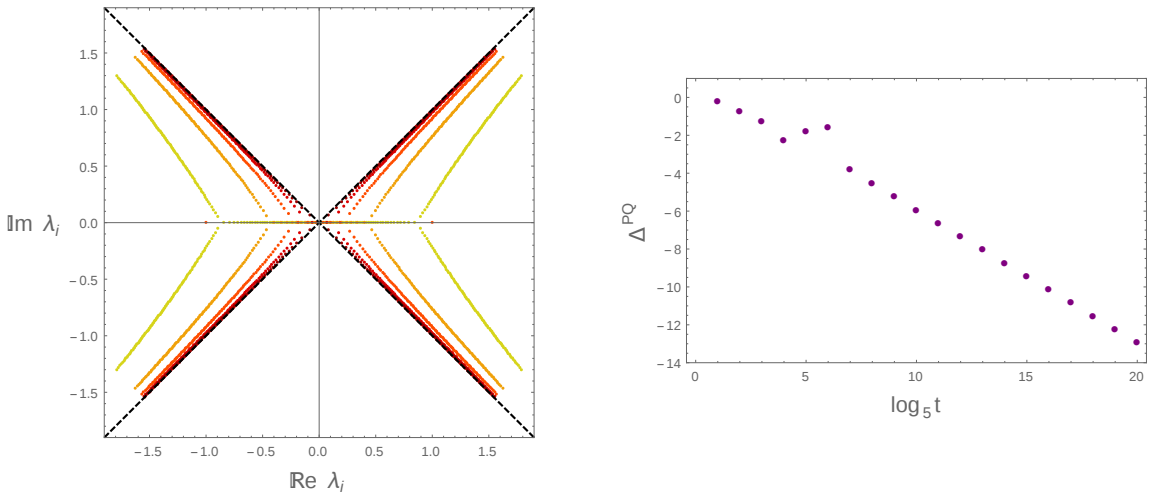

Figure 5.9: Left: eigenvalue distributions for $t = 10^k$, $k = 1, \ldots, 5$, going from light to dark. The last distribution is hardly distinguishable from the dashed asymptotes placed at $\pi/4$ angles; Right: Sum of distances between the eigenvalues of the "full" quartic and those of the "pure" quartic, $\Delta^{\rm PQ} \equiv \sum_i \left|\lambda_i - \lambda_i^{\rm PQ}\right|^2$, for $t = 5^k$ and $k = 1, \ldots, 20$. This is a log-log plot, so we have $\log \Delta^{\rm PQ}$ vs. k.

absorbed a scale factor of $t^{1/4}$ in the eigenvalues, but the pictures would not change without this. This re-scaling only helps to keep all the eigenvalue distributions in the same picture, as we have identified this to be the scaling of the eigenvalues. It is possible to predict this by looking back at the finite N equations of motion

$$-\frac{N}{t} V'(\lambda_i) + 2 \sum_{j \neq i} \frac{1}{\lambda_i - \lambda_j} = 0 \,. \tag{5.18}$$

[7] The pure quartic recursion amounts to taking only the term quadratic in r in (5.1).

In the limit of large t, the only way the two terms in the equation of motion remain of the same order is if the eigenvalues scale as $\lambda_i \sim t^{1/4}$. We can also take advantage of this limit to extract some information about the spectral curve. Concretely, in this limit the conditions (5.14) with $x_0 = 0$ yield the following result for the endpoints of the outer legs

$$\alpha = \mathrm{e}^{\frac{\mathrm{i}\pi}{4}} \left(\frac{24t}{\lambda}\right)^{1/4} + \mathcal{O}(t^0)\,. \tag{5.19}$$

The subleading corrections correspond to opening up the middle-cut, and they will break the $\mathbb{Z}_4$ symmetry. There is always the possibility of computing corrections to the endpoints order by order, for instance using a small x_0 as a parameter, and then comparing them both against numerics and against an analytical solution for the endpoints, as a safety check. It is also not hard to imagine having enough conditions to determine the endpoints but having them only defined implicitly. Then a power expansion could be a very useful check.

The pure quartic limit also conjures up other intriguing questions. For starters, when tackling it with orthogonal polynomials, one could hope to find an "exact" solution for the partition function, in the spirit of the Gaussian matrix model or the other examples discussed in [11]. But while there seems to be some structure emerging in the norms h_n we were not able to guess them completely. We should keep in mind that this still is a full-fledged interacting theory. If such an exact solution were available, we could contemplate introducing the Gaussian part of the potential as a perturbation [8] and this could be an alternative window into the trivalent phase. Additionally we could investigate if the asymptotic structure, presumed to be of the theta-function type, survives in this limit, or if the $1/N$ expansion somehow boils down to the traditional kind we had in the Stokes phases. But at this stage it would seem like an exact solution is not at hand, and as such the pure quartic limit will remain as an interesting limit to check the analytic predictions of the trivalent phase.

[8] We would essentially compute expectation values of powers $\mathrm{Tr}M^2$.

Chapter 6

Finite N from Resurgent Large N

The contents of this chapter appear in [2]:
"Finite N from Resurgent Large N",
R. Couso-Santamaría, R. Schiappa, and R. Vaz,
arXiv:1501.01007 [hep-th], Annals Phys. **356**, 1-28 (2015)
DOI: 10.1016/j.aop.2015.02.019

6.1 Introduction

We have spent the past few chapters exploring the different phases of the quartic matrix model and (successfully) testing the implications of resurgence. As we have stressed very often, the different sectors of the transseries are bound together by a web of large-order relations, and we saw this in detail in the two-cut quartic matrix model and in more detail in Painlevé II. But we now focus our attention on a different aspect of the large N expansion. It is a divergent (asymptotic) series which is not Borel summable. So how can one make sense of such an expansion, or more concretely, how can we obtain finite N results out of the large N expansion? It is our goal in this chapter to introduce and develop a rather general method to extract (eventually *exact*) finite N results out of the large N expansion.[1]

With the goal of having this chapter as self-contained as possible, we will review some of the ideas in play. We are also going to use a notation which is slightly different from the one used before, but more convenient in this setup. Let us focus upon the free energy, whose

[1] As originally emphasized by 't Hooft [26], it was then hoped that the large N expansion, and in particular the planar limit, would lead to "reasonable" approximations in spite of the physical interest in smaller values of N.

large N asymptotic expansion is

$$F(N,t) \simeq \sum_{g=0}^{+\infty} N^{2-2g} F_g(t). \tag{6.1}$$

One might hope to make sense out of this factorially divergent series via Borel resummation. In fact, the Borel transform (2.8) removes the factorial growth from the perturbative coefficients as

$$\mathcal{B}[N^{2-2\alpha}](s) = \frac{s^{2\alpha-3}}{(2\alpha-3)!}, \tag{6.2}$$

so that its (non-zero) radius of convergence is now dictated by the subleading exponential growth of the original perturbative coefficients. Upon analytic continuation of $\mathcal{B}[F](s)$ along the complex Borel s-plane, the Borel resummation follows whenever the ray of integration along the direction θ avoids the integrand's singularities. In this case one finds (2.9)

$$\mathcal{S}_\theta F(N,t) = \int_0^{\mathrm{e}^{\mathrm{i}\theta}\infty} \mathrm{d}s\, \mathcal{B}[F](s)\, \mathrm{e}^{-sN}. \tag{6.3}$$

The important point is that even when the choice of direction θ is such that the above integration is possible, *i.e.*, that one finds Borel summability along θ, this expression need not match the exact result due to the occurrence of Stokes phenomena [139]. In fact, the factorial large-order behavior was already telling us that one is missing nonperturbative corrections, typically of the form $\sim \exp(-N)$, which are invisible to the perturbative expansion (6.1). But in spite of that, these initially exponentially suppressed terms may not be neglected. In fact, upon variation of θ in (6.3), they may grow to become of order one or, eventually, exponentially enhanced with respect to (6.1), and thus completely obliterate any sense in which the resummation (6.3) may yield correct results. This is the essence of Stokes phenomena, implying that the perturbative series alone cannot properly define the free energy and it needs to be enlarged into a *transseries*.

That Borel resummation, if allowed, cannot be the whole story when it comes to the genus expansion was recently verified numerically to great precision in [140] (following earlier work on the quantum mechanical quartic oscillator [141, 142]). In the example of the large N ABJM gauge theory (but having also addressed other examples, such as topological strings in the local $\mathbb{P}^1 \times \mathbb{P}^1$ Calabi-Yau geometry), [140] showed numerically that even if this case satisfies the requirements of Borel summability, Borel resummation of the genus expansion does not agree with the exact value (computed via integrability), with the mismatch controlled by complex D2-brane instantons. As explained in the above paragraph, this is just explicitly verifying that, in general, Borel resummation is somewhat useless from a practical point-of-view due to Stokes phenomena: even if there are no obstructions to performing the inverse Borel transform in (6.3), and the asymptotic expansion is dubbed Borel summable,

the resulting resummation will yield the correct result *only if* Stokes phenomenon has not yet occurred. Otherwise it will always miss nonperturbative contributions: further terms in the transseries may have already been turned on by the crossing of Stokes lines and these are thus needed and crucial to obtain correct results.

Thus, as we shall explore in detail below, finite N results can only be obtained out of transseries (3.24); schematically of the form

$$F(N,t) = \sum_{g=0}^{+\infty} N^{2-2g} F_g^{(0)}(t) + \sigma\, \mathrm{e}^{-NA(t)} \sum_{g=0}^{+\infty} \frac{1}{N^g}\, F_g^{(1)}(t) + \sigma^2\, \mathrm{e}^{-2NA(t)} \sum_{g=0}^{+\infty} \frac{1}{N^g}\, F_g^{(2)}(t) + \cdots . \tag{6.4}$$

All these objects have been discussed at length before, but is important to recall that the transseries parameter σ encodes Stokes phenomena (we shall discuss this point carefully in the main body of the text, but see also [97] for general and very explicit formulae). Resurgent transseries are at the basis of Écalle's work [17–19], where by joining analytic and non-analytic building blocks they allow for representations (in some sense, for constructions and *definitions*) of broad classes of functions, including functions with singularities and branch cuts. This is why in many cases where one might only have large N expansions available, a large N resurgent transseries may allow for a *definition* of the finite N theory and (considering arbitrarily large numbers of components in the transseries) for a calculation of *exact* finite N results.

While the initial gauge theory was only defined for *integer* values of N, the resurgent transseries is constructing a function of N, eventually valid upon analytic continuation for *arbitrary complex* values of N. While at first this might sound unexpected for nontrivial interacting gauge theories, it is actually familiar in free gauge theories such as the Gaussian or Penner matrix models (see, *e.g.*, [11, 50] for brief reviews). For instance, the partition function of the Gaussian matrix model (normalized against the volume of its U(N) gauge group), while only defined for integer values of N via a matrix integral, may still be computed as[2]

$$Z_{\mathrm{G}}(N) = \frac{g_s^{\frac{N^2}{2}}}{(2\pi)^{\frac{N}{2}}}\, G_2\left(N+1\right), \tag{6.5}$$

where $G_2(z)$ is the Barnes G-function which is in fact an entire function on the complex plane (see, *e.g.*, [143]). Finding nontrivial gauge-theoretic examples where nonperturbative completions allow for results defined at arbitrary values of N is not as straightforward. But a class of very interesting such examples was recently addressed in [61], within the context of ABJM gauge theory on the three-sphere. In their examples, supersymmetry and integrability ensure that all (genus) contributions to the partition functions actually *truncate*

[2]The so-called string coupling g_s appears as the overall coupling in front of the quadratic potential inside the matrix integral defining the partition function, and relates to the 't Hooft coupling as $t = g_s N$.

to finite sums, allowing for the computation of closed-form expressions at arbitrary values of N. In particular, partition functions for these theories were also found to be entire functions on the complex N-plane.

One fascinating spin-off of the calculations in [61] is the possibility to study exact properties of the partition function of ABJM gauge theory as a function of N. As shown therein, the fact that all partition functions found in [61] were entire functions on the complex N-plane implies the non-existence of phase transitions in N; in particular the non-existence of a phase transition as one moves from (real) large N to small N. From a dual holographic viewpoint [27] this implies there is really no drastic distinction between a "quantum" small-distance and a "semiclassical" large-distance phase, at least in this class of theories. Furthermore [61], this is particularly striking given that if one just looks at the genus expansion by itself, the perturbative free energies do have branch cuts in the 't Hooft coupling t, misleading us on the understanding of the nonperturbative physics. This phenomenon where the perturbative singularity structure is nonperturbatively smoothened was also found earlier in [144], within the context of minimal string theory. Therein, certain observables such as the FZZT partition function, while having semiclassical branched domains, end up having entire analytical properties when addressed nonperturbatively. Interestingly enough, the mechanism by which this occurs is again based upon the aforementioned Stokes phenomena, whereby (initially) exponentially small contributions grow to take dominance and dramatically change the structure of the solutions. The large N resurgent transseries methods we develop in this chapter will allow for these types of analyses in broad classes of gauge theories, even those where neither supersymmetry nor integrability are present.

One final point to discuss is whether the resurgent transseries completion we propose, to non-integer (and complex) values of N, is the only possible such completion? In principle, gauge theory observables are only defined at positive integer values of N, and, clearly, many possible interpolating functions may exist through such a discrete set of points. It was already suggested in [61] that the familiar Gamma function serves as a good analogy. Certainly there are many other functions which solve the factorial interpolation problem, and which in fact behave much better (the Gamma function is meromorphic). One such example is the Hadamard Gamma function, which interpolates the factorials as an entire function, but many others exist; see [145] for an excellent review. What tells all these possible interpolating functions apart is, of course, whatever (differential or functional) equation defines them. In this regard, the usual Euler Gamma function is the *only*[3] function which satisfies the continuous (functional) version of the factorial recursion,

$$\Gamma(z+1) = z\,\Gamma(z). \tag{6.6}$$

When translating to our current large N problem, a rather similar situation still holds. As we shall see in the main text of this chapter, the partition function at finite integer

[3] To be correct, uniqueness is only achieved after adding the technical requirement of logarithmic convexity [145].

N is computed by solving a discrete recursion relation (the so-called string equation [49], but we shall discuss this at greater length later), while the large N resurgent transseries is obtained out of the *continuous* (functional) version of this discrete string equation [1, 16, 25]. Furthermore, this solution is very special, in the sense that it is a *resurgent* solution: all its perturbative and nonperturbative building blocks are very tightly bound together! Although we do not address this point in this work – and it should certainly be addressed in future research – it might be reasonable to expect that these two properties combined provide a *unique* analytic continuation of gauge theoretic observables to complex N (at least up to some choice of boundary conditions).

The problem of resummation of divergent asymptotic series in Physics has a long history; see, *e.g.*, [20]. In order to apply it, and extend it via the use of resurgent transseries, to the problem of the large N expansion one first needs data, on both perturbative and multi-instanton expansions. To the best of our knowledge, the gauge theories for which at present there is the largest amount of available large-N resurgent-transseries data are matrix models (and their double-scaling limits); in particular matrix models with polynomial potentials [1, 16, 25, 60, 103]. This type of matrix models is a very reasonable prototype for generic gauge theories. We shall perform our explicit calculations in the example of the quartic matrix model [1, 25], although we should stress that our methods are completely general within gauge theory.

This chapter is organized as follows. We begin in section 6.2 with a calculation of exact results in the quartic matrix model, at small (integer) values of N. This is done via standard methods using orthogonal polynomials, and several exact results are obtained for the partition function and the recursion coefficients. At fixed N, these quantities are still functions of the coupling, or, equivalently, of the 't Hooft coupling, and we address their corresponding non-trivial monodromy properties. In section 6.3 we then address the gauge-theoretic large N resurgent solution to our example. While the resurgence data of the quartic matrix model is reviewed in appendix A, section 6.3 shows how to make use of this data (or resurgence data from any other gauge theory) in order to address the resummation problem and produce finite N results. Comparison with the analytical results is achieved up to remarkable numerical accuracy. Finally, section 6.4 discusses Stokes phenomenon and how the full resurgent transseries is crucial to reproduce the analytical finite N results across the complex t-plane, including the distinct non-trivial monodromy properties one found earlier for different integer values of N. We conclude with a discussion of how the large N transseries may be analytically continued for any complex value of N, and what are the properties of the resulting partition function on the complex N-plane.

6.2 Exact Finite N Results

In order to check both the validity and the resulting accuracy of any large N transseries results, we need data to compare them against. As already mentioned in section 6.1, this

will be done within the gauge-theoretic context of the quartic matrix model, where orthogonal polynomial techniques [49] allow for straightforward calculations at small (integer) values of N. We refer the reader to [50] for an excellent overview of these methods. Most of them were introduced in section 3.2.2, but we go over them again to keep this chapter self-contained and to set the notation.

Let us begin by recalling the definition of the partition function for a one-cut matrix model, with polynomial potential $V(z)$, already written in diagonal gauge with eigenvalues z_i (as usual, the partition function was originally normalized against the volume of the gauge group $\mathrm{U}(N)$). One has:

$$Z(N) = \frac{1}{N!} \int \prod_{i=1}^{N} \frac{\mathrm{d}z_i}{2\pi} \, \Delta^2(z) \, \mathrm{e}^{-\frac{1}{g_s} \sum_{i=1}^{N} V(z_i)}, \tag{6.7}$$

where $\Delta^2(z) = \prod_{i<j}(z_i - z_j)^2$ is the Vandermonde determinant. In this expression we have chosen the standard convention (within the matrix model literature) of using the so-called string coupling, g_s, as the overall normalization, but this is of course just a notation choice and we could have likewise used a gauge-theoretic coupling $g_s \sim g^2_{\mathrm{YM}}$. In any case, in the large N 't Hooft limit one has $t = g_s N$ fixed and we shall thus mostly work with the 't Hooft coupling, t, and gauge group rank, N, in the following. Furthermore, we shall focus exclusively upon the quartic potential with quartic coupling[4] [5] λ,

$$V(z) = \frac{1}{2} z^2 - \frac{1}{4!} \lambda z^4. \tag{6.10}$$

It is a straightforward task to introduce orthogonal polynomials $p_n(z) = z^n + \cdots$, satisfying

$$\int_{\mathbb{R}} \mathrm{d}\mu(z) \, p_n(z) \, p_m(z) = h_n \, \delta_{nm} \tag{6.11}$$

with respect to the measure $\mathrm{d}\mu(z) = \frac{\mathrm{d}z}{2\pi} \, \mathrm{e}^{-\frac{1}{g_s} V(z)}$ inherited from the matrix potential. A

[4] It is important to notice that there are in fact less independent couplings in the problem than apparent at first sight. Changing variables as $w = \frac{z}{\sqrt{g_s}}$, leads to

$$Z(N) = \frac{g_s^{\frac{N^2}{2}}}{N!} \int \prod_{i=1}^{N} \frac{\mathrm{d}w_i}{2\pi} \, \Delta^2(w) \, \mathrm{e}^{-\sum_{i=1}^{N} W(w_i)}, \tag{6.8}$$

with a modified potential

$$W(w) = \frac{1}{2} w^2 + \frac{1}{4!} \kappa w^4, \tag{6.9}$$

where we have defined $\kappa \equiv -\lambda g_s$. It is then clear that there is a unique independent coupling in the matrix integral, although, as we said above, we shall mostly work with the 't Hooft coupling t.

[5] To make contact with chapter 5, we are going to integrate over the real line and eventually fix $\lambda = -1$. In the basis (5.2) this amounts to taking $\varrho_1 = \varrho_2 = 1/2$ and $\varrho_3 = 0$.

simple calculation [49, 50] then shows how the partition function may be written as a product of the above polynomial norms

$$Z(N) = \prod_{n=0}^{N-1} h_n = h_0^N \prod_{n=1}^{N} r_n^{N-n}, \tag{6.12}$$

or, equivalently, as a product of the recursion coefficients $r_n = \frac{h_n}{h_{n-1}}$. These coefficients are precisely the same as the ones appearing in the recursion relation explicitly constructing orthogonal polynomials (for an even potential as we have in our case)

$$p_{n+1}(z) = z\, p_n(z) - r_n\, p_{n-1}(z). \tag{6.13}$$

Conversely, these recursion coefficients may also be written in terms of the partition function:

$$r_N = \frac{Z(N+1)\, Z(N-1)}{Z(N)^2}. \tag{6.14}$$

Of course at the end of the day the partition function (6.7) is solely determined by the potential (6.10), which means that these coefficients must also be determined by this choice of potential. In fact they are; they obey the so-called string equation [49], a finite-difference recursive equation which in the case of the quartic potential is

$$r_n \left(1 - \frac{\lambda}{6}\left(r_{n-1} + r_n + r_{n+1}\right)\right) = n g_s. \tag{6.15}$$

Note that their relevance extends beyond the above formulae, as these are also the natural objects to address and compute when considering the 't Hooft large N limit, see [49]. Furthermore, these are also the natural quantities to work with when constructing the large N resurgent transseries expansion for the partition function (or for the free energy), *e.g.*, [1, 25].

Using these relatively standard techniques, one may now compute the exact partition function for a few values of the rank N. If N is small, one may proceed and compute the polynomial norms, h_n, directly. First introduce the moments (under appropriate convergence conditions)

$$\mathfrak{m}_n \equiv \int_{\mathbb{R}} \mathrm{d}\mu(z)\, z^n = \frac{1+(-1)^n}{4\pi}\, \Gamma\left(\frac{n+1}{2}\right) \left(-\frac{6g_s}{\lambda}\right)^{\frac{n+1}{4}} U\left(\frac{n+1}{4}, \frac{1}{2}\,\middle|\, -\frac{3}{2\lambda g_s}\right), \tag{6.16}$$

in terms of which all results that follow may be expressible. Of course odd moments vanish as the potential we are considering is an even function. The result is expressible in terms of the confluent hypergeometric function of the second kind $U\left(a, b \,|\, z\right)$ (see, *e.g.*, [143]), which

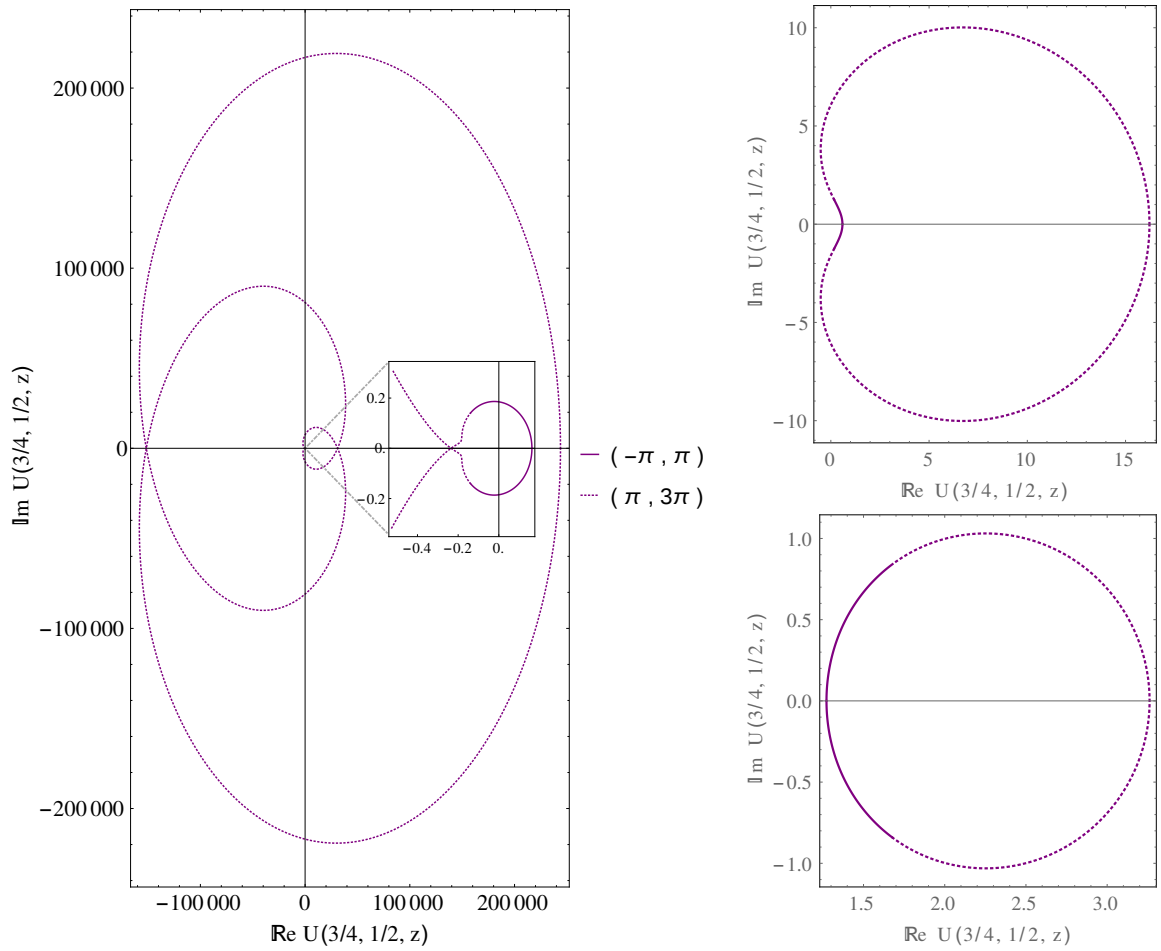

Figure 6.1: Illustration of the (double) monodromy of the confluent hypergeometric function of the second kind, for fixed values of $a = \frac{3}{4}$ and $b = \frac{1}{2}$, and different values of $|z| = 0.1$ (lower right), $|z| = 1.1$ (upper right), and $|z| = 10.1$ (left). The figures plot $U\,(a, b\,|\,z)$ over the complex z-plane as $\arg z \in (-\pi, 3\pi)$, with the solid line representing the first turn, $\arg z \in (-\pi, \pi)$, and the dotted line the second, $\arg z \in (\pi, 3\pi)$. Note the difference in scales between principal and secondary sheets, increasingly significant as $|z|$ grows. In the left plot we have enclosed a zoom-in close to the origin, in order to show the trajectory along the first sheet in more detail.

has a branch cut along the negative real axis in z, $\arg z = \pm\pi$, and integral representation

$$U\,(a, b\,|\,z) = \frac{1}{\Gamma(a)} \int_0^{+\infty} \mathrm{d}x\, x^{a-1}\,(1+x)^{b-a-1}\,\mathrm{e}^{-z\,x}, \tag{6.17}$$

when $\mathbb{R}\mathrm{e}\,a > 0$ and $|\arg z| < \frac{\pi}{2}$. Because of the branch cut, this function has non-trivial

monodromy, given by [143]

$$U\left(a,b\,|\,\mathrm{e}^{2\pi\mathrm{i}m}\,z\right)=\mathrm{e}^{-2\pi\mathrm{i}bm}\,U\left(a,b\,|\,z\right)+\frac{2\pi\mathrm{i}\,\mathrm{e}^{-\mathrm{i}\pi bm}}{\Gamma\left(1+a-b\right)\Gamma\left(b\right)}\,\frac{\sin\left(\pi bm\right)}{\sin\left(\pi b\right)}\,M\left(a,b\,|\,z\right),\qquad m\in\mathbb{Z},\tag{6.18}$$

where now $M\left(a,b\,|\,z\right)$ is the confluent hypergeometric function of the first kind; an entire function with integral representation

$$M\left(a,b\,|\,z\right)=\frac{\Gamma(b)}{\Gamma(a)\,\Gamma(b-a)}\int_0^1\mathrm{d}x\,x^{a-1}\left(1-x\right)^{b-a-1}\mathrm{e}^{z\,x},\tag{6.19}$$

when $\mathbb{R}\mathrm{e}\,b>\mathbb{R}\mathrm{e}\,a>0$. In our quartic-potential example (6.16) one always has $b=\frac{1}{2}$, implying from (6.18) that we have to rotate twice around the origin in the complex z-plane in order to return to the starting point, as illustrated in figure 6.1. This will also be a distinguishable feature for both recursion coefficients, free energy and partition function of our quartic gauge theory.

One may now explicitly construct the orthogonal polynomials of the quartic matrix model in terms of the moments, $\mathfrak{m}_n$, and find the following first few recursion coefficients

$$r_1=\frac{\mathfrak{m}_2}{\mathfrak{m}_0},\tag{6.20}$$

$$r_2=\frac{\mathfrak{m}_4}{\mathfrak{m}_2}-\frac{\mathfrak{m}_2}{\mathfrak{m}_0},\tag{6.21}$$

$$r_3=\frac{\mathfrak{m}_0}{\mathfrak{m}_2}\frac{\mathfrak{m}_4^2-\mathfrak{m}_6\,\mathfrak{m}_2}{\mathfrak{m}_2^2-\mathfrak{m}_4\,\mathfrak{m}_0},\tag{6.22}$$

$$r_4=\frac{\mathfrak{m}_8\,\mathfrak{m}_2}{\mathfrak{m}_6\,\mathfrak{m}_2-\mathfrak{m}_4^2}-\frac{\mathfrak{m}_4\,\mathfrak{m}_2}{\mathfrak{m}_4\,\mathfrak{m}_0-\mathfrak{m}_2^2}-\frac{\mathfrak{m}_6\,\mathfrak{m}_2\left(\mathfrak{m}_6\,\mathfrak{m}_0-\mathfrak{m}_4\,\mathfrak{m}_2\right)}{\left(\mathfrak{m}_6\,\mathfrak{m}_2-\mathfrak{m}_4^2\right)\left(\mathfrak{m}_4\,\mathfrak{m}_0-\mathfrak{m}_2^2\right)}.\tag{6.23}$$

Next, it is simple to use these results to find the partition functions at different values of the rank. Notice that while the polynomial norms and the recursion coefficients are, in general, rational functions, we can see from their structure that certain cancellations occur, ensuring that at the end of the day the partition functions are just a sum of products of hypergeometric functions. This could have been predicted from the start, since the Vandermonde determinant is a polynomial. Explicitly, the partition functions for $N=2,3,4,5$ are given

by

$$
\begin{aligned}
Z(2) &= \mathfrak{m}_2\,\mathfrak{m}_0, && (6.24)\\
Z(3) &= \mathfrak{m}_2\left(\mathfrak{m}_4\,\mathfrak{m}_0-\mathfrak{m}_2^2\right), && (6.25)\\
Z(4) &= \left(\mathfrak{m}_6\,\mathfrak{m}_2-\mathfrak{m}_4^2\right)\left(\mathfrak{m}_4\,\mathfrak{m}_0-\mathfrak{m}_2^2\right), && (6.26)\\
Z(5) &= \left(\mathfrak{m}_6\,\mathfrak{m}_2-\mathfrak{m}_4^2\right)\Big\{\mathfrak{m}_8\left(\mathfrak{m}_4\,\mathfrak{m}_0-\mathfrak{m}_2^2\right)+\mathfrak{m}_6\left(\mathfrak{m}_6\,\mathfrak{m}_0-\mathfrak{m}_4\,\mathfrak{m}_2\right)- \\
&\quad -\mathfrak{m}_4\left(\mathfrak{m}_6\,\mathfrak{m}_2-\mathfrak{m}_4^2\right)\Big\}. && (6.27)
\end{aligned}
$$

Note that for different values of N the above partition functions are not simply numbers, but *functions*. In these formulae they are implicitly functions of the couplings in the matrix integral via (6.16), which we trade for the 't Hooft coupling t as usual. As a consequence of (6.18), and as we shall now illustrate, these functions display intricate monodromy structures. For instance, in figure 6.2 we illustrate the monodromy properties of r_3, for three different values of $|t|$ and varying $\arg(t)$. Furthermore, the free energy[6] also displays distinctive monodromy features. The one novelty is that due to the logarithm the scale in the second sheet may be considerably larger than the corresponding one in the first sheet. This is illustrated in figure 6.3 for different values of N and t (in fact in these plots we do not show the entire range corresponding to the second sheet, in order to keep the pictures small enough for illustration purposes). Note that due to the logarithm, now the curves do not close upon themselves.

It is clear that the monodromy features displayed in figures 6.2 and 6.3 are quite non-trivial, and they change as we change the value of N. What is important to have in mind is that all these features must be precisely captured by the large N transseries which will be introduced in the following section. Furthermore, there is one single transseries describing the quartic matrix model, and this *one* transseries must be able to reproduce *all* these monodromies for *all* different values of N. As we shall see, this will be remarkably captured by instanton physics.

[6] A word on notation and normalizations: we shall follow standard practice of normalizing the partition function with respect to the Gaussian weight (6.5), which means in practice the partition function is in fact given by

$$\mathcal{Z}=\frac{Z}{Z_{\rm G}}. \tag{6.28}$$

However, with a slight abuse of notation and following common practice in earlier papers, this will always be implicitly assumed so that whenever we refer to Z this is always the normalized result $\mathcal{Z}$. The free energy will also always be normalized as $\mathcal{F}=\log\mathcal{Z}$, but in this case we shall keep it explicit in notation.

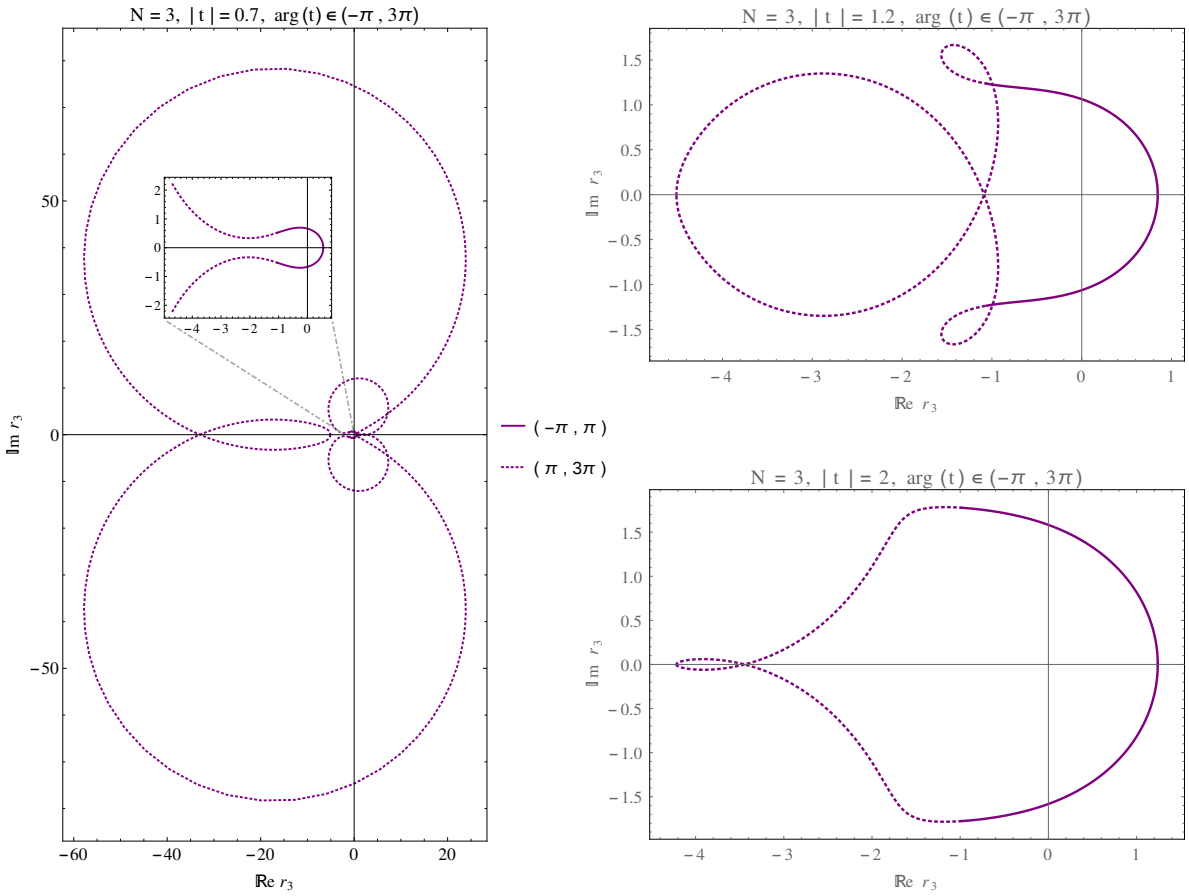

Figure 6.2: Monodromy of the recursion coefficient r_3, for different values of $|t| = 0.7$ (left), $|t| = 1.2$ (upper right), and $|t| = 2$ (lower right). The solid line corresponds to the first sheet, $\arg(t) \in (-\pi, \pi)$, and the dotted line to the second, $\arg(t) \in (\pi, 3\pi)$. In the left plot we enclose a zoom-in close to the origin, to see the trajectory along the first sheet in more detail.

6.3 Finite N from Resurgent Large N

The construction of the perturbative $1/N$ expansion has a long history. In the matrix model context it starts with a (planar) spectral curve [48], out of which one may recursively construct the full perturbative series – an endeavor which started out in [51] and culminated in [52]. But, as we shall now discuss, there is much more to gauge theory at finite N beyond its perturbative $1/N$ expansion. Depending on the values of the parameters, and on Stokes phenomenon, instantons may be crucial to achieve exponential accuracy in some results, or, instead, they become exponentially enhanced rather than suppressed to completely change the perturbative results and *correctly* reproduce many of the intricate monodromy features

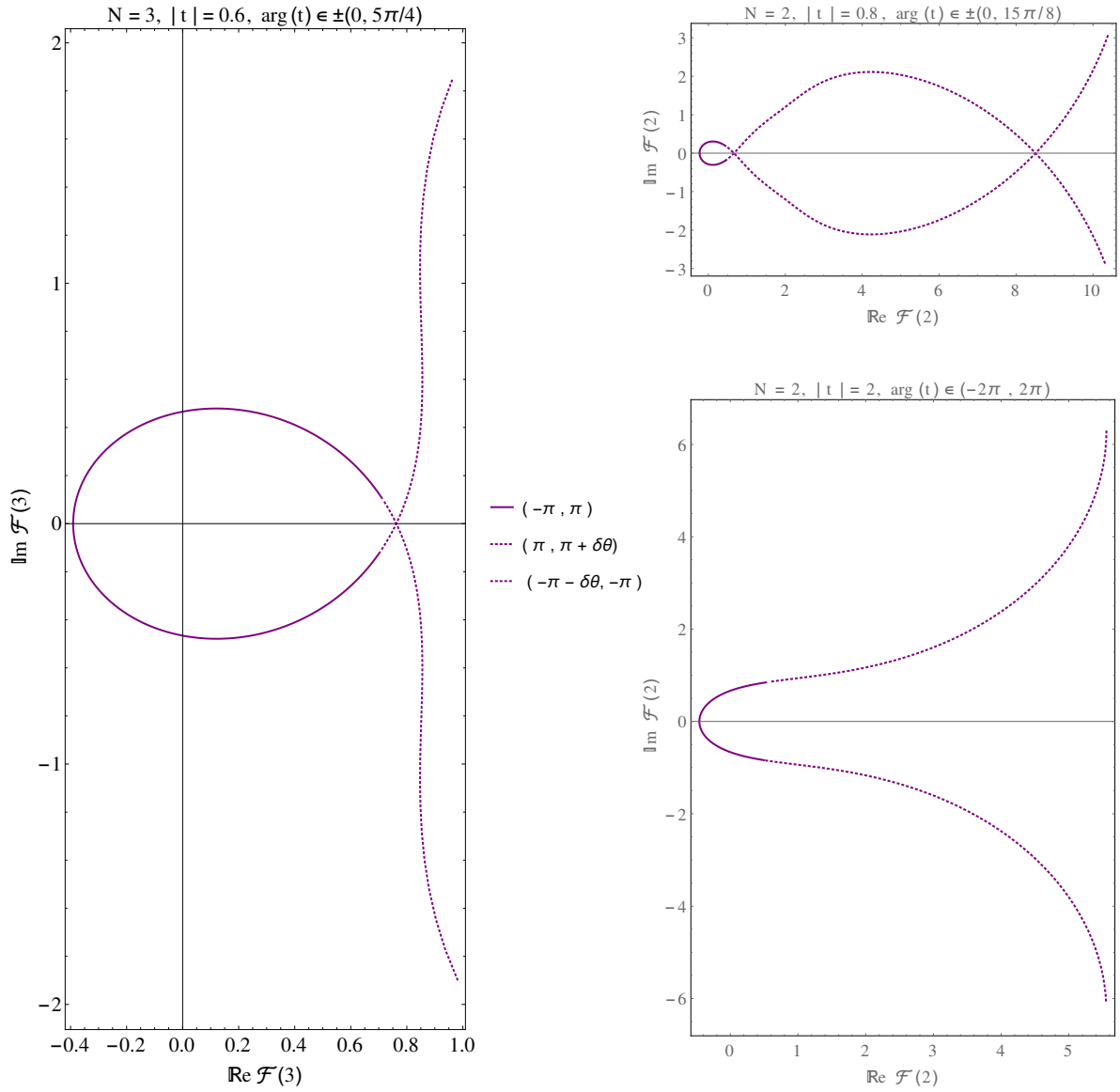

Figure 6.3: Monodromy of the free energy $\mathcal{F}(3)$, when $N = 3$, for $|t| = 0.6$ (left); and of the free energy $\mathcal{F}(2)$, when $N = 2$, for different values $|t| = 0.8$ (upper right) and $|t| = 0.6$ (lower right). As usual, the solid line corresponds to $\arg(t) \in (-\pi, \pi)$ while the dotted line now corresponds to $\arg(t) \in \pm(\pi, \pi + \delta\theta)$, where we set $\delta\theta = \pi/4$ (left), $\delta\theta = 7\pi/8$ (upper right), and $\delta\theta = \pi$ (lower right). In some plots we have not included the full dotted curves as they show no more relevant features beyond what is displayed (their range gets naturally enlarged by force of the logarithm).

we have discussed in the previous section. So, how are instantons incorporated into the large N expansion?

As already explained in the introduction, this is achieved via transseries which go beyond the large N expansion by including all its nonperturbative corrections. In practice one deals with a formal expression, such as (6.4). But it is important to notice that such transseries contain as much information as a would-be analytic expression for whatever function we are trying to describe. The explicit connection between the two is achieved by the resummation of the former into the latter. This is actually similar to the role that Taylor power-series play in describing or representing entire functions. In our case, while similar in spirit, the "power-series game" becomes a little bit harder in practice due to the existence of many singularities and branch cuts. The prominent role of transseries thus comes about, since finding analytic solutions is doomed to fail for most problems, while transseries representations yield natural completions to naïve perturbative approaches. These in fact include everything needed for a complete nonperturbative description of the solutions. Furthermore, treating parameters such as the rank N as formal variables removes any previous constraints on their domain of validity (*e.g.*, N must be an integer), so that after resummation they can even take real or complex values.

The observables we shall focus upon are the partition function and the free energy. Let us start with the free energy, $\mathcal{F}(N,t)$. In our example of the quartic matrix model, the construction of a large N transseries representation for the free energy starts by addressing the coefficients r_N (and we shall also display results for these). The large N transseries for r_N is a resurgent function of the form

$$\mathcal{R}(N,t) = \sum_{n=0}^{+\infty} \sigma^n \, \mathrm{e}^{-nN\frac{A(t)}{t}} \sum_{g=0}^{+\infty} N^{-g-\beta_n} \, t^{g+\beta_n} R_g^{(n)}(t), \tag{6.29}$$

which solves the continuous version of the string equation (6.15) when expressed in terms of the 't Hooft coupling. We refer to appendix A, and references therein, for a more detailed explanation of this transseries solution, *e.g.*, the choice of variables, the explicit instanton action, the coefficients β_n, the maximum orders up to which we have computed the g-coefficients, and a few explicit examples. Let us nonetheless stress a few points: there are two distinct sums, one in the instanton number, n, and the other in the perturbative order, g; the rank N is treated as a (continuous) formal parameter; at large N the nonperturbative exponential contributions are controlled by the ratio $A(t)/t$ involving the matrix model instanton action (A.8); the transseries parameter σ is so far arbitrary and needs to be fixed for any numerical evaluations; the perturbative coefficients $R_g^{(n)}(t)$ grow factorially fast with g, turning each instanton series in $1/N$ asymptotic; and that all building blocks of the transseries are in fact *functions* of the 't Hooft coupling t. Having determined the transseries for the coefficients r_N, one then uses equation (A.12) in order to obtain the transseries for

the free energy,

$$\mathcal{F}(N,t) = \sum_{n=0}^{+\infty} \sigma^n \, \mathrm{e}^{-nN\frac{A(t)}{t}} \sum_{g=0}^{+\infty} N^{-g-\beta_n^{\mathcal{F}}} \, t^{g+\beta_n^{\mathcal{F}}} \, \mathcal{F}_g^{(n)}(t). \tag{6.30}$$

We once more refer to the appendix for more technical details on this transseries construction. Note that when addressing any other gauge theory, the starting point and the method that now follows will be exactly the same. The only difference would be a distinct instanton action and multi-instanton perturbative coefficients, possibly computed diagrammatically, *i.e.*, the difference would essentially amount to having a distinct content in Appendix A.

One thing to notice is that expressions (6.29) or (6.30) are not the most general transseries solutions to the quartic matrix model; see [25]. Instead, it turns out that the instanton action has a symmetric companion of opposite sign which also solves the relevant differential equation. Consequently, the complete transseries solution will depend upon two parameters and it will include logarithmic monomials in N associated to resonant sectors. While knowledge of this complete transseries is necessary in order to understand the resurgence properties of the free energy – namely, how the coefficients of one sector grow and relate to coefficients from other sectors – it will not be needed for the particular resummations we address in the present context.

Finally, one still has to fix σ in order to obtain any numbers at the end of the day. Typically, a transseries with a given fixed choice of σ will be valid in a specific wedge of the coupling-constant complex-plane; in this case of the complex plane associated to the 't Hooft parameter t. Different wedges are separated by singular directions on the Borel plane, known as *Stokes lines*. This is where the multi-instanton singularities lie. For our present problem, these singular directions on the Borel plane are located at either $\theta = 0$ or $\theta = \pi$ [25, 97], but for the problems we shall address in the following we only need to consider the $\theta = 0$ case. Crossing this Stokes line implies that the transseries parameter will "jump" or "turn on", in the sense that any exponentially suppressed contributions previously neglected (as they were invisible behind the perturbative expansion) must now be taken into account as they will start growing and eventually may take dominance. To make this concrete, consider the free energy transseries (6.30) and write it explicitly as $\mathcal{F}(N,t,\sigma)$. Stokes phenomena then translates to the statement[7]

$$\mathcal{S}_{0^+}\mathcal{F}(N,t,\sigma) = \mathcal{S}_{0^-}\mathcal{F}(N,t,\sigma + S_1), \tag{6.31}$$

where the resummation $\mathcal{S}_\theta$ was defined in (6.3), and where the shift in the transseries parameter is controlled by the Stokes constant S_1. A particular case of (6.31) is when we start off with $\sigma = 0$, meaning the transseries has just the perturbative component, and then after crossing the Stokes line the nonperturbative contributions are turned on with a parameter $\sigma = S_1$.

[7] In the language of resurgence this jump is captured by the so-called Stokes automorphism; see, *e.g.*, [25, 97].

Now, as we want to bring together and compare the two representations of, say, the free energy, the one obtained analytically and the one obtained via resurgent transseries – in fact to show that they are equal at integer N – we need to resum the formal transseries into a function. Because the transseries is a double sum we must undergo a two-step process which bears the name of Borel-Écalle resummation. The first name deals with each of the asymptotic series in $1/N$, while the second takes care of the sum over multi-instantons. Both are important, in solving different problems, but, in practice, when we need to get a number out of a particular example the Borel resummation takes most of the attention. Let us fix an instanton sector, n, and consider the asymptotic series

$$\mathcal{F}^{(n)}(N,t) \simeq \sum_{g=0}^{+\infty} N^{-g-\beta_n^{\mathcal{F}}}\, t^{g+\beta_n^{\mathcal{F}}}\, \mathcal{F}_g^{(n)}(t). \tag{6.32}$$

As mentioned in the introduction for the perturbative case, Borel resummation first computes the Borel transform of the asymptotic series $\mathcal{F}^{(n)}(N,t)$ – a convergent series in s which may be analytically continued – and then evaluates its Laplace transform, yielding the resummation

$$\mathcal{S}_\theta \mathcal{F}^{(n)}(N,t) = \int_0^{\mathrm{e}^{i\theta}\infty} \mathrm{d}s\, \mathcal{B}[\mathcal{F}^{(n)}](s,t)\, \mathrm{e}^{-sN}. \tag{6.33}$$

The choice of the angle θ for the integration contour must be made carefully due to the singularities of the Borel transform. Once this is done and all perturbative and multi-instanton asymptotic series have been dealt with, one may take the second step and address the sum over multi-instantons. This is immediate, so the Borel-Écalle resummation of the transseries is, finally,

$$\mathcal{S}\mathcal{F}(N,t) = \sum_{n=0}^{+\infty} \sigma^n\, \mathrm{e}^{-nN\frac{A(t)}{t}}\, \mathcal{S}_\theta \mathcal{F}^{(n)}(N,t). \tag{6.34}$$

Note that the left-hand-side is nontrivially independent of θ; all one now has to take into account are the Stokes jumps (6.31), *i.e.*, keep track of which wedge in the complex plane are we on.

When we turn to implement equations (6.33) and (6.34) in an explicit example, such as ours for the quartic free energy, it is often the case that we cannot perform the Borel transform analytically. This is simply because in most problems nonlinearity prevents us from obtaining closed-form expression for the asymptotic coefficients and only a finite number of such coefficients are available for computation. The standard approach to circumventing this problem is found in using Padé approximants to mimic the analytic continuation of the Borel transform (see, *e.g.*, [106, 143]). Because the Padé approximant is a rational function of s we can capture some of the Borel singular behavior. Thus, the Borel-Padé resummation provides a numerical implementation of the exact Borel resummation. As such we will define

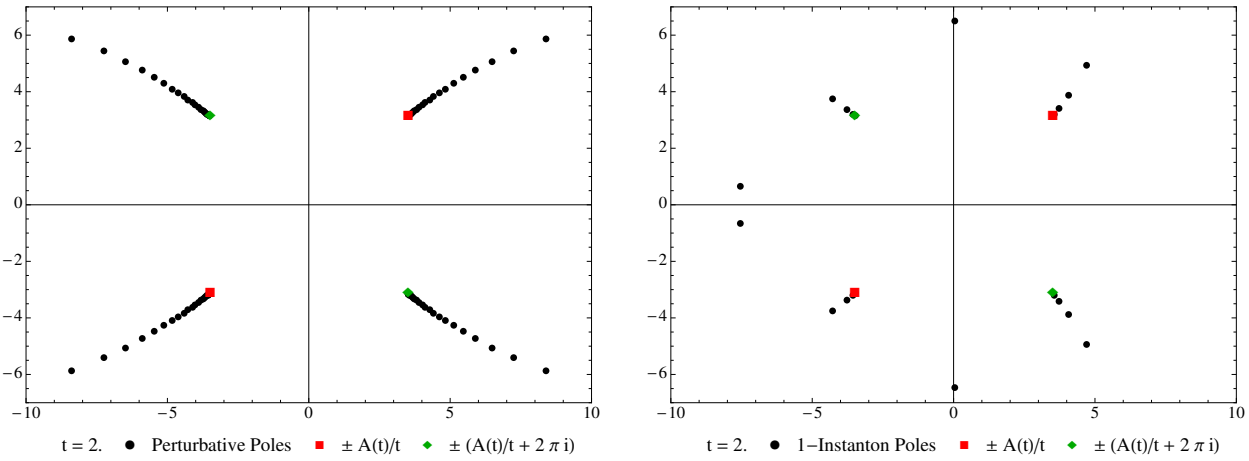

Figure 6.4: Approximate complex Borel s-planes for the perturbative (left, $\mathcal{F}^{(0)}$) and one-instanton (right, $\mathcal{F}^{(1)}$) free energies obtained by plotting poles of the Padé approximant when $t = 2$. Due to limited computational resources we have less points for higher instanton sectors, as compared to the perturbative sector. Still, the instanton action singularities are very clear, with the accumulation of poles signaling their associated logarithmic branch cuts.

the *Borel-Padé-Écalle* resummation of a transseries, up to the i-th instanton sector, as[8]

$$S_\theta^{(i)}\mathcal{F}(N,t) = \sum_{n=0}^{i} \sigma^n \, \mathrm{e}^{-nN\frac{A(t)}{t}} \, S_\theta \mathcal{F}^{(n)}(N,t), \tag{6.35}$$

$$S_\theta \mathcal{F}^{(n)}(N,t) = \int_0^{\mathrm{e}^{i\theta}s_{\max}} \mathrm{d}s \, \mathrm{BP}_\ell[\mathcal{F}^{(n)}](s,t) \, \mathrm{e}^{-sN}. \tag{6.36}$$

In the last definition $\mathrm{BP}_\ell[\mathcal{F}]$ denotes a (diagonal) order-ℓ Padé approximant of the Borel transform, and the numerical integration has a cut-off at $s_{\max}$. The "Écalle step" of the resummation is also truncated in practice, since only a few instanton terms are computed. As we shall see, this will nonetheless be more than enough to show the capabilities of transseries resummation.

Note that what we have described is *not* a numerical *method*, but rather a numerical *approximation* to an analytical procedure. As we already mentioned, the Borel-Écalle representation of a function is somewhat analogous to the Taylor power-series representation of (another) function, and this is what (6.33) and (6.34) set up, out of the transseries. Of course if one is to extract a *number* out of any of these analytical representations, some approximation (or truncation) must be considered. In Taylor power-series one just truncates at a given order and then sums. In the present Borel-Écalle framework, where the functional complexity is larger, one needs to implement the above Borel-Padé-Écalle resummation.

[8] To summarize, we are using S and BP_ℓ to define the numerical approximations to $\mathcal{S}$ and $\mathcal{B}$, respectively.

We can see an example in figure 6.4. The singularities on the Borel-Padé plane convey the image of branch cuts, where the branch points are given by the instanton actions that appear in the transseries. As we have commented before, instanton actions come in pairs of opposite signs. In here, we also notice the presence of a displacement of the instanton action $A(t)/t$ by a constant term $2\pi\mathrm{i}$. This is in agreement with general expectations of [46], where instanton actions in matrix models and topological strings should be linear combinations of spectral curve B-periods, such as in [10, 57], with spectral curve A-periods, such as in [11] (*i.e.*, the factor of $2\pi\mathrm{i}t$). Note however that due to the nature of the string equation, the sector associated with this other action is indistinguishable from that of $A(t)/t$ alone, and the two can be combined. In fact if we were to consider a two-parameter transseries[9] with sectors associated to A and $\widetilde{A} = A \pm 2\pi\mathrm{i}t$, denoted by $[n|\widetilde{n}]$, then after plugging such an *ansatz* into the string equation we would find that the "mixed" coefficients satisfy

$$R_g^{[n|\widetilde{n}]} = \frac{(n+\widetilde{n})!}{n!\,\widetilde{n}!} R_g^{[n+\widetilde{n}|0]}. \tag{6.37}$$

Plugging this result back into its two-parameter transseries would reduce it to the one-parameter transseries (6.29), with a simple shift in parameter $\sigma \to (1+\mathrm{e}^{\pm 2\pi\mathrm{i}N})\sigma$. In the case of integer N we have considered so far, the factor is equal to 2. But since the transseries parameter σ needs to be fixed in any case (which we will do next), the effect of the second instanton action with the $2\pi\mathrm{i}$ displacement is already automatically included in our results.

The final issue to address concerns the fact that equations (6.29) and (6.30) are actually representing a *family* of transseries, indexed by the transseries parameter σ. The resummation procedure cannot be complete until σ is specified. As we have discussed earlier, its particular value is subject to Stokes transitions that may add or subtract the Stokes constant S_1, but it still needs to be fixed at some point, with Stokes transitions then specifying it wherever else. In the present section we are focusing upon the case $t \in \mathbb{R}^+$, where one can numerically check that the transseries parameter is

$$\sigma = \mathrm{i}\sqrt{\frac{3}{\pi(-\lambda)}}, \tag{6.38}$$

equal to the Stokes constant S_1 [10, 16, 25]. Let us recall that λ is the quartic coupling-constant which we are going to set to -1 without loss of generality. More complicated gauge theories in more "physical" scenarios may eventually require that the fixing of transseries parameters must be done against some laboratory measurement.

Now that all the ingredients are on the table, we can explicitly show how adding more and more instanton contributions of the transseries gets us closer and closer to the exact result. In table 6.1 we display explicit numerical examples for the recursion coefficients (left)

[9] This should not be confused with the two-parameter transseries in [25], where the two actions are $\pm A$. The inclusion of this second action $\widetilde{A} = A \pm 2\pi\mathrm{i}t$ in that set-up would lead to a four-parameter transseries.

and the free energy (right). The first four rows correspond to the Borel-Padé resummations (6.36) of each sector, the fifth row is their sum (6.35), and the sixth has the analytical results, (6.22) and the logarithm of (6.25). In the total result we have labeled with different colors[10] the digits of the exact result that are matched after including the perturbative (blue), 1-instanton (green), 2-instanton (yellow) and 3-instanton (red) sectors. One can clearly see how the instanton contributions[11] provide exponentially small corrections with respect to the perturbative contribution, where the size of the correction is naturally controlled by the instanton action.

Sector	$S_0\mathcal{R}^{(n)}$	$S_0\mathcal{F}^{(n)}$
Perturbative	2.615 796 570 569 705 50 . . .	−1.973 899 279 493 161 74 . . .
1-Instanton	0.000 487 953 495 567 22 . . .	−0.000 020 359 080 917 15 . . .
2-Instanton	0.000 000 009 807 788 15 . . .	−0.000 000 000 300 789 88 . . .
3-Instanton	0.000 000 000 000 245 38 . . .	−0.000 000 000 000 004 71 . . .
Total	2.616 284 533 873 306 27 . . .	−1.973 919 638 874 873 50 . . .
Exact	2.616 284 533 873 306 26 . . .	−1.973 919 638 874 873 50 . . .

Table 6.1: Comparison of the truncated $\mathcal{R}$ and $\mathcal{F}$ transseries, up to the instanton sector $n = 0, 1, 2, 3$, against the exact result for $t = 6$ and $N = 3$. All digits displayed are stable. On the left table the last digit of the resummation must be corrected by the 4-instanton contribution.

We illustrate this visually in figure 6.5, also for different values of the rank. On the x-axis we vary N and on the y-axis we plot $-\log_{10}\left|S_0^{(i)}\mathcal{R} - r_N\right|$ (left) and $-\log_{10}\left|S_0^{(i)}\mathcal{F} - \mathcal{F}(N)\right|$ (right), where r_N are the exact recursion coefficients (6.20)-(6.23) and $\mathcal{F}(N)$ are the logarithms of the exact (normalized) partition functions (6.24)-(6.27). This quantity effectively tells us the number of decimal places to which the analytical result and the resummation agree, and as we saw in the example above we get closer and closer to the full answer as we add more and more instanton sectors. One can check that at $N = 3$ the matched digits are the ones shown in table 6.1. Note that we have chosen a relatively high value of t where the picture is clearer. As we move to lower t the instanton contributions get smaller in absolute value, and it may happen that if $S_0^{(0)}$ has not stabilized at enough digits it becomes harder to see their effect.

Having seen how the transseries so precisely captures the exact results, at small integer values of the rank, one may ask if it can go beyond this requirement and actually compute

[10] This is in fact the color code we shall be using in all subsequent plots.

[11] There is a slight abuse of notation in the column titles when we write them as $S_0\mathcal{R}^{(i)}$ and $S_0\mathcal{F}^{(i)}$. What we show is actually the whole contribution to the resummed objects, as in (6.35), so that herein $S_0\mathcal{R}^{(i)}$ and $S_0\mathcal{F}^{(i)}$ are in fact multiplied by the relevant powers of σ and $\exp(-NA(t)/t)$.

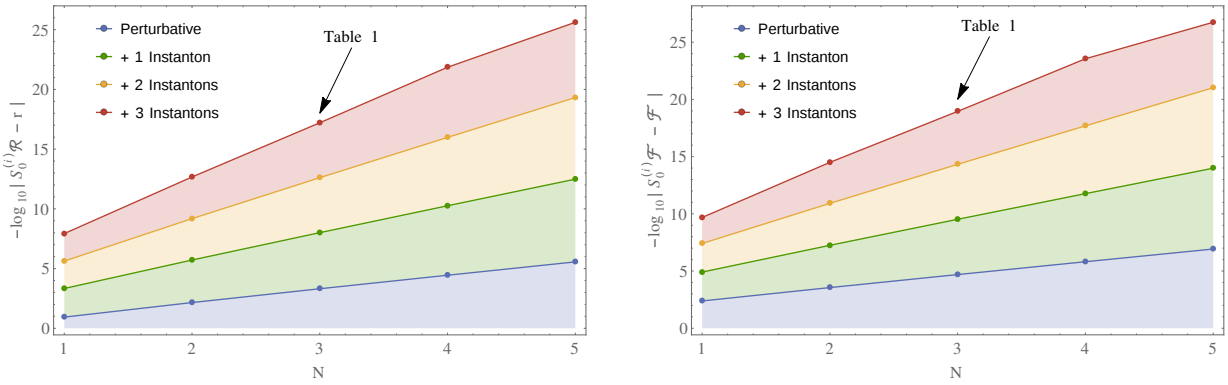

Figure 6.5: Number of decimal places up to which the resummation of the recursion coefficients (left) and the free energy (right) match their exact counterparts, with $N = 1, \ldots, 5$ and $t = 6$.

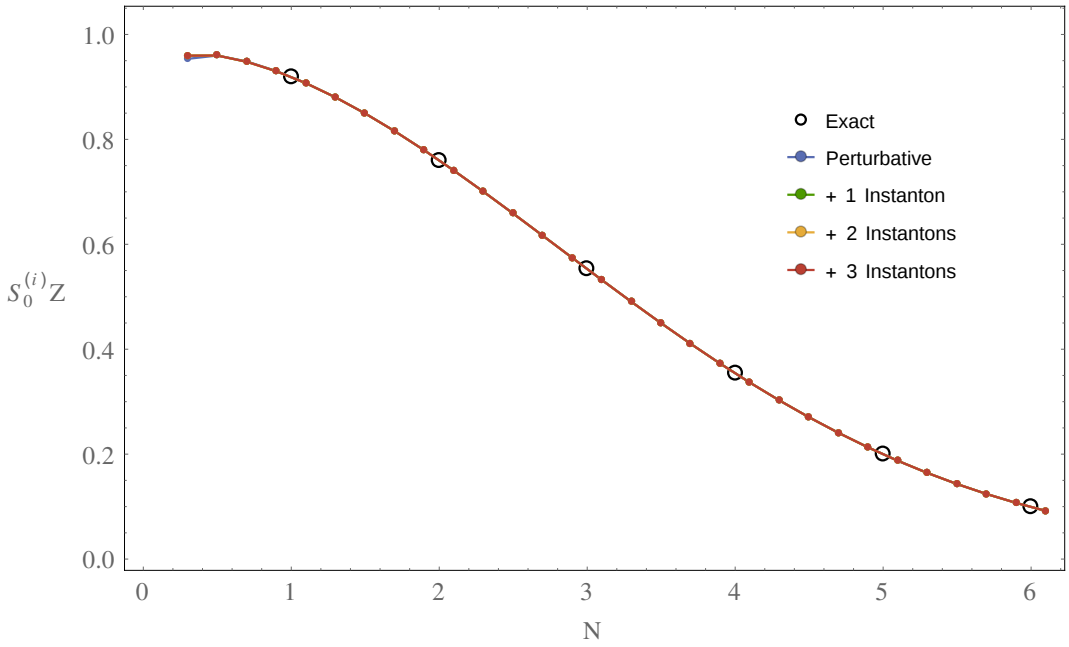

Figure 6.6: Resummation of the partition function for *continuous* $N \in (0, 6)$, $t = 1$, including up to 3-instantons (the lines are all superposed), and the exact results at integer values of N.

the free energy or partition function at *continuous* values of N. It should be clear that nothing changes as one considers the resummation for non-integer N. Furthermore, as we have analytical results for the exact partition function at integer values of N, we can ask how

the resummation interpolates between them. This is shown in figure 6.6, with $t = 1$, where it is clear that the resummation produces a smooth interpolation between the analytical results arising from the matrix integral. Of course these results are already going well beyond the exact matrix integral results, as the latter are not even defined when N is non-integer.

It is worth pointing out that we are not resumming Z in the same way we did for $\mathcal{F}$ or $\mathcal{R}$, since it is very inefficient to exponentiate the free energy transseries and then extract the $1/N$ coefficients at each order. Instead, we first resum the free energy and only then exponentiate the result. Furthermore, note that for the almost entirety of the plot in figure 6.6, the resummations including any or all instanton sectors are indistinguishable and the four lines are coincident. As we showed above, these distinctions only appear after a certain number of decimal places, and this is impossible to spot in these scales. However, in the next section we will also explore complex-valued t and we will see cases where there is a "macroscopic" distance between different resummations. Finally, we notice that the coincident lines seem to split apart as we get closer to $N = 0$. The fact that we are dealing with a normalized partition function means that $Z(0) = 1$. However, this is a point of infinitely strong coupling, and even the large amount of data we have is insufficient, from a numerical standpoint, to get consistent results at this point (*i.e.*, technically, at infinitely strong coupling we would need infinite terms in the Borel-Écalle transseries resummation, which is unachievable).

6.4 Analytic Continuations and Stokes Phenomenon

In the previous section we have limited our attention to the case where $t \in \mathbb{R}^+$. While definitely crediting the power of resurgent transseries in achieving to go beyond integer rank and actually *define* the gauge theory partition function at continuous values of N, the reader might get the wrong impression that other than that all the transseries is implementing is smaller and smaller instanton corrections to the perturbative expansion, piling on top of each other. This is certainly not the generic case and such picture will dramatically change as we consider the analytic continuation onto complex values of the 't Hooft parameter, due to Stokes phenomenon.

To understand how this works, let us first address an illustrative example. Consider the free energy when $N = 3$ and at fixed 't Hooft coupling $|t| = 0.6$ but varying argument $\arg(t) \in (-\pi, \pi + \pi/4)$. This is a continuous function with nontrivial monodromy, as shown in figure 6.3, computed from analytic expressions. In the 't Hooft limit, the large N resurgent transseries for $\mathcal{F}$, (6.30), must have all the required information in order to reproduce this plot. To extract it we not only have to resum it, as explained in the previous section, but also take into account Stokes phenomenon. This last step is crucial and in practice it implies selecting a particular member from the family of transseries parametrized by σ. For $t \in \mathbb{R}^+$ we saw that the correct value is given by (6.38), but as we now vary $\arg(t)$ we will need to implement Stokes transitions as shown in (6.31). This is a general feature of

representing functions as transseries: we need the whole family of solutions, as parametrized by the parameter σ, and a practical understanding of how Stokes phenomenon selects the right member as we move across the complex t-plane.

Stokes transitions take place at Stokes lines, the rays where multi-instanton singularities lie on the complex Borel plane. In the complex 't Hooft plane they satisfy $\mathbb{I}\mathrm{m}\,(A(t)/t) = 0$, and impose the familiar jump in the transseries parameter. One may also cross anti-Stokes lines, where $\mathbb{R}\mathrm{e}\,(A(t)/t) = 0$, with instantons taking dominance over the perturbative series – in fact at this point all contributions, perturbative and nonperturbative, are of the same order. As we move beyond it and into a region where $\mathbb{R}\mathrm{e}\,(A(t)/t) < 0$, the instanton contributions are no longer exponentially suppressed. However, this does not mean that the transseries representation breaks down. The transseries is a formal object that includes complex instantons in general, but where the label "exponentially suppressed" or "exponentially enhanced" only applies in the formal large N limit. In the resummation process where N becomes finite, even small, and where we may venture into the complex plane, this distinction is somewhat irrelevant and even not appropriate any more. The separation between perturbative and (multi) instanton sectors is only set up at the initial definition of the transseries, where one finds out that for some values of t the resummation of the perturbative series alone is enough to give the full answer, thus having $\sigma = 0$. But this washes away at finite N and complex t where the resummation of the transseries yields, in practice, a power-series in σ. All these features will be clear in the examples that follow.

Graphically we can represent the Stokes and anti-Stokes boundaries in the complex t-plane[12] and then, for each particular case, determine the corresponding lines as intersections with the path $|t| =$ constant. We show this in figure 6.7 for our example value $|t| = 0.6$, where the diagram on the left corresponds to the first sheet, $\arg(t) \in (-\pi, \pi)$, and the one on the right to the second sheet, $\arg(t) \in (\pi, 3\pi)$. We see that in the first sheet there are four Stokes lines at different arguments $\arg(t) \in (-\pi, \pi)$, and in the second sheet there are three anti-Stokes phase boundaries. There is also a symmetry with respect to the real line, so we can focus on $\arg(t) \geq 0$. Of course the information shown in figure 6.7 is incomplete without the actual resummation of the transseries, for the different values of $\arg(t)$, and that is displayed in figure 6.8. In the following we shall explain both these plots[13] at the same time, moving along the arrowed path drawn on the phase diagram, figure 6.7, and then looking at the relevant features of the resummed transseries, figure 6.8. For $\arg(t) = 0$ we are in a case similar to the one described in the previous section: we can reproduce the value of the free energy with increasing accuracy by piling up smaller and smaller instanton contributions on top of the (already quite accurate) perturbative result.

[12] These become the large N phase diagram for the quartic matrix model; see [125, 136, 137] for further discussions.

[13] A very pedagogical introduction to this type of Argand plots may be found in the excellent review [94], addressing the simple example of the Airy function (which is a linear problem with no multi-instanton sectors). A similar example but for the Bessel function (again linear and without multi-instantons) appears in [146].

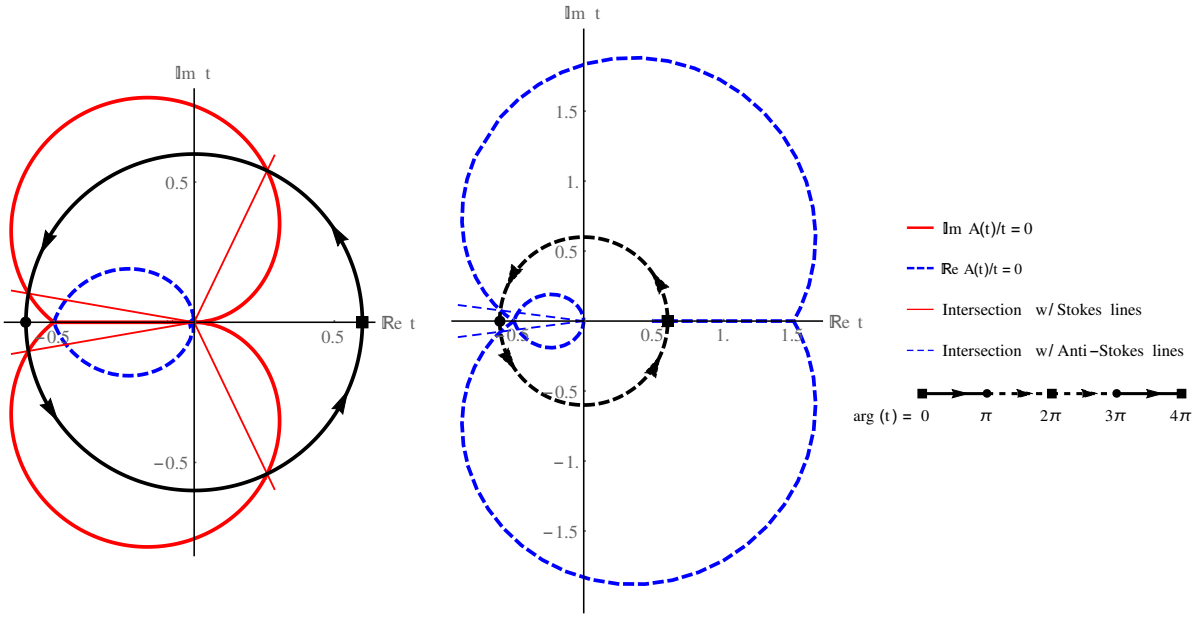

Figure 6.7: Phase diagrams showing anti-Stokes (thick, dashed, blue curved) and Stokes (thick, solid, red curved) boundaries along with the path $|t| = 0.6$ (arrowed black) and the intersections of this path with Stokes (thin, solid, red) and anti-Stokes (thin, dashed, blue) lines. The left plot represents $\arg(t) \in (-\pi, +\pi)$ while the one on the right is for $\arg(t) \in (\pi, 3\pi)$. In the last line of the caption we show how the motion on the two sheets takes place as $\arg(t)$ is changed from 0 (the solid square on the first diagram) all the way (back) to 4π. Note that there is a third intersection with an anti-Stokes line in the second sheet, for $\arg(t) = 2\pi$, but we do not draw the intersecting ray because it would lie along the positive real axis.

The value of the transseries parameter is (6.38), *i.e.*, the Stokes constant. The reader may also want to take another look at table 6.1 and figure 6.5 from the previous section[14]. As we increase $\arg(t)$ from 0 onwards we will cross the first Stokes line, where a transition occurs that selects the transseries with $\sigma = 0$. That is, we reach a region where perturbation theory alone is enough to reproduce the exact value of the free energy. To show that this is the case, we display the different instanton contributions in table 6.2. It is clear that if we were to add them to the perturbative result we would immediately deviate from the exact result! Pushing $\arg(t)$ further towards $+\pi$ we cross the second Stokes line. This restores the value

[14]Note that in the present section we focus on a smaller value of $|t|$ than in the previous section, to illustrate Stokes phenomena. However the precision of the results is reduced, due to the finite number of available transseries coefficients. In practice, the contributions of the second and third instantons do not provide stable digits to display. In any case, in figure 6.8 the different contributions cannot be distinguished with the naked eye.

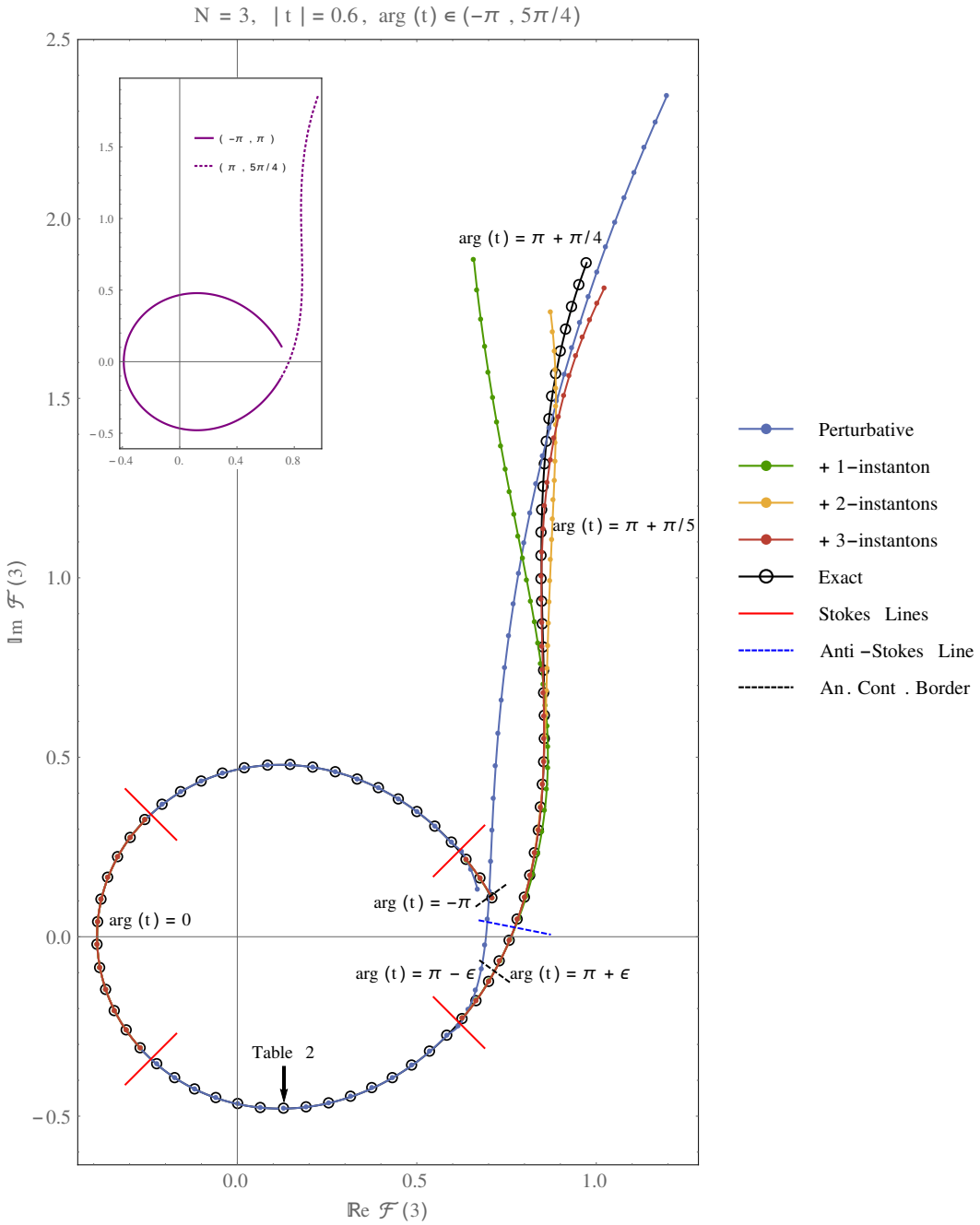

Figure 6.8: Resummation of the free energy transseries for $|t| = 0.6$ and $N = 3$, taking into account the different values of σ (due to Stokes phenomenon) depending on $\arg(t) \in (-\pi, \pi + \pi/4)$. The Stokes lines illustrate how in some regions $\sigma = 0$ and the perturbative resummation yields the correct result, while in other regions $\sigma = S_1$ and we need to include up to three instantons in order to reproduce the exact result (shown in the left plot of figure 6.3 and enclosed here). It is also clear how past the anti-Stokes phase boundary the perturbative contribution is no longer reliable and instantons need to take over in order to yield the correct monodromy results.

Sector	$\mathbb{R}\mathrm{e}\, S_0\mathcal{F}^{(n)}$	$\mathbb{I}\mathrm{m}\, S_0\mathcal{F}^{(n)}$
Perturbative	$+0.130\,991\,945\,237\,228\ldots$	$-0.478\,840\,360\,187\,836\ldots$
1-Instanton	$-0.000\,070\,474\,759\,944\ldots$	$-0.000\,010\,860\,987\,563\ldots$
2-Instanton	$-0.000\,000\,002\,360\,007\ldots$	$-0.000\,000\,001\,378\,327\ldots$
3-Instanton	$-0.000\,000\,000\,000\,097\ldots$	$-0.000\,000\,000\,000\,095\ldots$
Exact	$+0.130\,991\,945\,237\,228\ldots$	$-0.478\,840\,360\,187\,836\ldots$

Table 6.2: Comparison of the real and imaginary parts of the resummed $\mathcal{F}$-transseries, at the instanton sector $n = 0, 1, 2, 3$, and compared against the exact result for $N = 3$ and $t = \frac{3}{5}\,\mathrm{e}^{2\pi\mathrm{i}/3}$. All digits displayed are stable. Note that *all* the digits in the perturbative resummation already match the exact solution, so the transseries parameter must be 0.

of σ back to what it was at $\arg(t) = 0$, namely (6.38). After this point the perturbative result alone is already significantly different from the exact one, as can be clearly seen in figure 6.8. We could, in principle, stop at $\arg(t) = +\pi$, but we know that the partition function has monodromy 2 around $t = 0$ so we keep pushing the calculation. In order to do this, for the exact value of the free energy we will use the analytic continuation of the hypergeometric function, explained around equation (6.18). For the transseries we need to do an analytical continuation of both its coefficients and the instanton action. As we move beyond $\arg(t) > +\pi$ the first observation is that perturbation theory becomes less and less accurate. Shortly afterward we cross an anti-Stokes line, signaling a change in the sign of $\mathbb{R}\mathrm{e}\,(A(t)/t)$, from negative to positive. Now instanton contributions are roughly of the same order of magnitude as the perturbative contribution, and this effect is dramatically enhanced as $\arg(t)$ grows. Following the sequence of points in figure 6.8 we see how each new instanton contribution struggles to move the resummation line closer to the exact curve. As we get to $\arg(t) = +\pi + \frac{\pi}{4}$ not even three instanton terms can give an accurate result, and higher instanton sectors are needed to keep up with the analytical curve.

Figure 6.8 is a very rich picture which involves both Stokes and anti-Stokes lines, regions with $\sigma = 0$ and with $\sigma \neq 0$, and a crisp image of the importance of instanton corrections. In fact it shows how the instantons in the transseries are relevant for much more than achieving exponential accuracy in matching the exact results: they actually need to take *dominance* in order to properly describe the physics at small N. This should be extremely compelling evidence towards the relevance of resurgent transseries in describing the nonperturbative realm. We may now proceed with exploring the gauge-theory parameter space. In figures 6.9, 6.10, and 6.11, we expand our list of examples by keeping $N = 3$ but varying the value of $|t|$; and this time around we consider the orthogonal polynomial recursion coefficients $\mathcal{R}(N, t)$. In some of these figures for $\mathcal{R}(N, t)$ we can actually follow the entire monodromy and "close" the curves (the cases we are presently addressing are the ones shown earlier in

figure 6.2). These figures also show a rather interesting feature: the perturbative resummation has a tendency to follow along the *planar* approximation and thus, past anti-Stokes boundaries, it completely misses the correct features of the problem. It is the instantons that come to save the day and properly describe the monodromy properties we are trying to reproduce. Furthermore, we keep expanding our list of examples in figures 6.12 and 6.13, by now addressing the free energy at $N = 2$ and for new values of $|t|$; and these cases are in correspondence with the exact results shown in figure 6.3. In all these figures we can cleanly identify all the Stokes, anti-Stokes, and analytic continuation transitions which occur as we draw the constant $|t|$ paths on the phase diagram of figure 6.7.

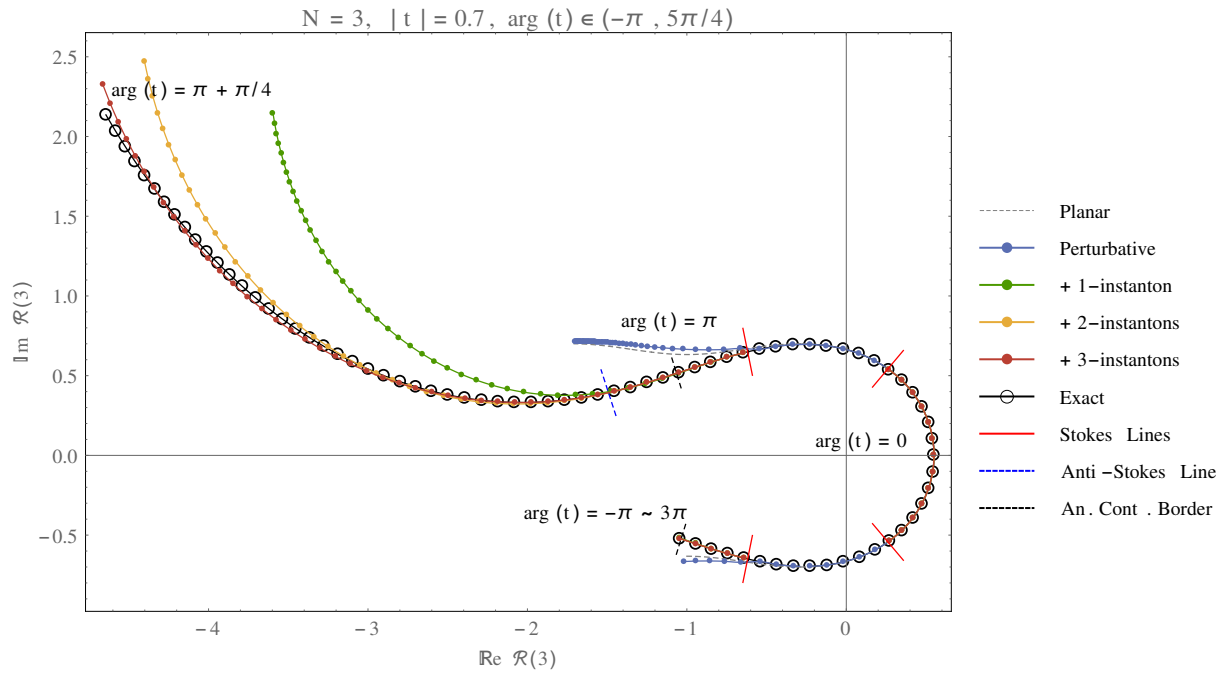

Figure 6.9: Resummation of r_3, for $|t| = 0.7$, in direct correspondence with the left plot in figure 6.2. Note the various Stokes lines in the principal domain for $\arg(t)$, and the anti-Stokes phase boundary in the second domain indicating that instanton corrections have become of order one.

Finally, we wish to study the partition function as a function of N, where N will be taken as an *arbitrary complex number*, and at fixed 't Hooft coupling t. The first thing one can try to do is extend our results towards negative N. This is shown in figure 6.14, for $t = \frac{1}{2}\, e^{\frac{5\pi i}{6}}$. At positive N the different lines smoothly interpolate between the exact results, and it is in fact impossible to tell them apart with the naked eye. Only very close to $N = 0$ do we notice the instanton contributions behaving incorrectly. As we have discussed earlier, this is a point of infinitely strong coupling where we do not have enough data – in fact at this point the pertur-

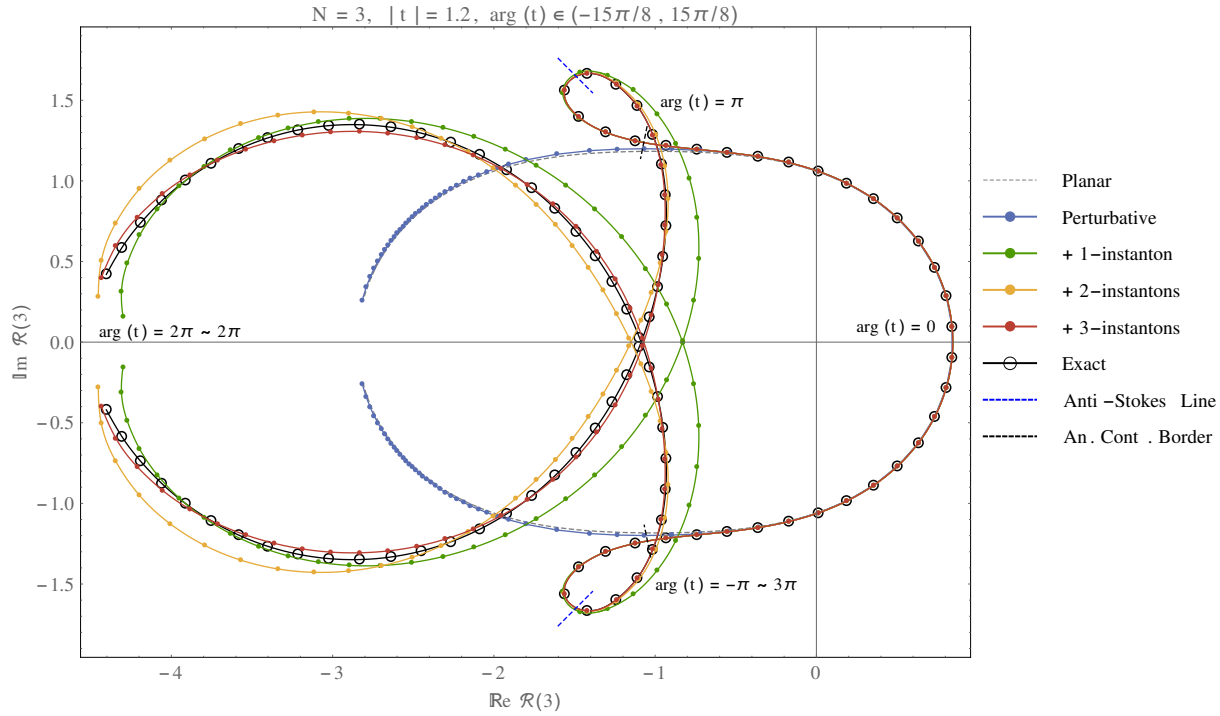

Figure 6.10: Resummation of r_3, for $|t| = 1.2$, in direct correspondence with the top right plot in figure 6.2. This plot illustrates very clearly how the perturbative resummation keeps following the planar approximation (and thus producing an incorrect result), while instanton effects take dominance in order to produce the correct monodromy results.

bative resummation is more reliable as we have more than twice the perturbative coefficients as compared to the (multi) instanton coefficients (see the appendix). As one moves towards $N < 0$, we should bear in mind that we have entered a region where $\exp(-NA(t)/t)$ has changed sign. This means that the perturbative sector is no longer a viable approximation to the full answer, since it just became of the same order as the instanton sectors. The plot in figure 6.14 illustrates how up until $N \approx -4$ the instanton sectors still look consistent, and are providing corrections which sit on top of the previous sector. However, as N gets increasingly negative we start getting wilder oscillations and the resummation can no longer be trusted. We would need more coefficients, and crucially higher instanton sectors, in order to carry on. In spite of this, it is clear how the transseries resummation allows us to define gauge theory at negative rank!

We can next look at complex values of N, and this is shown in figure 6.15, for $t = 10\,e^{\frac{99\pi i}{100}}$ (in this figure we are just plotting the third instanton contribution to the partition function, which visually is in fact indistinguishable from the perturbative or lower instanton resummations). Similarly to what we have found when looking at real N, positive or negative, we

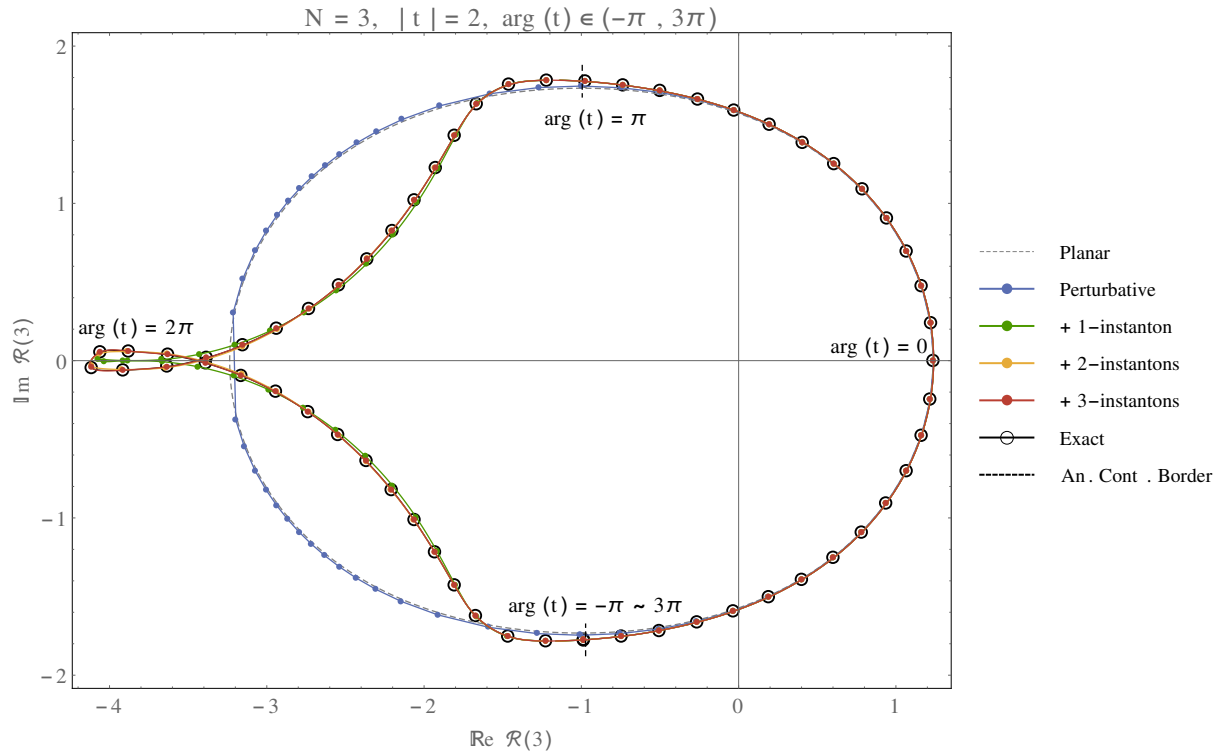

Figure 6.11: Resummation of r_3, for $|t| = 2$, in direct correspondence with the bottom right plot in figure 6.2. Note how the perturbative resummation keeps following the planar approximation.

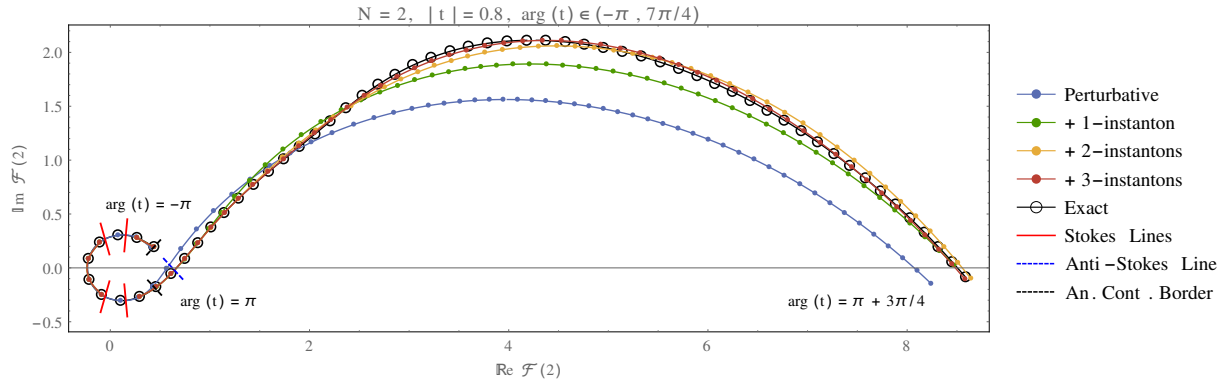

Figure 6.12: Resummation of $\mathcal{F}(2)$, for $|t| = 0.8$, in direct correspondence with the top right plot in figure 6.3. While the perturbative resummation still follows the general trend of the monodromy, it is no longer reliable past the anti-Stokes phase boundary.

have a function which oscillates and those oscillations can get milder or harsher as we move away from the real line. Note that in [61] the authors were able to analytically show that

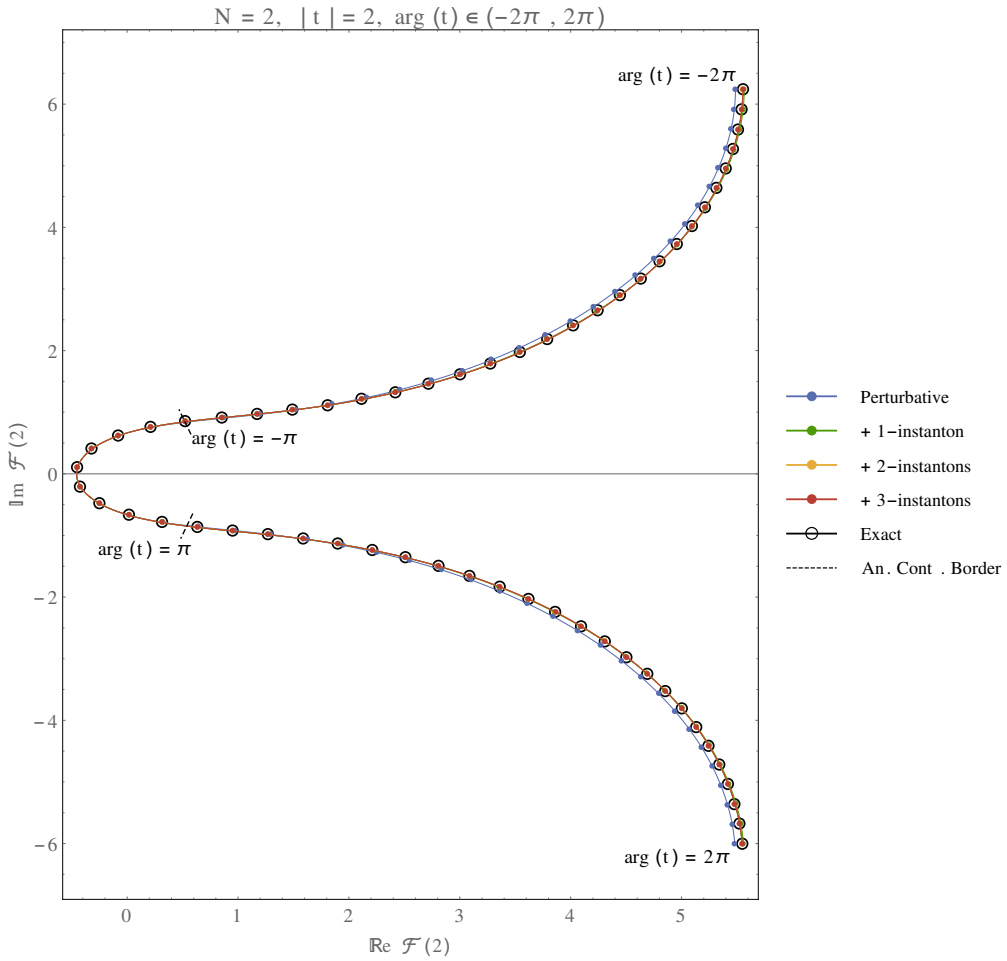

Figure 6.13: Resummation of $\mathcal{F}(2)$, for $|t| = 2$, in direct correspondence with the bottom right plot in figure 6.3. Unlike previous plots, note how here the perturbative result is pretty reliable.

the $\mathcal{N} = 8$ ABJ(M) partition function was an entire function of N. Crucial to that, as we have mentioned before, was the drastic simplification they found in their nonperturbative structure. The quartic matrix model partition function we address in the present work has no supersymmetry, milder integrability properties, and a full transseries to deal with, implying that such an analytical proof is at present still unachievable[15]. Generic gauge theories will be even more complicated. Nevertheless, we can carry out numerical tests, such as the ones illustrated above, and based on the evidence we have been able to produce we find encouraging signs that the partition function will indeed be an entire function of N, at fixed 't Hooft coupling. Future research should definitely address this issue, perhaps starting by

[15]Further studies of the partition function of the quartic matrix model will appear in [136, 137].

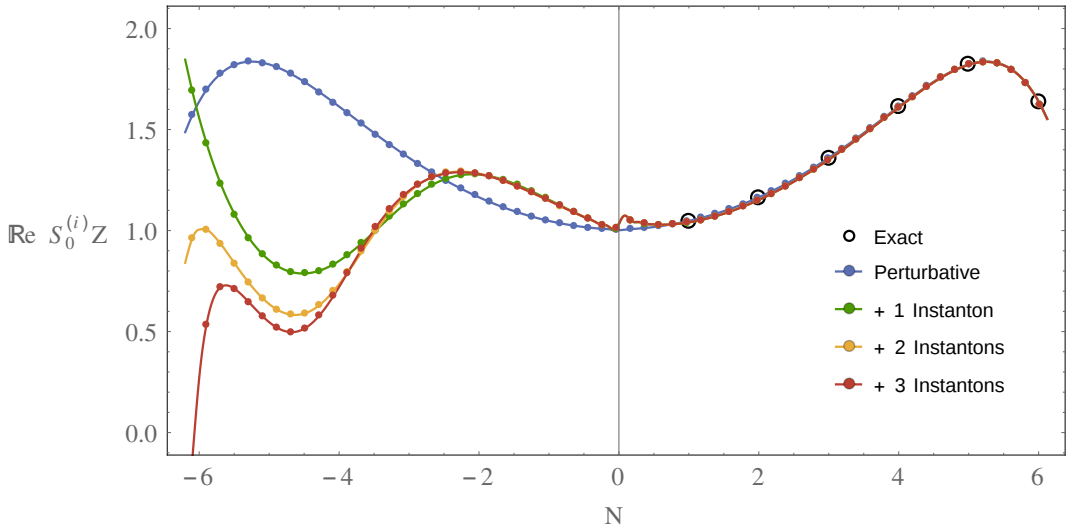

Figure 6.14: Real part of the resummed partition function, $S_0 Z$, for continuous negative to positive $N \in (-6, 6)$ and fixed $t = \frac{1}{2} e^{\frac{5\pi i}{6}}$. The accuracy is no longer reliable for $N \lesssim -4$.

producing more data, both higher $1/N$ coefficients in the sectors we have already computed and in higher instanton sectors. In any case, it is certainly remarkable that our one single transseries was able to correctly reproduce the many different (nonperturbative) monodromy structures at play, for different values of N and t. It is also extremely interesting that at the same time it went far beyond any available analytical results by extending the gauge theory to arbitrary complex N.

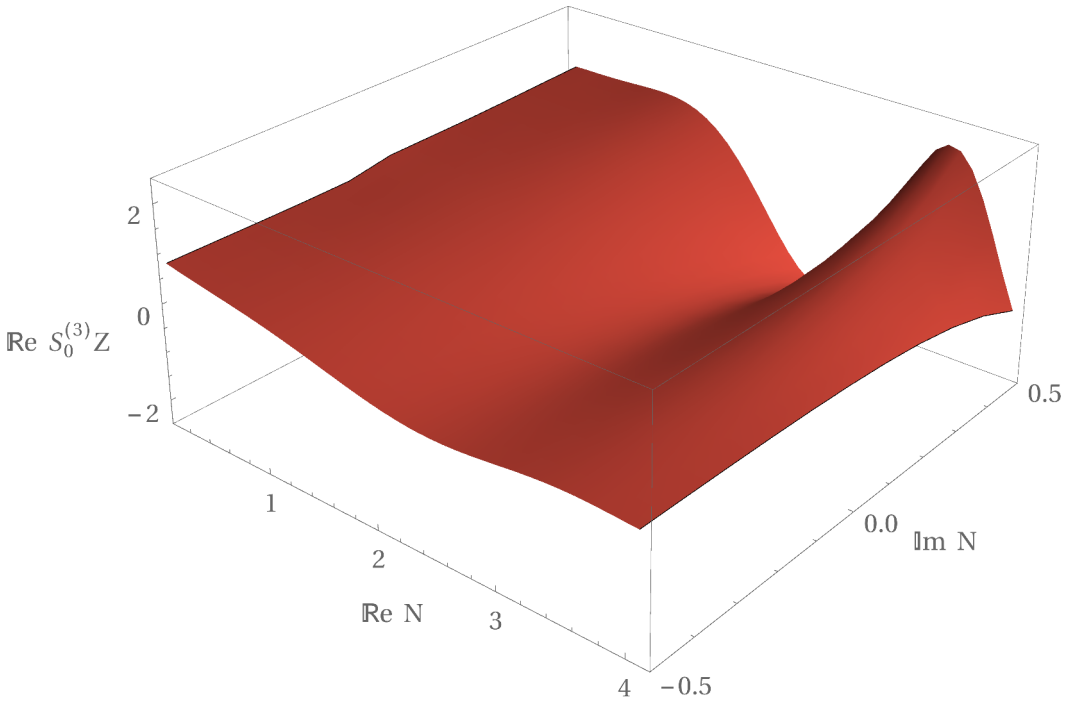

Figure 6.15: Real part of the partition function, resummed up to three instantons, $S_0^{(3)}Z$, for *complex* rank $\mathbb{R}\mathrm{e}(N) \in (0,4)$ and $\mathbb{I}\mathrm{m}(N) \in (-1/2, 1/2)$, and fixed $t = 10\,\mathrm{e}^{\frac{99\pi\mathrm{i}}{100}}$.

Chapter 7

Conclusions and Outlook

In this dissertation we have delved into recent developments concerning the application of the ideas of resurgence, particularly in the context of large N matrix models. The framework of resurgence, which we tried to describe in chapter 1, is complex and technically involved, but it teaches us many things. It teaches us that an asymptotic perturbative expansions should be generalized into transseries which are valid in a given wedge of the complex plane. Alien calculus then allows us to find out how solutions across different wedges are connected, and the transition lines are the Stokes lines where the singularities of the Borel transform lie. This connection amounts to jumps in the transseries parameter(s), and depends on a possibly infinite set of Stokes constants. These are invariants of the ODE or difference equation in question, and we will return to them in a bit. Finally, and very importantly, through alien calculus and the bridge equation, we can derive a multitude of large-order relations linking all multi-instanton sectors among themselves. This implies that the coefficients in the transseries are not a "random" collection of numbers but they are bound together in specific ways.

The choice of the $1/N$ expansion of matrix models as the testing ground for these ideas and the study of nonperturbative effects is justified in many ways. Even if we look past its connections to other, more complicated, string and gauge theories, it has two main advantages. It allows the extraction of large-order data both at perturbative and non-perturbative levels, and it provides a clean phsyical interpretation of the instanton effects, which we showed in our construction in section 3.3. We should underline that these derivations of the nonperturbative structure of matrix models via spectral geometry play this dual role of providing a physical understanding in terms of eigenvalue tunneling as well as an independent check on the transseries structure. In this work we have generalized many results [10, 11, 16, 57, 60, 103] to the multi-cut realm, with emphasis on proceeding with the nonperturbative study of the quartic matrix model initiated in [10, 16, 25], this time around in its two-cut phase with its Painlevé II double-scaling limit. Our results support the need for resurgent analysis and transseries, in particular the need for two-parameter transseries

solutions including new nonperturbative sectors. As in previous work, the question remains to explain, semi-classically, what these new sectors are: for example, in the Painlevé II context, while the physical multi-instanton sectors correspond to ZZ-branes [16, 30, 144] there is no similar understanding of the generalized sectors. Partial discussions may be found in [25, 60, 103, 147] but no conclusive answer as yet been reached. There is an interesting possibility that they may be related to anti-branes and super-matrix models [148] which needs to be explored. This question is also related to finding a first-principles calculation of the many "experimental" Stokes constants we have found: for one of these constants, $S_1^{(0)}$, in the Painlevé II framework, there are many analytical methods which determine it, see, *e.g.*, [16, 126, 131, 132, 149], but for all others finding one such analytical method is still an open problem. This is probably related to first determining how many truly independent Stokes constants there are for each problem, and further explaining the empirical relations we have found among them.

As one looks towards future research, some natural generalizations of our present work quickly come to mind. For example, one natural extension would be to "dig" deeper into the asymptotics of our examples, putting the full resurgent formulae on even stronger grounds. Recall that in [25], both for the one-cut quartic model and for its Painlevé I double-scaling limit, techniques of Borel-Padé resummation were used in order to analyze contributions to the large-order behavior arising at exponentially suppressed orders of 2^{-g}, 3^{-g}, and so on. It would be very interesting to extend those results within the present examples of the two-cut quartic model and its Painlevé II double-scaling limit. Yet another captivating line of work would be to address extensions of our Painlevé II results towards its deformations which arise within the type 0B minimal superstring context, when turning on RR flux or in the presence of charged ZZ-branes [128, 130]. This flux is controled by a parameter, q, and the equation which describes the minimal string set-up is now a deformation of Painlevé II, namely

$$u''(z) - 2u^3(z) + 2z\,u(z) = -\frac{q^2}{u^3(z)}. \tag{7.1}$$

This equation is certainly addressable within our framework and it would be very interesting to fully carry out its resurgent transseries analysis, extending our Painlevé II results.

In order to be fully explicit when addressing multi-cut Stokes phases, we have focused on the two-cut case where the Stokes phase is essentially related to the $\mathbb{Z}_2$ symmetry of the spectral curve configuration. But one may extend this calculation for an arbitrary number of cuts, k, as long as one keeps the corresponding spectral geometry configuration having a $\mathbb{Z}_k$ symmetry on its cuts. This symmetry will ensure that, although we are generically dealing with hyperelliptic configurations, at the end of the day all calculations reduce to elliptic integrals (very much along the same lines of the derivation in subsection 3.3.1). Afterwards, and still following our own guidelines from the $\mathbb{Z}_2$ case, a proper treatment of the

sum over instantons will further ensure that these elliptic functions will cancel in the end, thus producing adequate results for a Stokes phase. Setting up such $\mathbb{Z}_k$ symmetric spectral configurations is very simple, as it is to compute their corresponding instanton actions. The multi-instanton analysis should then follow with some extra work. Another attractive point of this example is its own double-scaling limit [133, 150] which seems to lead to new integrable hierarchies. For a $\mathbb{Z}_k$-symmetric configuration the string equations get more complicated, but are certainly solvable within our framework. In this way, it should be possible to say a lot about the nonperturbative structure of their corresponding solutions and, thus, about the general structure of these new integrable hierarchies.

The two-parameter transseries solution we have obtained for the Painlevé II equation is, in principle, its full nonperturbative solution. How may we understand the information encoded in this solution? When addressing 2d supergravity, or type 0B string theory, we are looking for a real solution to this equation, (4.58), for all $z \in \mathbb{R}$. Recall from, *e.g.*, [16] that this is naturally associated to the two phases of the Painlevé II solutions: the weak-coupling phase, when $z \to +\infty$, and the strong-coupling phase, when $z \to -\infty$, where one finds the asymptotic behaviors [131, 151]

$$u(z) \sim \sqrt{z}, \qquad z \to +\infty, \tag{7.2}$$

$$u(z) \sim \frac{1}{2^{1/12}\sqrt{2\pi}} (-z)^{-1/4} \, \mathrm{e}^{-\frac{2\sqrt{2}}{3}(-z)^{3/2}}, \qquad z \to -\infty. \tag{7.3}$$

There is in fact one such real solution, interpolating between the above weak and strong couplings, the Hastings-McLeod solution [151]. Notice that there are many solutions to the Painlevé II equation: for example, in [131] one finds a large class of global purely imaginary solutions, alongside another large class of global real solutions of which the Hastings-McLeod solution is a particular (singular limit) case–and the asymptotics of all these solutions are well known [131]. In particular, all these solutions should be encoded in our transseries solution, but in here we shall only discuss the Hastings-McLeod solution which was also addressed in [16]. This in itself is already a non-trivial problem: clearly, the "instanton action" in (7.3) is different from the Painlevé II instanton actions appearing in its two-parameter transseries solution. The natural question that follows is: how is the Hastings-McLeod solution encoded in our two-parameter transseries solution, and how can it provide for both types of weak and strong coupling behaviors, displayed above? In particular, how may A and $-A$ of Painlevé II "conspire" to yield the extra $\sqrt{2}$ factor? This question was partially addressed in [16], in the context of an one-parameter transseries solution. In there, it was shown that–upon Borel resummation–one may perform a median resummation [97] of the transseries along the Stokes line in the positive real axis to yield a real solution of the Painlevé II equation (see

the final discussion in [25] as well), *i.e.*,

$$u_{\mathbb{R}}(z,\sigma) \equiv \mathcal{S}_{+}u\left(z,\sigma-\frac{1}{2}S_1\right), \tag{7.4}$$

where $\mathcal{S}_{+}$ denotes a left Borel resummation along the positive real axis (see, *e.g.*, [25, 97]). Once this is done, the Hastings-McLeod solution is that particular real solution which has $\sigma = 0$ in the expression above [16]. In particular, this median resummation of the one-parameter transseries reproduces the Hastings-McLeod content for $z \in \mathbb{R}^{+}$. But one question remained open: what happens along the *negative* real axis instead? To answer this question one needs the full two-parameter transseries solution we have constructed in this dissertation, but yet this is not the full story: constructing a median resummation along the negative real axis, where one now finds an infinite number of highly non-trivial Stokes constants, is a much harder problem, and moving from positive z to negative z will also entail crossing Stokes lines. These crossings will make Stokes constants jump, not only as overall factors but also inside exponential terms due to the logarithmic sectors as we discussed in subsection 4.4.3. As such, it would be a very interesting project to make this strong/weak coupling interpolation completely explicit, within the resurgent transseries framework.

In chapter 5 we presented some preliminary results concerning the quartic matrix model phase diagram and the trivalent-tree phase. The full picture of the quartic matrix model should be complete in the near future [136–138]. This is expected to be anti-Stokes phase with oscillatory large-N asymptotics, and as such it is of natural interest to understand how the transseries reorganizes itself into a theta-function-like object. From a different perspective we also want to construct the spectral geometry of the trivalent phase, as it should be the gateway to understanding the nature of the nonperturbative effects, since they are not eigenvalue jumps (at least not in the traditional B-cycle instanton picture we discussed). We already have ample numeric evidence to guide us and test the results in this new phase. There is also the possibility that we will somehow be able to find an exact solution in the pure quartic $|t| \to +\infty$ limit, and reconstruct the trivalent phase out of this. In addition, we note that this is a novel type of phase, and it could mean that there are new phases in more relevant gauge theories to be uncovered. After the trivalent phase is well understood in the quartic matrix model, we have to start wondering if more complicated matrix models, particularly the ones derived from gauge theories via localization [43, 44], have these trivalent, or multivalent in general, types of eigenvalue configurations, and what their physical implications are. But even within the matrix model context, there are other engaging open questions to consider. We have not delved much into this direction, but there is more "geometry" in the matrix model than the spectral curve. In rough terms the spectral curve can be seen as a "subset" of a Calabi-Yau, and this is how matrix models are connected to topological strings (see [29, 50, 62] for more details). We should now consider a general, background independent, grand-canonical partition function as a sum over all background

choices [57–59, 110], schematically of the form

$$\mathcal{Z}(\varrho_i, t) = \sum_{N_1+N_2+N_3=N} \varrho_1^{N_1} \varrho_2^{N_2} \varrho_3^{N_3} Z(N_1, N_2, N_3)\,. \tag{7.5}$$

The ϱ_i are the weights associated to each of the three contours, as we discussed in chapter 5. The connection between these and the transseries parameter should be understood better, but for now we can see how in the sum above there are really only two parameters, because the sum of the N_i is fixed. In this picture the Stokes phases are easy to understand. We have a given background $\{N_i^\star\}$, or equivalently a choice of 't Hooft moduli $\{t_i^\star\}$, which corresponds to a certain Calabi-Yau geometry, and the sum over backgrounds is peaked around this "energetically favored" choice. This implies we have something of the form (3.87)

$$\mathcal{Z}(\varrho_i, t) = Z(N_i^\star) \left\{ 1 + \sum_\ell \frac{g_s^{\ell^2/2}}{(2\pi)^{\ell/2}} G_2(\ell+1)\, q^{\ell^2/2}\, \mathrm{e}^{-\ell A/g_s} (1 + \mathcal{O}(g_s)) \right\}, \tag{7.6}$$

or in other words, the grand-canonical partition function is dominated by a particular canonical background. These expressions are for fixed t, and as it changes the dominant background will change, and with it the geometry changes, until we cross an anti-Stokes line and picture changes. In the anti-Stokes regions we no longer have an adequate $1/N$ expansion, so it is not clear if there is still a dual holographic geometry. In a way, there is no instanton action in this case, and eigenvalues are free to move between cuts. So geometrically it would correspond to a multitude of backgrounds all contributing with the same "energy". This is a very engaging open problem.

Finally, in chapter 6 we made use of our knowledge of transseries and resurgence to take the $1/N$ expansion one step further, and that was to make use of our resurgent transseries in order to make finite N predictions. We then moved on to explore the full monodromy of the free energy and recursion coefficients at finite N, and saw how the multi-instanton contributions could be crucial to match the analytic results. In the end we looked at an analytic continuation to the complex N-plane and found some evidence that our resummed transseries could be the unique analytic continuation into the complex plane and moreover, that it might be an entire function. As such a natural extension of our work is the computation of more data, both to higher instanton sectors and to higher loop orders, so that we can add more strength to this claim. We also believe that many interesting problems may be addressed in the near future using the methods we introduce and develop in this chapter. For instance, one may consider gauge theories in higher dimensions. When considering supersymmetric gauge theories on compact manifolds where some observables localize, we may fall back into the realm of matrix models. The resurgent analysis of localizable observables in some three and four dimensional gauge theories was initialized in [152] and it would certainly be interesting to address finite N calculations in that realm. If we move away from

matrix models, the main difference will be that the (now diagrammatic) computation of perturbative and multi-instanton coefficients will be much more time consuming. Our uses of large N resurgent transseries, however, should hold step by step. Perhaps a good route where to start would be to follow the recent resurgence calculations for the $\mathbb{CP}^N$ model in [75–77] and address the corresponding large N limit in that context.

Via large N duality, another class of theories to explore are string theories. The simplest cases might be within topological string theory, whose resurgent analysis has also been steadily developed [10, 11, 16, 64, 65, 107] in recent years. In particular, the resurgence techniques introduced in [64] have allowed for the generation of large amounts of resurgence data concerning the local $\mathbb{P}^2$ geometry [65], and are easily extendable to generate equal amounts of data for other toric Calabi–Yau geometries such as local $\mathbb{P}^1 \times \mathbb{P}^1$. In this context, a very interesting comparison is actually now possible due to a recent proposal for obtaining nonperturbative results for topological strings in toric Calabi–Yau geometries [153] (following up on earlier work in [154, 155]). This proposal allows for the calculation of topological string free energies at continuous values of N for several local Calabi–Yau geometries; in particular it addresses the examples of local $\mathbb{P}^2$ and local $\mathbb{P}^1 \times \mathbb{P}^1$. It would be extremely interesting to use the aforementioned resurgence data for these geometries [64, 65], combined with the methods in the present dissertation, to investigate how accurate would be the match between both approaches, this time around at *continuous* N. On the subject of topological string theory, it is also worth considering an investigation into the A-model side. While at the present time it is still not clear how to proceed, this would be a way to study the resurgent properties of enumerative invariants, such as Gromov-Witten or Gopakumar-Vafa invariants.

Bibliography

[1] R. Schiappa and R. Vaz, *The Resurgence of Instantons: Multi-Cut Stokes Phases and the Painlevé II Equation*, *Commun.Math.Phys.* **330** (2014) 655–721, [arXiv:1302.5138].

[2] R. Couso-Santamaría, R. Schiappa, and R. Vaz, *Finite N from Resurgent Large N*, *Annals Phys.* **356** (2015) 1–28, [arXiv:1501.01007].

[3] C. P. Herzog, K.-W. Huang, and R. Vaz, *Linear Resistivity from Non-Abelian Black Holes*, *JHEP* **1411** (2014) 066, [arXiv:1405.3714].

[4] F. J. Dyson, *Divergence of perturbation theory in quantum electrodynamics*, *Phys. Rev.* **85** (Feb, 1952) 631–632.

[5] C. M. Bender and T. T. Wy, *Statistical analysis of feynman diagrams*, *Phys. Rev. Lett.* **37** (Jul, 1976) 117–120.

[6] L. Lipatov, *Divergence of the Perturbation Theory Series and the Quasiclassical Theory*, *Sov.Phys.JETP* **45** (1977) 216–223.

[7] S. Garoufalidis and T. T. Q. Le, *Gevrey series in quantum topology*, *ArXiv Mathematics e-prints* (Sept., 2006) [math/0609618].

[8] C. M. Bender and T. T. Wu, *Anharmonic oscillator*, *Phys. Rev.* **184** (Aug, 1969) 1231–1260.

[9] C. M. Bender and T. Wu, *Anharmonic oscillator. 2: A Study of perturbation theory in large order*, *Phys.Rev.* **D7** (1973) 1620–1636.

[10] M. Mariño, R. Schiappa, and M. Weiss, *Nonperturbative Effects and the Large-Order Behavior of Matrix Models and Topological Strings*, *Commun.Num.Theor.Phys.* **2** (2008) 349–419, [arXiv:0711.1954].

[11] S. Pasquetti and R. Schiappa, *Borel and Stokes Nonperturbative Phenomena in Topological String Theory and c=1 Matrix Models*, *Annales Henri Poincare* **11** (2010) 351–431, [arXiv:0907.4082].

[12] S. Shenker, *The Strength of Nonperturbative Effects in String Theory*, vol. 262 of *NATO ASI Series*. Springer US, 1991.

[13] J. Le Guillou and J. Zinn-Justin (eds.), *Large order behavior of perturbation theory*, *North Holland, Amsterdam* (1990).

[14] J. Boyd, *The devil's invention: Asymptotic, superasymptotic and hyperasymptotic series*, *Acta Applicandae Mathematica* **56** (1999), no. 1 1–98.

[15] M. Berry, *Stokes phenomenon; smoothing a victorian discontinuity*, *Publications Mathématiques de l'Institut des Hautes Études Scientifiques* **68** (1988), no. 1 211–221.

[16] M. Mariño, *Nonperturbative effects and nonperturbative definitions in matrix models and topological strings*, *JHEP* **0812** (2008) 114, [arXiv:0805.3033].

[17] J. Écalle, *Les Fonctions Résurgentes, vol. 1: Algèbres de fonctions résurgentes*, *Publ.Math. Orsay* **81-05** (1981).

[18] J. Écalle, *Les Fonctions Résurgentes, vol. 2: Les fonctions résurgentes appliquées à l'itération*, *Publ.Math. Orsay* **81-06** (1981).

[19] J. Écalle, *Les Fonctions Résurgentes, vol. 3: L'équation du pont et la classification analytique des objets locaux*, *Publ.Math. Orsay* **85-05** (1985).

[20] J. Zinn-Justin, *Perturbation Series at Large Orders in Quantum Mechanics and Field Theories: Application to the Problem of Resummation*, *Phys.Rept.* **70** (1981) 109.

[21] U. D. Jentschura and J. Zinn-Justin, *Instantons in quantum mechanics and resurgent expansions*, *Phys.Lett.* **B596** (2004) 138–144, [hep-ph/0405279].

[22] A. Voros, *Résurgence quantique*, *Ann.Inst.Fourier* **43** (1993), no. 5 1509–1534.

[23] O. Costin, *Exponential asymptotics, transseries, and generalized borel summation for analytic, nonlinear, rank-one systems of ordinary differential equations*, *International Mathematics Research Notices* (1995), no. 8 377–417.

[24] O. Costin, *On borel summation and stokes phenomena for rank- 1 nonlinear systems of ordinary differential equations*, *Duke Math. J.* **93** (06, 1998) 289–344.

[25] I. Aniceto, R. Schiappa, and M. Vonk, *The Resurgence of Instantons in String Theory*, *Commun.Num.Theor.Phys.* **6** (2012) 339–496, [arXiv:1106.5922].

[26] G. 't Hooft, *A Planar Diagram Theory for Strong Interactions*, *Nucl.Phys.* **B72** (1974) 461.

[27] J. M. Maldacena, *The Large N limit of superconformal field theories and supergravity*, *Int.J.Theor.Phys.* **38** (1999) 1113–1133, [hep-th/9711200].

[28] O. Aharony, S. S. Gubser, J. M. Maldacena, H. Ooguri, and Y. Oz, *Large N field theories, string theory and gravity*, *Phys.Rept.* **323** (2000) 183–386, [hep-th/9905111].

[29] R. Dijkgraaf and C. Vafa, *Matrix models, topological strings, and supersymmetric gauge theories*, *Nucl.Phys.* **B644** (2002) 3–20, [hep-th/0206255].

[30] S. Y. Alexandrov, V. A. Kazakov, and D. Kutasov, *Nonperturbative effects in matrix models and D-branes*, *JHEP* **0309** (2003) 057, [hep-th/0306177].

[31] E. J. Martinec, *The Annular report on noncritical string theory*, hep-th/0305148.

[32] M. Krblek and P. Seba, *The statistical properties of the city transport in cuernavaca (mexico) and random matrix ensembles*, *Journal of Physics A: Mathematical and General* **33** (2000), no. 26 L229.

[33] E. Bachmat, D. Berend, L. Sapir, S. Skiena, and N. Stolyarov, *Analysis of aeroplane boarding via spacetime geometry and random matrix theory*, *Journal of Physics A Mathematical General* **39** (July, 2006) L453–L459, [physics/0512020].

[34] A. Brini, B. Eynard, and M. Mariño, *Torus Knots and Mirror Symmetry*, *Annales Henri Poincaré* **13** (Dec., 2012) 1873–1910, [arXiv:1105.2012].

[35] J. P. Keating and N. C. Snaith, *Random Matrix Theory and $\zeta(1/2+it)$*, *Communications in Mathematical Physics* **214** (2000) 57–89.

[36] J. E. Andersen, L. O. Chekhov, R. C. Penner, C. M. Reidys, and P. Sułkowski, *Enumeration of RNA complexes via random matrix theory*, *ArXiv e-prints* (Mar., 2013) [arXiv:1303.1326].

[37] G. Akemann, J. Baik, and P. D. Francesco, eds., *The Oxford Handbook of Random Matrix Theory*. Oxford University Press, 2011.

[38] A. Morozov, *Faces of matrix models*, *Soviet Journal of Experimental and Theoretical Physics Letters* **95** (Aug., 2012) 586–593, [arXiv:1204.3953].

[39] L. F. Alday, D. Gaiotto, and Y. Tachikawa, *Liouville Correlation Functions from Four-dimensional Gauge Theories*, *Lett.Math.Phys.* **91** (2010) 167–197, [arXiv:0906.3219].

[40] N. Wyllard, *A_{N-1} Conformal Toda Field Theory Correlation Functions from Conformal $\mathcal{N} = 2$ $SU(N)$ Quiver Gauge Theories*, *JHEP* **0911** (2009) 002, [arXiv:0907.2189].

[41] R. Dijkgraaf and C. Vafa, *Toda Theories, Matrix Models, Topological Strings, and $\mathcal{N} = 2$ Gauge Systems*, arXiv:0909.2453.

[42] R. Schiappa and N. Wyllard, *An A_r Threesome: Matrix Models, 2d CFTs and 4d $\mathcal{N} = 2$ gauge theories*, *J.Math.Phys.* **51** (2010) 082304, [arXiv:0911.5337].

[43] V. Pestun, *Localization of gauge theory on a four-sphere and supersymmetric Wilson loops*, *Commun.Math.Phys.* **313** (2012) 71–129, [arXiv:0712.2824].

[44] A. Kapustin, B. Willett, and I. Yaakov, *Exact Results for Wilson Loops in Superconformal Chern-Simons Theories with Matter*, *JHEP* **1003** (2010) 089, [arXiv:0909.4559].

[45] N. Drukker, M. Mariño, and P. Putrov, *From Weak to Strong Coupling in ABJM Theory*, *Communications in Mathematical Physics* **306** (Sept., 2011) 511–563, [arXiv:1007.3837].

[46] N. Drukker, M. Mariño, and P. Putrov, *Nonperturbative aspects of ABJM theory*, *JHEP* **1111** (2011) 141, [arXiv:1103.4844].

[47] M. Mariño and P. Putrov, *ABJM theory as a Fermi gas*, *Journal of Statistical Mechanics: Theory and Experiment* **3** (Mar., 2012) 1, [arXiv:1110.4066].

[48] E. Brezin, C. Itzykson, G. Parisi, and J. Zuber, *Planar Diagrams*, *Commun.Math.Phys.* **59** (1978) 35.

[49] D. Bessis, C. Itzykson, and J. Zuber, *Quantum field theory techniques in graphical enumeration*, *Adv.Appl.Math.* **1** (1980) 109–157.

[50] M. Mariño, *Les Houches lectures on matrix models and topological strings*, hep-th/0410165.

[51] J. Ambjorn, L. Chekhov, C. Kristjansen, and Y. Makeenko, *Matrix model calculations beyond the spherical limit*, *Nucl.Phys.* **B404** (1993) 127–172, [hep-th/9302014].

[52] B. Eynard and N. Orantin, *Invariants of algebraic curves and topological expansion*, *Commun.Num.Theor.Phys.* **1** (2007) 347–452, [math-ph/0702045].

[53] B. Eynard and N. Orantin, *Algebraic methods in random matrices and enumerative geometry*, arXiv:0811.3531.

[54] O. Lechtenfeld, *On Eigenvalue tunneling in matrix models*, *Int.J.Mod.Phys.* **A7** (1992) 2335–2354.

[55] F. David, *Phases of the large N matrix model and nonperturbative effects in 2-d gravity*, *Nucl.Phys.* **B348** (1991) 507–524.

[56] F. David, *Nonperturbative Effects in Two-Dimensional Quantum Gravity*. World Scientific, 1992.

[57] M. Mariño, R. Schiappa, and M. Weiss, *Multi-Instantons and Multi-Cuts*, *J.Math.Phys.* **50** (2009) 052301, [arXiv:0809.2619].

[58] B. Eynard, *Large N expansion of convergent matrix integrals, holomorphic anomalies, and background independence*, *JHEP* **0903** (2009) 003, [arXiv:0802.1788].

[59] B. Eynard and M. Mariño, *A Holomorphic and background independent partition function for matrix models and topological strings*, *J.Geom.Phys.* **61** (2011) 1181–1202, [arXiv:0810.4273].

[60] A. Klemm, M. Mariño, and M. Rauch, *Direct Integration and Non-Perturbative Effects in Matrix Models*, *JHEP* **1010** (2010) 004, [arXiv:1002.3846].

[61] S. Codesido, A. Grassi, and M. Mariño, *Exact results in $\mathcal{N} = 8$ Chern-Simons-matter theories and quantum geometry*, *JHEP* **07** (2015) 011, [arXiv:1409.1799].

[62] R. Dijkgraaf and C. Vafa, *On geometry and matrix models*, *Nucl.Phys.* **B644** (2002) 21–39, [hep-th/0207106].

[63] M. Vonk, *A Mini-course on topological strings*, hep-th/0504147.

[64] R. Couso-Santamaría, J. D. Edelstein, R. Schiappa, and M. Vonk, *Resurgent Transseries and the Holomorphic Anomaly*, arXiv:1308.1695.

[65] R. Couso-Santamaría, J. D. Edelstein, R. Schiappa, and M. Vonk, *Resurgent Transseries and the Holomorphic Anomaly: Nonperturbative Closed Strings in Local $\mathbb{CP}^2$*, *Commun.Math.Phys.* **338** (2015), no. 1 285–346, [arXiv:1407.4821].

[66] M. Vonk, *Resurgence and Topological Strings*, arXiv:1502.05711.

[67] M. Bershadsky, S. Cecotti, H. Ooguri, and C. Vafa, *Kodaira-Spencer theory of gravity and exact results for quantum string amplitudes*, *Commun.Math.Phys.* **165** (1994) 311–428, [hep-th/9309140].

[68] A. Cherman and M. Ünsal, *Real-Time Feynman Path Integral Realization of Instantons*, arXiv:1408.0012.

[69] A. Behtash, T. Sulejmanpasic, T. Schaefer, and M. Ünsal, *Hidden topological angles and Lefschetz thimbles*, arXiv:1502.06624.

[70] A. Cherman, D. Dorigoni, G. V. Dunne, and M. Ünsal, *Resurgence in Quantum Field Theory: Nonperturbative Effects in the Principal Chiral Model*, *Phys.Rev.Lett.* **112** (2014) 021601, [arXiv:1308.0127].

[71] G. Başar, G. V. Dunne, and M. Ünsal, *Resurgence theory, ghost-instantons, and analytic continuation of path integrals*, *JHEP* **1310** (2013) 041, [arXiv:1308.1108].

[72] G. Başar and G. V. Dunne, *Resurgence and the Nekrasov-Shatashvili limit: connecting weak and strong coupling in the Mathieu and Lamé systems*, *JHEP* **1502** (2015) 160, [arXiv:1501.05671].

[73] G. V. Dunne, M. Shifman, and M. Ünsal, *Infrared Renormalons versus Operator Product Expansions in Supersymmetric and Related Gauge Theories*, *Phys.Rev.Lett.* **114** (2015), no. 19 191601, [arXiv:1502.06680].

[74] G. V. Dunne and M. Ünsal, *Resurgence and Dynamics of O(N) and Grassmannian Sigma Models*, arXiv:1505.07803.

[75] A. Cherman, D. Dorigoni, and M. Ünsal, *Decoding perturbation theory using resurgence: Stokes phenomena, new saddle points and Lefschetz thimbles*, arXiv:1403.1277.

[76] G. V. Dunne and M. Ünsal, *Resurgence and Trans-series in Quantum Field Theory: The CP(N-1) Model*, *JHEP* **1211** (2012) 170, [arXiv:1210.2423].

[77] G. V. Dunne and M. Ünsal, *Continuity and Resurgence: towards a continuum definition of the $\mathbb{CP}$(N-1) model*, *Phys.Rev.* **D87** (2013) 025015, [arXiv:1210.3646].

[78] P. Argyres and M. Ünsal, *A semiclassical realization of infrared renormalons*, *Phys.Rev.Lett.* **109** (2012) 121601, [arXiv:1204.1661].

[79] P. C. Argyres and M. Ünsal, *The semi-classical expansion and resurgence in gauge theories: new perturbative, instanton, bion, and renormalon effects*, *JHEP* **1208** (2012) 063, [arXiv:1206.1890].

[80] N. Beisert, B. Eden, and M. Staudacher, *Transcendentality and Crossing*, *J.Stat.Mech.* **0701** (2007) P01021, [hep-th/0610251].

[81] I. Aniceto, *The Resurgence of the Cusp Anomalous Dimension*, arXiv:1506.03388.

[82] D. Dorigoni and Y. Hatsuda, *Resurgence of the Cusp Anomalous Dimension*, arXiv:1506.03763.

[83] M. P. Heller and M. Spalinski, *Hydrodynamics Beyond the Gradient Expansion: Resurgence and Resummation*, *ArXiv e-prints* (Mar., 2015) [arXiv:1503.07514].

[84] D. Dorigoni, *An Introduction to Resurgence, Trans-Series and Alien Calculus*, arXiv:1411.3585.

[85] T. Seara and D. Sauzin, *Resumació de Borel i Teoria de la Ressurgència*, *Butl.Soc.Catalana Mat.* **18** (2003) 131.

[86] D. Sauzin, *Introduction to 1-summability and resurgence*, *ArXiv e-prints* (May, 2014) [arXiv:1405.0356].

[87] M. Mariño, *Lectures on non-perturbative effects in large N gauge theories, matrix models and strings*, *Fortsch.Phys.* **62** (2014) 455–540, [arXiv:1206.6272].

[88] B. Candelpergher, J. Nosmas, and F. Pham, *Premiers Pas en Calcul Étranger*, *Ann.Inst.Fourier* **43** (1993) 201.

[89] E. Delabaere, *Introduction to Écalle Theory*. Computer Algebra and Differential Equations. Cambridge University Press, 1994.

[90] O. Costin, *Asymptotics and Borel Summability*, vol. 141 of *Monographs and Surveys in Pure and Applied Mathematics*. CRC Press, 2012.

[91] B. L. Braaksma, *Transseries for a class of nonlinear difference equations.*, *J. Difference Equ. Appl.* **7** (2001), no. 5 717–750.

[92] B. Braaksma and R. Kuik, *Resurgence relations for classes of differential and difference equations*, *Annales de la faculté des sciences de Toulouse* **13** (2004), no. 4 479–492.

[93] G. Edgar, *Transseries for Beginners*, *Real Anal. Exchange* **35** (2009) 253, [arXiv:0801.4877].

[94] M. Berry, *Asymptotics, Superasymptotics, Hyperasymptotics...*, vol. 284 of *NATO ASI Series*. Springer US, 1991.

[95] E. Bogomolny, *Calculation of instanton-anti-instanton contributions in quantum mechanics*, *Physics Letters B* **91** (1980), no. 34 431 – 435.

[96] J. Zinn-Justin, *Multi-instanton contributions in quantum mechanics*, *Nuclear Physics B* **192** (1981), no. 1 125 – 140.

[97] I. Aniceto and R. Schiappa, *Nonperturbative Ambiguities and the Reality of Resurgent Transseries*, *Commun.Math.Phys.* **335** (2015), no. 1 183–245, [arXiv:1308.1115].

[98] S. Garoufalidis and M. Mariño, *Universality and asymptotics of graph counting problems in nonorientable surfaces*, arXiv:0812.1195.

[99] B. Candelpergher, J. Nosmas, and F. Pham, *Approche de la résurgence*. Actualités mathématiques. Hermann (14-Bayeux), Paris, 1993.

[100] J. C. Collins and D. E. Soper, *Large order expansion in perturbation theory*, *Annals of Physics* **112** (May, 1978) 209–234.

[101] P. Di Francesco, P. H. Ginsparg, and J. Zinn-Justin, *2-D Gravity and random matrices*, *Phys.Rept.* **254** (1995) 1–133, [hep-th/9306153].

[102] M. Hanada, M. Hayakawa, N. Ishibashi, H. Kawai, T. Kuroki, et al., *Loops versus matrices: The Nonperturbative aspects of noncritical string*, *Prog.Theor.Phys.* **112** (2004) 131–181, [hep-th/0405076].

[103] S. Garoufalidis, A. Its, A. Kapaev, and M. Mariño, *Asymptotics of the instantons of Painlevé I*, arXiv:1002.3634.

[104] L. F. Richardson and J. A. Gaunt, *The deferred approach to the limit. part i. single lattice. part ii. interpenetrating lattices*, *Philosophical Transactions of the Royal Society of London. Series A* **226** (1927) pp. 299–361.

[105] F. David, *Nonperturbative effects in matrix models and vacua of two-dimensional gravity*, *Phys.Lett.* **B302** (1993) 403–410, [hep-th/9212106].

[106] C. M. Bender and S. A. Orszag, *Advanced Mathematical Methods for Scientists and Engineers*. 1978.

[107] M. Mariño, *Open string amplitudes and large order behavior in topological string theory*, *JHEP* **0803** (2008) 060, [hep-th/0612127].

[108] M. Mariño, S. Pasquetti, and P. Putrov, *Large N duality beyond the genus expansion*, *JHEP* **1007** (2010) 074, [arXiv:0911.4692].

[109] B. Eynard, M. Mariño, and N. Orantin, *Holomorphic anomaly and matrix models*, *JHEP* **0706** (2007) 058, [hep-th/0702110].

[110] G. Bonnet, F. David, and B. Eynard, *Breakdown of universality in multicut matrix models*, *J.Phys.* **A33** (2000) 6739–6768, [cond-mat/0003324].

[111] G. Akemann, *Higher genus correlators for the Hermitian matrix model with multiple cuts*, *Nucl.Phys.* **B482** (1996) 403–430, [hep-th/9606004].

[112] J. Ambjorn and G. Akemann, *New universal spectral correlators*, *J.Phys.* **A29** (1996) L555–L560, [cond-mat/9606129].

[113] N. Deo, *Orthogonal polynomials and exact correlation functions for two cut random matrix models*, *Nuclear Physics B* **504** (1997), no. 3 609 – 620.

[114] E. Kanzieper and V. Freilikher, *Two-band random matrices*, *Phys. Rev. E* **57** (Jun, 1998) 6604–6611.

[115] E. Brézin and N. Deo, *Correlations and symmetry breaking in gapped matrix models*, *Phys. Rev. E* **59** (Apr, 1999) 3901–3910, [cond-mat/9805096].

[116] Wolfram Functions Site, "Elliptic integrals." http://functions.wolfram.com/EllipticIntegrals/.

[117] Wolfram Functions Site, "Elliptic functions." http://functions.wolfram.com/EllipticFunctions/.

[118] L. Molinari, *Phase structure of matrix models through orthogonal polynomials*, *Journal of Physics A: Mathematical and General* **21** (1988), no. 1 1.

[119] K. Demeterfi, N. Deo, S. Jain, and C.-I. Tan, *Multiband structure and critical behavior of matrix models*, *Phys.Rev.* **D42** (1990) 4105–4122.

[120] J. Jurkiewicz, *Chaotic behavior in one matrix models*, *Phys.Lett.* **B261** (1991) 260–268.

[121] D. Senechal, *Chaos in the Hermitian one matrix model*, *Int.J.Mod.Phys.* **A7** (1992) 1491–1506.

[122] R. C. Brower, N. Deo, S. Jain, and C.-I. Tan, *Symmetry breaking in the double well Hermitian matrix models*, *Nucl.Phys.* **B405** (1993) 166–190, [hep-th/9212127].

[123] M. Bertola and M. Mo, *Commuting difference operators, spinor bundles and the asymptotics of orthogonal polynomials with respect to varying complex weights*, *Advances in Mathematics* **220** (2009), no. 1 154 – 218.

[124] M. Bertola, *Boutroux curves with external field: equilibrium measures without a variational problem*, *Analysis and Mathematical Physics* **1** (2011), no. 2-3 167–211, [arXiv:0705.3062].

[125] M. Bertola and A. Tovbis, *Asymptotics of Orthogonal Polynomials with Complex Varying Quartic Weight: Global Structure, Critical Point Behaviour and the First Painlevé Equation*, arXiv:1108.0321 .

[126] P. Bleher and A. Its, *Semiclassical asymptotics of orthogonal polynomials, riemann-hilbert problem, and universality in the matrix model.*, *Annals of Mathematics. Second Series* **150** (1999), no. 1 185–266.

[127] M. R. Douglas, N. Seiberg, and S. H. Shenker, *Flow and Instability in Quantum Gravity*, *Phys.Lett.* **B244** (1990) 381–386.

[128] I. R. Klebanov, J. M. Maldacena, and N. Seiberg, *D-brane decay in two-dimensional string theory*, *JHEP* **0307** (2003) 045, [hep-th/0305159].

[129] N. Seiberg and D. Shih, *Branes, rings and matrix models in minimal (super)string theory*, *JHEP* **0402** (2004) 021, [hep-th/0312170].

[130] N. Seiberg and D. Shih, *Flux vacua and branes of the minimal superstring*, *JHEP* **0501** (2005) 055, [hep-th/0412315].

[131] P. A. Deift and X. Zhou, *Asymptotics for the painlevé ii equation*, *Communications on Pure and Applied Mathematics* **48** (1995), no. 3 277–337.

[132] H. Kawai, T. Kuroki, and Y. Matsuo, *Universality of nonperturbative effect in type 0 string theory*, *Nucl.Phys.* **B711** (2005) 253–274, [hep-th/0412004].

[133] C. Crnkovic and G. W. Moore, *Multicritical multicut matrix models*, *Phys.Lett.* **B257** (1991) 322–328.

[134] M. Mariño and P. Putrov, *Multi-instantons in large N Matrix Quantum Mechanics*, arXiv:0911.3076.

[135] I. R. Klebanov, J. M. Maldacena, and N. Seiberg, *Unitary and complex matrix models as 1-d type 0 strings*, *Commun.Math.Phys.* **252** (2004) 275–323, [hep-th/0309168].

[136] R. Couso-Santamaría, R. Schiappa, and R. Vaz, *to appear*, .

[137] I. Aniceto, R. Schiappa, and M. Vonk, *to appear*, .

[138] R. Schiappa and M. Vonk, *to appear*, .

[139] G. G. Stokes, *On the Discontinuity of Arbitrary Constants which Appear in Divergent Developments*, *Trans.Camb.Phil.Soc.* **10** (1864) 106.

[140] A. Grassi, M. Mariño, and S. Zakany, *Resumming the string perturbation series*, *JHEP* **1505** (2015) 038, [arXiv:1405.4214].

[141] R. Balian, G. Parisi, and A. Voros, *Discrepancies from Asymptotic Series and their Relation to Complex Classical Trajectories*, *Phys.Rev.Lett.* **41** (1978) 1141.

[142] R. Balian, G. Parisi, and A. Voros, *Quartic oscillator*, vol. 106 of *Lecture Notes in Physics*. Springer Berlin Heidelberg, 1979.

[143] F. W. J. Olver, D. W. Lozier, R. F. Boisvert, and C. W. Clark, eds., *NIST Handbook of Mathematical Functions*. Cambridge University Press, New York, NY, 2010.

[144] J. M. Maldacena, G. W. Moore, N. Seiberg, and D. Shih, *Exact vs. semiclassical target space of the minimal string*, *JHEP* **0410** (2004) 020, [hep-th/0408039].

[145] P. Luschny, *Hadamard versus Euler: Who Found the Better Gamma Function?*, *(http://www.luschny.de/math/factorial/hadamard/HadamardsGammaFunctionMJ.html)* (2006).

[146] A. Cherman, P. Koroteev, and M. Ünsal, *Resurgence and Holomorphy: From Weak to Strong Coupling*, *J.Math.Phys.* **56** (2015) 053505, [arXiv:1410.0388].

[147] C.-T. Chan, H. Irie, and C.-H. Yeh, *Analytic Study for the String Theory Landscapes via Matrix Models*, *Phys.Rev.* **D86** (2012) 126001, [arXiv:1206.2351].

[148] C. Vafa, *Brane / anti-brane systems and U(N—M) supergroup*, hep-th/0101218.

[149] C.-T. Chan, H. Irie, and C.-H. Yeh, *Stokes Phenomena and Non-perturbative Completion in the Multi-cut Two-matrix Models*, *Nucl.Phys.* **B854** (2012) 67–132, [arXiv:1011.5745].

[150] C.-T. Chan, H. Irie, S.-Y. D. Shih, and C.-H. Yeh, *Macroscopic loop amplitudes in the multi-cut two-matrix models*, *Nucl.Phys.* **B828** (2010) 536–580, [arXiv:0909.1197].

[151] S. Hastings and J. McLeod, *A boundary value problem associated with the second painlevé transcendent and the korteweg-de vries equation*, *Archive for Rational Mechanics and Analysis* **73** (1980), no. 1 31–51.

[152] I. Aniceto, J. G. Russo, and R. Schiappa, *Resurgent Analysis of Localizable Observables in Supersymmetric Gauge Theories*, *JHEP* **1503** (2015) 172, [arXiv:1410.5834].

[153] A. Grassi, Y. Hatsuda, and M. Mariño, *Topological Strings from Quantum Mechanics*, arXiv:1410.3382.

[154] Y. Hatsuda, M. Mariño, S. Moriyama, and K. Okuyama, *Non-perturbative effects and the refined topological string*, *JHEP* **1409** (2014) 168, [arXiv:1306.1734].

[155] J. Kallen and M. Mariño, *Instanton effects and quantum spectral curves*, arXiv:1308.6485.

Appendix A

The One-Cut Quartic Matrix Model: Structural Data

Our resurgence approach to extract finite N results out of the (nonperturbative) large N expansion was illustrated throughout chapter 6 within the example of the transseries solution to the one-cut quartic matrix model. In this appendix we briefly overview the data for this gauge theory, and the methods required in order to obtain it. These methods, first developed in [16] to construct one-parameter transseries solutions to the one-cut quartic matrix model, were later extensively used in [1, 25] to construct full two-parameter transseries solutions to the one- and two-cut quartic matrix models, resulting in large amounts of data for both perturbative and multi-instanton sectors. For the purposes of our current numerical analysis, however, the full data in [1, 25] is not needed but just about "half". The transseries written down in [1, 25] were written as asymptotic expansions in the matrix-model string coupling, g_s, being a bit closer in spirit to the string theoretic literature. In this case, remaining closer to the gauge theoretic literature, we shall slightly rewrite these results using the 't Hooft coupling instead, where $t = g_s N$.

The starting point is the so-called string equation, an equation computing the recursion coefficients r_n, (6.12), given some choice of polynomial potential in the matrix integral for the partition function. As discussed earlier, if one is able to compute these coefficients, then the partition function itself follows. For the case of the quartic potential, the string equation takes the form

$$r_n \left(1 - \frac{\lambda}{6}\left(r_{n-1} + r_n + r_{n+1}\right)\right) = n g_s. \tag{A.1}$$

The standard procedure starts by considering a continuum limit, where we introduce a new continuous variable $x = n g_s$ and where the recursion coefficients r_n get promoted to functions $\mathcal{R}(x)$ (we shall take the value $x = t$ in the following). This function is then written as a

transseries,

$$\mathcal{R}(N,t) = \sum_{n=0}^{+\infty} \sigma^n \, \mathcal{R}^{(n)}(N,t), \tag{A.2}$$

$$\mathcal{R}^{(n)}(N,t) \simeq \mathrm{e}^{-nN\frac{A(t)}{t}} \sum_{g=0}^{+\infty} N^{-g-\beta_n} \, t^{g+\beta_n} R_g^{(n)}(t), \tag{A.3}$$

where σ is the transseries parameter and $A(t)$ is the instanton action. The coefficient β_n may be regarded as a "characteristic exponent". In the present case $\beta_n = n/2$ (but see [25] for tables indicating the different values of β_n for the transseries of the quartic model). Note that in general one actually needs to consider a *two*-parameter transseries, with instanton actions $\pm A(t)$, leading to generalized instantons as one needs to consider many new nonperturbative sectors $(n) \to (n|m)$. Moreover, all these nonperturbative sectors are related to each other via resurgence; see [1, 25]. For most of the numerical analysis we have carried out, the above one-parameter transseries is enough. Another thing to notice is that the instanton action and the asymptotic coefficients have "attached" adequate powers of t. This is just so that what we herein call $A(t)$ and $R_g^{(n)}(t)$ are the *exact* same quantities as those computed in [25]. Now, by plugging this transseries expansion into the (continuous) string equation[1]

$$\mathcal{R}(t)\left\{1 - \frac{\lambda}{6}\left(\mathcal{R}\left(t-g_s\right) + \mathcal{R}(t) + \mathcal{R}\left(t+g_s\right)\right)\right\} = t, \tag{A.4}$$

we can recursively solve for the coefficients $R_g^{(n)}(t)$, as well as compute the instanton action (see [25] for details). The equations one finds are differential when $n = 1$ and algebraic in all other cases. The coefficients $R_g^{(n)}(t)$ can be written in terms of the variable $r \equiv \frac{1}{\lambda}\left(1 - \sqrt{1-2\lambda\, t}\right)$ and they have a pattern of the form

$$R_g^{(n)}(t) = \frac{(\lambda\, r)^{p_1}}{r^{p_2}\,(3-3\lambda\, r)^{p_3}\,(3-\lambda\, r)^{p_4}}\, P_g^{(n)}(r). \tag{A.5}$$

The exponents in the prefactor are functions of n and g,

$$\begin{aligned} p_1 &= \frac{1}{2}\left(3n-2\right), \\ p_2 &= n+g-1, \\ p_3 &= \frac{1}{4}\left(5n+10g-4\right), \\ p_4 &= \frac{1}{4}\left(3n+6g+2\delta-4\right), \end{aligned} \tag{A.6}$$

[1] Not to clutter notation too much, we sometimes omit the first argument in $\mathcal{R}(N,t)$.

with $\delta = n \bmod 2$, and the $P_g^{(n)}(r)$ are polynomials of degree $(n+6g+\delta-2)/2$. For the purposes of the numerical analysis in the main text, we have focused only on instanton sectors up to $n=3$. The maximum order of the asymptotic coefficients computed in each sector is shown below, in table A.1. For completeness let us also write down the first coefficients in

n	0	1	2	3
$g_{\max}$	200	50	50	50

Table A.1: Highest order g for which we have calculated $R_g^{(n)}(t)$.

each sector. For $n=0$,

$$R_0^{(0)} = r, \qquad R_2^{(0)} = \frac{\lambda^2 r}{6\left(1-\lambda r\right)^4}, \qquad R_4^{(0)} = \frac{7\lambda^4 r\left(5+2\lambda r\right)}{72\left(1-\lambda r\right)^9}. \tag{A.7}$$

With $n=1$ the equation at order N^{-g} gives a solution for $R_{g-1}^{(1)}(t)$. At order N^0 we compute the instanton action (see as well [10, 16, 57])

$$A = -\frac{r}{2}\left(2-\lambda r\right)\operatorname{arccosh}\left(\frac{3-2\lambda r}{\lambda r}\right) + \frac{1}{2\lambda}\sqrt{\left(3-\lambda r\right)\left(3-3\lambda r\right)}, \tag{A.8}$$

and the first coefficients that follow are

$$R_0^{(1)} = \frac{\sqrt{\lambda r}}{\left(3-\lambda r\right)^{1/4}\left(3-3\lambda r\right)^{1/4}}, \qquad R_1^{(1)} = -\frac{9\sqrt{\lambda r}\left(6-3\lambda r-6\lambda^2 r^2+2\lambda^3 r^3\right)}{8r\left(3-\lambda r\right)^{7/4}\left(3-3\lambda r\right)^{11/4}}. \tag{A.9}$$

Finally, for $n=2,3$, we have

$$R_0^{(2)} = -\frac{\lambda^2 r}{2\left(3-\lambda r\right)^{1/4}\left(3-3\lambda r\right)^{3/2}}, \qquad R_1^{(2)} = \frac{3\lambda^2\left(18+117\lambda r-102\lambda^2 r^2+22\lambda^3 r^3\right)}{8\left(3-\lambda r\right)^2\left(3-3\lambda r\right)^4}, \tag{A.10}$$

$$R_0^{(3)} = \frac{3\left(\lambda r\right)^{7/2}\left(2-\lambda r\right)}{8r^2\left(3-\lambda r\right)^{7/4}\left(3-3\lambda r\right)^{11/4}}, \qquad R_1^{(3)} = \frac{27\left(\lambda r\right)^{7/2}\left(18+\lambda r-12\lambda^2 r^2+4\lambda^3 r^3\right)}{16r^3\left(3-\lambda r\right)^{11/4}\left(3-3\lambda r\right)^{19/4}}. \tag{A.11}$$

Having addressed the transseries multi-instanton structure of $\mathcal{R}(N,t)$, one may proceed and address the free energy next. The relation between these quantities is encapsulated in a Toda-like equation (which is in fact nothing more than the continuous version of (6.14)),

$$\mathcal{F}\left(t+g_s\right) - 2\mathcal{F}(t) + \mathcal{F}\left(t-g_s\right) = \log\left(\frac{\mathcal{R}(t)}{t}\right). \tag{A.12}$$

Here $\mathcal{F} = F - F_{\mathrm{G}}$ denotes the free energy of the quartic matrix model normalized against the Gaussian contribution. By force of the above relation, the free energy will inherit the

transseries structure of $\mathcal{R}(N,t)$, such that again one finds

$$\mathcal{F}(N,t) = \sum_{n=0}^{+\infty} \sigma^n \, \mathcal{F}^{(n)}(N,t), \tag{A.13}$$

with

$$\mathcal{F}^{(0)}(N,t) \;\simeq\; \sum_{g=0}^{+\infty} N^{2-2g}\, t^{2g-2} \mathcal{F}_{2g}^{(0)}(t), \tag{A.14}$$

$$\mathcal{F}^{(n)}(N,t) \;\simeq\; \mathrm{e}^{-nN\frac{A(t)}{t}} \sum_{g=0}^{+\infty} N^{-g-\beta_n^{\mathcal{F}}}\, t^{g+\beta_n^{\mathcal{F}}} \mathcal{F}_g^{(n)}(t)\,, \tag{A.15}$$

where $\beta_n^{\mathcal{F}} = n/2$. Plugging this back in (A.12) and expanding in powers of σ we find

$$\mathcal{F}^{(n)}\left(t+g_s\right) - 2\mathcal{F}^{(n)}(t) + \mathcal{F}^{(n)}\left(t-g_s\right) = \Phi^{(n)}(t), \tag{A.16}$$

where $\Phi^{(n)}(t)$ is the n-th instanton sector of $\log\left(\frac{\mathcal{R}(t)}{t}\right)$. The first few sectors, which we will be using, are

$$\Phi^{(0)}(t) = \log\left(\frac{R^{(0)}(t)}{t}\right), \qquad \Phi^{(1)}(t) = \frac{R^{(1)}(t)}{R^{(0)}(t)}, \qquad \Phi^{(2)}(t) = \frac{R^{(2)}(t)}{R^{(0)}(t)} - \frac{1}{2}\left(\frac{R^{(1)}(t)}{R^{(0)}(t)}\right)^2. \tag{A.17}$$

The standard course of action, *e.g.*, [1, 16, 25, 49], essentially amounts to inverting (A.12) and finding explicit equations for each transseries component $\mathcal{F}_g^{(n)}(t)$. Herein we have taken a slightly different route, already starting at the perturbative level, $n=0$, which turns out to be much more computationally efficient at high genus. What we do is simply to use (A.12) directly: start by expanding its right-hand-side in powers of $1/N$, where the expansion of the logarithm is now written as a sum over partitions

$$\log\left(\frac{R^{(0)}(t)}{t}\right) = \log\left(\frac{R_0^{(0)}(t)}{t}\right) + \sum_{k=1}^{+\infty} \frac{t^{2k}}{N^{2k}} \sum_{s\geq 1} \frac{(-1)^{s-1}}{s} \sum_{\ell_1+\cdots+\ell_s=k} \frac{R_{\ell_1}^{(0)}(t)}{R_0^{(0)}(t)} \cdots \frac{R_{\ell_s}^{(0)}(t)}{R_0^{(0)}(t)}. \tag{A.18}$$

Now on the left-hand-side, at order $1/N^{2g}$, we see that the highest order coefficients cancel out and we are left with a differential equation for $\partial_t^2 \mathcal{F}_{2g}^{(0)}$. Knowing that the perturbative free energies follow a pattern[2] written in terms of the variable r (see [25]),

$$\mathcal{F}_{2g}^{(0)} = \frac{\lambda^{2g-1}}{(2-\lambda\, r)^{2g-2}\,(1-\lambda\, r)^{5(g-1)}}\, \mathcal{P}_{2g}^{(0)}(r), \tag{A.19}$$

[2] With exceptions at $g = 0, 1$.

with $\mathcal{P}^{(0)}_{2g}(r)$ a polynomial of degree $3g-3$, it is a computationally straightforward task to plug this *ansatz* into the equation and solve for the coefficients of the polynomial. The boundary conditions amount to setting $\mathcal{F}^{(0)}_{2g}\Big|_{\lambda=0} = 0$, which is a consequence of the Gaussian normalization. The highest order to which we computed $\mathcal{F}^{(0)}_{2g}$ is shown in table A.2. The first coefficients are

$$\mathcal{F}^{(0)}_0 = \frac{r^2}{96}\left(\lambda r\left(9\lambda r-16\right)+12\left(2-\lambda r\right)^2\log\left(\frac{2}{2-\lambda r}\right)\right), \tag{A.20}$$

$$\mathcal{F}^{(0)}_2 = -\frac{1}{12}\log\left(\frac{2-2\lambda r}{2-\lambda r}\right), \tag{A.21}$$

$$\mathcal{F}^{(0)}_4 = \frac{\lambda^3\left(41\lambda^2 r^3-185\lambda r^2+200r\right)}{2880\left(\lambda r-2\right)^2\left(1-\lambda r\right)^5}. \tag{A.22}$$

Proceeding with the one and two instanton coefficients, the calculation follows in a straightforward fashion. The equations at order $\sigma^n\, g_s^g$ are now algebraic equations for $\mathcal{F}^{(n)}_g$, and we solve them using the same method of plugging-in an *ansatz* and reducing the problem to one of finding coefficients of a polynomial. The maximum orders of the coefficients we found for $n=1,2,3$ are shown in table A.2. Essentially, we are limited by the number of $R^{(n)}_g$ we calculated beforehand. The functions $\mathcal{F}^{(n)}_g$, which we computed for $n=1,2,3$, are of the

n	0	1	2	3
$g_{\max}$	130	50	50	50

Table A.2: Highest order g for which we have calculated $\mathcal{F}^{(n)}_g(t)$.

form[3]

$$\mathcal{F}^{(n)}_g = \frac{\left(\lambda\, r\right)^{p_1+1}}{r^{p_2+1}\left(3-3\lambda\, r\right)^{p_3+1}\left(3-\lambda\, r\right)^{p_4+1-\delta}}\,\mathcal{P}^{(n)}_g(r), \qquad n\geq 1, \tag{A.23}$$

where the $\mathcal{P}^{(n)}_g(r)$ are polynomials of degree $(6g+n-\delta)/2$, and the exponents p_i were defined

[3]We note that there is a small typo in the formulae for the free energy coefficients in [25]. The factors of $t-\alpha^2$ therein, where $\alpha^2=r$, should in fact be α^2-t.

in (A.6). At lowest order, the $n = 1, 2$ and 3 coefficients are

$$\mathcal{F}_0^{(1)} = \frac{\lambda^{3/2}\, r^{1/2}}{2\,(3-3\lambda r)^{5/4}\,(3-\lambda r)^{1/4}}, \tag{A.24}$$

$$\mathcal{F}_1^{(1)} = -\frac{9\lambda^{3/2}\,(6+75\lambda r-54\lambda^2 r^2+10\lambda^3 r^3)}{16 r^{1/2}\,(3-3\lambda r)^{15/4}\,(3-\lambda r)^{7/4}}, \tag{A.25}$$

$$\mathcal{F}_0^{(2)} = -\frac{\lambda^3 r\,(3-2\lambda r)}{8\,(3-3\lambda r)^{5/2}\,(3-\lambda r)^{3/2}}, \tag{A.26}$$

$$\mathcal{F}_1^{(2)} = \frac{3\lambda^3\,(54+531\lambda r-846\lambda^2 r^2+462\lambda^3 r^3-92\lambda^4 r^4)}{32\,(3-3\lambda r)^{5}\,(3-\lambda r)^{3}}, \tag{A.27}$$

$$\mathcal{F}_0^{(3)} = -\frac{\lambda^{9/2} r^{3/2}\,(6-5\lambda r)}{48\,(3-3\lambda r)^{15/4}\,(3-\lambda r)^{7/4}}, \tag{A.28}$$

$$\mathcal{F}_1^{(3)} = \frac{3\lambda^{9/2} r^{1/2}\,(-108-1044\lambda r+1917\lambda^2 r^2-1086\lambda^3 r^3+212\lambda^4 r^4)}{128\,(3-3\lambda r)^{25/4}\,(3-\lambda r)^{13/4}}. \tag{A.29}$$

Finally, let us note that even though we have presented several results for the partition function in chapter 6, we have actually not addressed its transseries representation. In fact, it is computationally very inefficient to exponentiate the free energy transseries and then extract the transseries coefficients for the partition function. If we had done that, we would have ended up only going to much lower orders than what we have achieved for the free energy. As such, we have instead always performed any required resummation first, for the free energy transseries, and only then exponentiated the result.

Appendix B

The Two-Cut Quartic Matrix Model: Structural Data

In this appendix we present some explicit results concerning the two-parameter transseries solution to the two-cut quartic matrix model. Let us recall that in subsection 4.3 we have solved the string equations of this model, (4.24) and (4.25), by introducing the *ansatz*

$$\mathcal{P}(x) = \sum_{n=0}^{+\infty} \sum_{m=0}^{+\infty} \sigma_1^n \sigma_2^m \, \mathcal{P}^{(n|m)}(x), \tag{B.1}$$

with

$$\mathcal{P}^{(n|m)}(x) \simeq \mathrm{e}^{-(n-m)A(x)/g_s} \sum_{g=\beta_{nm}}^{+\infty} g_s^g \, P_g^{(n|m)}(x), \tag{B.2}$$

and similarly for $\mathcal{Q}(x)$. In the table below we show the maximum order (in g) in the string coupling to which we have recursively computed the above nonperturbative coefficients:

m \ n	0	1	2	3	4
0	60	10	10	10	5
1		10	5	5	5

Table B.1: Values for the highest g for which we have calculated $P_g^{(n|m)}$ and $Q_g^{(n|m)}$.

Do note that, since the sums in (B.2) have a "starting genus" which is (in general) $\beta_{nm} = -\min(m,n) \leq 0$, the actual number of coefficients that we have computed is *bigger* than the numbers displayed in table B.1. It is also worth pointing out that in the cases where $n = m$ the asymptotic expansions contain only even powers of g_s, which implies half of the indicated coefficients vanish. Finally, the sectors $(m|n)$ and $(n|m)$ are trivially related via

(similar for $Q(x)$)

$$P_g^{(n|m)}(x) = (-1)^g\, P_g^{(m|n)}(x). \tag{B.3}$$

Let us begin by presenting explicit results for the first few coefficients in the perturbative sector[1]

$$P_0^{(0|0)} = \frac{1}{\lambda}(3-p), \qquad Q_0^{(0|0)} = \frac{1}{\lambda}(3+p), \tag{B.4}$$

$$P_1^{(0|0)} = \lambda\,\frac{162-27p-9p^2}{2p^5}, \qquad Q_1^{(0|0)} = \lambda\,\frac{-162-27p+9p^2}{2p^5}, \tag{B.5}$$

$$P_2^{(0|0)} = \lambda^3\,\frac{1915812-314928p-181521p^2+18711p^3+1944p^4}{8p^{11}}, \tag{B.6}$$

$$Q_2^{(0|0)} = \lambda^3\,\frac{-1915812-314928p+181521p^2+18711p^3-1944p^4}{8p^{11}}. \tag{B.7}$$

Proceeding with the multi-instanton sectors (and just explicitly showing results for $\mathcal{P}(x)$ from now on), the first few coefficients in the $(1|0)$ sector are

$$P_0^{(1|0)} = -\sqrt{\frac{3-p}{p}}, \tag{B.8}$$

$$P_1^{(1|0)} = \lambda\,\frac{459-45p^2+6p^3}{8\,p^{7/2}\,(3+p)\,(3-p)^{1/2}}, \tag{B.9}$$

$$P_2^{(1|0)} = \lambda^2\,\frac{9}{128\,p^{13/2}\,(3+p)^2\,(3-p)^{3/2}}\times \tag{B.10}$$
$$\times\left(-122553-15552p+27270p^2+2844p^3-1593p^4-132p^5+4p^6\right),$$

while in the $(2|0)$ sector we find

$$P_0^{(2|0)} = -\lambda\,\frac{3-p}{2p^2}, \tag{B.11}$$

$$P_1^{(2|0)} = \lambda^2\,\frac{1107+108p-117p^2-6p^3}{8\,p^5\,(3+p)}, \tag{B.12}$$

$$P_2^{(2|0)} = \lambda^3\,\frac{9}{64\,p^8\,(3+p)^2\,(3-p)}\times$$
$$\times\left(-442341-65448p+102330p^2+12924p^3-6669p^4-636p^5+80p^6\right) \tag{B.13}$$

One of the main features of using multi-parameter transseries is the appearance of generalized multi-instanton sectors, which may have different signs of the instanton action within the nonperturbative exponential contribution. This may lead, sometimes, to the cancellation of

[1]Recall from the main body of the text that we are using the variable $p=\sqrt{9-6\lambda x}$.

all terms in this exponential contribution – for example, in the present setting this happens when $n = m$ – and we will be left with a (perturbative) expansion in the closed string coupling. The first sector with this feature is the $(1|1)$ sector, where the first few coefficients are

$$P_0^{(1|1)} = \lambda \frac{9-p}{p^2}, \tag{B.14}$$

$$P_2^{(1|1)} = \lambda^3 \frac{70713 - 10125p - 4617p^2 + 261p^3}{8\,p^8}, \tag{B.15}$$

$$P_4^{(1|1)} = \lambda^5 \frac{1}{128\,p^{14}} \left(8806981203 - 1369011699p - 959100102p^2 + 103563198p^3 + \right.$$
$$\left. + 18833715p^4 - 787563p^5\right). \tag{B.16}$$

The general case $n \neq m$ is more complicated. Generically, asymptotic expansions will be in powers of the string coupling, g_s, and the "starting genus" may start taking negative values. Furthermore, logarithmic contributions begin to appear [25]. For example, one may compute the following coefficient in the $(2|1)$ sector (this is the second non-vanishing coefficient in this sector):

$$P_0^{(2|1)} = \lambda^2 \frac{1}{16\,p^{7/2}\,(3+p)\,(3-p)^{1/2}} \left\{ \left(-432 - 180p + 24p^2 + 12p^3\right) + \right.$$
$$\left. + \left(153 - 15p^2 + 2p^3\right) \log\left(\frac{p^6}{9-p^2}\right)\right\}. \tag{B.17}$$

Even though we have not produced as much data as in the one-cut solution discussed in [25], we are still able to conjecture the general form of all these coefficients. Our data, together with the experience gathered in [25], indicate that the nonperturbative coefficients take the form

$$P_g^{(n|m)}(x) = \sum_{k=0}^{\min(n,m)} \log^k\left(f(x)\right) \cdot P_g^{(n|m)[k]}(x), \tag{B.18}$$

where

$$P_g^{(n|m)[k]}(x) = \frac{\lambda^{c_1}}{p^{c_2}\,(3-p)^{c_3}\,(3+p)^{c_4}}\,\mathfrak{P}_g^{(n|m)[k]}(x), \tag{B.19}$$

and where the function $f(x)$, written in terms of the variable p, is

$$f(p) = \frac{p^6}{9-p^2}. \tag{B.20}$$

Above, the coefficients c_i are given by

$$c_1 = n+m+g-1, \tag{B.21}$$

$$c_2 = \frac{3}{2}(n+m)+3g-1, \tag{B.22}$$

$$c_3 = (1-\delta_{nm})\frac{1}{2}(3m-n+2g), \tag{B.23}$$

$$c_4 = (1-\delta_{nm})(m+g), \tag{B.24}$$

and they are valid whenever $n \geq m$. The $\mathfrak{P}_g^{(n|m)[k]}(x)$ are polynomials in p of degree $3(m+g)$. When $n=m$, these polynomials get reduced and have degree $n+g$. Concerning the pattern for the $Q_g^{(n|m)}(x)$ coefficients, we find a similar result, but with the roles of c_3 and c_4 interchanged,

$$Q_g^{(n|m)[k]}(x) = \frac{\lambda^{c_1}}{p^{c_2}(3-p)^{c_4}(3+p)^{c_3}}\mathfrak{Q}_g^{(n|m)[k]}(x), \tag{B.25}$$

and with the extra condition

$$\mathfrak{Q}_g^{(n|m)[k]}(p) = -\mathfrak{P}_g^{(n|m)[k]}(-p). \tag{B.26}$$

Finally, upon further analyzing our data, a relation emerges between the coefficients in the $(n|m)[k]$ and the $(n-k|m-k)[0]$ sectors (this is very similar to the relation (4.76) which we have found for the nonperturbative Painlevé II coefficients in the main body of the text). We find

$$P_g^{(n|m)[k]} = \frac{1}{k!}\left(\frac{\lambda(n-m)}{6}\right)^k P_{g+k}^{(n-k|m-k)[0]}. \tag{B.27}$$

For completeness, let us be fully specific on a few of the polynomials $\mathfrak{P}_g^{(n|m)[k]}$, which we have explicitly computed. These polynomials take the form $c\sum a_i p^i$, where p is their variable and c and a_i their coefficients. We list these coefficients in the tables that follow.

g	0	1	2
c	$-\frac{3}{4}$	$\frac{1}{32}$	$-\frac{3}{512}$
p^0	36	670680	811753164
p^1	15	8991	163196127
p^2	-2	-159732	-277986654
p^3	-1	486	-53318331
p^4		11340	33149088
p^5		-261	6037173
p^6		-208	-1519542
p^7			-264789
p^8			16680
p^9			3068

g	-1	0	1
c	$-\frac{1}{6}$	$\frac{1}{16}$	$-\frac{3}{256}$
p^0	1	153	122553
p^1		0	15552
p^2		-15	-27270
p^3		2	-2844
p^4			1593
p^5			132
p^6			-4

Table B.2: Prefactor c and coefficients of the polynomials $\mathfrak{P}_g^{(2|1)[0]}$ (left) and $\mathfrak{P}_g^{(2|1)[1]}$ (right).

g	0	1	2
c	$-\frac{1}{4}$	$\frac{1}{8}$	$-\frac{3}{128}$
p^0	297	528525	2176342749
p^1	54	69255	368793810
p^2	-27	-118584	-766103913
p^3	-4	-12744	-118696752
p^4		7533	96370155
p^5		549	13149378
p^6		-94	-4972095
p^7			-549324
p^8			81696
p^9			5288

g	-1	0	1
c	$-\frac{1}{6}$	$\frac{1}{8}$	$-\frac{3}{64}$
p^0	1	369	442341
p^1		36	65448
p^2		-39	-102330
p^3		-2	-12924
p^4			6669
p^5			636
p^6			-80

Table B.3: Prefactor c and coefficients of the polynomials $\mathfrak{P}_g^{(3|1)[0]}$ (left) and $\mathfrak{P}_g^{(3|1)[1]}$ (right).

g	0	1	2
c	$-\frac{3}{16}$	$\frac{3}{128}$	$-\frac{9}{2048}$
p^0	351	2998377	14430217473
p^1	54	451980	2674565406
p^2	−33	−654156	−4961854665
p^3	−4	−82620	−841785048
p^4		39393	605366703
p^5		3600	90717246
p^6		−382	−29788263
p^7			−3633804
p^8			442368
p^9			30856

g	−1	0	1
c	$-\frac{1}{8}$	$\frac{3}{64}$	$-\frac{9}{1024}$
p^0	1	1269	3852765
p^1		126	593892
p^2		−135	−876582
p^3		−8	−115236
p^4			55341
p^5			5544
p^6			−572

Table B.4: Prefactor c and coefficients of the polynomials $\mathfrak{P}_g^{(4|1)[0]}$ (left) and $\mathfrak{P}_g^{(4|1)[1]}$ (right).

Appendix C

Perturbative Free Energy in the Quartic Matrix Model

In the main text we have discussed how the Euler-Maclaurin formula (suitably adapted to the period-two case) provides for a recipe in order to extract the genus g perturbative free energies, $\mathcal{F}_g^{(0|0)}$, out of the recursion coefficients in the orthogonal polynomial framework. However, it is important to notice that this method is computationally very time consuming (even more so that in the one-cut case addressed in [25]) and thus ends up providing for less data in the resurgence tests than directly using the coefficients $P_g^{(0|0)}$ or $Q_g^{(0|0)}$. Nonetheless, we explicitly need to know these coefficients as they are used to determine the Stokes coefficient out of the large-order sequence (4.47). In here, we shall explicitly list a few of these results for the $\mathcal{F}_g^{(0|0)}$ (as usual, written in terms of the variable p). We find

$$\mathcal{F}_0^{(0|0)} = \frac{(9-p^2)^2}{576\lambda^2}\log\left(\frac{1296}{\lambda^4}\right), \tag{C.1}$$

$$\mathcal{F}_1^{(0|0)} = \frac{1}{4}\log\left(\frac{3+p}{2p}\right), \tag{C.2}$$

$$\begin{aligned}\mathcal{F}_2^{(0|0)} = {} & \frac{\lambda^2}{320\,p^6\,(9-p^2)^2}\times \\ & \times\left(787320-174960p-215055p^2+43740p^3+18630p^4-3780p^5-471p^6\right),\end{aligned} \tag{C.3}$$

$$\begin{aligned}\mathcal{F}_3^{(0|0)} = {} & \frac{\lambda^4}{1792\,p^{12}\,(9-p^2)^4}\times \\ & \times\big(1214950653504-234633327264p-653277037896p^2+119905844184p^3+ \\ & +141553030437p^4-24374010024p^5-15592951332p^6+2467933272p^7+ \\ & +895852062p^8-125778744p^9-23861628p^{10}+2857680p^{11}+181989p^{12}\big).\end{aligned} \tag{C.4}$$

As the genus increases, the expressions become exponentially longer and we shall not show any more explicit formulae. However, our results do indicate a clear pattern for the perturbative genus g free energies: for genus $g \geq 2$ they have the form

$$\mathcal{F}_g^{(0|0)}(\lambda, p) = \frac{\lambda^{2(g-1)}}{p^{6(g-1)}\left(9-p^2\right)^{2(g-1)}}\,\mathfrak{F}_g(p), \tag{C.5}$$

where $\mathfrak{F}_g(p)$ is a polynomial in p of degree $6(g-1)$. Finally, as we have discussed in subsection 4.4.3, applying the double-scaling limit to these results, and taking two derivatives, yields a precise match with (the square of) the perturbative data arising within the Painlevé II equation.

Appendix D

The Painlevé II Equation: Structural Data

In this appendix we present some explicit results concerning the two-parameter transseries solution to the Painlevé II equation. Let us recall that in subsection 4.4.1 we have solved this equation, (4.58), by introducing the *ansatz*

$$u\left(w,\sigma_1,\sigma_2\right)=\sum_{n=0}^{+\infty}\sum_{m=0}^{+\infty}\sigma_1^n\sigma_2^m\,\mathrm{e}^{-(n-m)A/w^2}\,\Phi_{(n|m)}(w), \tag{D.1}$$

with

$$\Phi_{(n|m)}(w)\simeq\sum_{k=0}^{\min(n,m)}\log^k w\cdot\sum_{g=0}^{+\infty}u_g^{(n|m)[k]}\,w^g. \tag{D.2}$$

For shortness we introduce

$$\Phi^{[k]}_{(n|m)}(w)\simeq\sum_{g=0}^{+\infty}u_g^{(n|m)[k]}\,w^g. \tag{D.3}$$

As we discussed in the main text, this *ansatz* turns the original differential equation into a recursive equation for the coefficients $u_g^{(n|m)[k]}$. In table D.1 we show the maximum order in w to which we have calculated these coefficients. We have only listed the $n\geq m$ cases, but we shall see below how the $(m|n)$ and $(n|m)$ sectors are trivially related. We shall also see that there is a relation between the $[k]$th and the $[0]$th logarithmic sectors. In the following we will reproduce a few examples concerning all this data.

m \ n	0	1	2	3	4
0	1000	1000	1000	500	500
1		1000	100	100	100
2			100	100	100
3				100	100
4					100

Table D.1: Maximum order in w for which we have calculated $u_g^{(n|m)[k]}$.

The first few $(n|0)$ sectors we found are:

$$\Phi^{[0]}_{(0|0)} = 1 - \frac{1}{16}w^4 - \frac{73}{512}w^8 - \frac{10657}{8192}w^{12} - \frac{13912277}{524288}w^{16} - \cdots, \tag{D.4}$$

$$\Phi^{[0]}_{(1|0)} = w - \frac{17}{96}w^3 + \frac{1513}{18432}w^5 - \frac{850193}{5308416}w^7 + \frac{407117521}{2038431744}w^9 - \cdots, \tag{D.5}$$

$$\Phi^{[0]}_{(2|0)} = \frac{1}{2}w^2 - \frac{41}{96}w^4 + \frac{5461}{9216}w^6 - \frac{1734407}{1327104}w^8 + \frac{925779217}{254803968}w^{10} - \cdots. \tag{D.6}$$

The lowest $\Phi^{[0]}_{(n|1)}$ are

$$\Phi^{[0]}_{(1|1)} = -3w^2 - \frac{291}{128}w^6 - \frac{447441}{32768}w^{10} - \frac{886660431}{4194304}w^{14} - \cdots, \tag{D.7}$$

$$\Phi^{[0]}_{(2|1)} = w^3 - \frac{115}{48}w^5 + \frac{30931}{18432}w^7 - \frac{4879063}{663552}w^9 + \cdots. \tag{D.8}$$

The first time we encounter logarithmic terms is for $n = 2$, $m = 1$, where we have

$$\Phi^{[1]}_{(2|1)} = -8w + \frac{17}{12}w^4 - \frac{1513}{2304}w^6 + \frac{850193}{663552}w^8 + \cdots. \tag{D.9}$$

From the full list of data we computed, one finds a relation between the coefficients in sectors $(n|m)[k]$ (logarithmic) and $(n-k|m-k)[0]$ (non-logarithmic), which is the following

$$u_g^{(n|m)[k]} = \frac{1}{k!}\left(8\,(m-n)\,\right)^k u_g^{(n-k|m-k)[0]}. \tag{D.10}$$

Finally, the sectors with $n < m$ are very closely related to the ones with $n > m$ as[1]

$$u_g^{(m|n)[k]} = \left|u_g^{(n|m)[k]}\right|, \qquad \text{for } n > m. \tag{D.11}$$

[1]Similarly to what was found in [25] for the Painlevé I equation, we may suspect that this is just an "apparent" relation, only to be falsified at some high n, m and g (in [25] one had to go to $n = 3$, $m = 4$ and genus $g = 11$ to falsify it). However, all the data we have produced is consistent with this relation.

As a final note, we add that all our off-criticality transseries results, *i.e.*, the results for the two-cut quartic matrix model partially presented in appendix B, match the present transseries solution of Painlevé II, when in the double-scaling limit. A *Mathematica* notebook with the complete explicit results we have obtained is available upon request.